CHARACTERIZATION OF LIGHTNING USING OPTICAL TECHNIQUES

By

SANDIP NALLANI

A THESIS PRESENTED TO THE GRADUATE SCHOOL
OF THE UNIVERSITY OF FLORIDA IN PARTIAL FULFILLMENT
OF THE REQUIREMENTS FOR THE DEGREE OF
MASTER OF SCIENCE

UNIVERSITY OF FLORIDA

2008

To my parents, to whom I owe everything.

ACKNOWLEDGMENTS

I am deeply indebted to Dr. Rakov and Mr. Rob Olsen for their incredible patience and tireless guidance. Dr. Rakov, is a brilliant scientist and researcher who introduced me to the field of lightning. I cannot thank Rob Olsen enough for assisting me whenever possible, even on a couple of weekends, when he had a family and a job to attend to. I would also like to thank Dr. Uman and Dr. Doug Jordan for the brain storming sessions in the lightning lab meetings. I would also like to thank Amitabh Nag, Jason Jerauld, Jens Schoene, and Dimitris Tsalikis for all those fun lightning lab moments interspersed with serious technical discussions. Lastly, I would like to acknowledge my family. Without them, graduate school would have been a mere fantasy dream.

.

TABLE OF CONTENTS

LIST OF TABLES

LIST OF FIGURES

Abstract of Dissertation Presented to the Graduate School
of the University of Florida in Partial Fulfillment of the
Requirements for the Degree of Master of Science

CHARACTERIZATION OF LIGHTNING USING OPTICAL TECHNIQUES

By

SANDIP NALLANI

May 2008

Chair: V.A. Rakov
Major: Electrical Engineering

We analyzed optical (photodiode array) records for 31 lightning flashes obtained at Camp Blanding, Florida, in summer 2005. Of these 31 flashes, 8 (containing 11 strokes) were triggered- lightning flashes and the remaining 23 were natural lightning flashes. The overall return-stroke speeds and return-stroke speed profiles as a function of height were obtained for triggered lightning strokes. The slope-intercept point and the 20% of peak point were used as reference points in estimating return-stroke speeds. Based on higher resolution LeCroy data, the triggered-lightning return-stroke speeds are found to vary between 1.48 x 10^8 m/s and 1.59 x 10^8 m/s. The average return-stroke optical risetimes for 11 triggered-lightning events were found to be 0.81 μs and 2.83 μs at the bottom and top of the lightning channel, respectively. Leader speeds for 5 triggered-lightning strokes have been estimated. The leader speeds are found to vary between 1.3 x 10^7 m/s and 2.5 x 10^7 m/s. All 23 natural lightning records acquired in 2005 at Camp Blanding using photodiodes viewing various heights are presented and characterized. An image converter camera was used at the University of Florida to obtain optical images of natural lightning processes in summer 2006. Only limited analysis of these images was possible due to lack of resolution. In order to improve the performance characteristics of the image converter camera, a new triggering circuit for this camera was designed, built, and successfully tested.

CHAPTER 1
INTRODUCTION

Lightning is one of the most beautiful displays in nature as well as one of the most deadliest natural phenomena known to man. With lightning channel temperatures hotter than the surface of the Sun, lightning is a lesson in science and humility.

In the Indian mythological story of Ramayana, written by a poet Valmiki some 2000 years ago, Lord Hanuman (‘pavan-putra’ in Sanskrit) was the son of the wind god ‘Vayu’. Hanuman possessed immense physical strength with the power to fly and was capable of divine levels of endurance .When the young immature Hanuman started tossing around the Sun playfully, the distressed Sun called out to Lord Indira, the son of lightning, heaven, and Earth who carried thunderbolts on his chariot. The skies grew dark and made way for Lord Indira who shot the young mischievous Hanuman with a thunder bolt when he disagreed to let the Sun go, and so goes the story. Thus, we see that lightning and thunder have always been feared and respected by mankind and have played a significant role in the religions and mythologies of all but the most modern of civilizations.

CHAPTER 2
LITERATURE REVIEW

The first scientific study of lightning was carried out by Benjamin Franklin in the later half of the eighteenth century. Much of Franklin's reputation was as a result of his phenomenal demonstration of intercepting lightning and bringing it safely to the Earth without harming people of property. Franklin was the first to propose an experiment to prove that lightning was electrical and thus so were the clouds that produced lightning, using an iron rod [Uman, 1987]. In this experiment a man on ground was to draw sparks between an iron rod and a grounded wire held by an insulating handle. In France in May 1752, Thomas-Francois D'Alibard successfully performed Franklin's suggested experiment and sparks were observed to jump from the iron rod during a thunderstorm. It was proved that thunderclouds contained electrical charge [Uman, 1987]. In 1752, he thought of a better experiment where the kite was to take the place the rod, since it could achieve greater elevation. In the same year, he was successful in drawing sparks out of a key tied to the bottom of the kite string separated from his hand by an insulating silk string [Uman, 1987]. He then proposed a version of the lightning rod that is still the primary means of protecting structures against lightning [Franklin, 1774, p.169].

2.2 Natural Lightning

Research into natural lightning was renewed because of the hazards faced by electrical circuits, aircraft and spacecraft due to the voltages and currents by direct of nearby lightning strikes. Very small voltages are capable of causing malfunction of electronics. Natural lightning flashes are produced by thunderclouds which are formed when warm moist air rises and cools via an adiabatic expansion, eventually condensing into water droplets which form the visible cloud. It is usually assumed that there is net positive charge at the top, a negative charge in the middle followed by an additional smaller positive charge at the bottom. The top two charges are

usually the main charges and are often specified to be equal in magnitude whereas the lower positive charge may not always be present [Rakov 2002]. Lightning is a transient, high current discharge whose path length is measured in kilometers. Well over half of all flashes occur wholly within the cloud and are called IC discharges. However, we are mainly concerned with cloud-to-ground (CG) lightning because of its practical importance and also because it can be relatively easily studied. In Figure 2-1 below the four different categories of CG flashes are illustrated. Category 1 lightning begins with a negatively charged leader moving downward, while Category 3 has a positively charged downward moving leader. Category 2 has a positively charged upward moving leader while Category 4 has a negatively charged upward moving leader. In Categories 1 and 2, negative charge is effectively transported to ground and in Categories 3 and 4 positive charge is lowered to ground.

Upward-initiated flashes (Categories 2 and 4) are relatively rare and generally occur from tall man-made structures or moderate heights structures on mountain tops. Because of the nature and unpredictability of natural lightning, there has been a growing interest in the use of rocket-and-wire techniques (see Section 2.3) in lightning research.

Lightning discharge is composed of several distinct processes which occur in less than 1 second, mostly along the same spatial path. A schematic of these various distinct processes is shown in Figure 2-2. The discharge begins with a preliminary electrical breakdown in the cloud, which is not shown in this figure, followed by a stepped leader, followed by the first return stroke. This first return stroke could then be followed by a series of dart leader and subsequent return stroke combination events separated by intervals of several tens of milliseconds. During these intervals, after some return strokes, steady currents of hundreds of amperes continue to flow to ground, which are called continuing currents. During the continuing current phase,

discharges not shown in the Figure 2-2 brighten the channel and are called the M-components. Continuing currents cease prior to a subsequent leader return stroke sequence.

2.3 Artificially Initiated (Triggered) Lightning

In rocket-and-wire lightning triggering technique, a small (~1m) rocket trailing a grounded wire is used to initiate a lightning flash. This allows the researcher to have advance knowledge of the time and location of a lightning flash, and hence of the exact distance to the termination point of the lightning channel. This allows one to measure currents and propagation speeds of the leader/return-stroke sequences. The rocket is launched in the presence of a sufficiently charged cloud overhead. When the wire is grounded, the triggering is called the "classical" triggering and is illustrated in Figure 2-3. The electric field below the cloud is measured, with -4 to -10 kV/m typically being the experimentally-determined critical field. When this occurs, a rocket is launched. It ascends at a speed of about 200 m/s. When it is typically 200-300 m high, the electric field enhancement near the upper end of the wire is sufficient to trigger a positively charged leader propagating towards the cloud (in the predominant case when there is negative charge at the bottom of the cloud).

The upward leader melts and vaporizes the trailing wire and establishes the so-called "initial continuous current" of the order of some hundreds of amperes along the wire trace, which effectively serves to transport negative charge from the cloud charge source to the ground via the triggering facility and current-measuring instrumentation. After the cessation of the initial continuation current, several downward leader/upward return stroke sequences often traverse the same path to the triggering facility. The initial current variation stage is illustrated in Figure 2-4 adapted from Olsen et al. (2006). A typical initial current variation (ICV) waveform exhibits a relatively slow increase in current magnitude to a maximum of some hundreds of amperes, which generally but not always coincides with the beginning of current decay, shown here at

point A. The relatively rapid current reduction between points A and B1 is associated with the explosion of the triggering wire. The interval between B1 and B2 can vary between some hundreds of microseconds to some milliseconds, during which little or no current flows. There may be small pulses (not seen in this figure) during this interval. At point C, a relatively large and sharp pulse reestablishes current between the upward positive leader (UPL) and ground. For the purposes of estimating charge and action integral (AI), current is integrated over the interval between the beginning of the record (which is prior to the beginning of the initial stage, when no current is flowing) and the time labeled B1 on the waveform. ‘‘Peak before’’ denotes the peak current prior to wire explosion, which is generally but not always observed at the onset of current reduction at point A. ‘‘Decay’’ denotes the duration of the time interval during which the current decays to or nearly to zero, between points A and B1 on the diagram. ‘‘Zero current interval’’ denotes the duration of the time interval over which the current is equal to (or nearly equal to) zero, represented by the interval between B1 and B2. ‘‘Peak after’’ denotes the maximum current in the pulse (shown at point C) associated with reconnection of the UPL to ground.

2.4 Optical Studies of Lightning: An Overview

The luminous features of lightning discharges to ground have been widely studied and have provided considerable insights in to the physics of the lightning processes. Scientists first studied the light intensity of the lightning flash late in the 19th century. Their main intention was to determine the sequence of events in a lightning flash. Kayser (1884) was the first to observe that the lightning process consisted of multiple strokes down the same spatial path or the channel formed by the first leader and return stroke processes. Hoffert (1889) and Weber (1889) used moving cameras to separate the individual lightning events on film. Photographs were obtained by Walter (1902, 1903, 1910, 1912, 1918) which showed for the first time that the lightning process was initiated by a branched initial process followed by a return stroke traveling up the

same channel. Therefore by the 20th century a coarse view of the lightning discharge had been revealed.

Sir Charles V. Boys (1929) invented a camera system in 1900 which revolutionized the study of lightning. The camera produced relative motion between the film and the lenses by having the lenses rotate in front of the film. This system allowed the camera to remain stationary but still allowed the camera to separate different events that occurred on the same path. The investigation of optical properties of lightning during the period between 1930 and 1960 was dominated by Schonland, Malan, Collens and coworkers in South Africa. Boys cooperated with this team and loaned his camera to be used as a prototype. In their first experiments with Boys' rotating lens camera design (Schonland, Malan and Collens, 1934), they verified previous findings by Halliday (1933) which showed lightning intensity moving up and down the lightning channel. They observed that the lightning intensity decreased as the return stroke front passed each branch point and finally vanished after it passed the last branch before entering the cloud. The Boys camera was later modified to have still lenses and a rotating film drum (Schonland, Malan, and Collens, 1935), as shown in Figure 2-6. The apertures of the camera lenses were set independently which allowed sufficient dynamic range to examine the processes whose light intensity varied greatly. It was observed that the stepped leader paused for approximately 100 microseconds between steps. The authors also discovered that the effective stepped leader speeds increased near the ground. Orville and Indone (1982) also showed that the stepped leader speed increases near the ground.

In this way, optical lightning research in the early years mainly concentrated on the subjective analysis of film records to determine lightning properties. As technology improved, it became possible to use calibrated photoelectric detectors to determine quantitative parameters of

lightning processes. Mackerras (1973) used photomultiplier tubes and a wide-angle camera system to perform a quantitative study of the integrated lightning output of both cloud and ground flashes.

2.5 Leader and Return-Stroke Speeds and Light-Pulse Risetimes Obtained from Optical Observations

A parameter of great interest to researchers developing return stroke models, is the speed of the return stroke front as it propagates up the channel. Return stroke is a fundamental parameter of the cloud-to-ground flash and is also one of the two input parameters (channel base current and return stroke speeds) in the transmission line model (TLM) of the return stroke for calculating currents (Jordan 1989). Orville et al (1978) presented daytime lightning data acquired with a streak camera system including measurements of return stroke speeds ranging from 1.2 x 10^8 to 1.4 x 10^8 m/s. The return stroke speed was computed using a still image from a 35 mm camera as a reference image and measuring the displacement of the streaked image from the still image. The displacement was a function of the height along the channel and the return stroke speed.

Orville and Idone (1982) presented streak camera records for 21 dart leaders, 4 dart–stepped leaders and 3 stepped leaders from Kennedy Space Center, Florida, and Socorro, New Mexico, in mostly daylight conditions. Dart leader speeds were computed at two heights along the channel with the mean speed in the bottom 800 meters being 11 x 10^6 m/sec. They also found a correlation between the dart leader luminous intensity and the resulting return stroke luminous intensity. They found no correlation between the dart leader speed and luminous intensity of the dart and little correlation between the luminous intensity of the dart and resulting return stroke speed. Inconclusive results were found for dart leader speed versus return-stoke luminous

intensity as well. Idone, 1984 observed two-dimensional leader and return stroke speeds over the same channel section, to be 1.7 x 10^7 m/s and 1.3 x 10^8 m/s respectively.

Jordan et al. (1992) examined dart leader speeds as a function of the initial electric field peak, of the following return stroke current peak, and of the duration of the previous inter-stroke interval (excluding the duration of continuing currents, if present). For 11 natural lightning strokes in Florida they observed an average leader speed of 1.4 x 10^7 m/s, whereas for 36 triggered lightning strokes in Florida they observed an average leader speed of 1.6 x 10^7 m/s. Jordan (1990) presented the luminosity of dart leaders and return strokes versus height (shown in Figure 2-8) and observed average leader speeds of 1.2 x 10^7 m/sec.

Mach and Rust (1989) used data from a mobile photoelectric device and presented two-dimensional return stroke velocities. Their return stroke velocity device (RSV) consisted of eight levels solid state detectors, each with a 41 degree horizontal view and 0.1 degree vertical field view. The velocity measurements were divided into two groups: "short channel" values with channel segments starting near the ground and less than 500 m in length and "long-channel" that start near the ground and exceed 500 m in length. The average long channel velocity was found to be 1.3 $\pm$ 0.3 x 10^8 m/s for natural return strokes and 1.2 $\pm$ 0.3 x 10^8 m/s for triggered return strokes. In the case of "short-channel" the natural return strokes had an average velocity of 1.9 $\pm$ 0.7 x 10^8 m/s and the triggered return strokes had an average velocity of 1.4 $\pm$ 0.4 x 10^8 m/s. Mach and Rust (1997) reported the velocities, rise-times and other optical measurements of a set of 35 natural and 26 triggered dart leaders. All of the dart leaders were from negative strokes and the data were collected using the same return stroke velocity (RSV) device. The average two-dimensional speed for natural leaders was found to be 1.9 $\pm$ 0.2 x 10^7 m/s, while for the triggered dart leaders, average 2-D speed turned out to be 1.3 $\pm$ 0.1 x 10^7 m/s. Also there was no

significant change in the dart leader 2-D speed with height. The mean 10-90% optical rise time for the dart leaders was 2.6 ± 0.4 microseconds. The optical rise-time for triggered leaders was observed to be 1.4 ± 0.4 microseconds. Mach and Rust (1993) reported the velocities and optical rise-times for seven natural and positive return strokes using the same RSV device. The average 2-D positive return stroke velocity for channel segments of smaller than 500 m in length was 0.8 ± 0.3 x 10^8 m/s which was slower than the corresponding average velocity for natural negative first return stroke, 1.7 ± 0.7 x 10^8 m/s. In the case of long channels, greater than 500 m in length, the average return stroke speed in the case of natural negative first stroke was 1.2 ± 0.6 x 10^8 m/s while it was 0.9 ± 0.4 x 10^8 m/s in the case of positive return strokes. They observed no significant change of velocity for the positive return strokes with height. Further, they observed rise times of 9.4± 3.0 microseconds in the case of positive return strokes and 3.5 ± 1.7 microseconds in the case of negative strokes.

Wang (1999) used a high speed digital optical system, to find the the propagation characteristics of two leader/return stroke sequences in the bottom 400 m of the channel of two lightning flashes triggered at Camp Blanding, Florida. The optical data were acquired using the digital optical imaging system ALPS which consisted of a 256 (16x16) pin photodiodes, each 1.3 x 1.3 mm^2 size, with a separation of 1.5 mm between the centers of individual diodes. Each of the diodes operated at wavelengths from 400 to 1000 nm with response time of less than 3 ns. The time resolution of the measuring system was 100 ns, and the spatial resolution was about 30 m. The leaders exhibited increasing speeds when propagating downwards over the bottom some hundreds of meters, while the return strokes showed a decrease in speed when propagating upwards over the same distance. Propagation speeds and luminosity pulses for two leaders are shown in Figures 2-9 and 2-10. Their finding represents the first experimental evidence that the

luminosity pulses associated with the steps of a downward moving leader propagate upwards with speeds ranging from 1.9 x 10^7 m/se to 1.0 x 10^8 m/s with a mean value of 6.7 x 10^7 m/s. The return stroke speeds within the bottom 60 meters or so of the channel were 1.3 x 10^8 m/s and 1.5 x 10^8 m/s with a potential error of less than 20%.

Olsen et al. (2004) presented the return stroke propagation speeds of five strokes from a seven stroke triggered lightning flash, measured with a 2 ns sampling interval, using a vertical array of photodiodes. Various reference points were used to determine the return stroke speed vs. height for the captured flashes. The EG&G C30807 PIN photodiodes used here were arranged in a vertical array, rated at 5 ns rise-time and 10 ns fall time. Each diode's amplifying circuit had a 10-90% rise-time of about 220 ns. The diodes were arranged in 7 x 1.9 x 30 cm^3 rectangular aluminum enclosure with interior painted matte black and were arranged at varying angles as shown in the Figure 2-12. The overall (7-170 m) return stroke speeds for Flash F0336 and the return stroke speeds versus height are shown in the Tables 2-1 and 2-2 below. There was an interesting trend in the data which concerns the variation in the measured speed in the three channel segments between 7-170 m. Specifically for strokes 2, 4 , 5 and 6 it was observed that the measured speed was the greatest in the segment between 63 and 117 m, slightly lower in the segment between 117 and 170 and lowest in the segment between 7 and 63 m.

2.6 Correlation Between Current and Light

Figure 2-12, adapted from Olsen et al (2006), shows an interesting correlation between the lightning discharge currents and associated optical streak records for the ICV (initial current variation) stage. Panels (a) and (b) show the optical streak film and the channel base current records, respectively for flash F0348 showing two attempted reconnection pulses (ARP1 and ARP2) and a reconnection pulse (RP). The streak record and the current record were manually

aligned. This was done by selecting the point of most rapid increase in optical streak record luminosity at the channel base to be zero time for alignment with the current record.

Idone and Orville (1985) estimated dart-leader peak currents for 22 leaders in two rocket-triggered flashes using two different optical techniques. In method (i), the ratio of the dart-leader and return-stroke currents was taken as equal to the ratio of the dart-leader and return-stroke speeds; this assumes a simple model in which an equal charge per unit length is involved in each process. The speed ratio and the return-stroke current were measured, allowing a calculation of the dart-leader current. In method (ii) the relation between return-stroke peak current I_R and return-stroke peak relative light intensity L_R in each of two flashes ($L_R=1.5I_R^{1.6}$ $L_R=6.4\,I_R^{1.1}$) was applied to the dart-leader relative light intensities in the flash to determine the dart-leader current. The two techniques produced very similar results, a mean current of 1.8 KA for method (ii) and 1.6 KA for method (i). Individual values ranged from 100 A to 6 kA. The ratio of dart-leader to return-stroke current ranged from 0.03 to 0.3 with a mean of 0.17 from method (ii) and 0.16 from method (i). The largest dart-leader to return-stroke current ratios were associated with the largest return-stroke currents and relative light intensities. Idone and Orville (1985) discussed the validity of the techniques used to find dart-leader currents, which, as they stated, are certainly open to question.

Wang et al. (2005) performed a comparative analysis of channel-base current and light waveforms for four different rocket-triggered lightning strokes. Their study supported the idea of evaluating the variation of return-stroke current along the lightning return-stroke channel using light signals, provided the evaluation was limited to the rising portions of those signals and assuming that the light/current relationship observed at the bottom of the channel holds at other heights. It was found that the current and light signals at the bottom of the channel exhibited a

linear relationship (direct proportionality) in their rising portions. However, just after the peaks the linearity disappears, and the light signals usually decrease faster than the currents during the next several microseconds as shown in Figure 2-13. From Figures 2-13 and 2-14, the relation between the current and the light could be divided into four stages. In stage 1 (from t=0 to t=1.3 us), both the current and light increase sharply, and they exhibit a strong linear relationship. In stage 2 (t=1.3 μs to t=7 μs), both the current and light signals decrease, but the decrease in the light signal is much more pronounced than the decrease in the current. In stage 3 (t=7 μs to t=55 μs) the light signal remains at more or less constant level, but the current exhibits a continuing decrease. In stage 4 (after t=55 μs), both current and the light signals show a relatively slow decay.

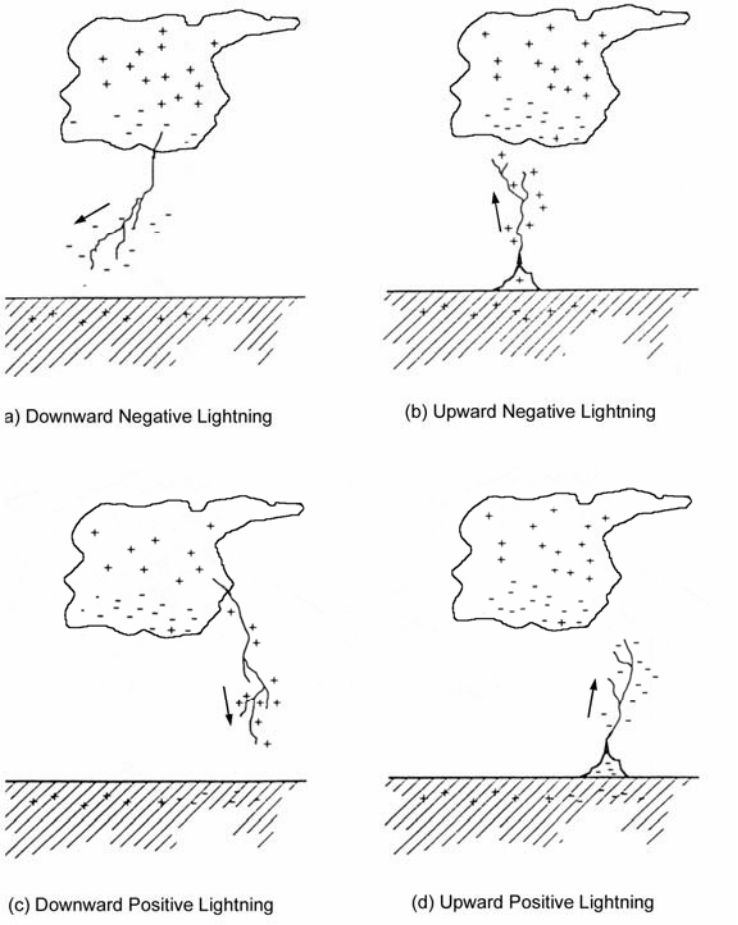

Figure 2-1: The four types of cloud-to-ground flashes. Adapted from Rakov and Uman, 2003.

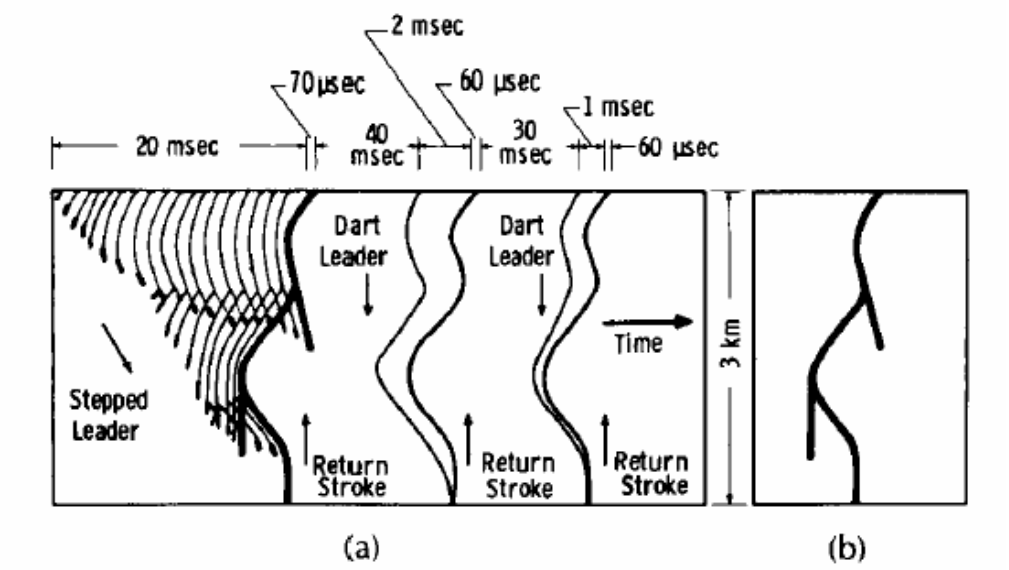

Figure 2-2: The various processes in a single lightning flash. Adapted from Uman (1987).

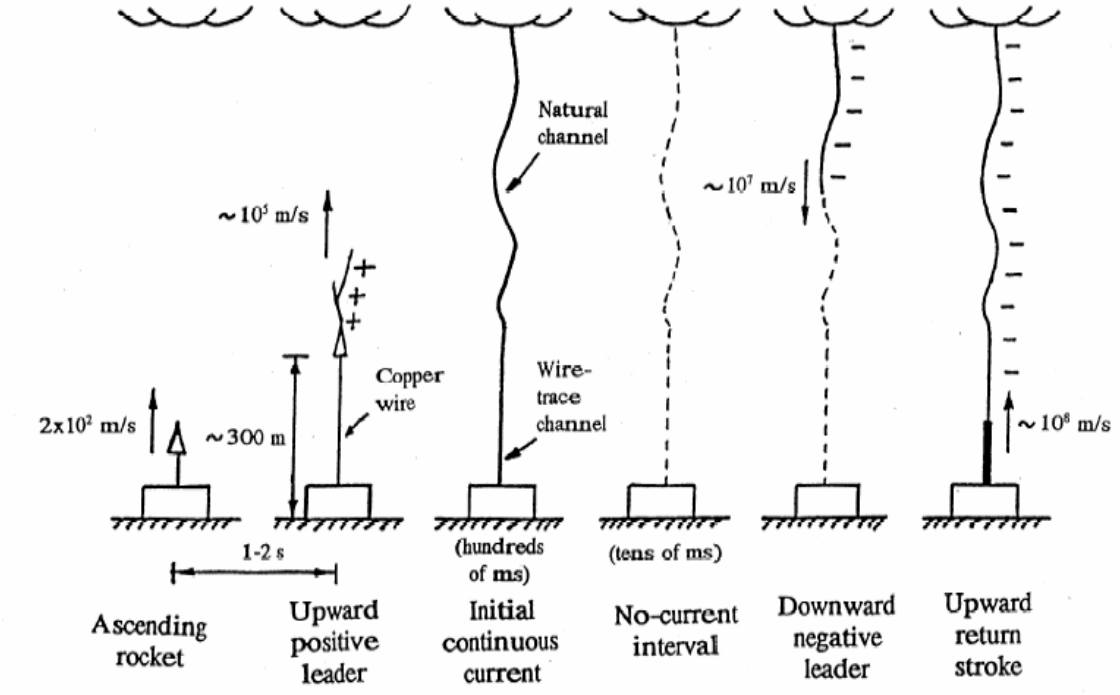

Figure 2-3: The classical rocket-triggered lightning process. Adapted from Rakov et. al. (1998).

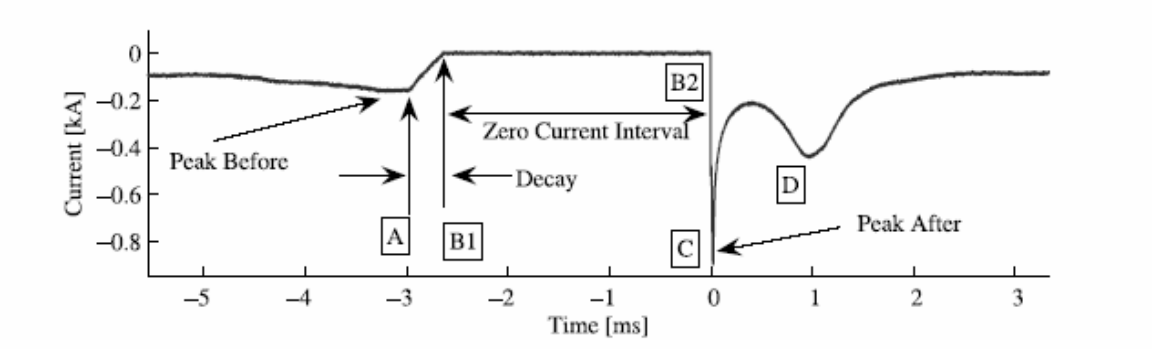

Figure 2-4: The initial current variation stage in rocket triggered lightning. Adapted from Olsen et. al. (2006).

Figure 2-5: Upward lightning initiated from the Eiffel Tower. Photograph taken June 3, 1902, at 9.20 p.m., by M. G. Loppé. Published in the *Bulletin de la Société Astronomique de France* (May, 1905).

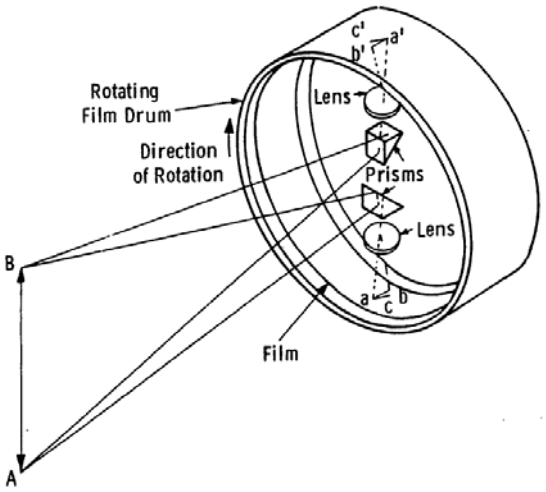

Figure 2-6: Diagram of improved Boys camera with moving film and stationary lenses. Adapted from McEachron (1939).

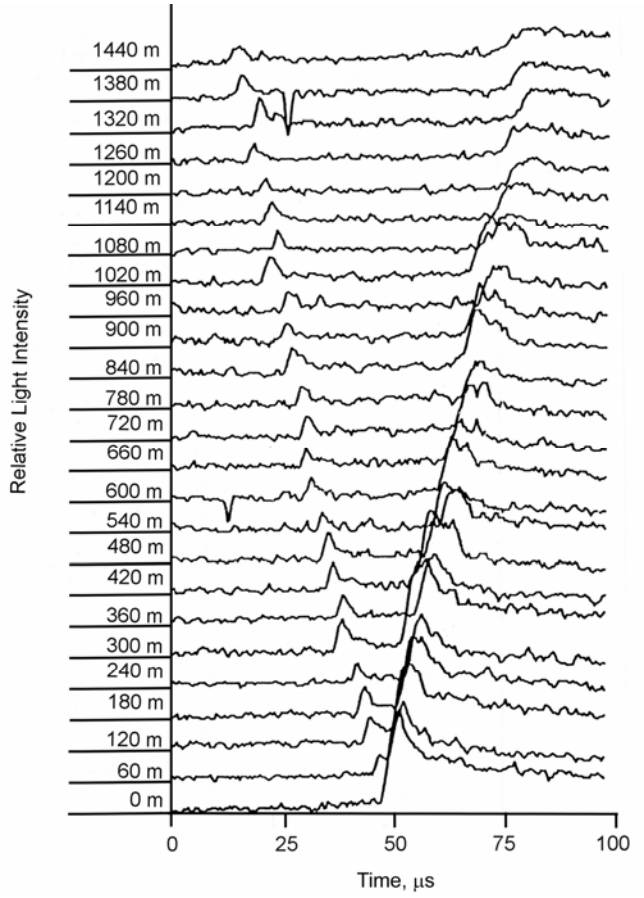

Figure 2-7: Luminosity of dart leaders and return strokes versus time. Adapted from Jordan (1990).

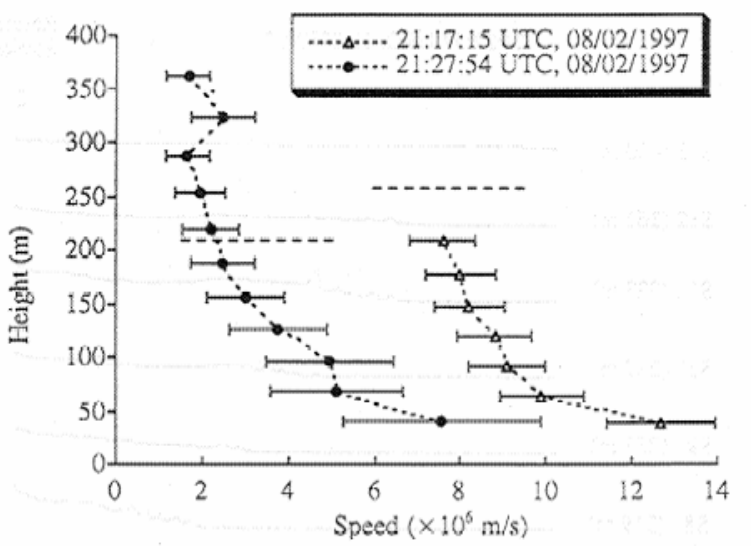

Figure 2-8: Propagation speeds of two leaders analyzed by Wang et al. (1999). The events were triggered on August 2, 1997 (a) 2117:15 UTC and (b) 2127:54 UTC.

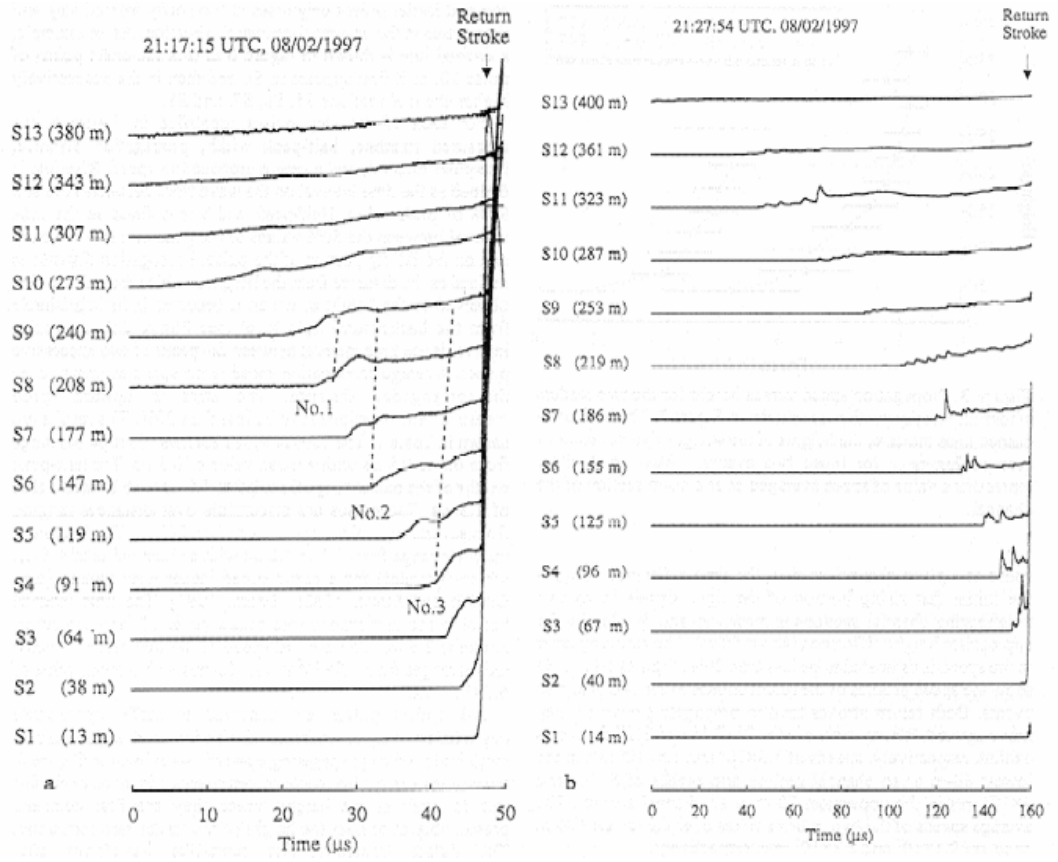

Figure 2-9: Leader light pulses versus time waveforms at different heights above the ground for events triggered on August 2, 1997 at (a) 2117:15 UTC and (b) 2127:54 UTC analyzed by Wang et al. (1999).

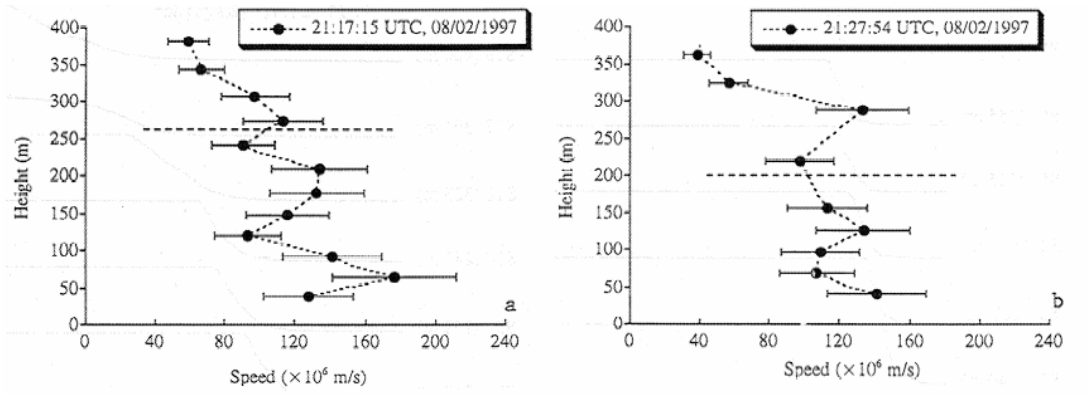

Figure 2-10: The propagation speeds versus heights for two return-strokes. The events were triggered on August 2, 1997 (a) 2117:15 UTC and (b) 2127:54 UTC analyzed by Wang et al. (1999). Each solid circle represents a value of the speed averaged over a 60 m section of the channel.

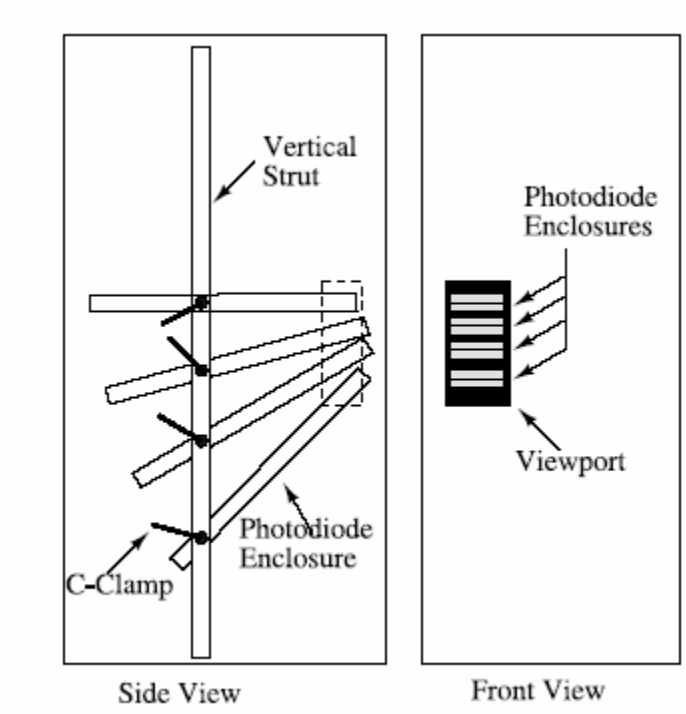

Figure 2-11: The pin photodiode array used by Olsen et al. (2004).

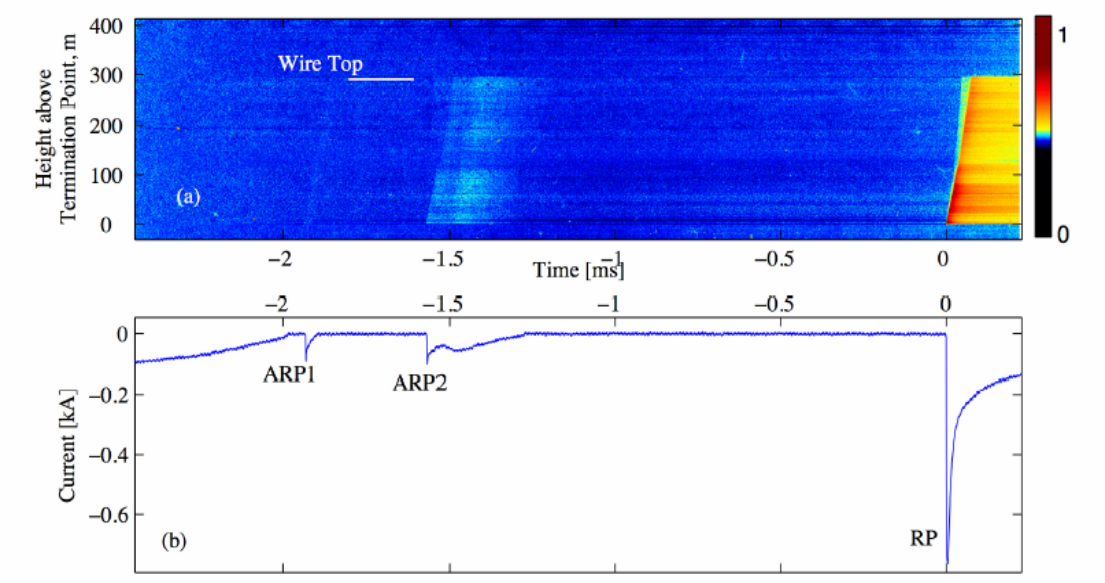

Figure 2-12: Correlation between the lightning discharge current (b) and associated optical streak record (a) for the ICV (initial current variation) stage of rocket-triggered lightning. Adapted from Olsen et al. (2006).

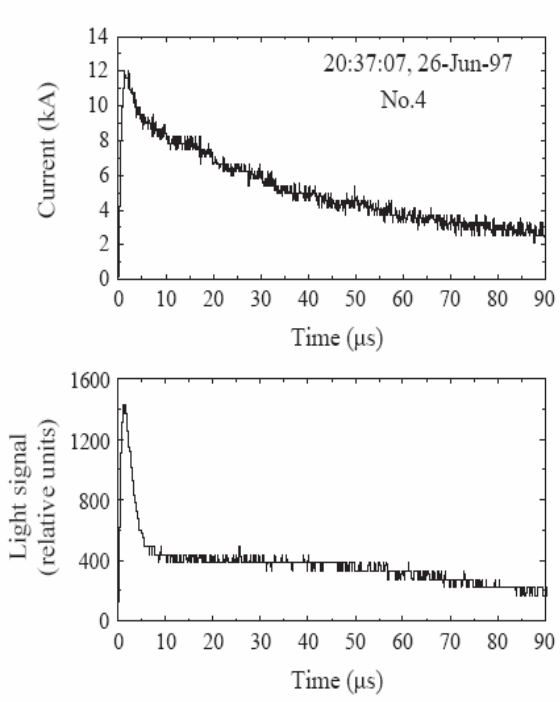

Figure 2-13: Channel-base current and light waveforms of the return-stroke in the flash triggered at 20:37:07, 6/26/1997 (event No. 4) at Camp Blanding, Florida. Adapted from Wang et. al. (2005).

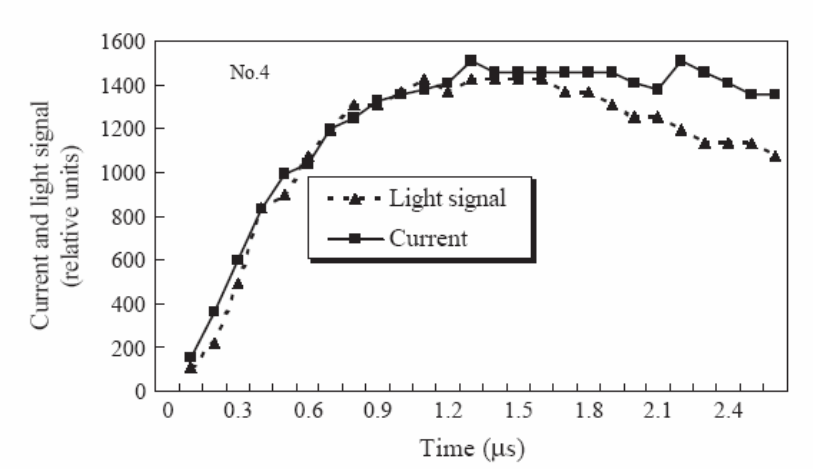

Figure 2-14: Comparison between the current and light waveforms shown in Figure 2-13 for the initial 2.7 microseconds. Adapted from Wang et. al. (2005).

Table 2-1: Overall return stroke speeds for F0336. Adapted from Olsen (2003).

	Stroke Order				
	1	2	4	5	6
Reference Point	Speed, $\times 10^8$ m s^{-1}				
10%[a]	1.98	1.73	1.81	2.21	1.81
20%	1.53	1.36	1.46	1.50	1.41
90%	0.774	0.621	0.653	0.628	0.630
100%	0.579	0.462	0.368	0.449	0.493
Max dL/dt[b]	1.29	1.27	0.609	1.32	1.45
Slope-intercept	2.02	1.81	2.26	2.00	1.78

Table 2-2: Return stroke speed profile versus height for F0336 using the 20% point and the slope point intercept as references. Adapted from Olsen (2003).

Stroke Order	Reference Point	Return Stroke Speed $\times 10^8$ m s^{-1}		
		7 m–63 m	63 m–117 m	117 m–170 m
1	20%	1.34	1.62	1.70
	slope-intercept	1.81	1.99	2.33
2	20%	1.19	1.81	1.22
	slope-intercept	1.94	2.59	1.32
4	20%	1.19	1.83	1.50
	slope-intercept	2.04	2.74	2.13
5	20%	1.24	1.78	1.61
	slope-intercept	2.00	2.36	1.74
6	20%	1.24	1.58	1.47
	slope-intercept	1.94	2.09	1.44

CHAPTER 3
EXPERIMENTAL SETUP

3.1 ICLRT Overview

In this section, an overview of the International Center for Lightning Research and Testing (ICLRT) is presented. The ICLRT is located at Camp Blanding, Florida, at coordinates 29°56' N, 82° 02' W, 8 km east of Starke. It was constructed by Power Technologies under a contract from the Electric Power Research Institute (EPRI) in 1993 to study the effects of lightning on power lines. It has been operated by the University of Florida since 1994. The rocket-and-wire technique (e.g., Rakov et al., 1998) was used to artificially initiate (trigger) lightning from natural thunderclouds. The research facility extends over 1 square kilometer of sand, scrub and young growth forest. Air space over the site is restricted and controlled by the Camp Blanding range control, ensuring no air-borne vehicles are harmed by the rockets used in the experiments performed at ICLRT. A variety of structures have been installed over the years at ICLRT, as summarized below. A schematic of the Camp Blanding research facility is shown in Figure 3-1. The Office Building (OB) contains office space for researchers, a conference room, a machine shop / workshop area, and laboratory space for the operation of experiments and data gathering apparatus. The Launch Control Trailer is a facility which contains experiment control equipment such as rocket launcher control, a computer system for the control of measurement devices; data digitization and storage equipment such as oscilloscopes; and various cameras.

During Summers 2002 and 2003, this was the primary control center for all rocket-launching operations and data collection. The Launch Control Trailer is located near the center of the research facility, to the north side of the Tower Launcher. SATTLIF is a self-contained transportable launch facility built by Sandia National Laboratories for rocket-triggered lightning experiments. It contains rocket launcher control equipment, experiment control equipment, data

storage instrumentation, and various cameras. The SATTLIF control equipment can be used independently of the equipment in the Launch Control trailer.

3.2 Rockets and Launchers

Rockets used at the ICLRT are small, fiberglass, solid-fuel rockets approximately 1 meter in length. The nose cone of the rocket contains a parachute which is released when the motor's fuel is exhausted. A spool of wire is mounted coaxially at the bottom of the rocket. The wire used is copper, has a diameter of 0.2 mm, and is covered in Kevlar for mechanical strength. Total length of wire on the spool is typically 750 m. Vertical velocity of the rocket is designed to be about 100 m/sec to 200 m/sec when the rocket reaches a suitable height for triggering.

As stated above, the Tower Launcher, shown in Figure 3-2, is an 11-m tall wooden tower, located near the center of the ICLRT grounds A platform located immediately below the top level of the tower allows access to camera boxes located on the tower. A rocket launcher consisting of several aluminum tubes is mounted on the top level of the tower. The unit is mounted on fiberglass legs. The top of each tube is about 2 m above the platform atop the tower. Each tube can contain a single rocket. The trailing end of the wire spool is connected mechanically and electrically to the launcher frame. Operators located in the Launch Control Trailer initiate the launch of a rocket by sending a pulse of high pressure air over a pneumatic line. The pulse closes a contact, connecting a battery across the leads of a "squib" igniter placed in the exhaust orifice of the rocket motor. This "squib" ignites the motor and the rocket accelerates out of the tube.

The Bucket Truck Launcher, shown in Figure 3-3, is a transportable launching facility. Six aluminum rocket launcher tubes, about 3 meters long, are mounted in the bucket at the end of the articulated arm on a truck formerly used for power line maintenance. A pneumatic trigger assembly similar to that employed on the Tower Launcher is used on the truck launcher as well.

In this case, however, the initiating high pressure air pulse is released from a high pressure air tank mounted on the truck, and is initiated via computer control over a wireless radiofrequency data link between the Launch Control Trailer and the Bucket Truck Launcher. The height of the launcher above ground can be varied using the hydraulic power of the articulated arm. A Hoffman box containing a current viewing resistor (CVR) and fiber-optic transmitter apparatus is mounted next to the rocket tubes. The trailing wires are grounded to the aluminum launcher tubes, which are in turn connected to the CVR with 2 cm copper braid. The other end of the CVR is connected via copper braid to ground rods at the rear of the truck. Typically, three to four ground rods are driven into the ground at each new location for the Bucket Truck Launcher.

3.3 The BIFO K004M Image Converter Camera

The attachment process in lightning [Rakov and Uman 2003] is a very difficult process to image. The process is very fast, occurs in a small volume, and is much less luminous than the processes which immediately follow it. Some success has been made using Image Converter cameras to image the attachment process in long sparks, which are thought to be similar in nature to lightning discharges. The advantages of an image converter camera include very high recording rates, immediate view ability of captured images, and very high sensitivity to light.

The K004M image converter camera made by BIFO Company in Moscow, Russia, specifically for studying the attachment process in rocket-triggered lightning was deployed during Summer 2003 and Summer 2005 at Camp Blanding and in 2006 at the University of Florida Campus (2006 cupola experiments). The camera is capable of operating in framing mode or in streak mode.

In streak mode, the camera can operate at a recording rate from 0.1 μs/cm to ms/cm over the 3.55 cm wide rear phosphor readout. The fastest recording rate, 0.1 μs/cm, corresponds to temporal resolution of about 1 ns. In framing mode, the camera can collect 1, 2, 4, 6, or 9 images

consecutively. Frame duration is adjustable from 0.1 μs to 10 μs, and inter-frame interval is adjustable from 0.5 μs to 999.9 μs. The consecutive frames are arrayed across the readout screen in a pattern shown in Figure 3-4.

An objective lens is used to construct an image upon the photocathode marked as 3_1 in Figure 3-5. The photocathode converts the optical image to an electronic image. The electronic image passes through an electronics focussing lens and is constructed upon the micro-channel plate 1 (MCP1), designated as 3_8 in Figure 3-5. MCP1 and MCP 2 intensify the image and project it onto a phosphor screen (3_9 in Figure 3-5) which converts the electronic image into a luminous image. A video camera attached to the rear of the K004M reads the image and sends the video signal to a PC which digitizes the signal and stores it. The shut pulse generator enables or disables the passage of images from the photocathode to the MCP's. The sweep generator controls the position of the image on the MCP's, which effectively controls the position of the image on the phosphor screen. The sweep generator is the mechanism by which consecutive frames are arrayed on the rear phosphor in multi-framing mode and the mechanism by which the image is swept across the phosphor in streak mode.

The camera is triggered by a two-channel photosensor (PS-001), also manufactured by BIFO. One channel is used to initiate the exposure and the other channel engages a gain reduction circuit which reduces the gain of the second MCP. The trigger threshold on each channel is adjustable. Each channel of the PS-001 includes an adjustable slit for limiting the viewable area, both in terms of altitude and width. This allows for high optical gain during the early stages of the attachment process, and then when the return stroke is initiated the gain should be reduced to avoid saturation. Initial testing of the K004M showed that operation was as

specified. Several images of sparks were obtained in every mode of operation. Additionally, images were obtained for 5 to 30 mm long sparks.

As stated above, the unit was tested, along with other image converter cameras, using long (up to 6 m) sparks at the high-voltage facility in Istra, Russia. The performance was good. However, the unit did not operate properly during Summer 2003 when it was moved to Camp Blanding for triggered lightning experiments. Internal arcing was observed, which required repair procedures. After these had been corrected, false triggering of the unit was observed. Finally, the K004M failed to power up at all. Dr. Vitali Lebedev of BIFO Company came to Gainesville and repaired the K004M in September of 2003. After the repair was completed, the camera was set up in a cupola atop the Engineering Building on the campus of the University of Florida in Gainesville. A large, active thunderstorm passed through the area and several nearby lightning flashes were observed. Under the direction of Dr. Lebedev, the camera was operated during this storm. Several flashes triggered the camera and were recorded. None of these images contained features which could be identified. Two images were captured with the K004M during the summer 2003. During the camera's functional period an insufficient number of events occurred to allow proper calibration of the camera for capturing processes of interest.

The BIFO K004M trigger circuit was designed by the author in Fall 2007. The PS001 which was initially employed for triggering the BIFO K004M camera was found to be insufficiently sensitive to luminosity of leader channels. The PS001 has a highly complex schematic and so modifying the internal circuitary to achieve leader triggering was a non-trivial task. This was the motivation behind prototyping a simple triggering circuit that would allow full control over the triggering light levels. The triggering levels can be changed suitably to make either leader or return-stroke as K004M trigger.

This newly-developed trigger circuit is shown in Figures 3.6 and 3.7. Two avalanche photodiode circuits are employed to get correlated triggers based on either the leader or the return-stroke optical intensity in the lightning channel. The avalanche photodiode circuits were designed and manufactured by Rob Olsen. They were employed during summer 2005 at Camp Blanding and in 2006 at the University of Florida for the characterization of lightning strokes. This circuit is described in detail in section 3.4. Each sensor input channels is then compared to two reference voltage levels (V_{ref1} and V_{ref2}) via an AD8564, a high speed quad comparator with a propagation delay of 7 ns. V_{ref1} corresponds to a voltage reference level to expected to be exceeded by a leader optical pulse, whereas V_{ref2} corresponds to a voltage reference expected to be exceeded by a return-stroke optical pulse. A facility has been provided to vary the levels of V_{ref1} and V_{ref2} by the means of an on chip surface mount variable potentiometer. When both the sensors observe the same leader optical pulse, voltage on both the input channels is above the leader reference voltage levels (V_{ref1}). This produces a voltage pulse of approximately 3-4 volts at the output of both the comparators, corresponding to V_{ref1} as the reference voltage level. These two voltage pulses at the comparator output corresponding to a leader (leader trigger) are then combined by means of 74LS00, a quad NAND logic gate (a NAND gate produces a low output when all the inputs are high). The NAND gate produces a low output signal. This low output signal is then inverted by employing another NAND gate, configured as an inverter, thus producing a relatively high voltage pulse (approximately 3-4 V) at the output. This output is then connected to the K004M trigger channels via a line driver octal buffer SCT25244 to avoid loading the NAND gate by an output stage. The same process repeats if the sensors detect a return-stroke. In this case, the comparators corresponding to V_{ref2} (the voltage reference level expected to be exceeded when a return-stroke is observed by the sensors) provide the outputs for

the NAND gate and the line driver, which can then be used to trigger the gain reduction channel of the K004M camera.

3.4 The Photodiode Array

A vertical array of 9 avalanche photodiode optical detectors designed and manufactured by Rob Olsen was employed during summer 2005 at Camp Blanding and in 2006 at the University of Florida for the characterization of lightning strokes. Each photo-diode was mounted in a rectangular aluminum tube whose interiors were painted matte black to prevent reflections. The inner cross-section dimensions of the tubes were measured to be 2.75 wide and 0.75 in tall. Each tube was 1 m in length.

All photodiodes were the C30737 type avalanche photodiodes that have high responsivity between 400 nm and 1000 nm with a response time of 300 ps at all wavelengths with a frequency response of up to 1.2 GHz. They have 0.5 mm active diameter, a breakdown voltage of 160 volts, and very low noise floor of 0.2 pA/$\sqrt{Hz}$ **.** Signals from photodiodes were relayed to the oscilloscope via an active amplifier whose circuit diagram is shown in Figure 3-8.

The active circuit was designed and manufactured by Rob Olsen around a high-speed operational amplifier AD8066, configured in transimpedance mode. The impedance seen by the photodiode was thus very close to zero thus moving the high frequency roll off higher in frequency, and improved the risetime of the circuit. The first amplifier stage was set in the inverting mode, therefore a second inverting gain stage was provided to restore the correct waveform polarity. A 50 Ω resistor was placed in series with the output for impedance matching with the co-axial cable and to provide the op amp with a higher load. On July 2, 2005, the response of the actively coupled photodiode circuit was found, using a General Radio Strobotac as the signal source, to be on the order of 600 ns.

Nine slit and tube assemblies were mounted in a shielded aluminum rack. The end of each tube with the slit end cap was bolted to a frame which allowed the tube to rotate about a horizontal axis roughly congruent with the slit itself. The nine tubes were arrayed vertically. The uppermost tube was aimed nearly horizontally, with successively lower tube aimed higher as shown in Figure 3-12. This resulted in all nine slits being very close and reduced the size of the hole that had to be cut in the cabinet to allow light to enter. An additional vertical strut was mounted in the rack and each tube was clamped to the strut using standard C-clamps. One meter RG-223 cables with BNC connectors on both ends were used to connect the photodiode outputs to the oscilloscope input channels. The breakdown (Avalanche breakdown is a current multiplication process that occurs only in strong electric field. The breakdown voltage, is the voltage that creates this high electric field across the in the photodiodes.) voltages for each of the photodiode assemblies was supplied by a high voltage supply unit. The entire oscilloscopes, power supply unit, and photodiode array assembly was thus enclosed in a shielded enclosure and isolated from radiated and conducted interferences. The aluminum tubes provided a second layer of shielding for the very sensitive photodiode and preamplifier section.

3.5 The Photodiode Experimental Setup used in 2005 and 2006

The experimental setup that was used for the capture of the Summer 2005 data is is shown in Figure 3-9. The same experimental setup was used for summer 2006 lightning captures at University of Florida. The Avalanche Photo Diodes were arranged such that APD 1 looked at the lower channel height and the highest part of the channel was seen by APD 9. These were then assigned to the Yokogawa as well as the LeCroy digital oscilloscopes using appropriate terminations.

Table 3-1 shown below summarizes the angles that each of the APDs was set to along with the respective channel heights seen by them. Initially, the rockets were launched from the

Bucket launcher (July 2nd). In this case the experimental setup was at distance of 706 meters from the lightning channel. Starting from July 13th onwards, the rockets were launched from the Tower. In this case the experimental setup was at a distance of 476 meters from the lightning channel.

In summer 2006 the APDs were setup at the same viewing angles. But since the distance to channel termination is unknown the actual heights viewed by each sensor from the photodiode array are unknown.

As stated previously, the BIFO K004M was used to record natural lightning events in summer of 2006 at University of Florida. Figure 3-10 shows the setup used for the PS001 photosensor and the BIFO K004M image converter camera (ICC). A metal frame with a flat surface on top was used in such a way that it was possible to mount the photosensor on top of the ICC. This is because the photosensor was responsible for triggering the BIFO, which would then record the event in streak mode. The photosensor and ICC setup (shown in Figure 3-10) was mounted on a wooden tripod with wheels. This made the heavy apparatus sufficiently mobile in the event that the pointing direction needed to be changed depending on the location of the thunderstorm.

Figure 3-11 shows the complete setup along with the photodiode array and the oscilloscopes. The LeCroys (scopes 16 and 6 in Figure 3-11) and Yokogawa (scope 7 in Figure 3-11) were mounted securely in a rack. The avalanche photodiodes were fixed onto this rack in such a way that the lowermost channel height viewed was just above the tree line. The photosensor and BIFO were also adjusted to view above the tree line. Figure 3-12 shows the avalanche photodiode array that was fixed behind the oscilloscope rack. Inter-scope delays were

computed for the following scope pairs: Scope 16 –Scope 6, Scope 6 –Scope 17 and Scope 16-Scope 17. These delays are presented in Table 3-2.

3.6 Modified Return-Stroke Speed Equation

In the summer 2005 experimental setup block diagram, shown in Figure 3-9, the LeCroy Scope-16 was used to trigger the LeCroy Scope 6 which would then trigger the LeCroy Scope 17. The oscilloscopes had their own internal finite time delays which resulted in an inter-scope delay when one scope was used to trigger another. It is therefore imperative to find time delays between scopes and include them in the return-stroke speed calculations along the channel for each of the rocket-triggered lightning event from summer 2005. For such a calibration, the photodiode array, shown in Figure 3-12, was exposed to rapid flashes produced by a strobe light. These flashes were recorded on the LeCroy DSOs via the array of photodiode sensors in the form of pulses. Figure 3-13 shows an example of the calibration pulses recorded by LeCroy Scope 16 and LeCroy Scope 17. As seen in this Figure, there is a difference in amplitude as well as time delay between these two waveforms. These waveforms were then filtered using a 11 ns window moving average filter, amplitude-scaled and shifted to find the best possible time delay between them. Automatic Matlab sub-routines were built for the above processing. The resulting shifted and processed waveforms are shown in Figure 3-14. The time delay between LeCroy Scope 16 and LeCroy Scope 17 for CAL001, Stroke 2 was found to be 78 nanoseconds. The time delays between the other LeCroy DSOs have been similarly computed using CAL001 and CAL002 date sets and are summarized in Table 3-2.

Accordingly, the new formula (modified relative to that used by Olsen et al. (2004) to account for interscope delays) for the return-stroke speed calculation is given as follows:

$$v_{RS} = \frac{h_2 - h_1}{t_2 - t_1 - \Delta t - \Phi t}$$

Δt = *Time Correction*
Φt = *Time Delay Between Scopes*
t_2 = *Higher Channel Time*
t_1 = *Lower Channel Time*
$h_2 - h_1$ = *Height Difference Between the two Channels*

The above formula states that for each set of times, the return-stroke speeds, v_{RS}, were calculated by dividing the vertical distance between adjacent viewed heights, h_2 - h_1, by the time interval, t_2 - t_1 (obtained, using techniques explained in chapter 5). Assuming a vertical channel, the light signal propagation path from the uppermost segment of the channel was some 133 m (433 nanoseconds) longer than the propagation path from the lowermost segment before July 2, 2005 and some 80 m (266 nanoseconds) longer than the propagation path from the lowermost segment after July 12, 2005. When measuring the time of arrival of the waveform, this time correction factor, Δt, has to be accounted for in the return-stroke speed equation. Also, Φt, the time delay between the LeCroy DSOs (explained in the previous paragraph), has been introduced into the return-stroke speed equation.

There are three primary sources of measurement error: angle error, distance error, and timing error [Olsen et al., 2004]. The angle error is due primarily to potential inaccuracy in the measurement of the angle of the photodiode assembly relative to the ground and is expected to be less than 0.35˚ which results in a height interval error of less than 15%. The distance error is a function of the accuracy of the GPS measurement made at the observation point and the lightning channel termination point, and is estimated to be no greater than ±10 m, or less than 3%. Finally the error in the time intervals due to inaccuracy of the reference point, whether using the "slope-intercept" method or the "percentage of peak" method, as explained in chapter 5, is estimated to be about 25 nanoseconds. As these speed errors are uncorrelated, the total speed error for each segment may be taken as the square root of the sum of squares of the three

individual error components. This results in a speed error of less than 20% for all lightning segments along the return-stroke channel for the summer 2005 data.

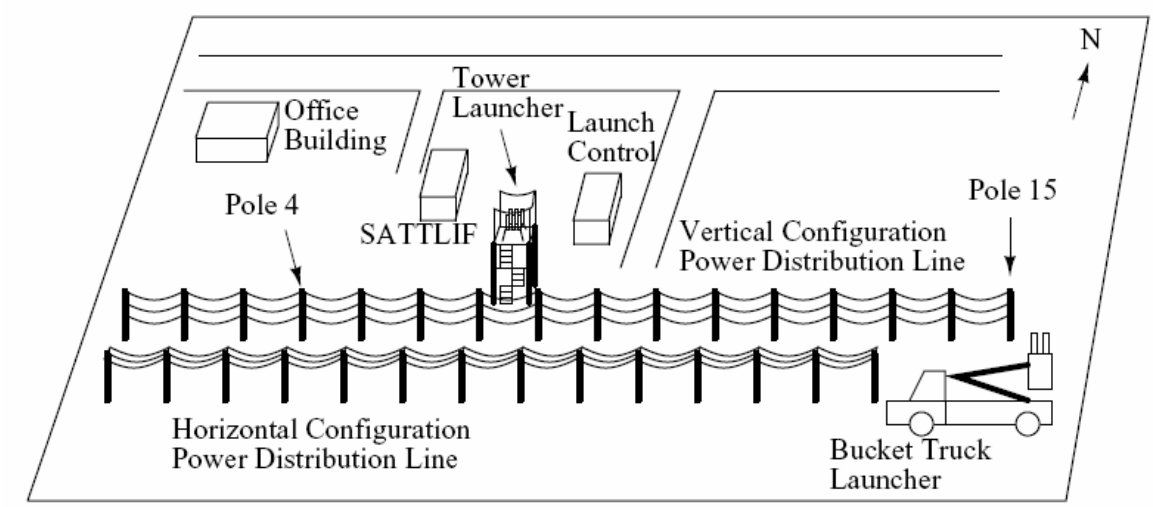

Figure 3-1: Overview of the ICLRT. Adapted from Olsen (2003)

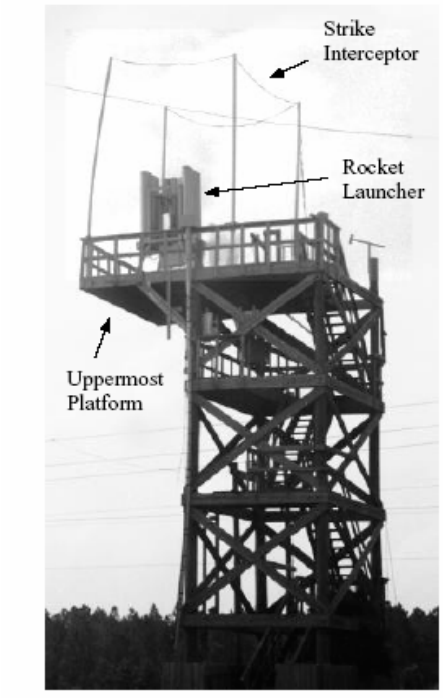

Figure 3-2: Tower launcher

Figure 3-3: Bucket truck launcher at ICLRT

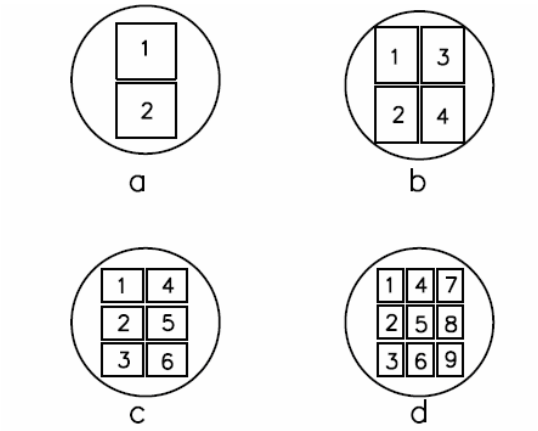

Figure 3-4: The K004M Multi-Framing Mode Display Patterns (a) 2-frame mode.(b) 4-frame mode. (c) 6-frame mode. (d) 9-frame mode.

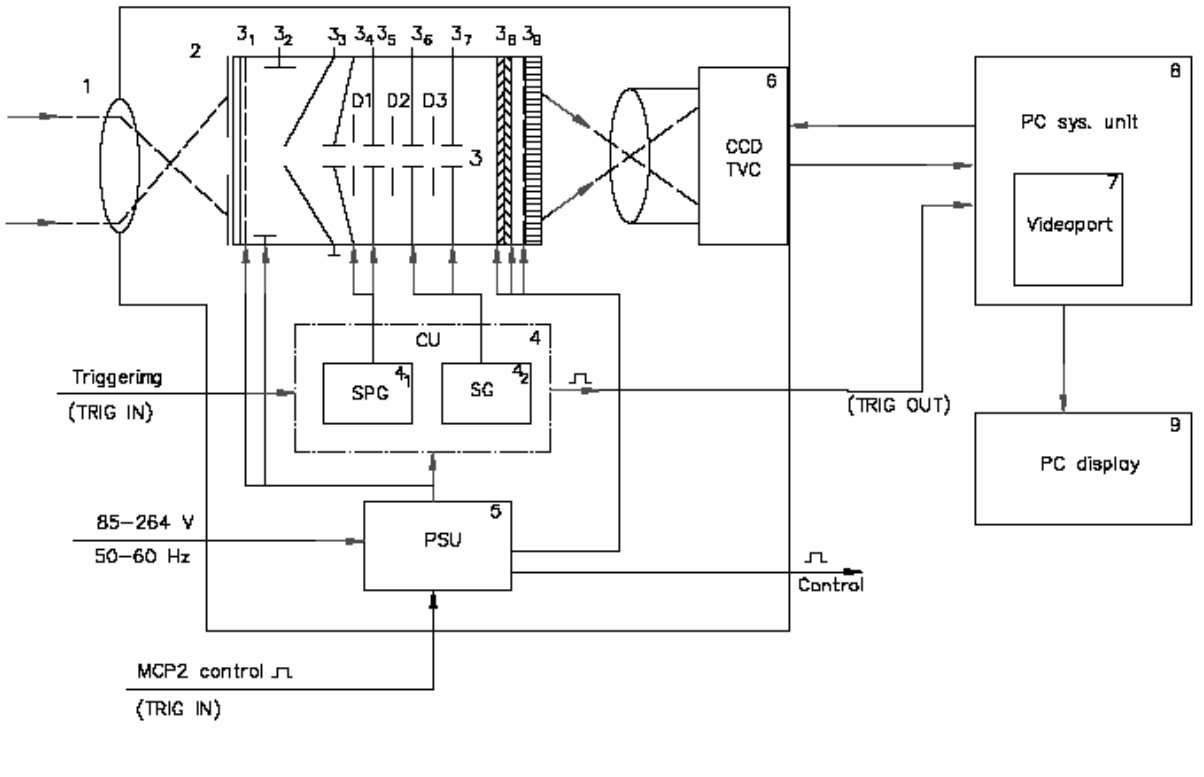

Figure 3-5: The BIFO K004M Image Converter Camera (ICC) –Block Diagram. 1. Input Objective Lens; 2. Slit, Frame Window or Test – object; 3. ICT (3_1 –Photocathode; 3_2 – Focusing Electrode; 3_3 – Anode; 3_4 ,3_5 – Shutter Plates; 3_6 , 3_7 – Deflection Plates; D1-D3 – Shielding Diaphragms; 3_8 – Two MCPs; 3_9 – Luminescent Screen); 4 – CU (4_1 – Shut Pulse Generator; 4_2 – Sweep Genetrator); 5 – Power Supply Unit; 6 – CCD TV camera; 7 – Video Port; 8 – PC System Unit; 9 – PC Display. Adapted from K004M Documentation , BIFO Company (2002).

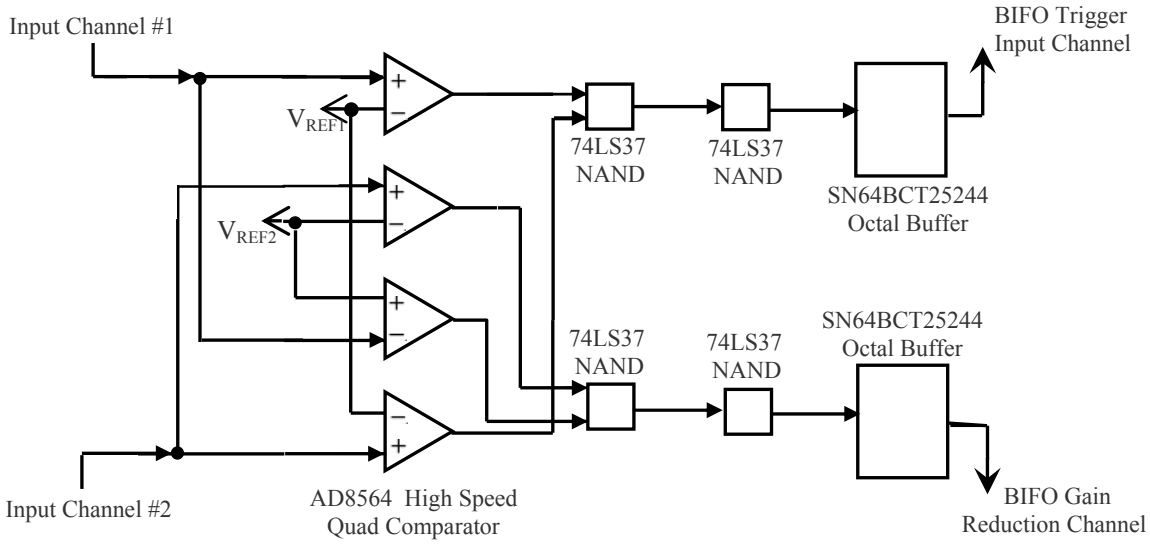

Figure 3-6: The BIFO K004M trigger circuit.

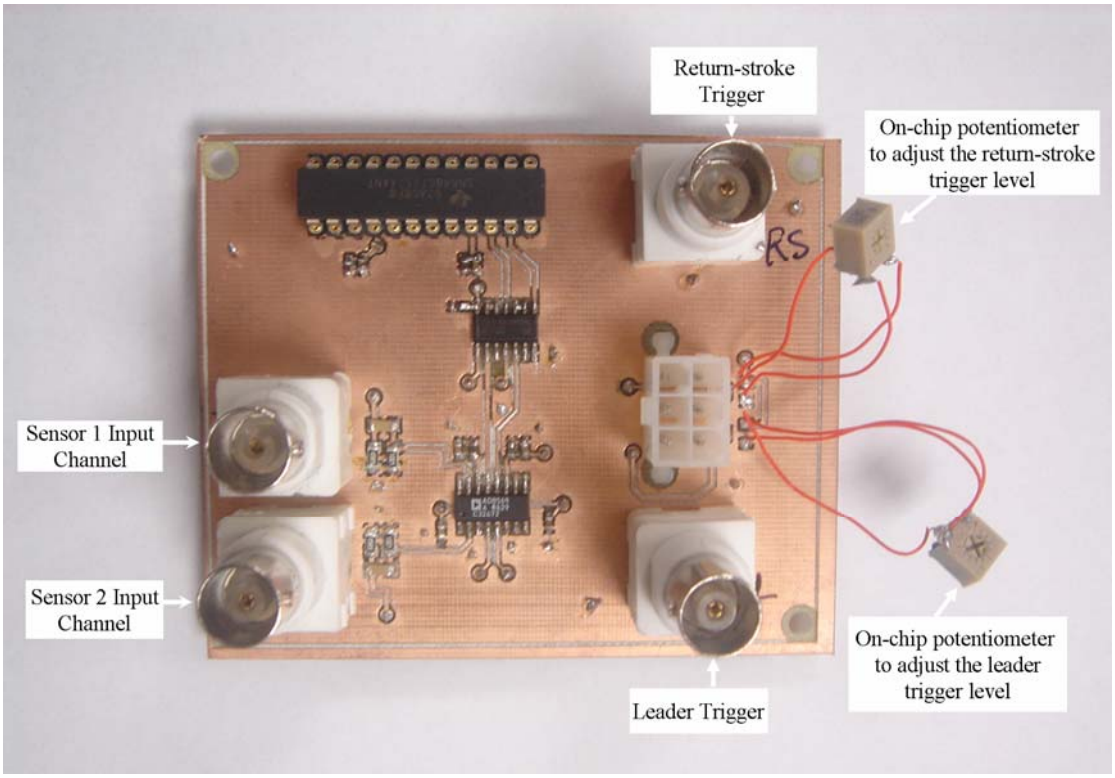

Figure 3-7: The BIFO K004M trigger circuit printed circuit board (PCB). Two avalanche photodiode circuits can be connected to the two BNC connectors on the left hand side of the PCB. The two BNC connectors on the right hand side represent the correlated leader and return-stroke triggers respectively. Also, seen are two potentiometers that can be used to adjust the leader and return-stroke trigger levels. The rest of the PCB components and the general circuit operation are described in section 3.3.1.

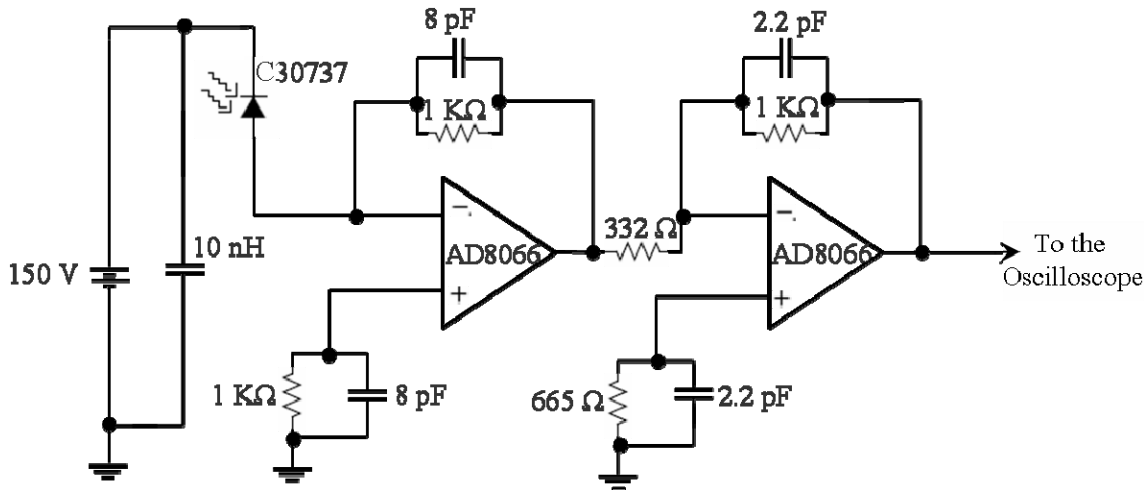

Figure 3-8: Actively-coupled photodiode circuit used during the summer 2005 Camp Blanding experiments as well as in the 2006 University of Florida experiments.

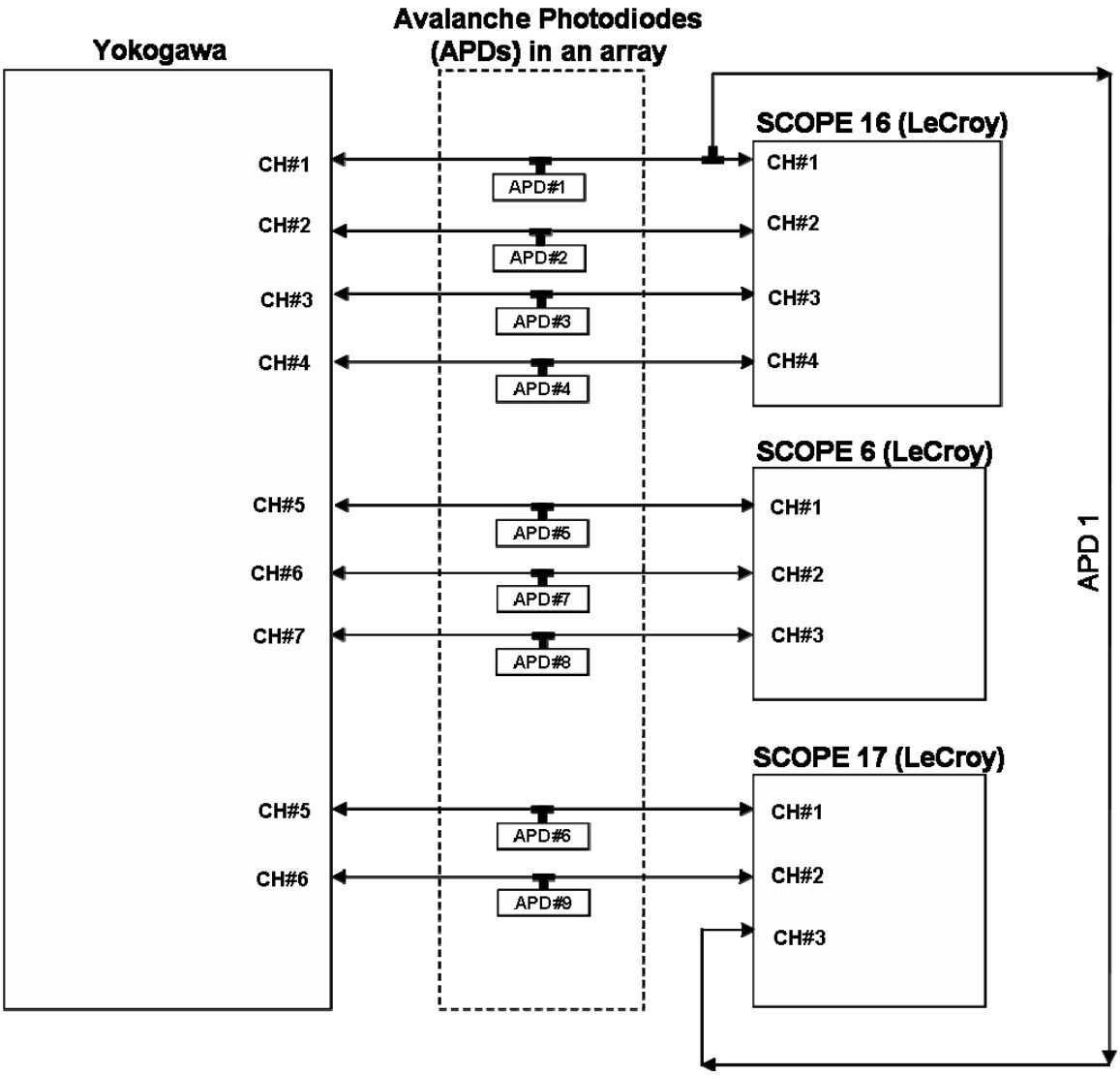

Figure 3-9: Block diagram of the 2005 Camp Blanding and 2006 University of Florida experiments. (APD= Avalanche Photodiode).

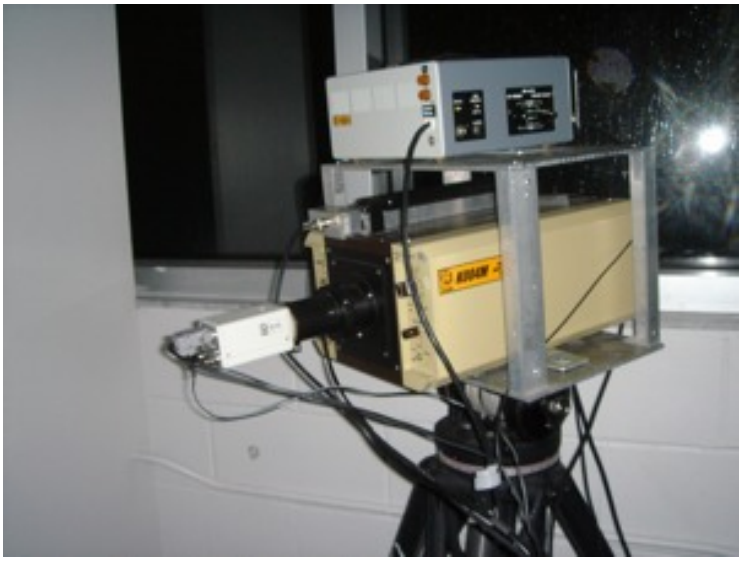

Figure 3-10: The BIFO K004M and PS001 photosensor setup used in the summer 2006 cupola lightning experiments.

Figure 3-11: Complete experimental setup used during the summer 2006 experiments. Shown in the figure are the LeCroy and the Yokogawa oscilloscopes mounted into a rack. The avalanche photo diodes (not visible in this image) were fixed behind this rack. The BIFO K004M camera and photosensor setup was placed near the rack in such a way that the photodiode array and the BIFO were focused at the same point.

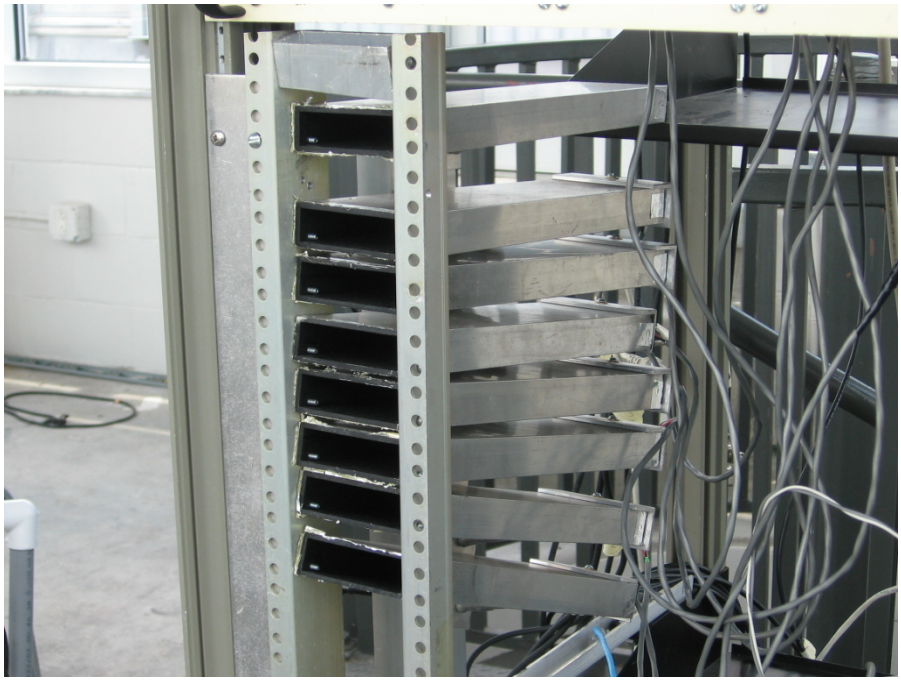

Figure 3-12: The Avalanche Photodiode (APD) array attached on the back side of the oscilloscope rack shown in Figure 3-10 and used for the summer 2005, rocket-triggered and summer 2006, natural lightning experiments. The angles viewed by the sensors are given in Table 3-1.

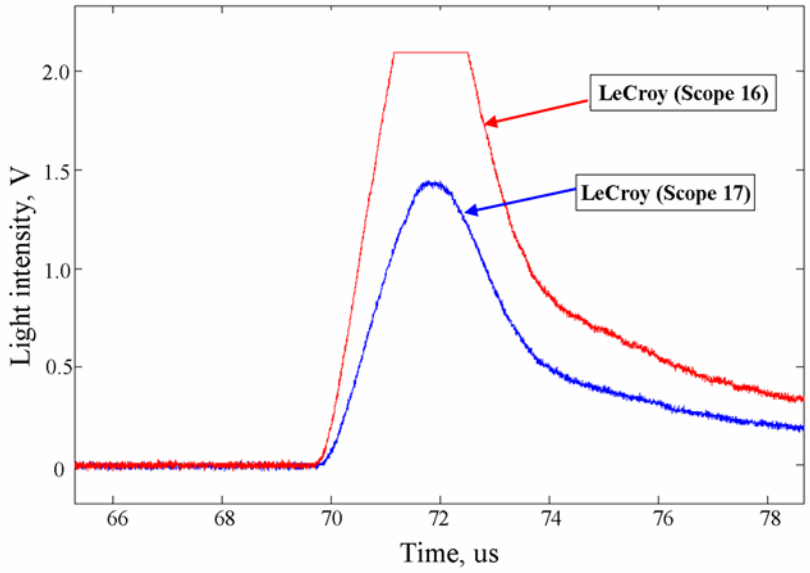

Figure 3-13: Calibration waveforms (CAL001, Stroke 2) recorded on the LeCroy DSOs mounted on the rack shown in Figure 3-10 in summer 2005. There is a delay between the waveforms even though they were simultaneously captured by the avalanche photodiode array. This is termed time delay between scopes (Φt) and is included in the return-stroke speed calculation formula.

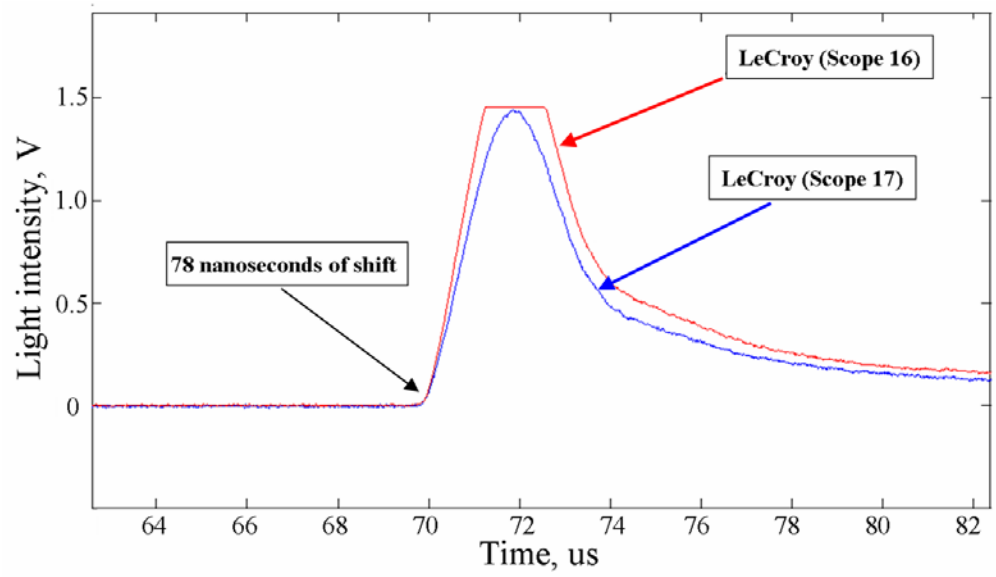

Figure 3-14: Calibration waveforms (CAL001, Stroke 2) shown in Figure 3-12 but filtered, amplitude scaled, and shifted using Matlab sub-routines until the best possible coincidence was achieved. This time shift is the time delay between scopes (Φt) which is included in the return-stroke speed calculation formula.

Table 3-1: The ICLRT Summer 2005 avalanche photodiode array angles and viewed heights along the lightning channel.

APDs	Angles (Degrees)	Viewed Channel Heights (July 2nd 2005 to July 12th)	Viewed Channel Heights (July 13th 2005 Onwards)
1	1.3	16	11
2	3.6	44	30
3	6.8	84	57
4	9.3	116	78
5	13.6	171	115
6	19.1	245	165
7	24.0	314	212
8	27.0	360	243

Table 3-2: Interscope delay or "Time Delay Between Scopes" (Φt) between the LeCroy DSOs estimated using the Summer 2005 calibration data..

LeCroy DSO	Delay, ns
Scope 16 – Scope 17	62
Scope 16 – Scope 6	69
Scope 6 – Scope 17	11

CHAPTER 4
DATA PRESENTATION

Optical records for 31 lightning flashes were obtained in Summer 2005. Of these 31, 8 were triggered lightning and the remaining 23 were natural lightning. The natural lightning optical records are listed in Table 4-1. A listing of all triggered lightning optical records is given in Table 4-2.

4.1 Triggered Lightning Events

4.1.1 Event F0501

Event F0501 was triggered on July 2, 2005 at 23:22:46 UTC. The triggering rocket was launched from the mobile launcher which was 706 m away from the photodiode array. Such a distance was chosen to maximize the viewable height of the channel for the photodiodes.

Figure 4-1 shows the optical waveforms captured on the photodiode array at different heights along the lightning channel on the LeCroy Digital Oscilloscopes. One stroke was observed for this event on the photodiode array. The angles of the individual tubes in the photodiode array relative to the horizontal along with the corresponding channel height viewed by each sensor are given in Table 4-3. The approximate vertical length of lightning channel imaged by each sensor was 1 m. The LeCroy's have sampling rate of 500 MHz (that is, a time interval of 2 nanoseconds between adjacent data points).

Figure 4-2 shows the optical waveforms captured by the photodiode array on the Yokogawa oscilloscope. The Yokogawa has a sampling rate of 10 MHz (that is, a time interval of 100 nanoseconds between adjacent data points). The smallest channel height seen by the photodiode array for this event was on the order of 30 meters (between sensors 3 and 4), that is, a time interval of 100 nanoseconds assuming the speed of propagation of light (3×10^8 m/s). Typical rise times for lightning events are on the order of microseconds, and hence the

Yokogawa waveforms have at least ten to fifteen points on the rising portion of return-stroke waveform. So, even though the rising portion of the waveforms have fewer points as compared to the waveforms captured on the LeCroy's, the Yokogawa data are also suitable for data analysis.

4.1.2 Event F0503

Event F0503 was triggered on July 2, 2005 at 23:37:27 UTC. The triggering rocket was launched from the mobile launcher which was 706 m away from the photodiode array. Such a distance was chosen to maximize the viewable height of the channel for the photodiodes.

Figures 4-3, 4-4, 4-5 and 4-6 show the optical waveforms captured by the photodiode array at on the LeCroy Digital Oscilloscopes for all four return-strokes. Four strokes were observed for this event on the photodiode array. The angles of the individual tubes in the photodiode array relative to the horizontal along with the corresponding channel height viewed by each sensor are given in Table 4-3. The approximate vertical length of lightning channel imaged by each sensor was 1 m. The LeCroys have sampling rate of 500 MHz (that is, a time interval of 2 nanoseconds between adjacent data points).

Figures 4-7, 4-8, 4-9 and 4-10 show the optical waveforms captured by the photodiodes on the Yokogawa oscilloscope. The Yokogawa has a sampling rate of 10 MHz (that is, a time interval of 100 nanoseconds between adjacent data points). The smallest channel height seen by the photodiode array for this event was on the order of 30 meters (between sensors 3 and 4), that is, a time interval of 100 nanoseconds assuming the speed of propagation of light ($3x10^8$ m/s). Typical rise-times for lightning events are on the order of micro seconds, and hence the Yokogawa waveforms have at least ten to fifteen points on the rising portion of return-stroke. So, even though the rising portion of the waveforms have fewer points as compared to the waveforms captured on the LeCroy's, the Yokogawa data are also suitable for data analysis.

4.1.3 Event F0510

Event F0510 was triggered on July 31, 2005 at 20:03:33 UTC. The triggering rocket was launched from the tower launcher which was 476 m away from the photodiode array. Such a distance was chosen to maximize the viewable height of the channel for the photodiodes. The photodiode array was operated during this event.

One stroke was observed for this event on the photodiode array. Figure 4-11 shows the optical waveforms at various channel heights, captured by the photodiode array on the LeCroy Digital Oscilloscopes. The angles of the individual tubes in the photodiode array relative to the horizontal along with the corresponding channel height viewed by each sensor are shown in Table 4-4. The approximate vertical length of lightning channel imaged by each sensor was 1 m. There were no records on the Yokogawa oscilloscope for this particular triggered-lightning event.

4.1.4 Event F0512

Event F0512 was triggered on July 31, 2005 at 20:14:47 UTC. The triggering rocket was launched from the tower launcher which was 476 m away from the photodiode array. Such a distance was chosen to maximize the viewable height of the channel for the photodiodes. The photodiode array was operated during this event.

One stroke was observed for this event on the photodiode array. Figure 4-12 shows the optical waveforms at various channel heights, captured by the photodiode array on the LeCroy Digital Oscilloscopes. The angles of the individual tubes in the photodiode array relative to the horizontal along with the corresponding channel height viewed by each sensor are shown in Table 4-4. The approximate vertical length of lightning channel imaged by each sensor was 1 m. There were no records on the Yokogawa oscilloscope for this particular triggered-lightning event.

4.1.5 Event F0514

Event F0514 was triggered on Aug 4, 2005 at 18:44:38 UTC. The triggering rocket was launched from the tower launcher which was 476 m away from the photodiode array. Such a distance was chosen to maximize the viewable height of the channel for the photodiodes. The photodiode array was operated during this event.

One stroke was observed for this event on the photodiode array. Figure 4-13 shows the optical waveforms at various channel heights, captured by the photodiode array on the LeCroy Digital Oscilloscopes. The angles of the individual tubes in the photodiode array relative to the horizontal along with the corresponding channel height viewed by each sensor are shown in Table 4-4. The approximate vertical length of lightning channel imaged by each sensor was 1 m.

Figure 4-14 shows the optical waveforms captured by the sensors on the Yokogawa oscilloscope. The Yokogawa has a sampling rate of 10 MHz (that is, a time interval of 100 nanoseconds assuming the speed of propagation of light. between adjacent data points). The smallest channel height seen by the photodiode array for this event was on the order of 30 meters (between sensors 2 and 3), that is, a time interval of 100 nanoseconds. Typical rise-times for lightning events are on the order of micro-seconds, and hence the Yokogawa waveforms have at least ten to fifteen points on the rising portion of return-stroke. So, even though the rising portion of the waveforms have fewer points as compared to the waveforms captured on the LeCroy's, the Yokogawa data are also suitable for data analysis.

4.1.6 Event F0517

Event F0517 was triggered on Aug 4, 2005 at 19:32:47 UTC. The triggering rocket was launched from the tower launcher which was 476 m away from the photodiode array. Such a distance was chosen to maximize the viewable height of the channel for the photodiodes. The photodiode array was operated during this event.

Two strokes were observed for this event on the photodiode array. Figures 4-15 and 4-16 show the optical waveforms at various channel heights, captured by the photodiode array on the LeCroy Digital Oscilloscopes. The angles of the individual tubes in the photodiode array relative to the horizontal along with the corresponding channel height viewed by each sensor are shown in Table 4-4. The approximate vertical length of lightning channel imaged by each sensor was 1 m.

Figures 4-17 and 4-18 show the optical waveforms captured by the photodiodes at various heights along the lightning channel, on the Yokogawa oscilloscope. The Yokogawa has a sampling rate of 10 MHz (that is, a time interval of 100 nanoseconds assuming the speed of propagation of light. between adjacent data points). The smallest channel height seen by the photodiode array for this event was on the order of 30 meters (between sensors 2 and 3), that is, a time interval of 100 nanoseconds. Typical rise-times for lightning events are on the order of micro-seconds, and hence the Yokogawa waveforms have at least ten to fifteen points on the rising portion of return-stroke. So, even though the rising portion of the waveforms have fewer points as compared to the waveforms captured on the LeCroy's, the Yokogawa data are also suitable for data analysis.

4.1.7 Event F0521

Event F0521 was triggered on August 5, 2005 at 21:30:57 UTC. The triggering rocket was launched from the tower launcher which was 476 m away from the photodiode array. Such a distance was chosen to maximize the viewable height of the channel for the photodiodes. The photodiode array was operated during this event.

One stroke was observed for this event on the photodiode array. Figure 4-19 shows the optical waveforms at various channel heights, captured by the photodiode array on the LeCroy Digital Oscilloscopes. The angles of the individual tubes in the photodiode array relative to the

horizontal along with the corresponding channel height viewed by each sensor are shown in Table 4-4. The approximate vertical length of lightning channel imaged by each sensor was 1 m. There were no records on the Yokogawa oscilloscope for this particular triggered-lightning event.

4.2 Natural Lightning Events

4.2.1 Event NAT0503

Event NAT0503 occurred on July 2, 2005 at 23:29:13 UTC. The termination point of the lightning channel is unknown. The photodiode array was operated during this event. One stroke was observed for this event on the photodiode array. Figure 4-20 shows the optical waveforms captured by the photodiode array on the LeCroy Digital Oscilloscopes. Except for sensor 1 (which viewed the lowest channel height), all the sensors were able to view the event clearly. No significant analysis of this event is possible.

4.2.2 Event NAT0504

Event NAT0504 occurred on July 2, 2005 at 23:33:24 UTC. The termination point of the lightning channel is unknown. The photodiode array was operated during this event. One stroke was observed for this event on the photodiode array. Figure 4-21 shows the optical waveforms captured by the photodiode array on the LeCroy Digital Oscilloscope. Except for sensor 1 (which viewed the lowest channel height), all the sensors were able to view the event clearly. No significant analysis of this event is possible.

4.2.3 Event NAT0506

Event NAT0506 occurred on July 14, 2005 at 21:05:37 UTC. The termination point of the lightning channel is unknown. The photodiode array was operated during this event. One stroke was observed for this event on the photodiode array.Figure 4-22 shows the optical waveforms

captured by the photodiode array on the LeCroy Digital Oscilloscopes. Only sensors 2, 3, 4 and 5 were able to view the event clearly. No significant analysis of this event is possible.

4.2.4 Event NAT0507

Event NAT0507 occurred on July 14, 2005 at 21:06:05 UTC. The termination point of the lightning channel is unknown. The photodiode array was operated during this event. One stroke was observed for this event on the photodiode array.Figure 4-23 shows the optical waveforms captured by the photodiode array on the LeCroy Digital Oscilloscopes. Except for sensor 1 (which viewed the lowest channel height), all the sensors were able to view the event. No significant analysis of this event is possible.

4.2.5 Event NAT0508

Event NAT0508 occurred on July 14, 2005 at 21:13:14 UTC. The termination point of the lightning channel is unknown. The photodiode array was operated during this event. One stroke was observed for this event on the photodiode array. Figure 4-24 shows the optical waveforms captured by the photodiode array on the LeCroy Digital Oscilloscopes. Except for sensor 1 (which viewed the lowest channel height), all the sensors were able to view the event clearly. No significant analysis of this event is possible.

4.2.6 Event NAT0509

Event NAT0509 occurred on July 14, 2005 at 21:14:02 UTC. The termination point of the lightning channel is unknown. The photodiode array was operated during these event. Two strokes were observed for this event on the photodiode array. Figures 4-25 and 4-26 show the optical waveforms captured by the photodiode array on the LeCroy Digital Oscilloscopes for both return the return-strokes. Except for sensor 1 (which viewed the lowest channel height), all the sensors were able to view the events clearly. No significant analysis of this event is possible.

4.2.7 Event NAT0510

Event NAT0510 occurred on July 14, 2005 at 21:14:23 UTC. The termination point of the lightning channel is unknown. The photodiode array was operated during this event. One stroke was observed for this event on the photodiode array.Figure 4-27 shows the optical waveforms captured by the photodiode array on the LeCroy Digital Oscilloscope. Except for sensor 1 (which viewed the lowest channel height), all the sensors were able to view the events clearly. No significant analysis of this event is possible.

4.2.8 Event NAT0511

Event NAT0511 occurred on July 14, 2005 at 21:16:17 UTC. The termination point of the lightning channel is unknown. The photodiode array was operated during this event. One stroke was observed for this event on the photodiode array. Figure 4-28 shows the optical waveforms captured by the photodiode array on the LeCroy Digital Oscilloscopes. Except for sensor 1 (which viewed the lowest channel height), all the sensors were able to view the events clearly. No significant analysis of this event is possible.

4.2.9 Event NAT0512

Event NAT0512 occurred on July 14, 2005 at 21:28:37 UTC. The termination point of the lightning channel is unknown. Two strokes were observed by the photodiode array for this event. Two strokes were observed for this event on the photodiode array. Figures 4-29 and 4-30 show the optical waveforms captured by the photodiode array on the LeCroy Digital Oscilloscopes for both the return-strokes. Except for sensor 1 (which viewed the lowest channel height), all the sensors were able to view the events clearly. No significant analysis of this event is possible.

4.2.10 Event NAT0513

Event NAT0513 occurred on July 14, 2005 at 21:16:59 UTC. The termination point of the lightning channel is unknown. The photodiode array was operated during this event. One stroke was observed for this event on the photodiode array. Figure 4-31 shows the optical waveforms captured by the photodiode array on the LeCroy Digital Oscilloscopes. Except for sensor 1 (which viewed the lowest channel height), all the sensors were able to view the events clearly. No significant analysis of this event is possible.

4.2.11 Event NAT0514

Event NAT0514 occurred on July 14, 2005 at 21:31:25 UTC. The termination point of the lightning channel is unknown. The photodiode array was operated during this event. One stroke was observed for this event. Figure 4-32 shows the optical waveforms captured by the photodiode array on the LeCroy Digital Oscilloscopes. Except for sensor 1 (which viewed the lowest channel height), all the sensors were able to view the events clearly. No significant analysis of this event is possible.

4.2.12 Event NAT0515

Event NAT0515 occurred on July 14, 2005 at 23:13:58 UTC. The termination point of the lightning channel is unknown. The photodiode array was operated during this event. One stroke was observed for this event on the photodiode. Figure 4-33 shows the optical waveforms captured by the photodiode array on the LeCroy Digital Oscilloscopes. Only sensors 2, 3 and 4 were able to view the event clearly. No significant analysis of this event is possible.

4.2.13 Event NAT0516

Event NAT0516 occurred on July 14, 2005 at 23:19:46 UTC. The termination point of the lightning channel is unknown. The photodiode array was operated during this event. One stroke was observed for this event on the photodiode array. Figure 4-34 shows the optical waveforms

captured by the photodiode array on the LeCroy Digital Oscilloscopes. Only sensors 2, 3, 4 and 5 were able to view the event clearly. No significant analysis of this event is possible.

4.2.14 Event NAT0517

Event NAT0517 occurred on July 14, 2005 at 23:20:40 UTC. The termination point of the lightning channel is unknown. The photodiode array was operated during this event. One stroke was observed for this event on the photodiode array. Figure 4-35 shows the optical waveforms captured by the photodiode array on the LeCroy Digital Oscilloscopes. Only sensors 2, 3, and 4 were able to view the event clearly. No significant analysis of this event is possible.

4.2.15 Event NAT0518

Event NAT0518 occurred on July 14, 2005 at 23:21:24 UTC. The termination point of the lightning channel is unknown. The photodiode array was operated during this event. One stroke was observed for this event on the photodiode array. Figure 4-36 shows the optical waveforms captured by the photodiode array on the LeCroy Digital Oscilloscopes. Except for sensor 1 (which viewed the lowest channel height), all the sensors were able to view the events clearly. No significant analysis of this event is possible.

is unknown, and therefore the height viewed by each sensor cannot be determined.

4.2.16 Event NAT0519

Event NAT0519 occurred on July 14, 2005 at 16:56:56 UTC. The termination point of the lightning channel is unknown. The photodiode array was operated during this event. One stroke was observed for this event on the photodiode array. Figure 4-37 shows the optical waveforms captured by the photodiode array on the LeCroy Digital Oscilloscopes. Except for sensor 1 (which viewed the lowest channel height), all the sensors were able to view the events clearly. No significant analysis of this event is possible.

4.2.17 Event NAT0520

Event NAT0520 occurred on July 14, 2005 at 17:06:22 UTC. The termination point of the lightning channel is unknown. The photodiode array was operated during this event. One stroke was observed for this event on the photodiode array. Figure 4-38 shows the optical waveforms captured by the photodiode array on the LeCroy Digital Oscilloscopes. Except for sensor 1 (which viewed the lowest channel height), all the sensors were able to view the events clearly. No significant analysis of this event is possible

4.2.18 Event NAT0521

Event NAT0521 occurred on July 14, 2005 at 17:21:55 UTC. The termination point of the lightning channel is unknown. The photodiode array was operated during this event. One stroke was observed for this event on the photodiode array. Figure 4-39 shows the optical waveforms captured by the photodiode array on the LeCroy Digital Oscilloscopes. Except for sensor 1 (which viewed the lowest channel height), all the sensors were able to view the events clearly. No significant analysis of this event is possible.

4.2.19 Event NAT0522

Event NAT0522 occurred on July 14, 2005 at 17:23:57 UTC. The termination point of the lightning channel is unknown. The photodiode array was operated during this event. One stroke was observed for this event on the photodiode array. Figure 4-40 shows the optical waveforms captured by the photodiode array on the LeCroy Digital Oscilloscopes. Except for sensor 1 (which viewed the lowest channel height), all the sensors were able to view the events clearly. No significant analysis of this event is possible.

4.2.20 Event NAT0523

Event NAT0523 occurred on July 14, 2005 at 17:25:22 UTC. The termination point of the lightning channel is unknown. The photodiode array was operated during this event. Two strokes

were observed for this event on the photodiode array. Figures 4-41 and 4-42 show the optical waveforms captured by the photodiode array on the LeCroy Digital Oscilloscopes for both the return-strokes. Except for sensor 1 (which viewed the lowest channel height), all the sensors were able to view the events clearly. No significant analysis of this event is possible.

4.2.21 Event NAT0524

Event NAT0524 occurred on July 14, 2005 at 17:54:45 UTC. The termination point of the lightning channel is unknown. The photodiode array was operated during this event. One stroke was observed for this event on the photodiode array. Figures 4-43 shows the optical waveforms captured by the photodiode array on the LeCroy Digital Oscilloscopes. Only sensors 2, 3, 4 and 5 were able to view the event clearly. No significant analysis of this event is possible.

4.2.22 Event NAT0525

Event NAT0525 occurred on July 14, 2005 at 17:59:31 UTC. The termination point of the lightning channel is unknown. The photodiode array was operated during this event. One stroke was observed for this event on the photodiode array. Figure 4-44 shows the optical waveforms captured by the photodiode array on the LeCroy Digital Oscilloscopes. Only sensors 2, 3, 4 and 5 were able to view the event clearly. No significant analysis of this event is possible.

4.2.23 Event NAT0526

Event NAT0526 occurred on July 14, 2005 at 18:01:10 UTC. The termination point of the lightning channel is unknown. The photodiode array was operated during this event. One stroke was observed for this event on the photodiode array. Figure 4-45 shows the optical waveforms captured by the photodiode array on the LeCroy Digital Oscilloscopes. Only sensors 2, 3, 4 and 5 were able to view the event clearly. No significant analysis of this event is possible.

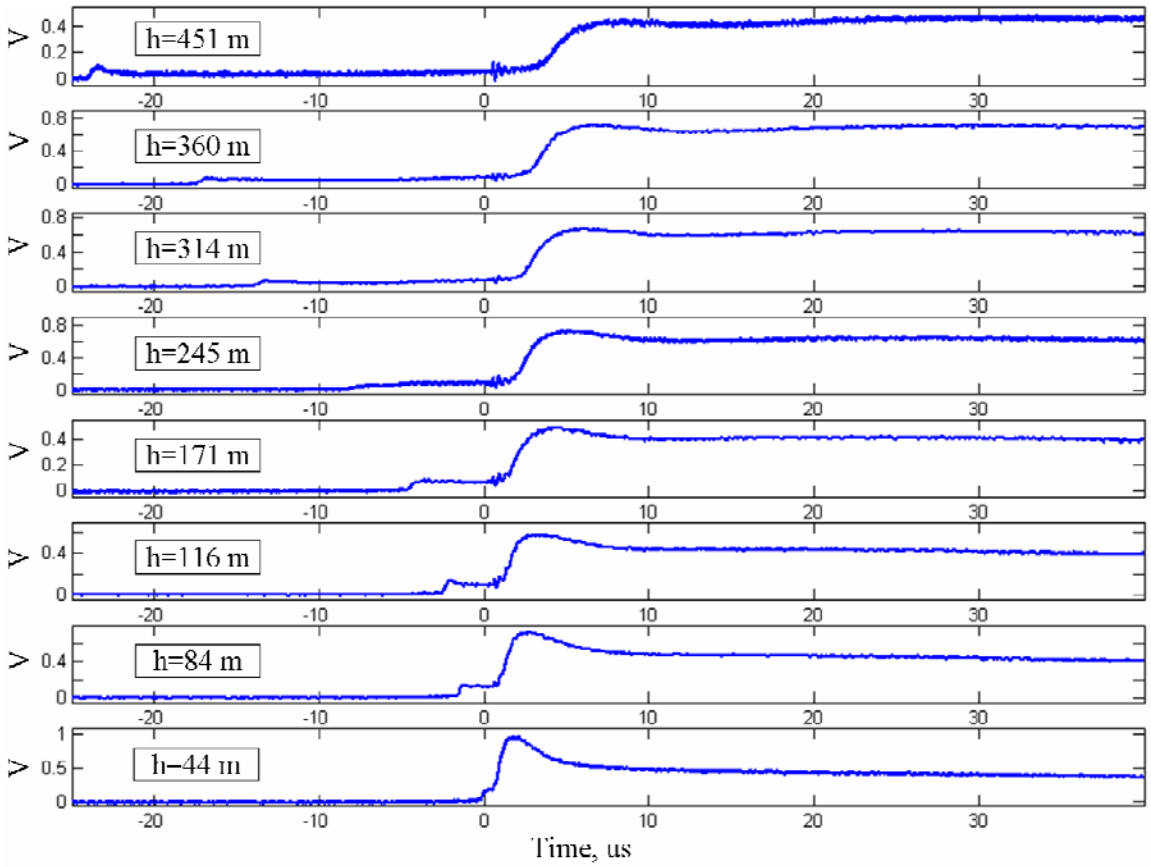

Figure 4-1: Event F0501, photodiode array waveforms recorded on the LeCroy DSOs. The vertical scale indicates relative light intensity and is given in terms of voltage at the oscilloscope input. This record was obtained using an active configuration (a trans-impedance amplifier was used in the photodiode circuit for achieving higher gain) of the photodiode array. The lightning channel termination point was the bucket launcher.

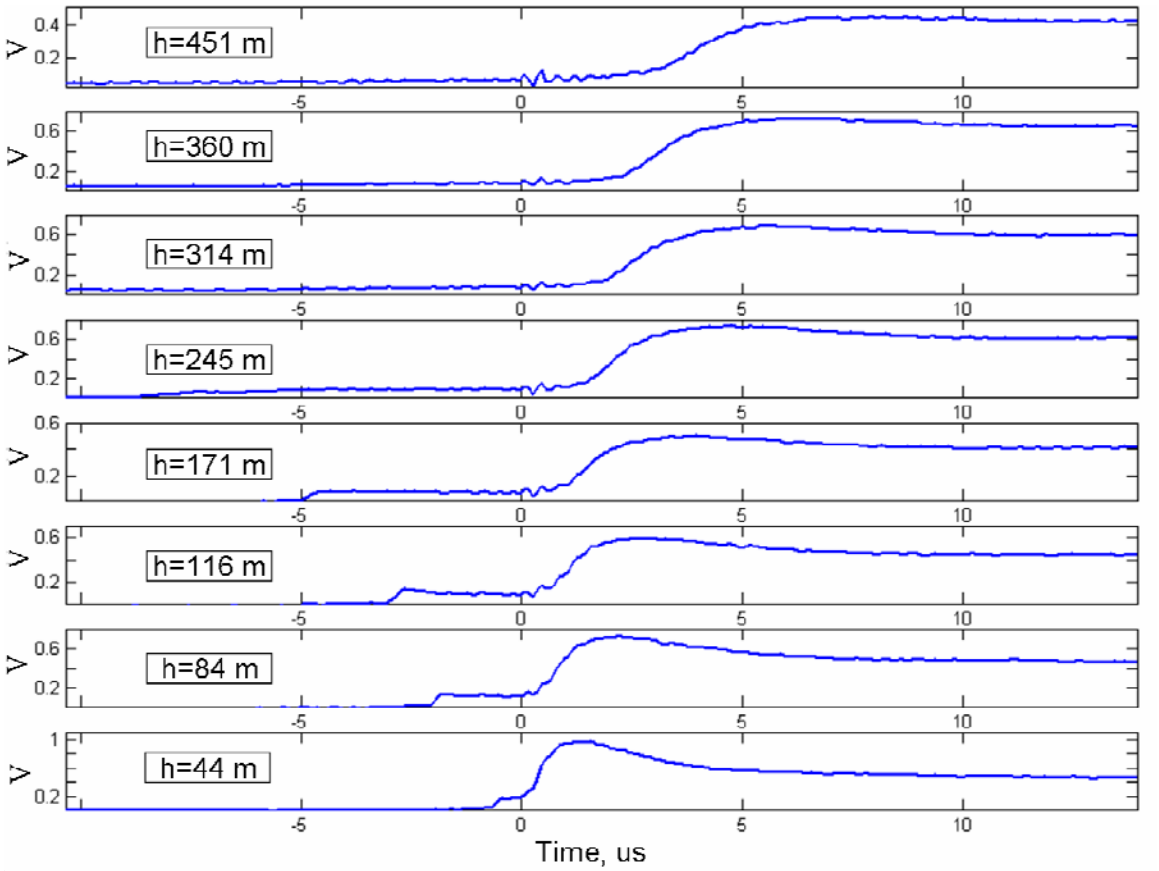

Figure 4-2: Event F0501, photodiode array recorded on the Yokogawa. The vertical scale indicates relative light intensity and is given in terms of voltage at the oscilloscope input. This record was obtained using an active configuration (a trans-impedance amplifier was used in the photodiode circuit for achieving higher gain) of the photodiode array. The lightning channel termination point was the bucket launcher.

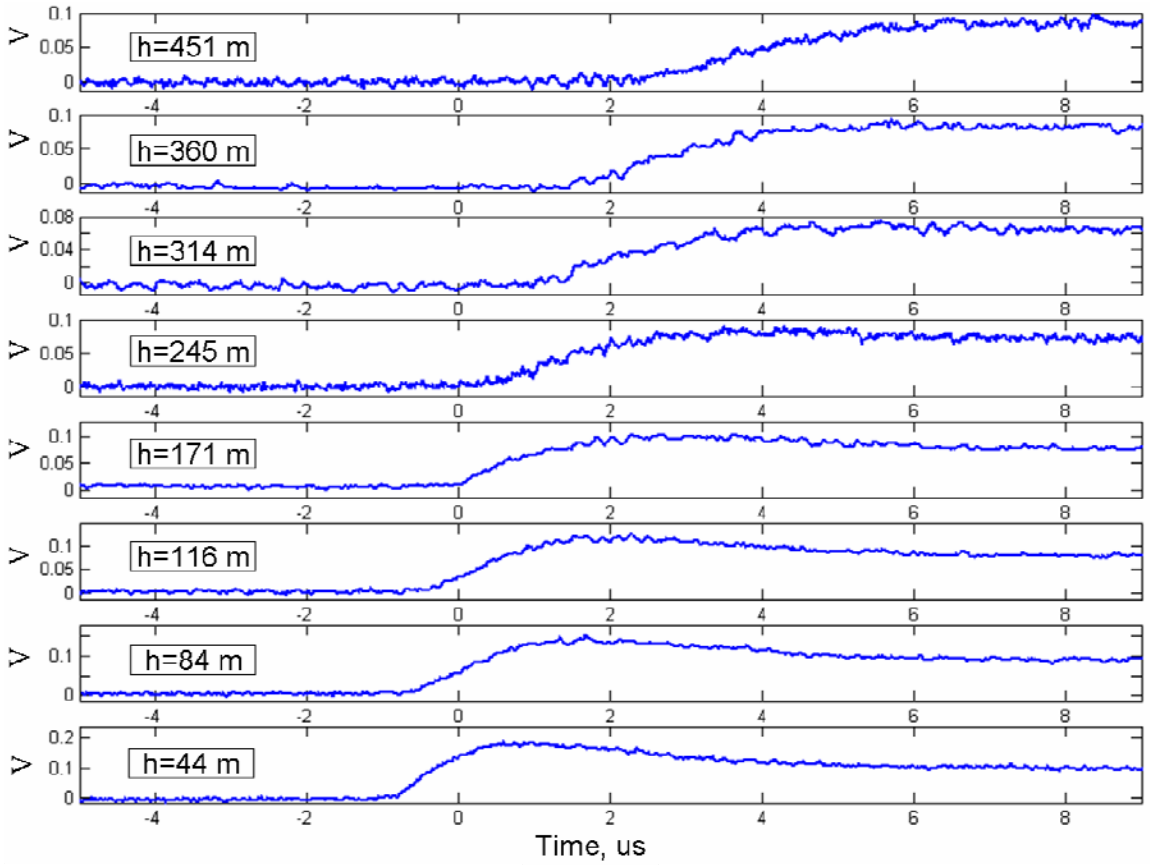

Figure 4-3 Event F0503, stroke 1, photodiode array recorded on the LeCroy DSOs. The vertical scale indicates relative light intensity and is given in terms of voltage at the oscilloscope input. This record was obtained using an active configuration (a trans-impedance amplifier was used in the photodiode circuit for achieving higher gain) of the photodiode array. The lightning channel termination point was the bucket launcher.

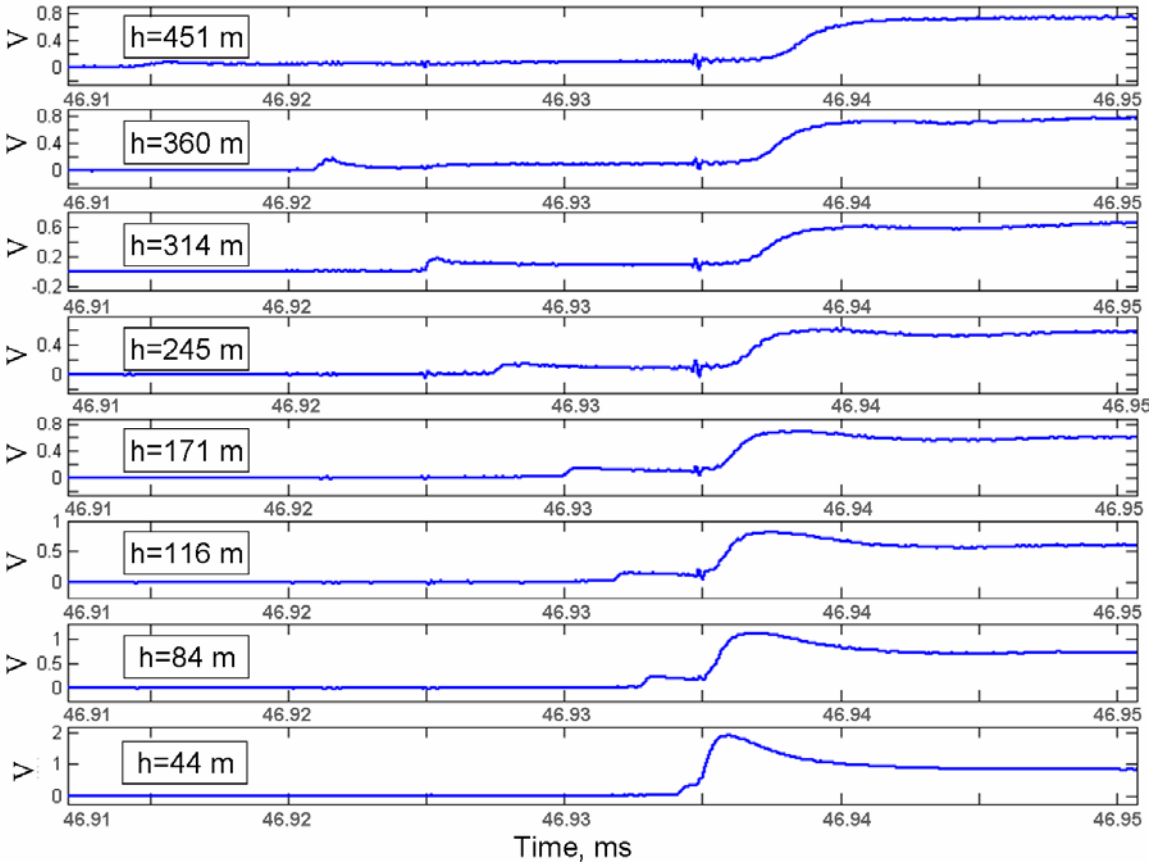

Figure 4-4 Event F0503, stroke 2, photodiode array recorded on the LeCroy DSOs. The vertical scale indicates relative light intensity and is given in terms of voltage at the oscilloscope input. This record was obtained using an active configuration (a trans-impedance amplifier was used in the photodiode circuit for achieving higher gain) of the photodiode array. The lightning channel termination point was the bucket launcher.

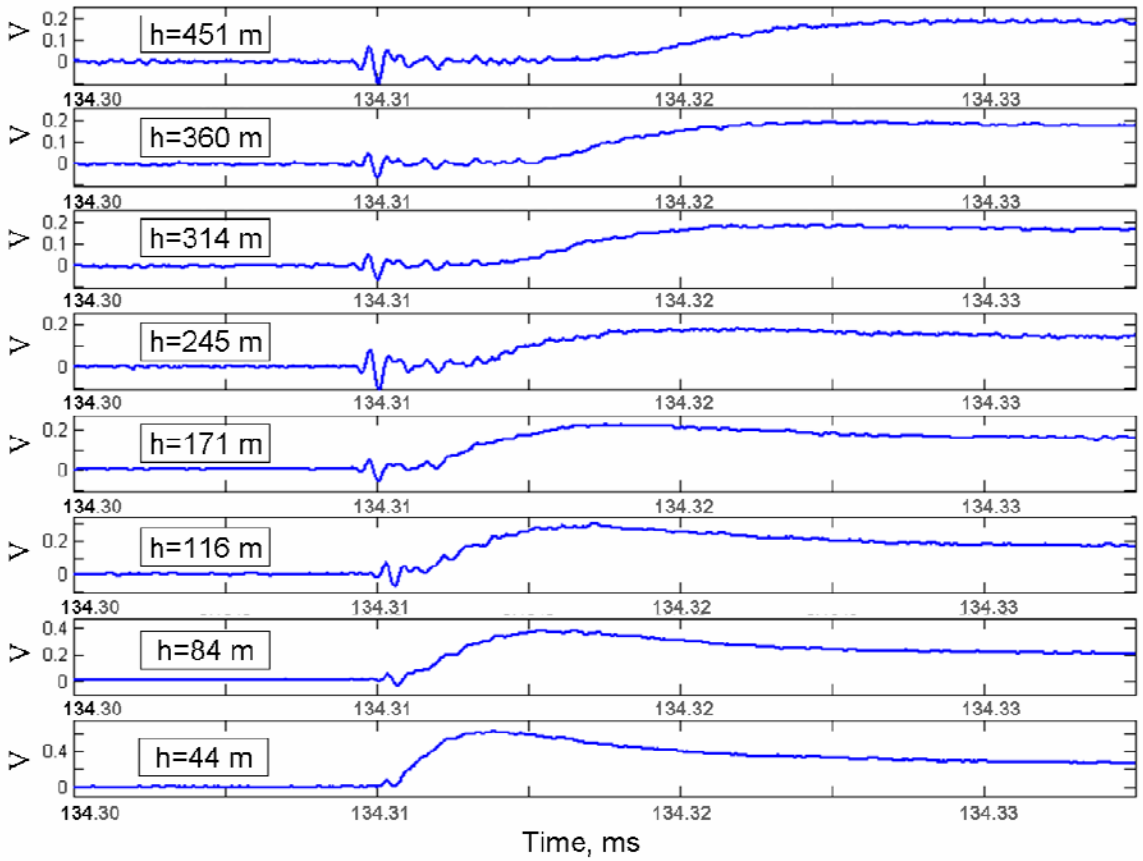

Figure 4-5 Event F0503, stroke 3, photodiode array recorded on the LeCroy DSOs. The vertical scale indicates relative light intensity and is given in terms of voltage at the oscilloscope input. This record was obtained using an active configuration (a trans-impedance amplifier was used in the photodiode circuit for achieving higher gain) of the photodiode array. The lightning channel termination point was the bucket launcher.

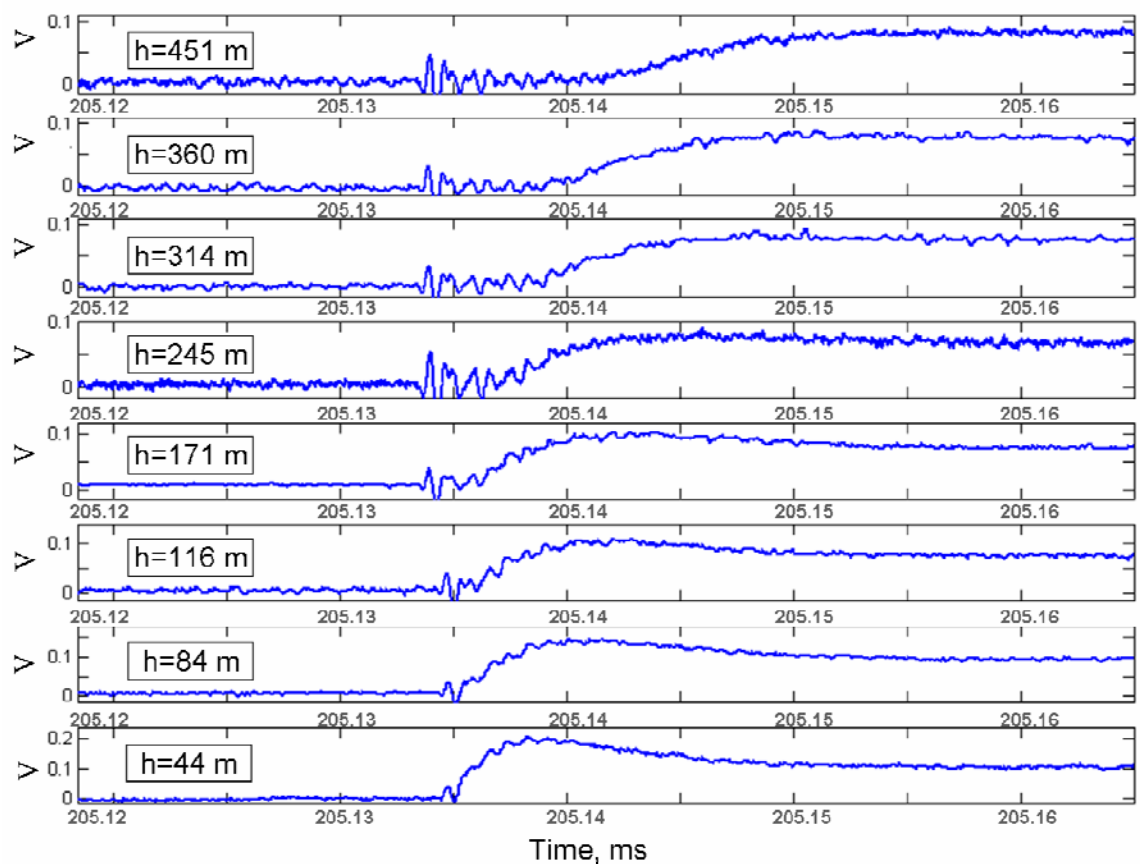

Figure 4-6 Event F0503, stroke 4, photodiode array recorded on the LeCroy DSOs. The vertical scale indicates relative light intensity and is given in terms of voltage at the oscilloscope input. This record was obtained using an active configuration (a trans-impedance amplifier was used in the photodiode circuit for achieving higher gain) of the photodiode array. The lightning channel termination point was the bucket launcher.

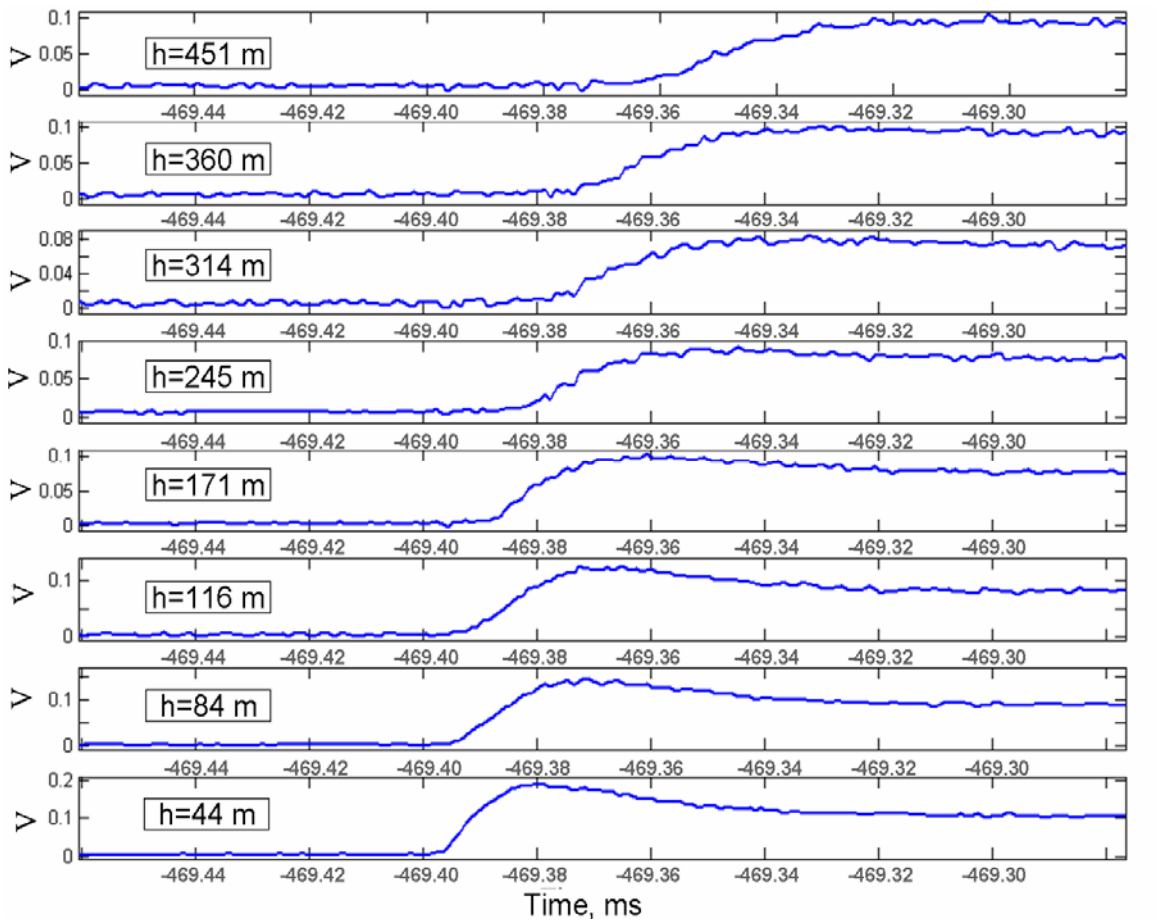

Figure 4-7 Event F0503, stroke 1, photodiode array recorded on the Yokogawa. The vertical scale indicates relative light intensity and is given in terms of voltage at the oscilloscope input. This record was obtained using an active configuration (a trans-impedance amplifier was used in the photodiode circuit for achieving higher gain) of the photodiode array. The lightning channel termination point was the bucket launcher.

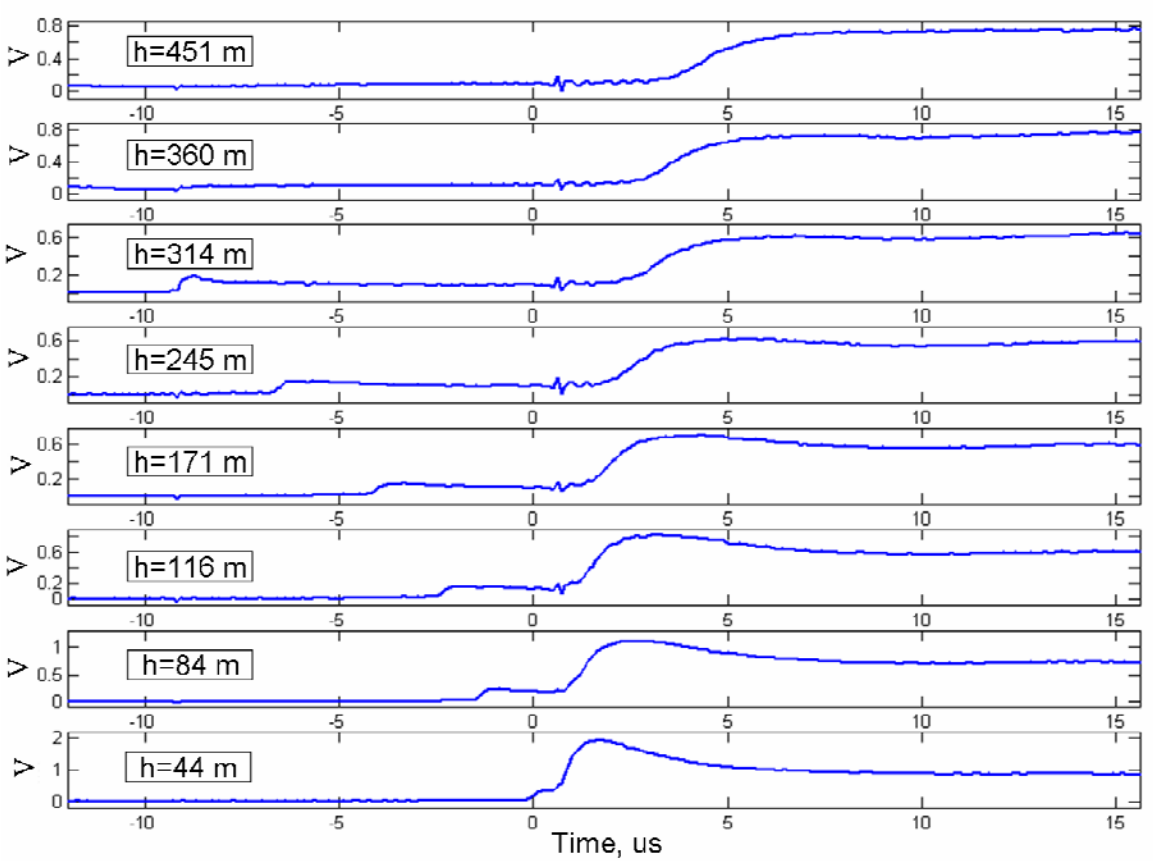

Figure 4-8 Event F0503, stroke 2, photodiode array recorded on the Yokogawa. The vertical scale indicates relative light intensity and is given in terms of voltage at the oscilloscope input. This record was obtained using an active configuration (a trans-impedance amplifier was used in the photodiode circuit for achieving higher gain) of the photodiode array. The lightning channel termination point was the bucket launcher.

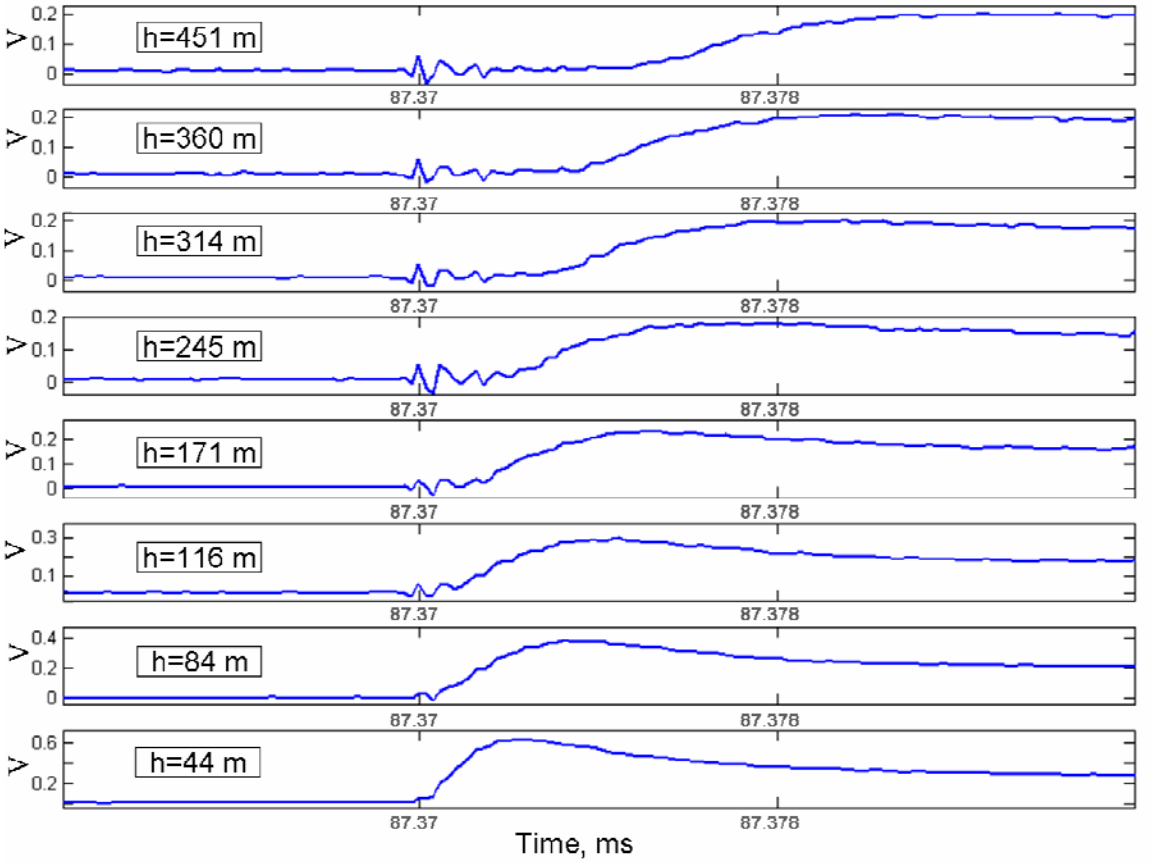

Figure 4-9 Event F0503, stroke 3, photodiode array recorded on the Yokogawa. The vertical scale indicates relative light intensity and is given in terms of voltage at the oscilloscope input. This record was obtained using an active configuration (a trans-impedance amplifier was used in the photodiode circuit for achieving higher gain) of the photodiode array. The lightning channel termination point was the bucket launcher.

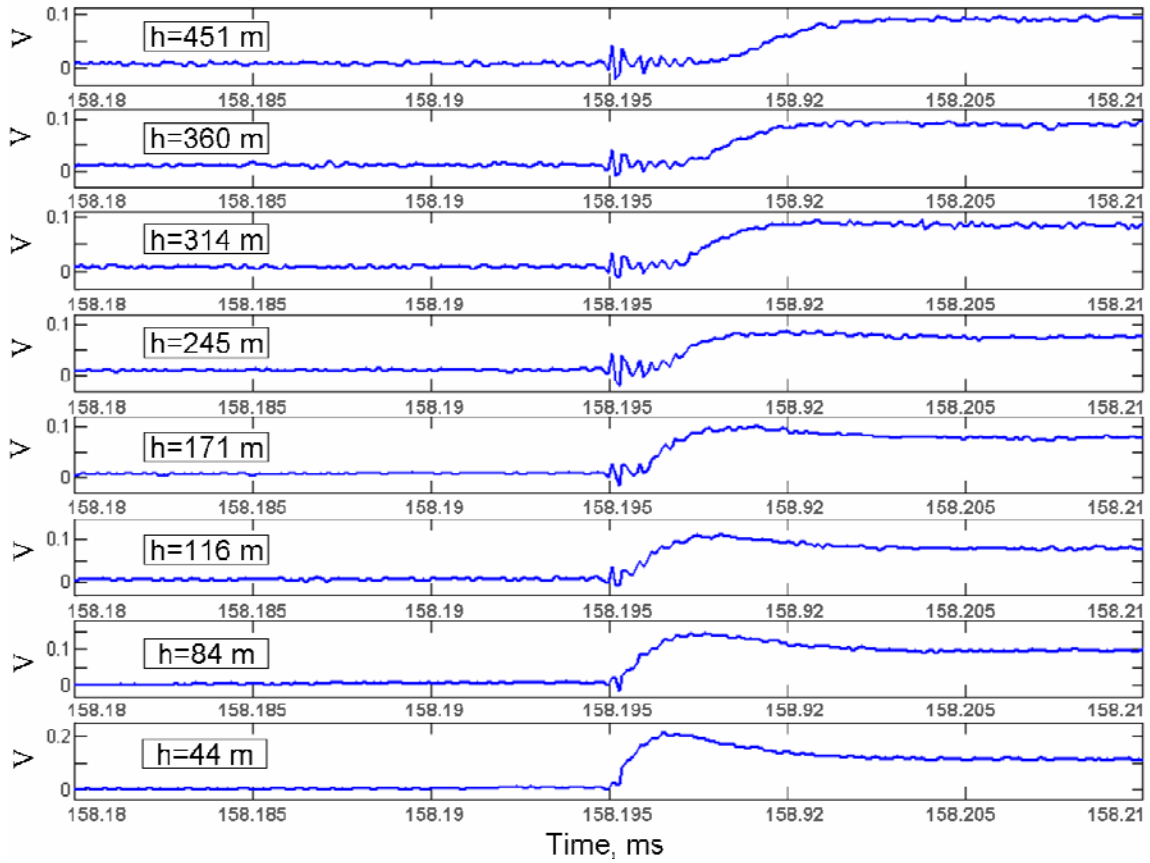

Figure 4-10 Event F0503, stroke 4, photodiode array recorded on the Yokogawa. The vertical scale indicates relative light intensity and is given in terms of voltage at the oscilloscope input. This record was obtained using an active configuration (a trans-impedance amplifier was used in the photodiode circuit for achieving higher gain) of the photodiode array. The lightning channel termination point was the bucket launcher.

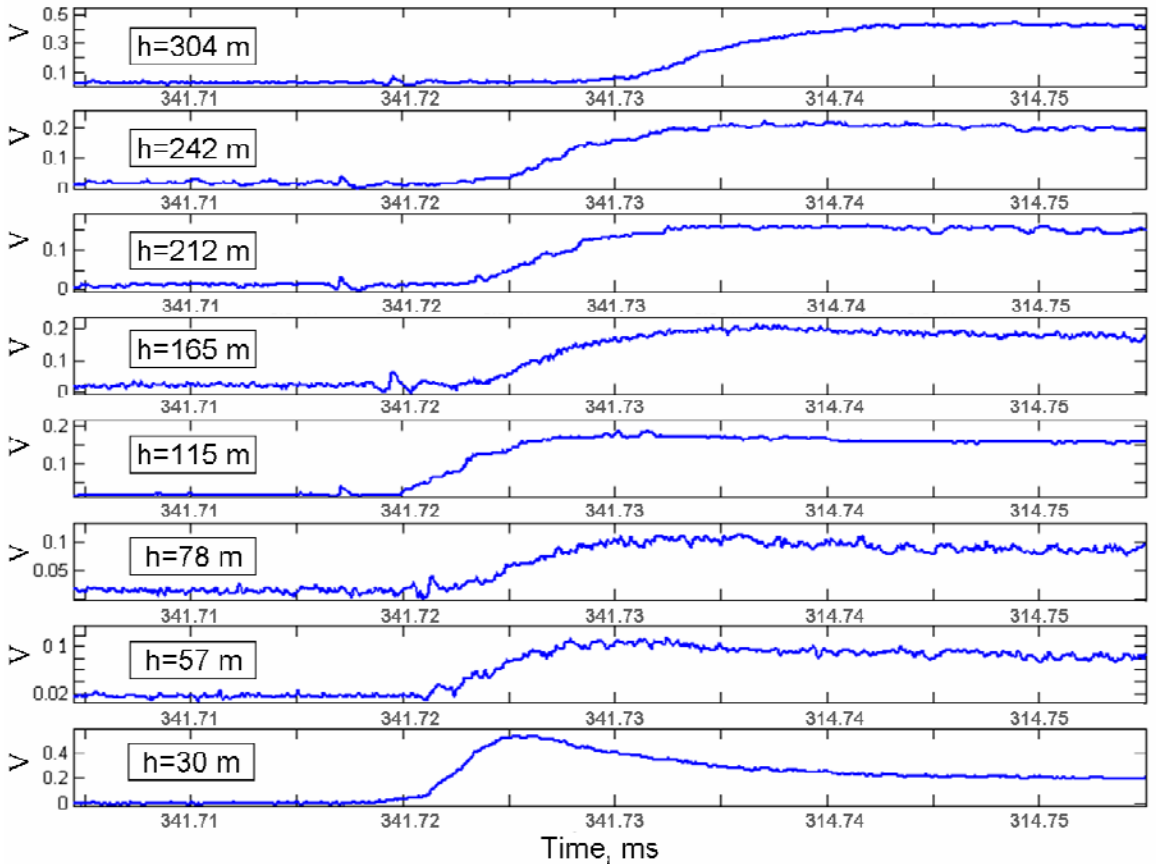

Figure 4-11 Event F0510, photodiode array recorded on the LeCroy DSOs. The vertical scale indicates relative light intensity and is given in terms of voltage at the oscilloscope input. This record was obtained using an active configuration (a trans-impedance amplifier was used in the photodiode circuit for achieving higher gain) of the photodiode array. The termination point was the tower launcher

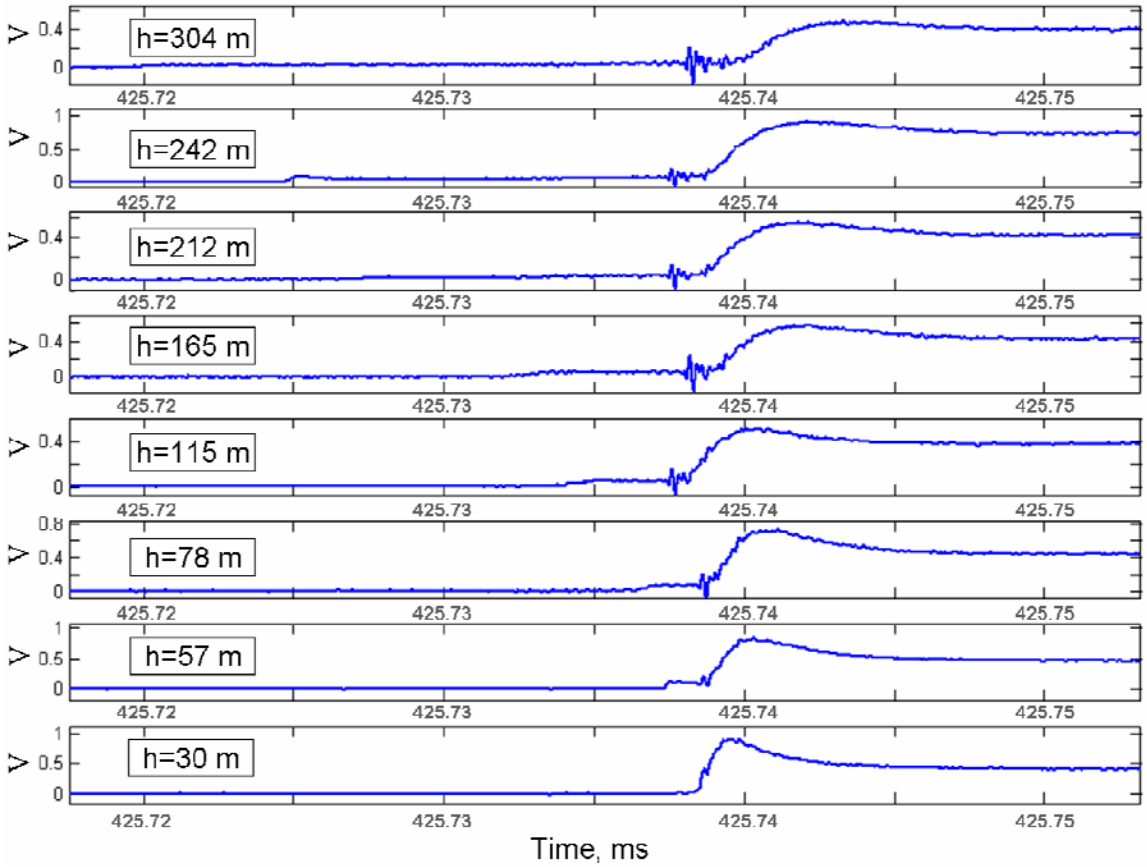

Figure 4-12 Event F0512, photodiode array recorded on the LeCroy DSOs. The vertical scale indicates relative light intensity and is given in terms of voltage at the oscilloscope input. This record was obtained using an active configuration (a trans-impedance amplifier was used in the photodiode circuit for achieving higher gain) of the photodiode array. The termination point was the tower launcher

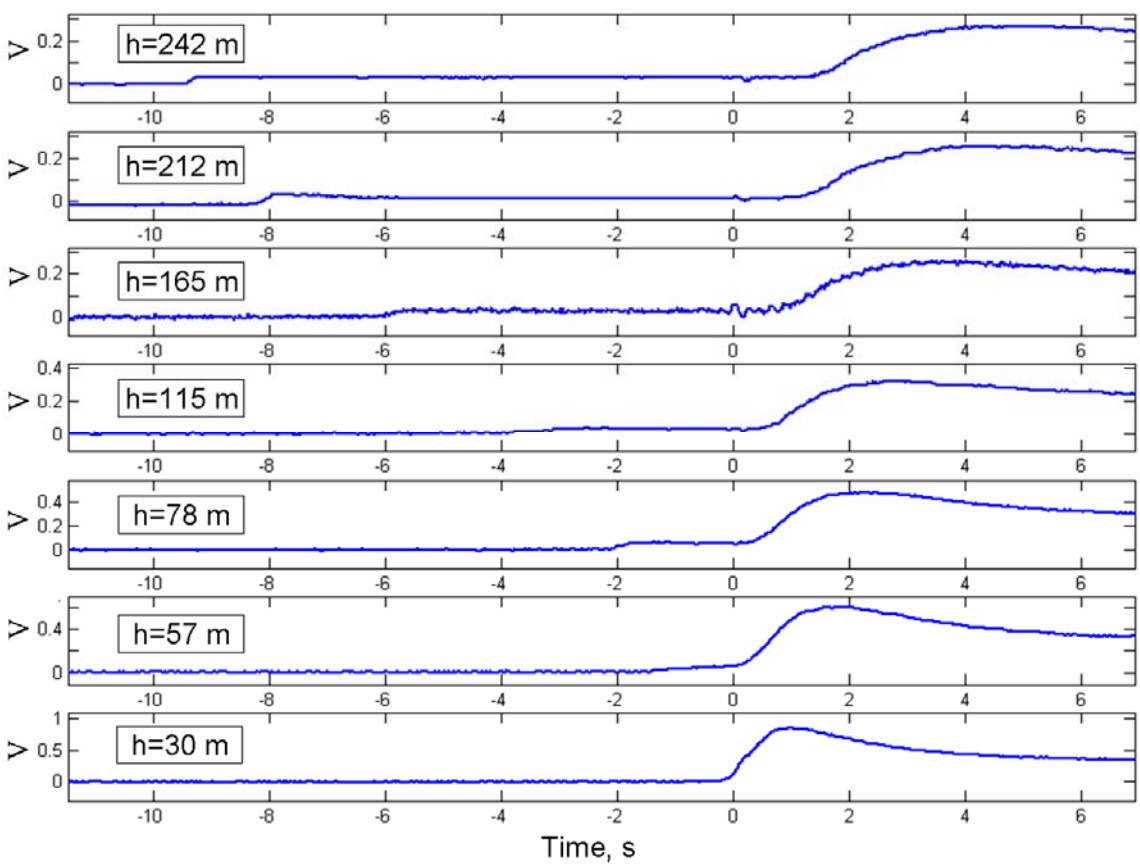

Figure 4-13 Event F0514, photodiode array recorded on the LeCroy DSOs. The vertical scale indicates relative light intensity and is given in terms of voltage at the oscilloscope input. This record was obtained using an active configuration (a trans-impedance amplifier was used in the photodiode circuit for achieving higher gain) of the photodiode array. The termination point was the tower launcher.

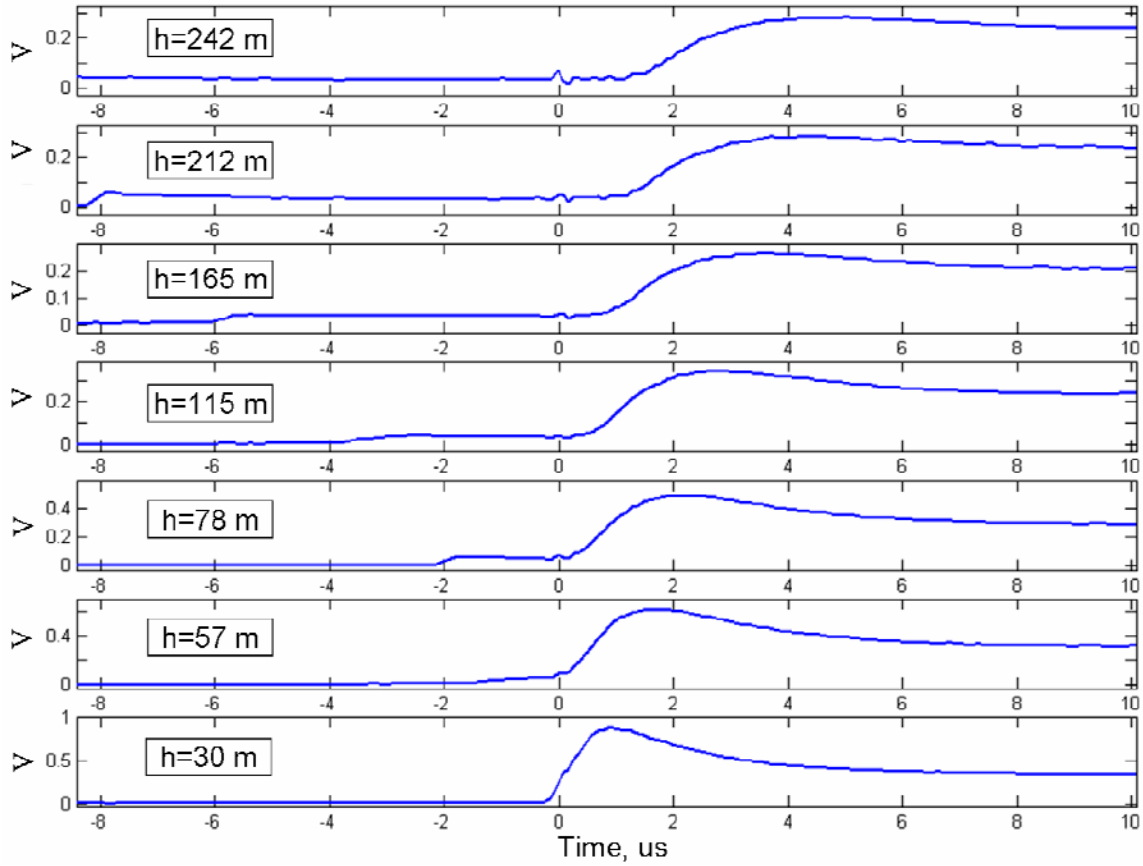

Figure 4-14 Event F0514, photodiode array recorded on the Yokogawa oscilloscope. The vertical scale indicates relative light intensity and is given in terms of voltage at the oscilloscope input. This record was obtained using an active configuration (a trans-impedance amplifier was used in the photodiode circuit for achieving higher gain) of the photodiode array. The termination point was the tower launcher.

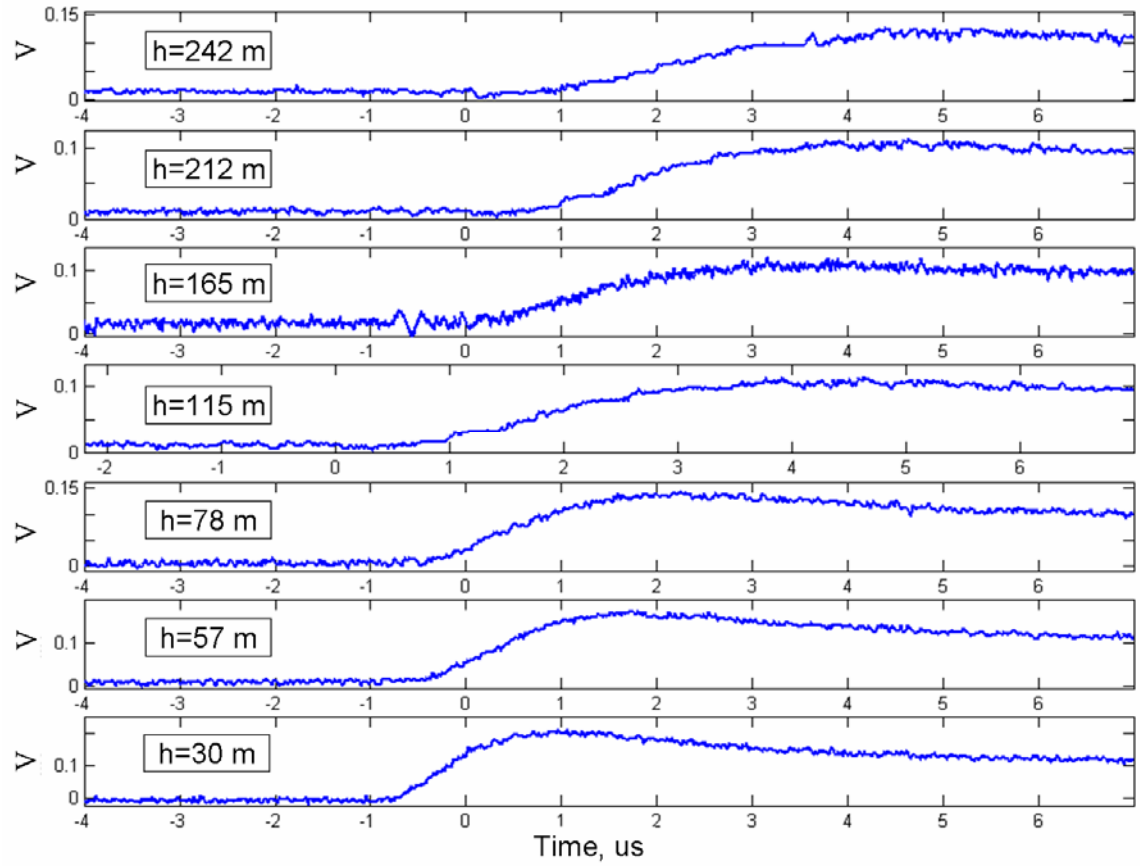

Figure 4-15 Event F0517, stroke 1, photodiode array recorded on the LeCroy DSOs. The vertical scale indicates relative light intensity and is given in terms of voltage at the oscilloscope input. This record was obtained using an active configuration (a trans-impedance amplifier was used in the photodiode circuit for achieving higher gain) of the photodiode array. The termination point was the tower launcher.

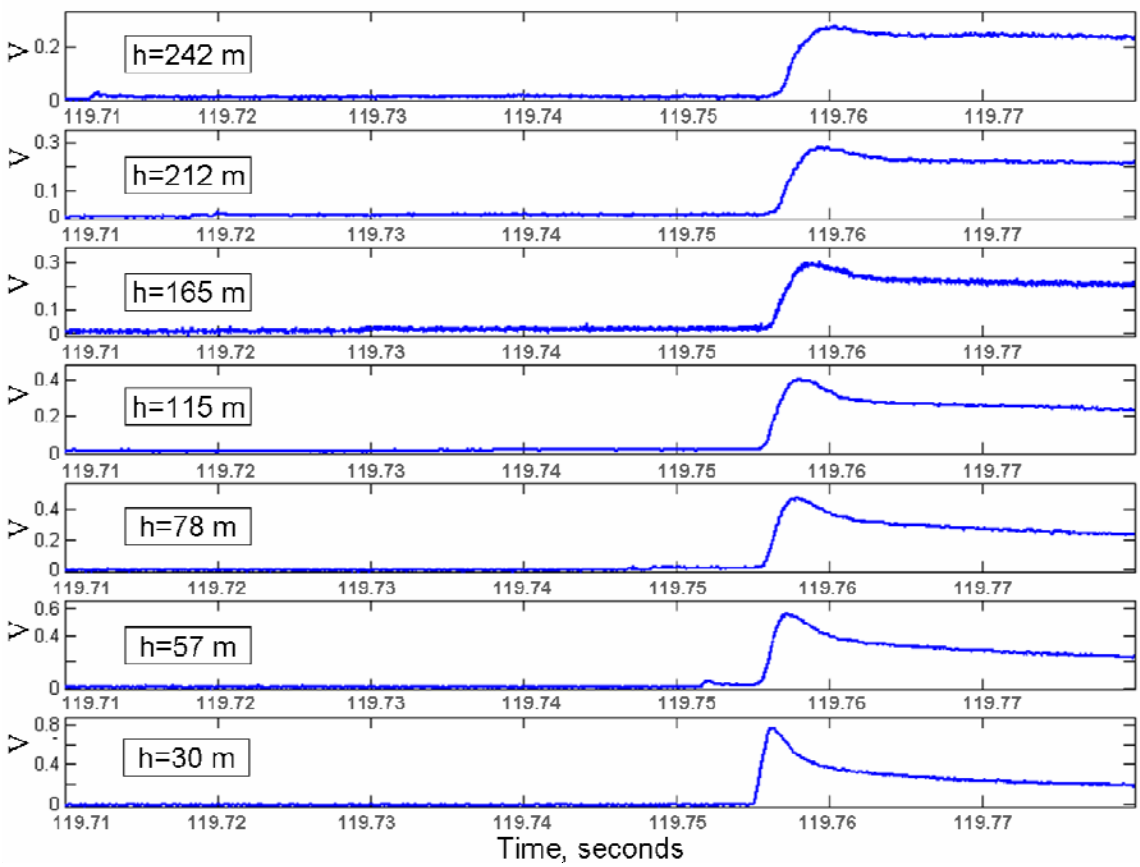

Figure 4-16 Event F0517, stroke 2, photodiode array recorded on the LeCroy DSOs. The vertical scale indicates relative light intensity and is given in terms of voltage at the oscilloscope input. This record was obtained using an active configuration (a trans-impedance amplifier was used in the photodiode circuit for achieving higher gain) of the photodiode array. The termination point was the tower launcher.

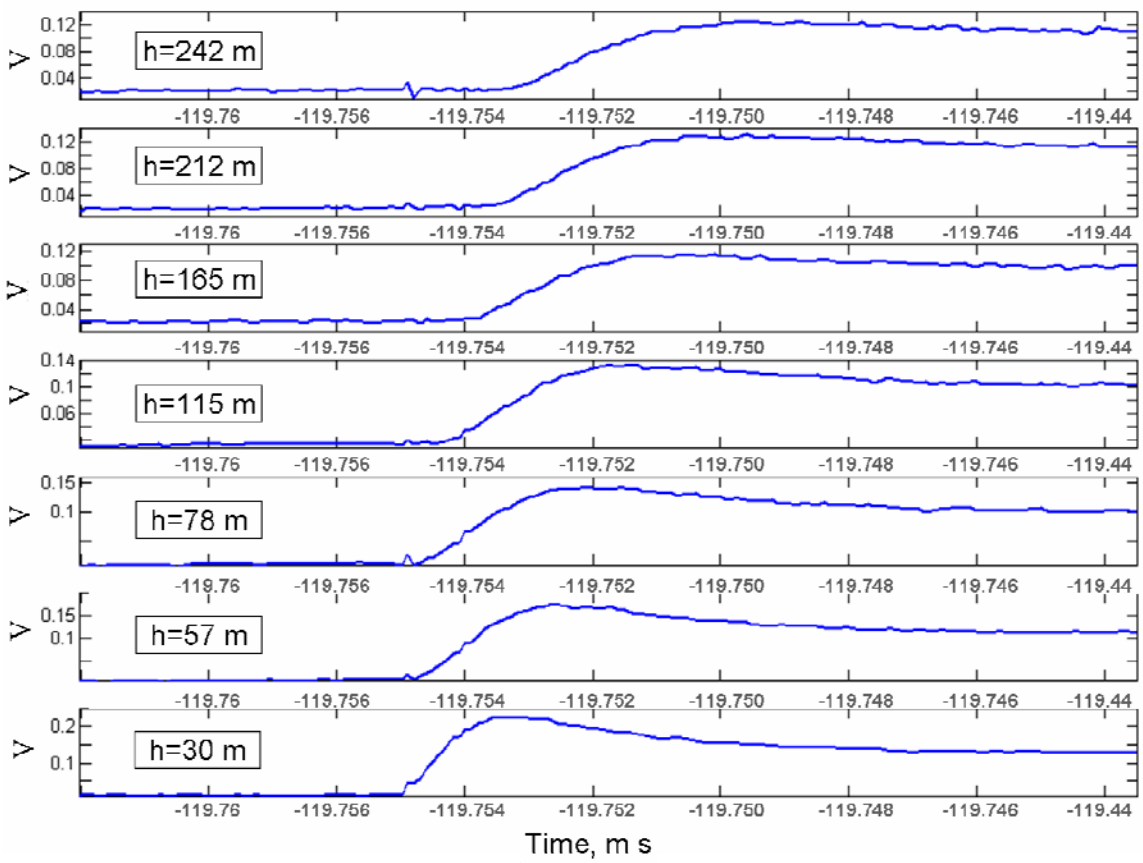

Figure 4-17 Event F0517, stroke 1, photodiode array recorded on the Yokogawa oscilloscope. The vertical scale indicates relative light intensity and is given in terms of voltage at the oscilloscope input. This record was obtained using an active configuration (a trans-impedance amplifier was used in the photodiode circuit for achieving higher gain) of the photodiode array. The termination point was the tower launcher.

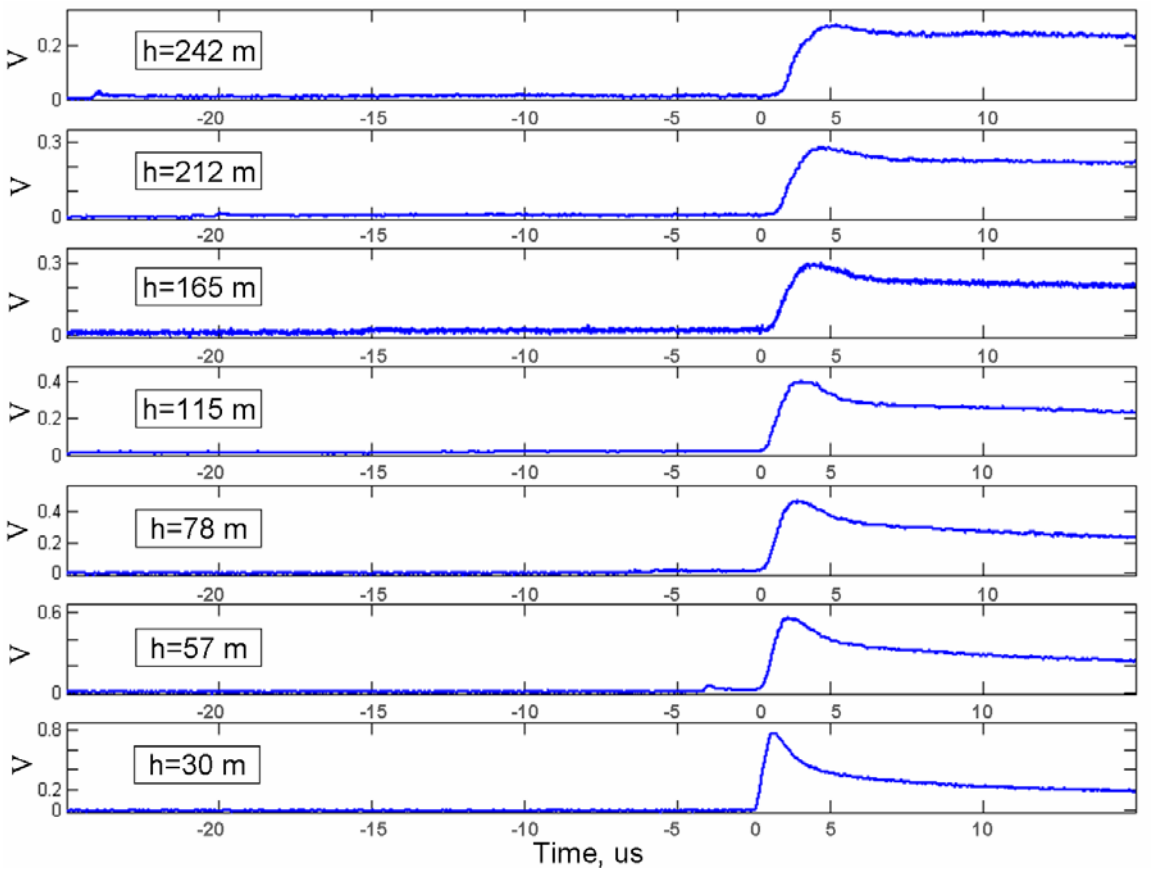

Figure 4-18 Event F0517, stroke 2, photodiode array recorded on the Yokogawa oscilloscope. The vertical scale indicates relative light intensity and is given in terms of voltage at the oscilloscope input. This record was obtained using an active configuration (a trans-impedance amplifier was used in the photodiode circuit for achieving higher gain) of the photodiode array. The termination point was the tower launcher.

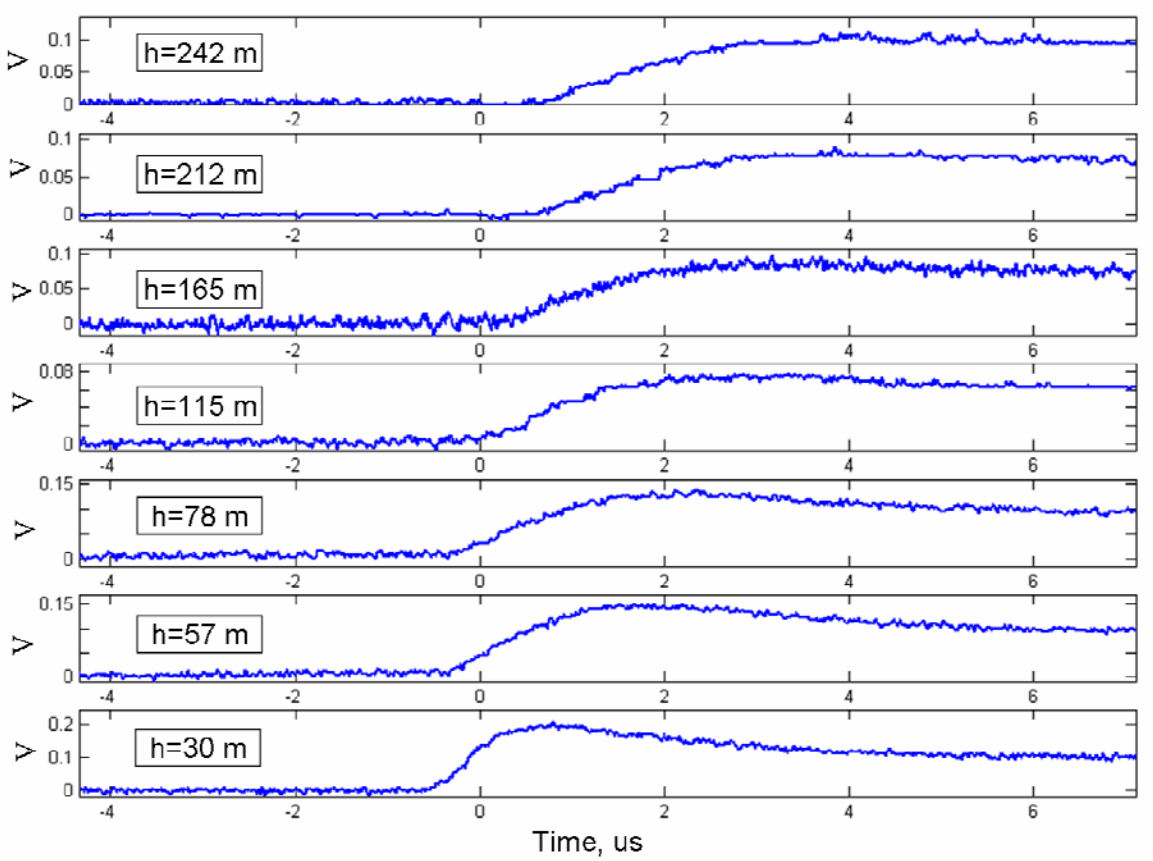

Figure 4-19 Event F0521, photodiode array recorded on the LeCroy DSOs. The vertical scale indicates relative light intensity and is given in terms of voltage at the oscilloscope input. This record was obtained using an active configuration (a trans-impedance amplifier was used in the photodiode circuit for achieving higher gain) of the photodiode array. The termination point was the tower launcher.

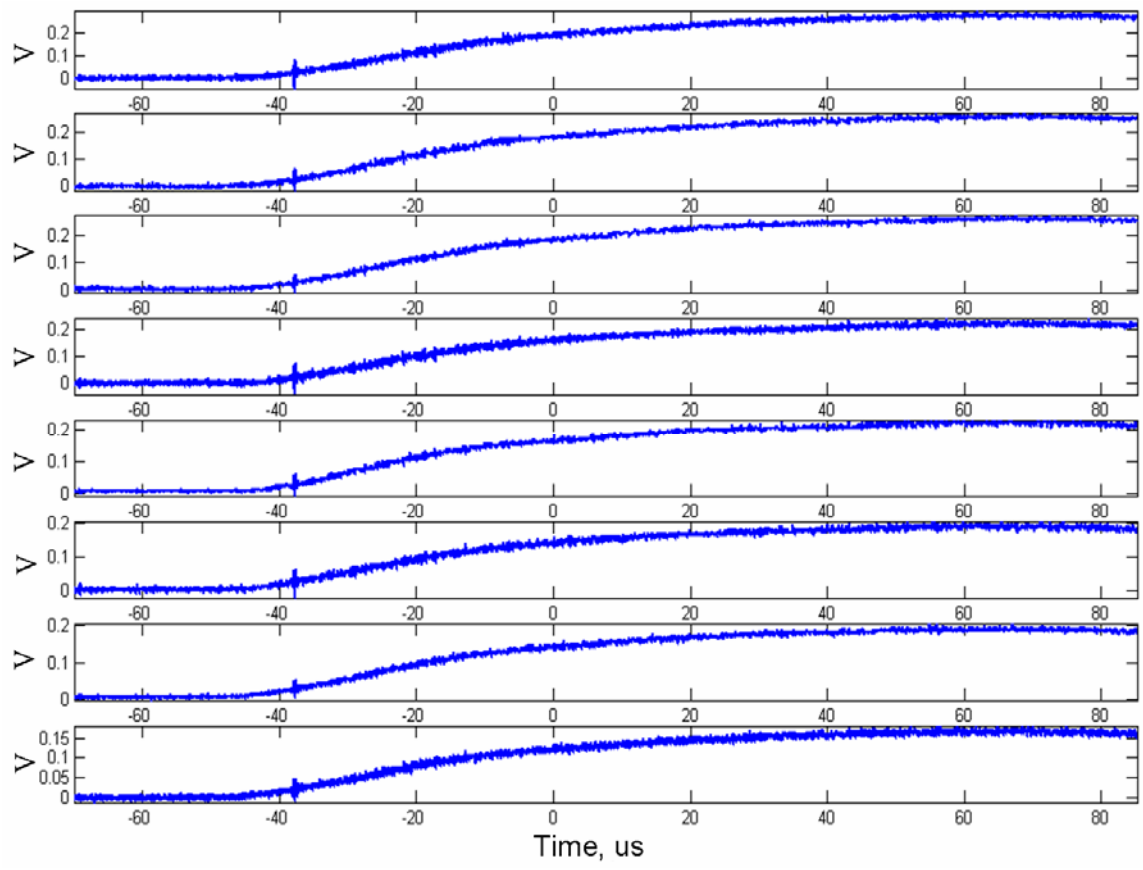

Figure 4-20 Event NAT0503 photodiode array record. The vertical scale indicates relative light intensity in terms of voltage at the oscilloscope input. The distance to the termination point is unknown, and therefore the height viewed by each sensor cannot be determined.

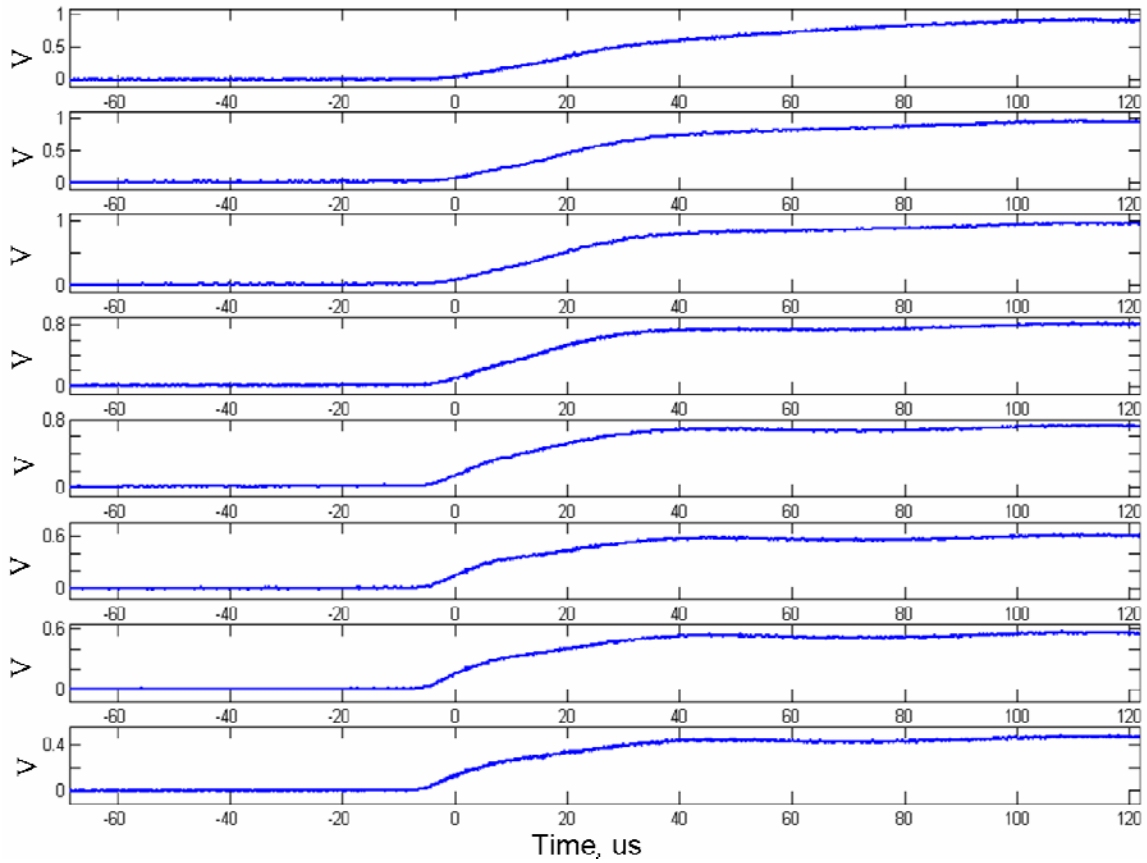

Figure 4-21 Event NAT0504 photodiode array record. The vertical scale indicates relative light intensity in terms of voltage at the oscilloscope input. The distance to the termination point is unknown, and therefore the height viewed by each sensor cannot be determined.

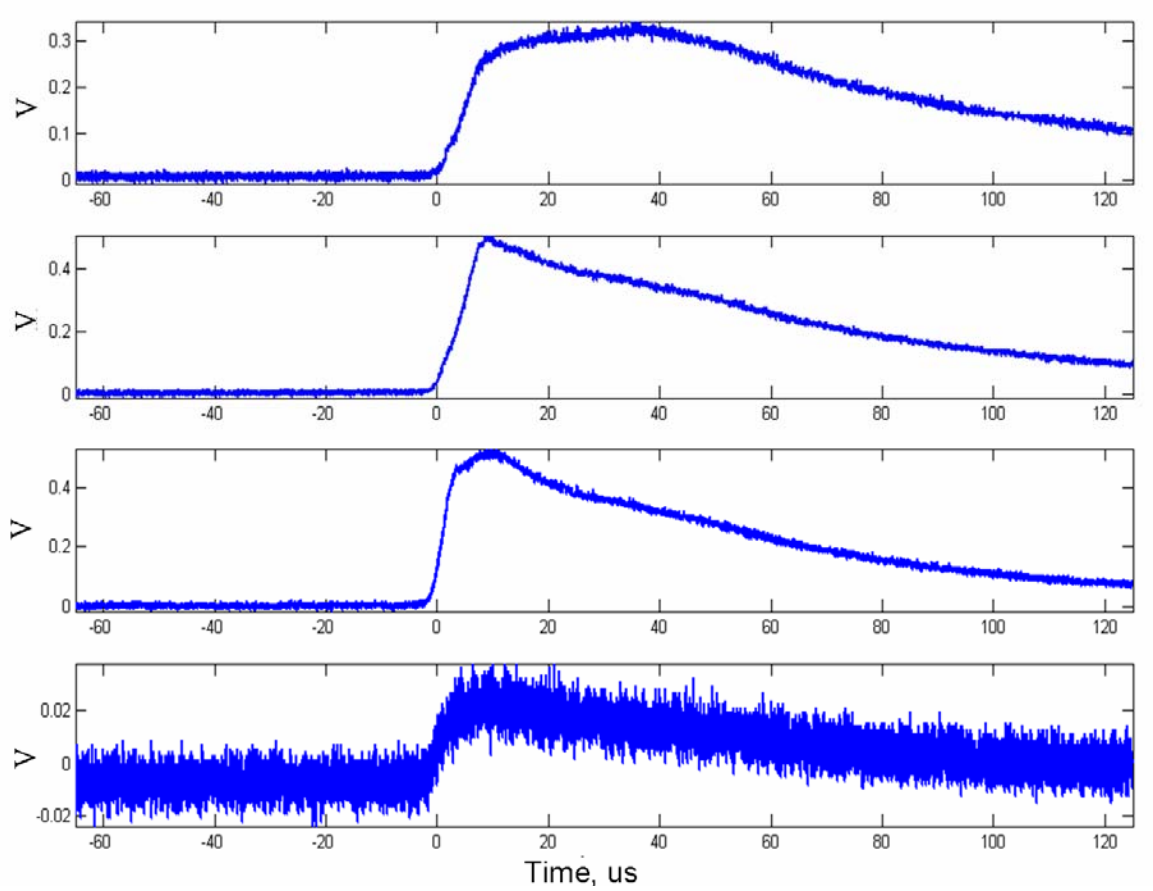

Figure 4-22 Event NAT0506 photodiode array record. The vertical scale indicates relative light intensity in terms of voltage at the oscilloscope input. The distance to the termination point is unknown, and therefore the height viewed by each sensor cannot be determined.

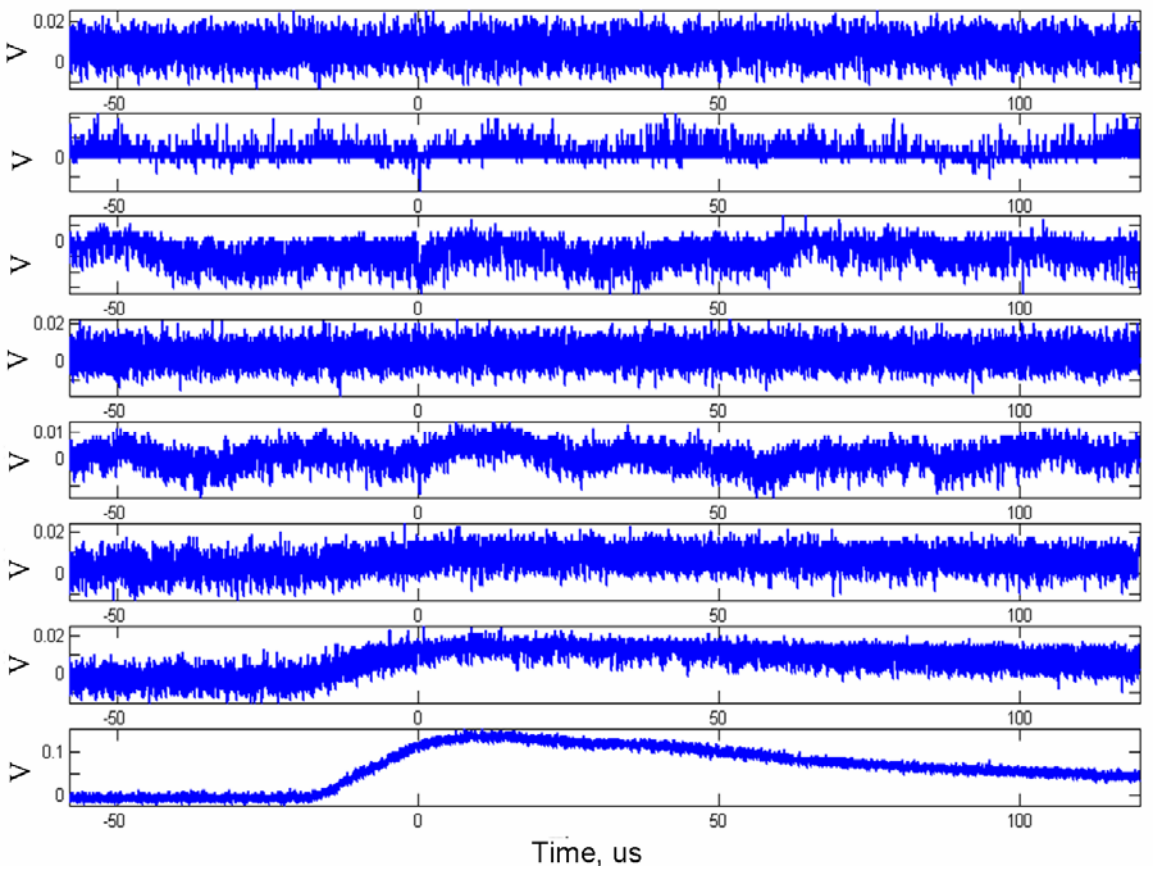

Figure 4-23 Event NAT0507 photodiode array record. The vertical scale indicates relative light intensity in terms of voltage at the oscilloscope input. The distance to the termination point is unknown, and therefore the height viewed by each sensor cannot be determined.

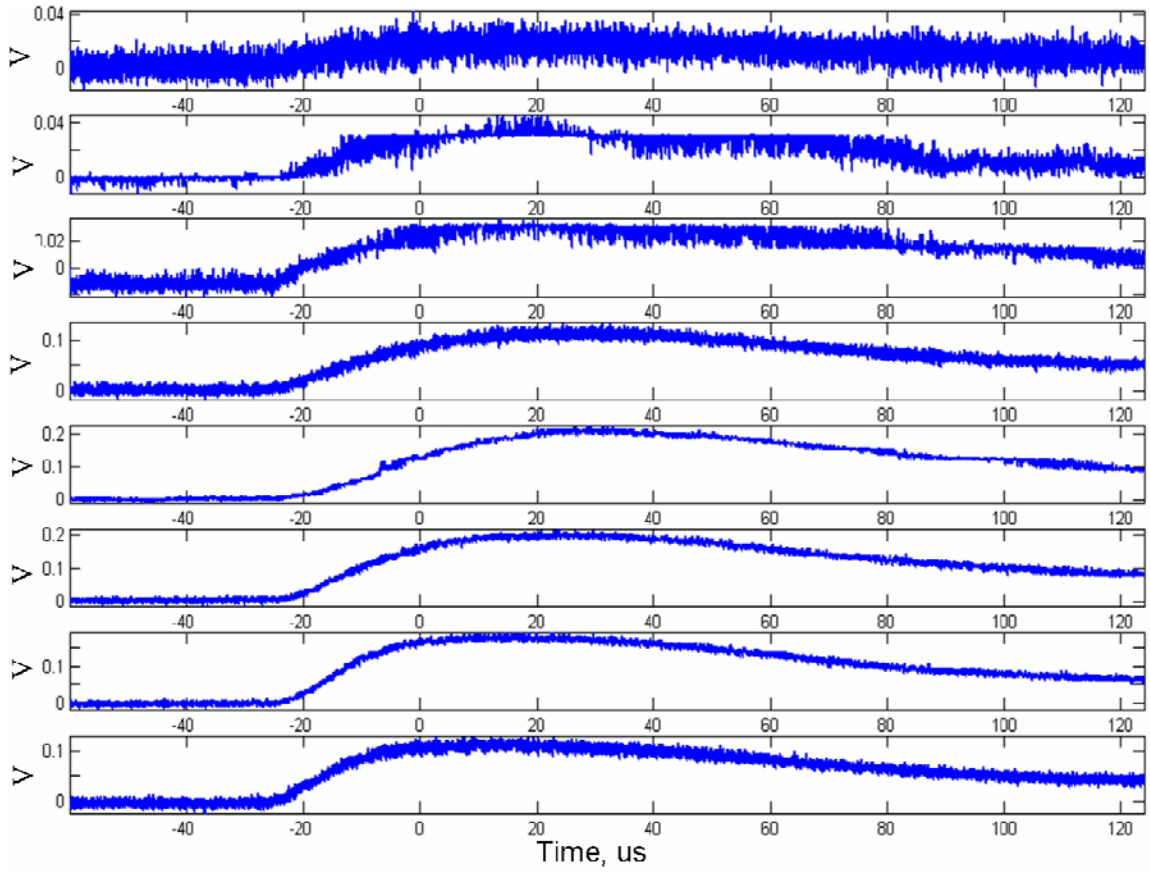

Figure 4-24 Event NAT0508 photodiode array record. The vertical scale indicates relative light intensity in terms of voltage at the oscilloscope input. The distance to the termination point is unknown, and therefore the height viewed by each sensor cannot be determined.

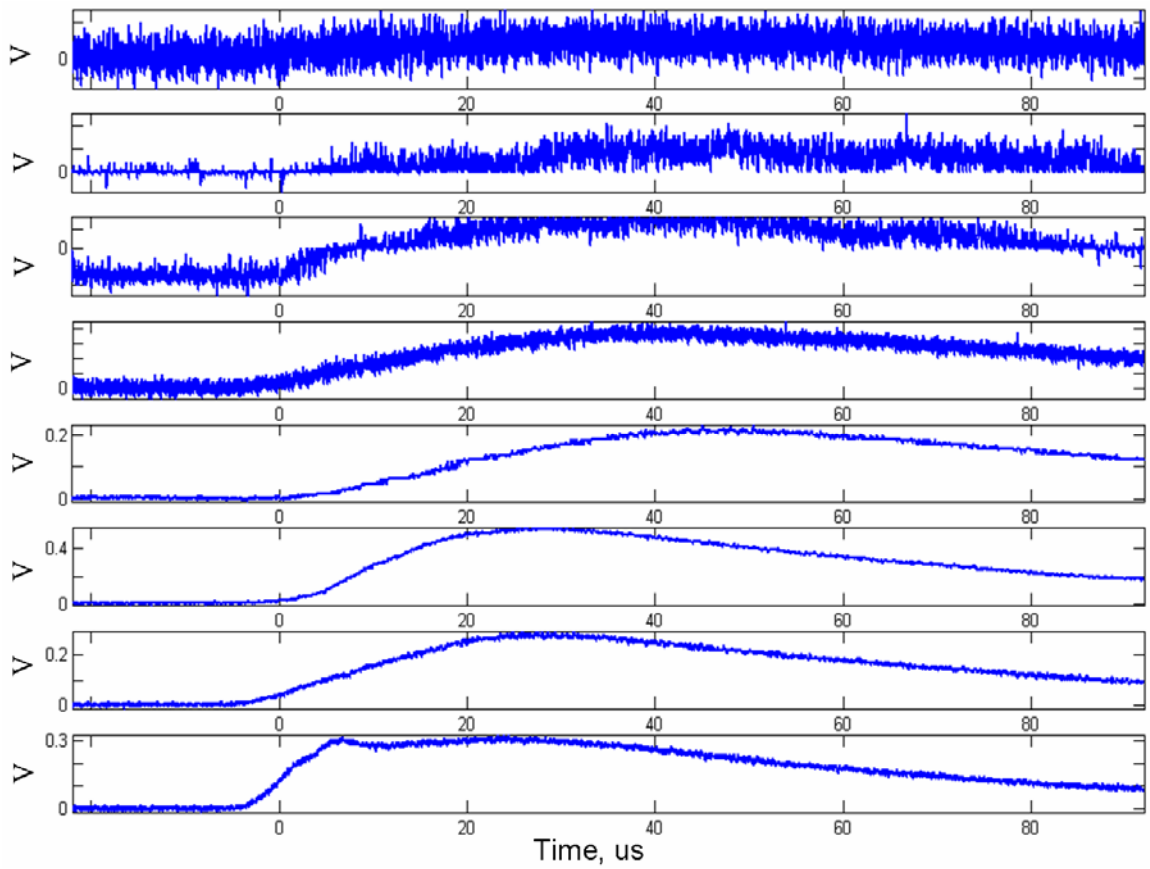

Figure 4-25 Event NAT0509, stroke 1, photodiode array record. The vertical scale indicates relative light intensity in terms of voltage at the oscilloscope input. The distance to the termination point is unknown, and therefore the height viewed by each sensor cannot be determined.

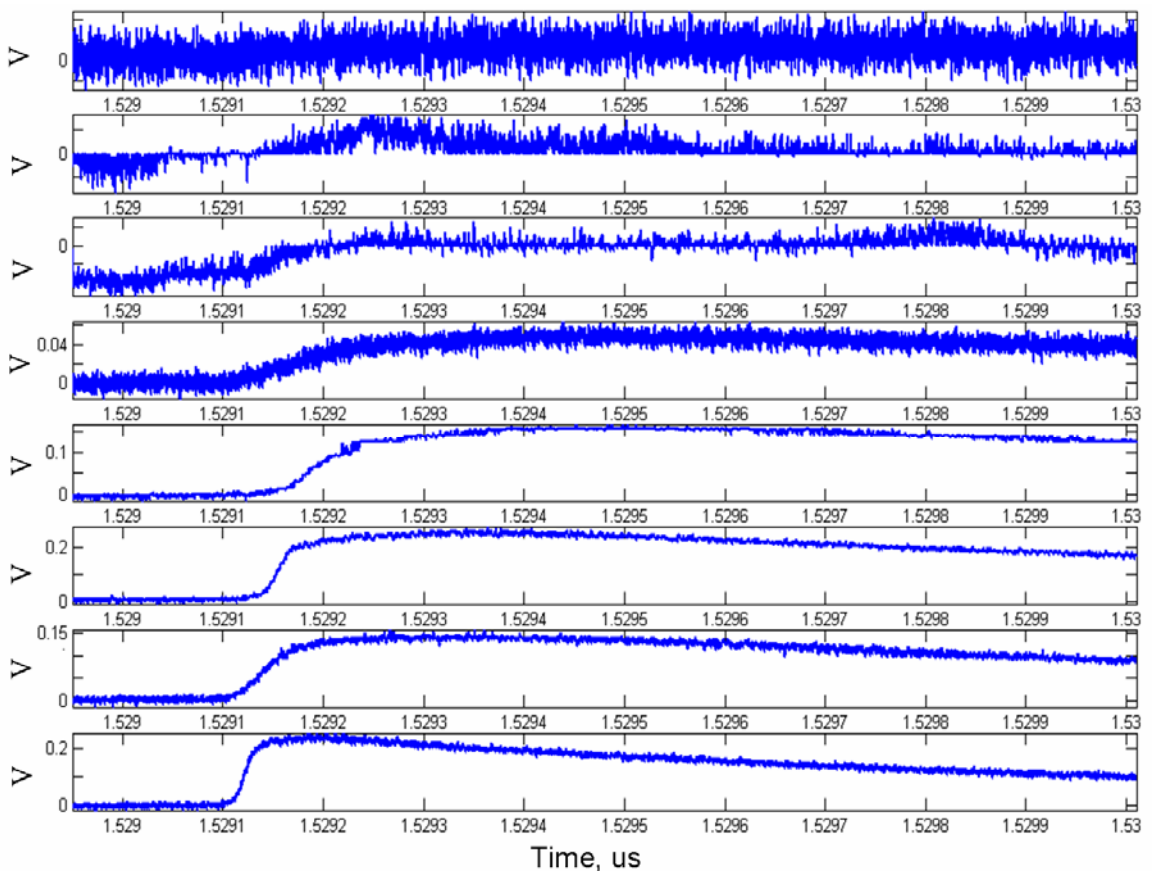

Figure 4-26 Event NAT0509, stroke 2, photodiode array record. The vertical scale indicates relative light intensity in terms of voltage at the oscilloscope input. The distance to the termination point is unknown, and therefore the height viewed by each sensor cannot be determined.

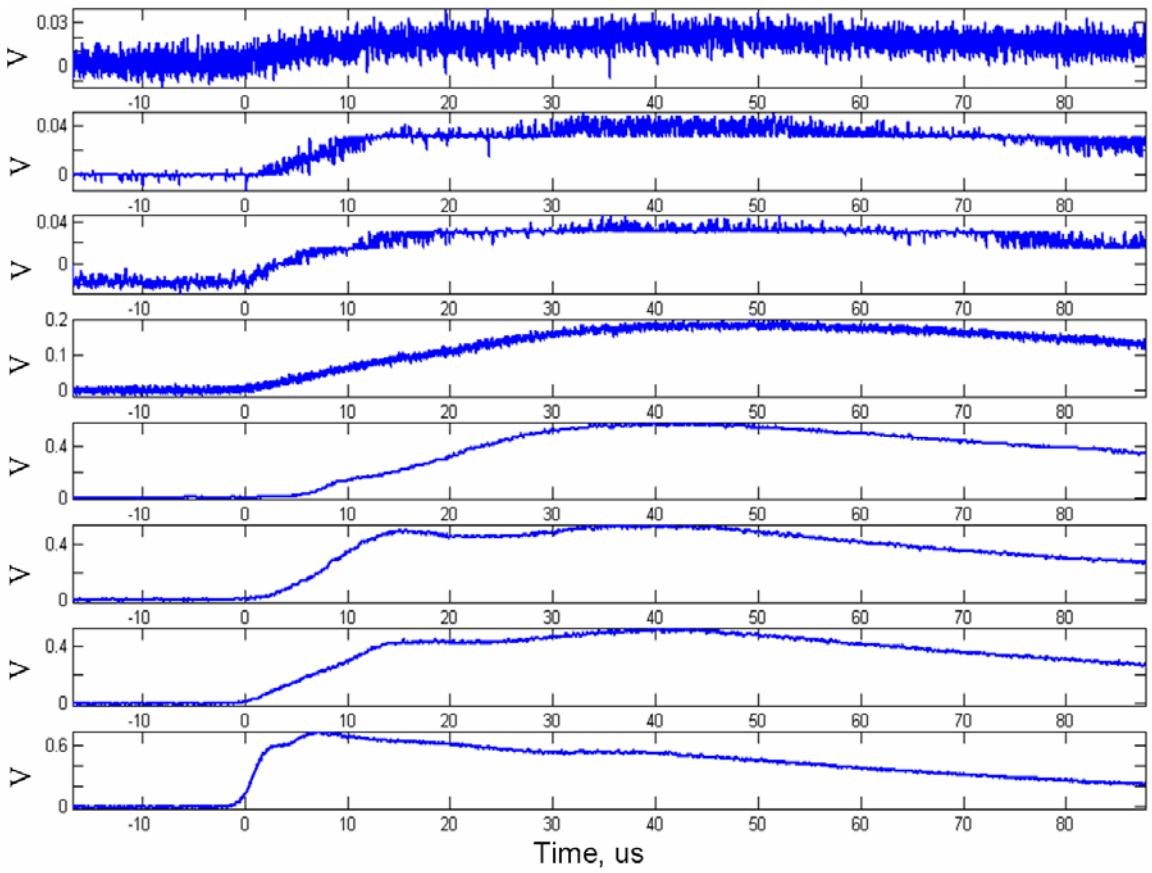

Figure 4-27 Event NAT0510 photodiode array record. The vertical scale indicates relative light intensity in terms of voltage at the oscilloscope input. The distance to the termination point is unknown, and therefore the height viewed by each sensor cannot be determined.

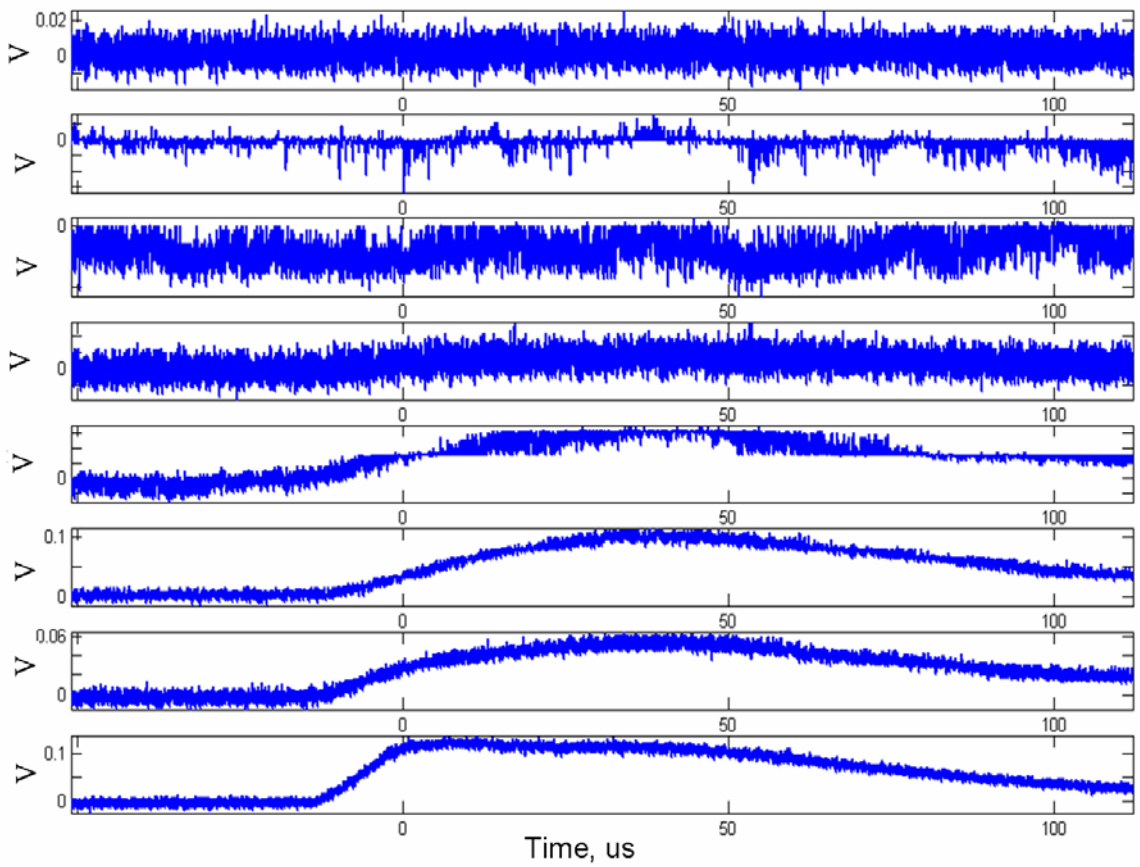

Figure 4-28 Event NAT0511 photodiode array record. The vertical scale indicates relative light intensity in terms of voltage at the oscilloscope input. The distance to the termination point is unknown, and therefore the height viewed by each sensor cannot be determined.

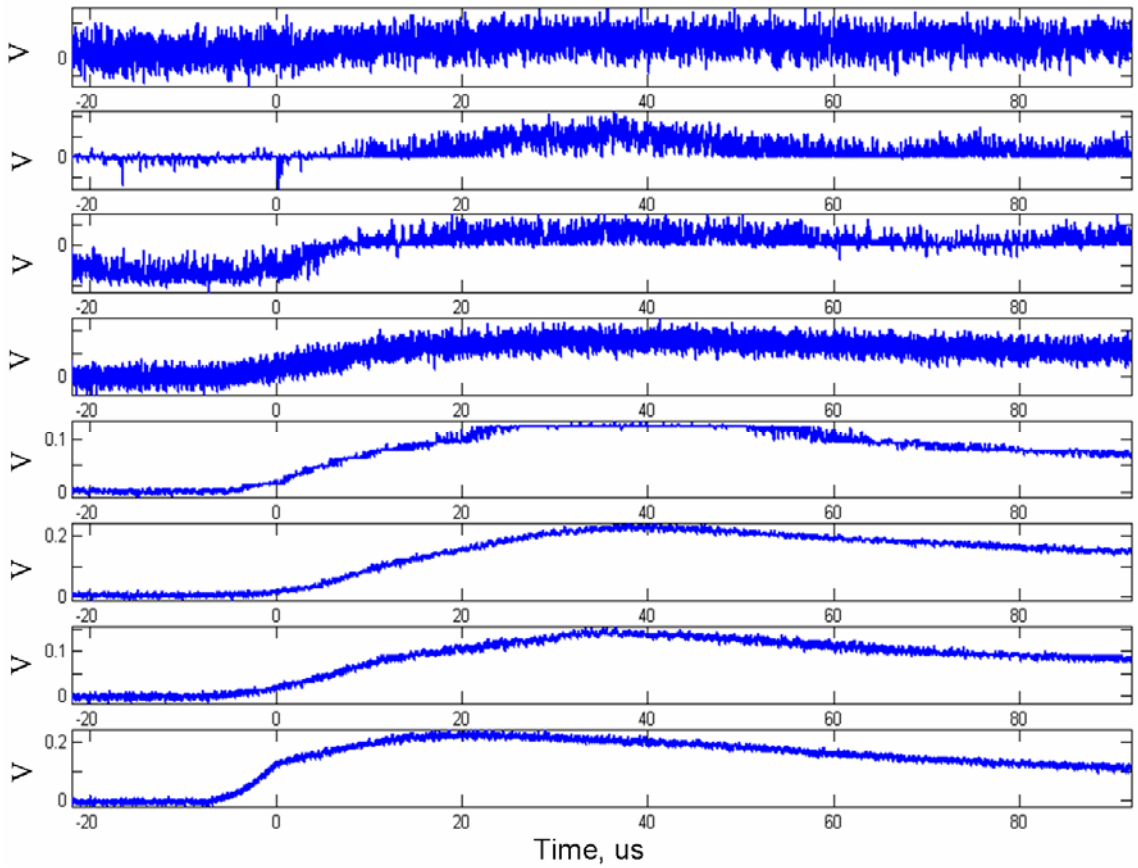

Figure 4-29 Event NAT0512, stroke 1, photodiode array record. The vertical scale indicates relative light intensity in terms of voltage at the oscilloscope input. The distance to the termination point is unknown, and therefore the height viewed by each sensor cannot be determined.

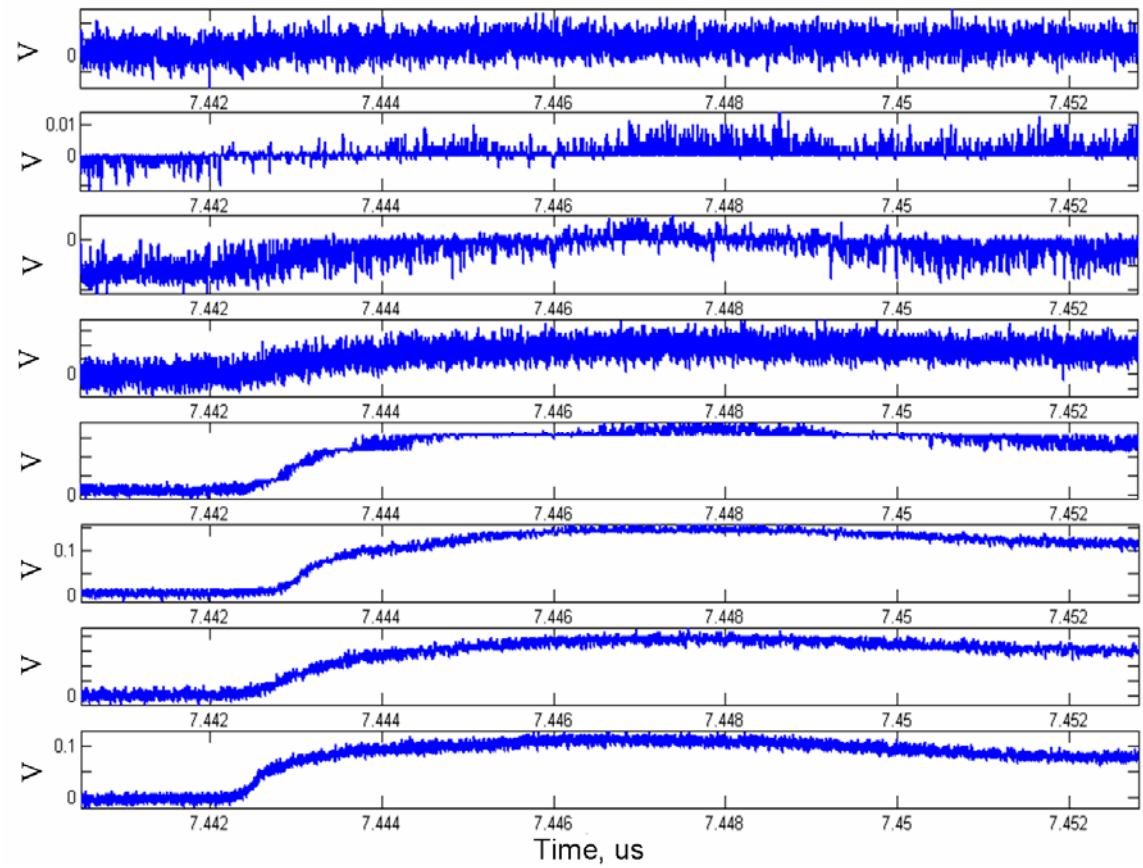

Figure 4-30 Event NAT0512, stroke 2, photodiode array record. The vertical scale indicates relative light intensity in terms of voltage at the oscilloscope input. The distance to the termination point is unknown, and therefore the height viewed by each sensor cannot be determined.

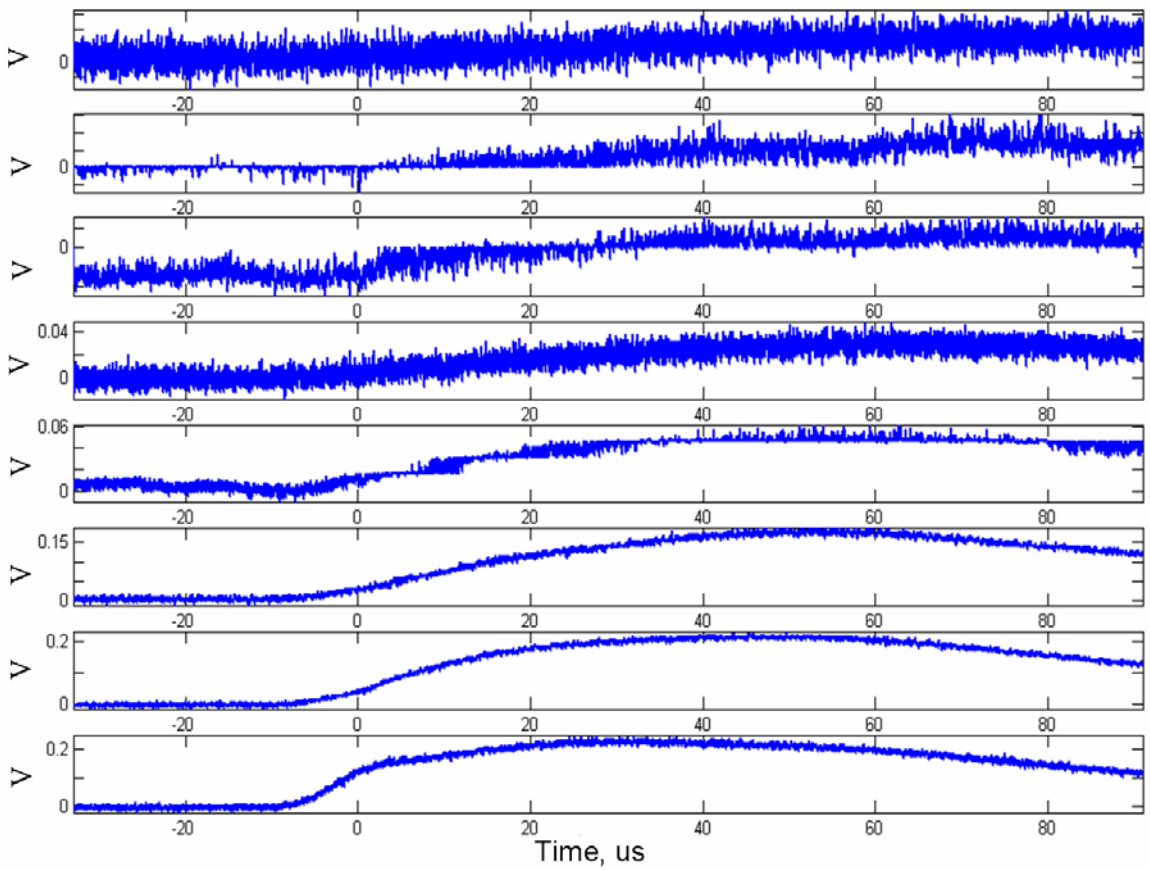

Figure 4-31 Event NAT0513 photodiode array record. The vertical scale indicates relative light intensity in terms of voltage at the oscilloscope input. The distance to the termination point is unknown, and therefore the height viewed by each sensor cannot be determined.

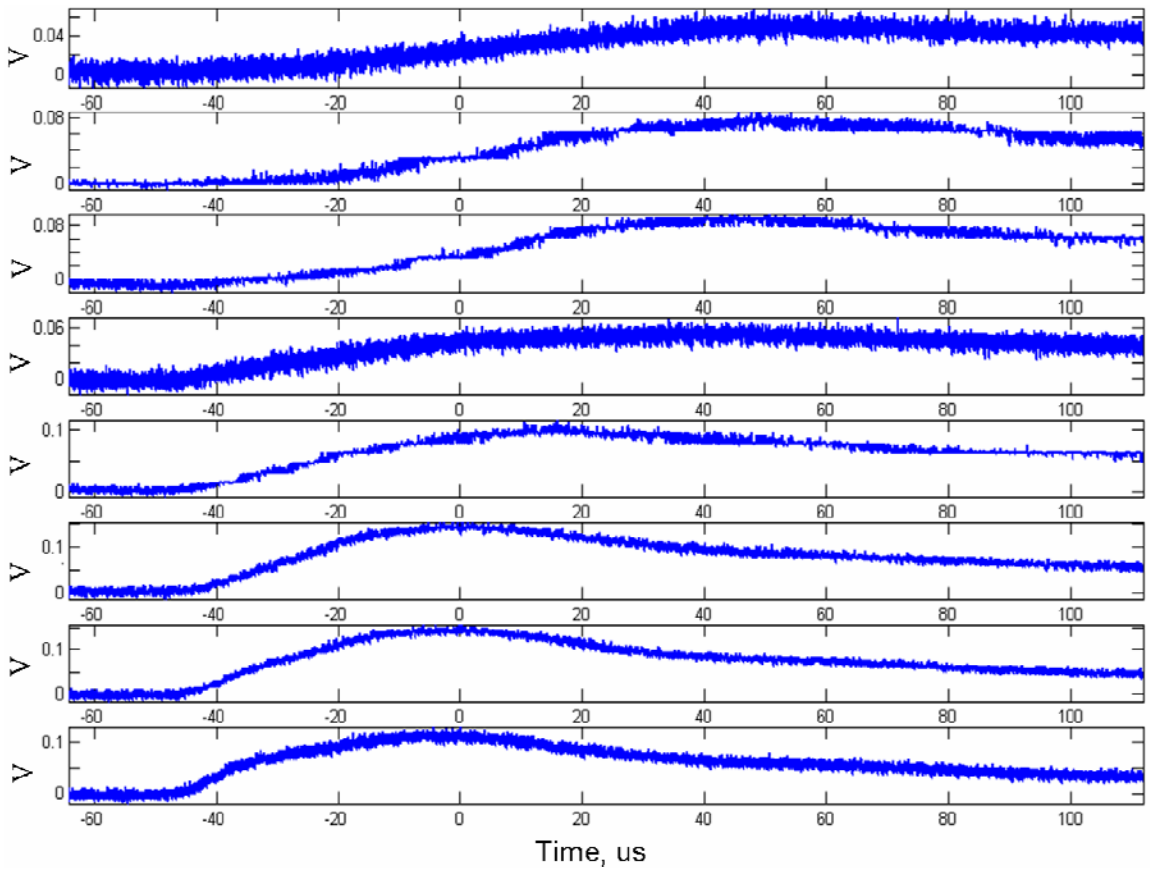

Figure 4-32 Event NAT0514 photodiode array record. The vertical scale indicates relative light intensity in terms of voltage at the oscilloscope input. The distance to the termination point is unknown, and therefore the height viewed by each sensor cannot be determined.

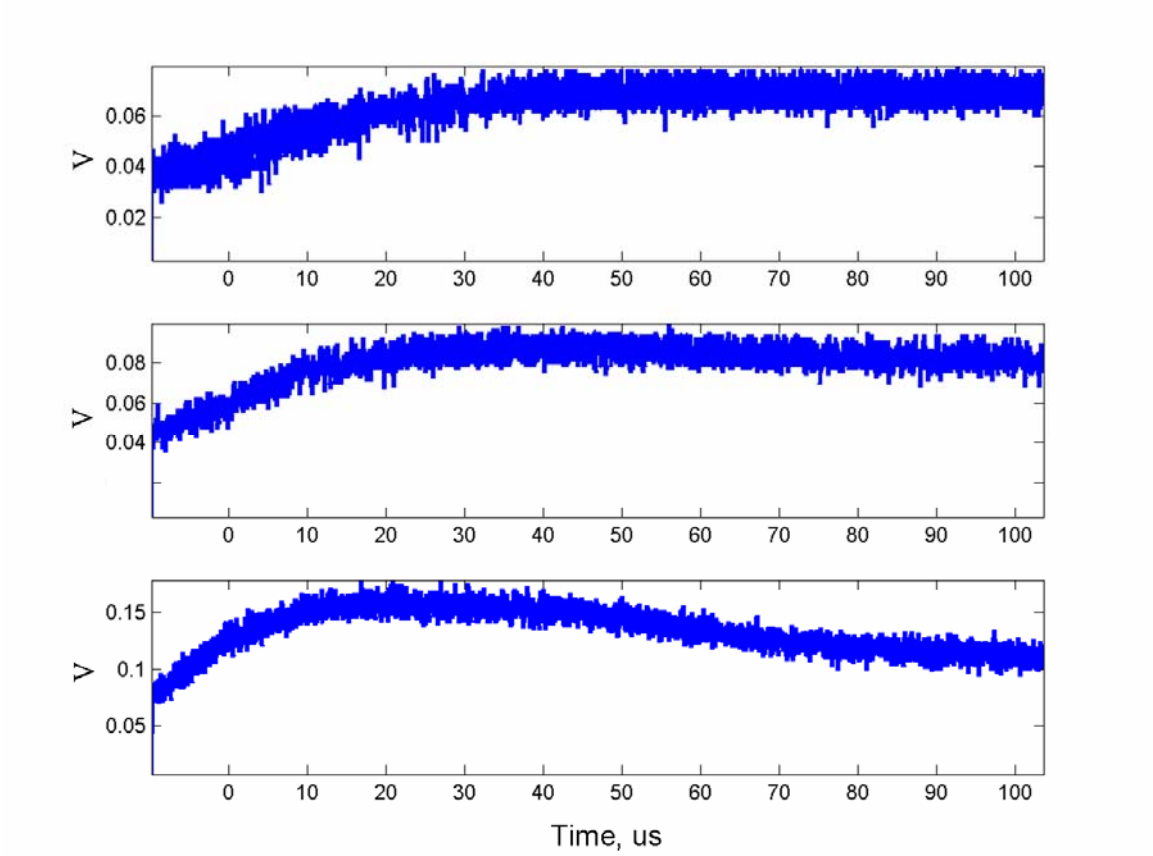

Figure 4-33 Event NAT0515 photodiode array record. The vertical scale indicates relative light intensity in terms of voltage at the oscilloscope input. The distance to the termination point is unknown, and therefore the height viewed by each sensor cannot be determined.

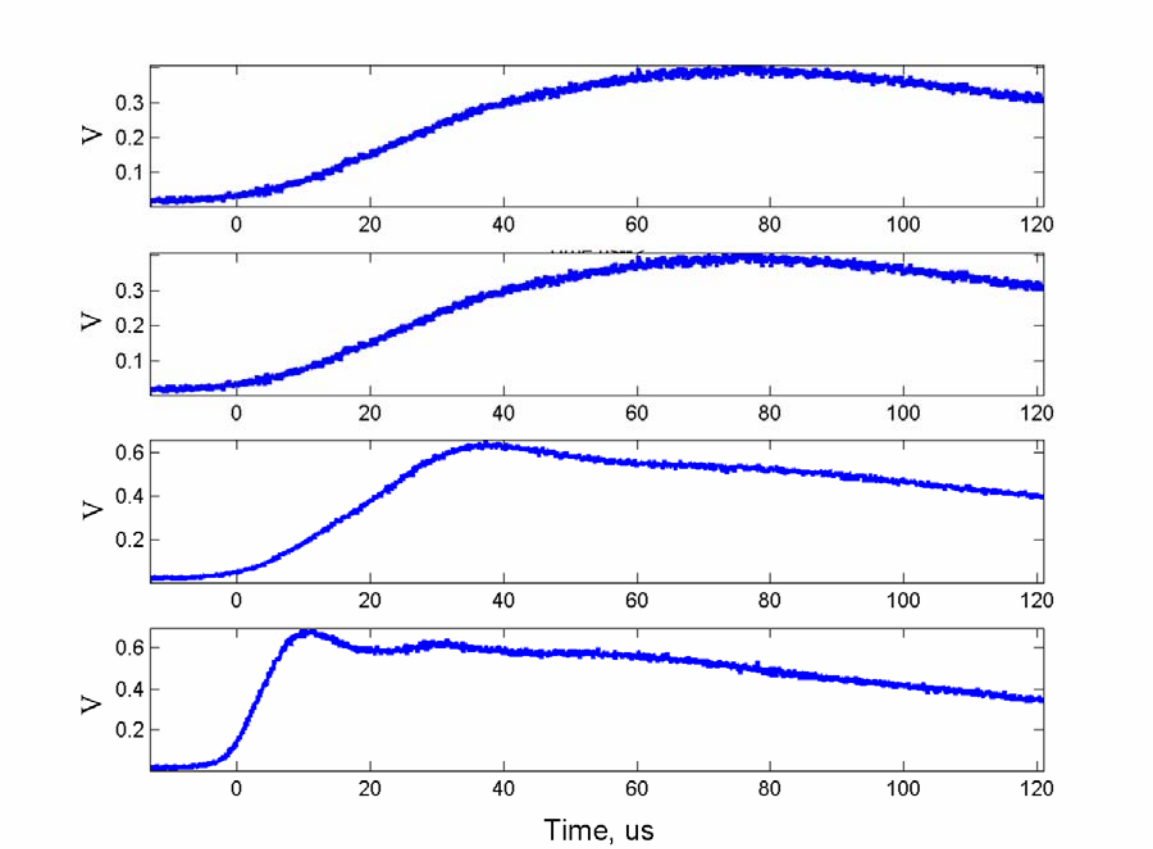

Figure 4-34 Event NAT0516 photodiode array record. The vertical scale indicates relative light intensity in terms of voltage at the oscilloscope input. The distance to the termination point is unknown, and therefore the height viewed by each sensor cannot be determined.

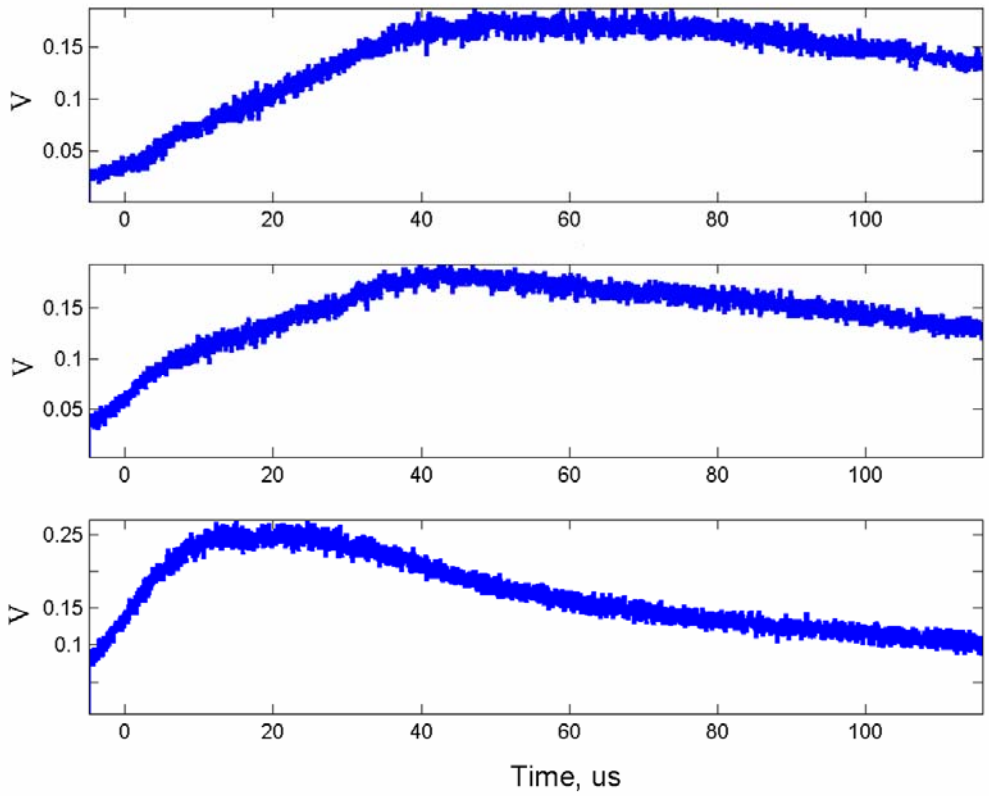

Figure 4-35 Event NAT0517 photodiode array record. The vertical scale indicates relative light intensity in terms of voltage at the oscilloscope input. The distance to the termination point is unknown, and therefore the height viewed by each sensor cannot be determined.

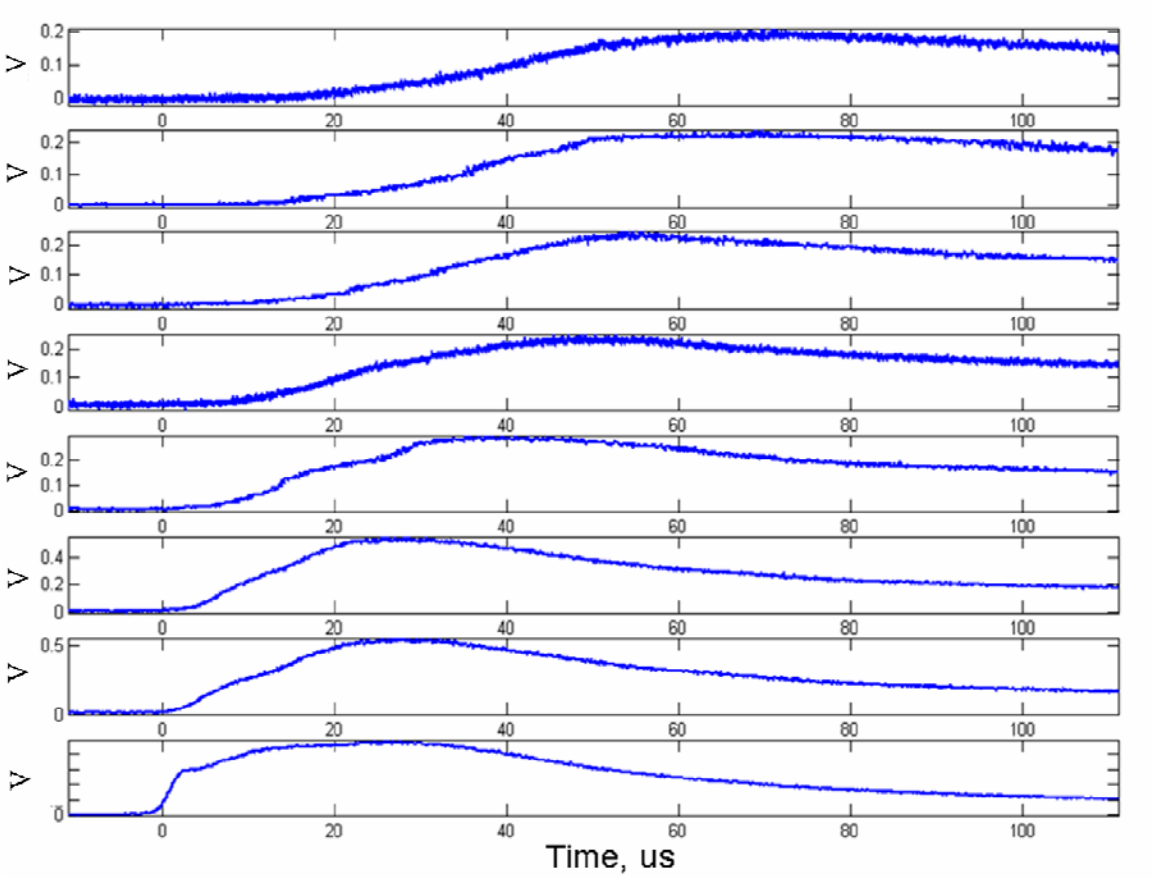

Figure 4-36 Event NAT0518 photodiode array record. The vertical scale indicates relative light intensity in terms of voltage at the oscilloscope input. The distance to the termination point

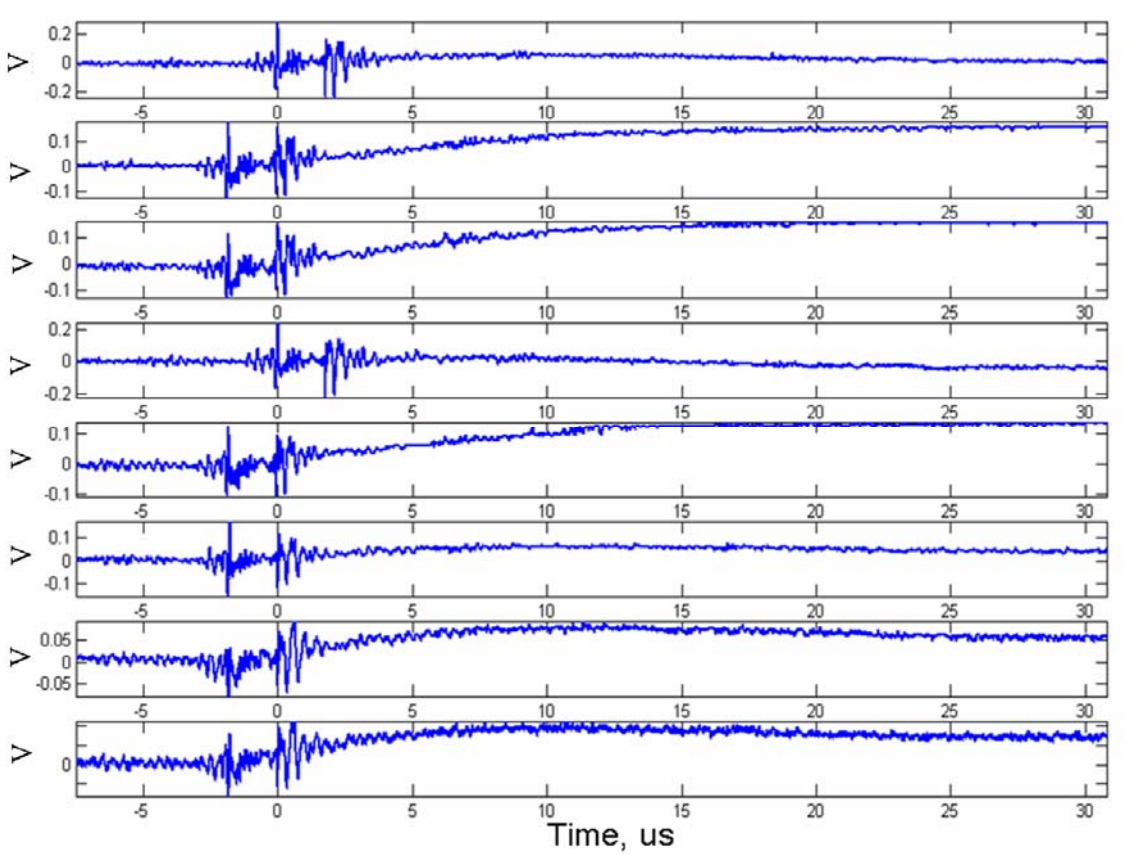

Figure 4-37 Event NAT0519 photodiode array record. The vertical scale indicates relative light intensity in terms of voltage at the oscilloscope input. The distance to the termination point is unknown, and therefore the height viewed by each sensor cannot be determined.

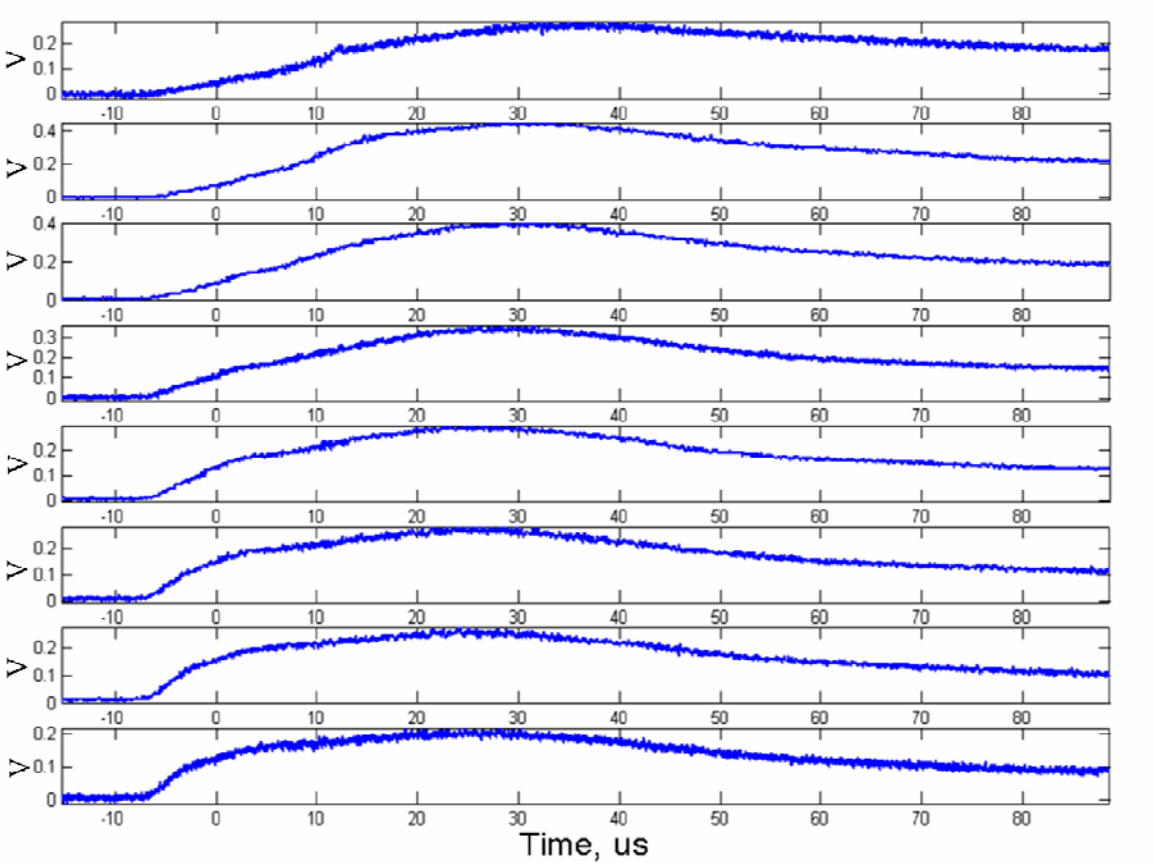

Figure 4-38 Event NAT0520 photodiode array record. The vertical scale indicates relative light intensity in terms of voltage at the oscilloscope input. The distance to the termination point is unknown, and therefore the height viewed by each sensor cannot be determined.

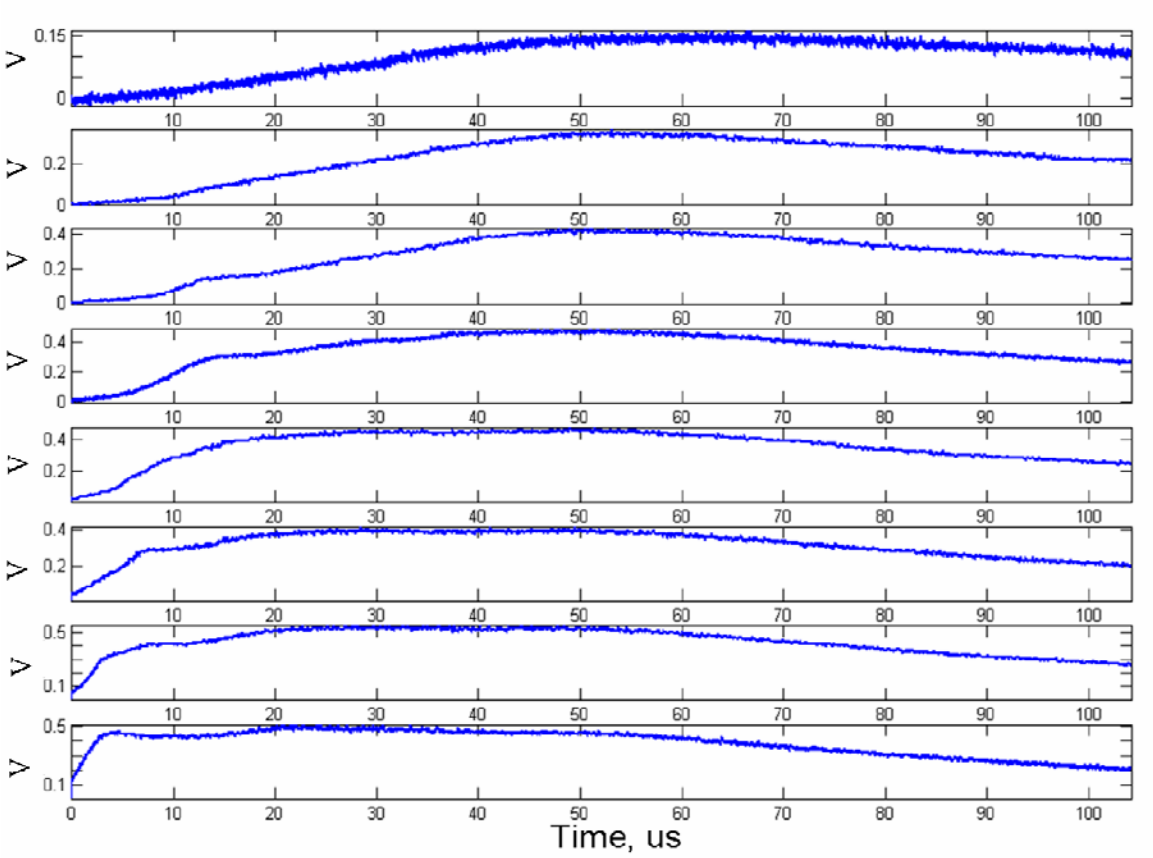

Figure 4-39 Event NAT0521 photodiode array record. The vertical scale indicates relative light intensity in terms of voltage at the oscilloscope input. The distance to the termination point is unknown, and therefore the height viewed by each sensor cannot be determined.

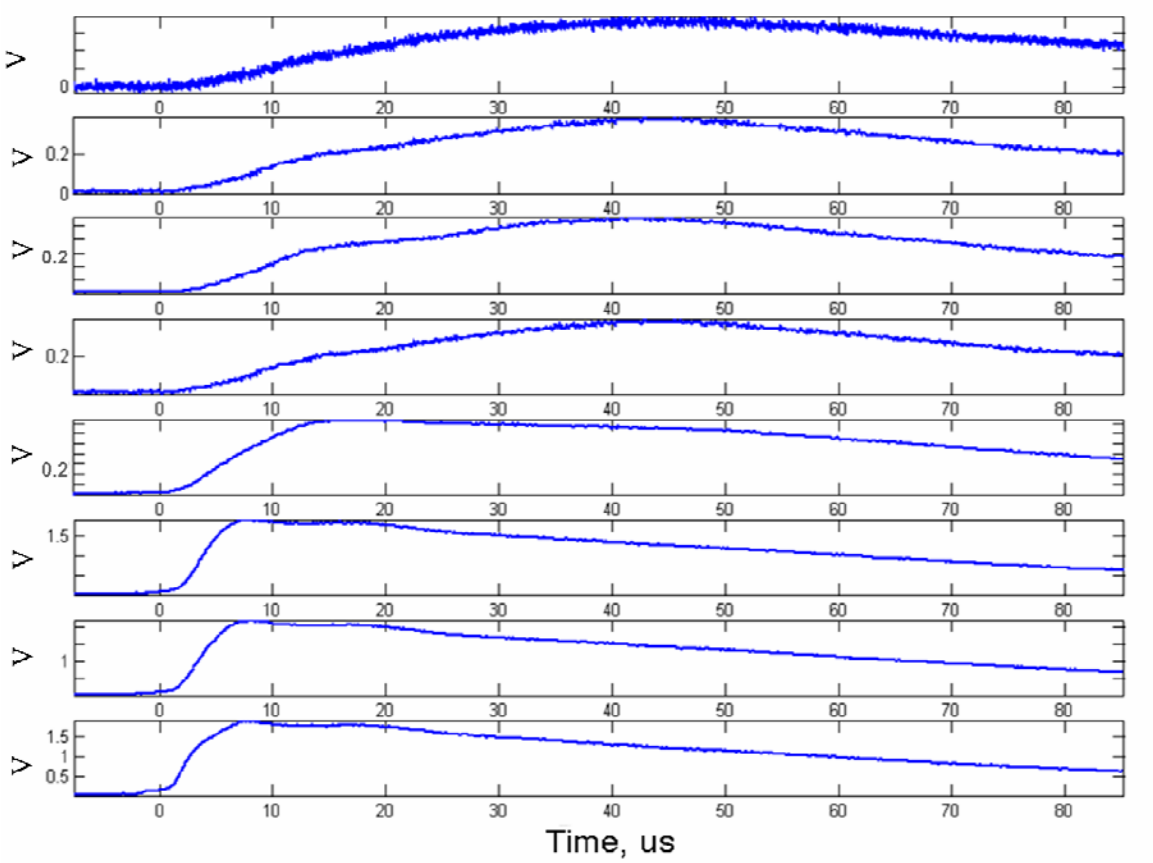

Figure 4-40 Event NAT0522 photodiode array record. The vertical scale indicates relative light intensity in terms of voltage at the oscilloscope input. The distance to the termination point is unknown, and therefore the height viewed by each sensor cannot be determined.

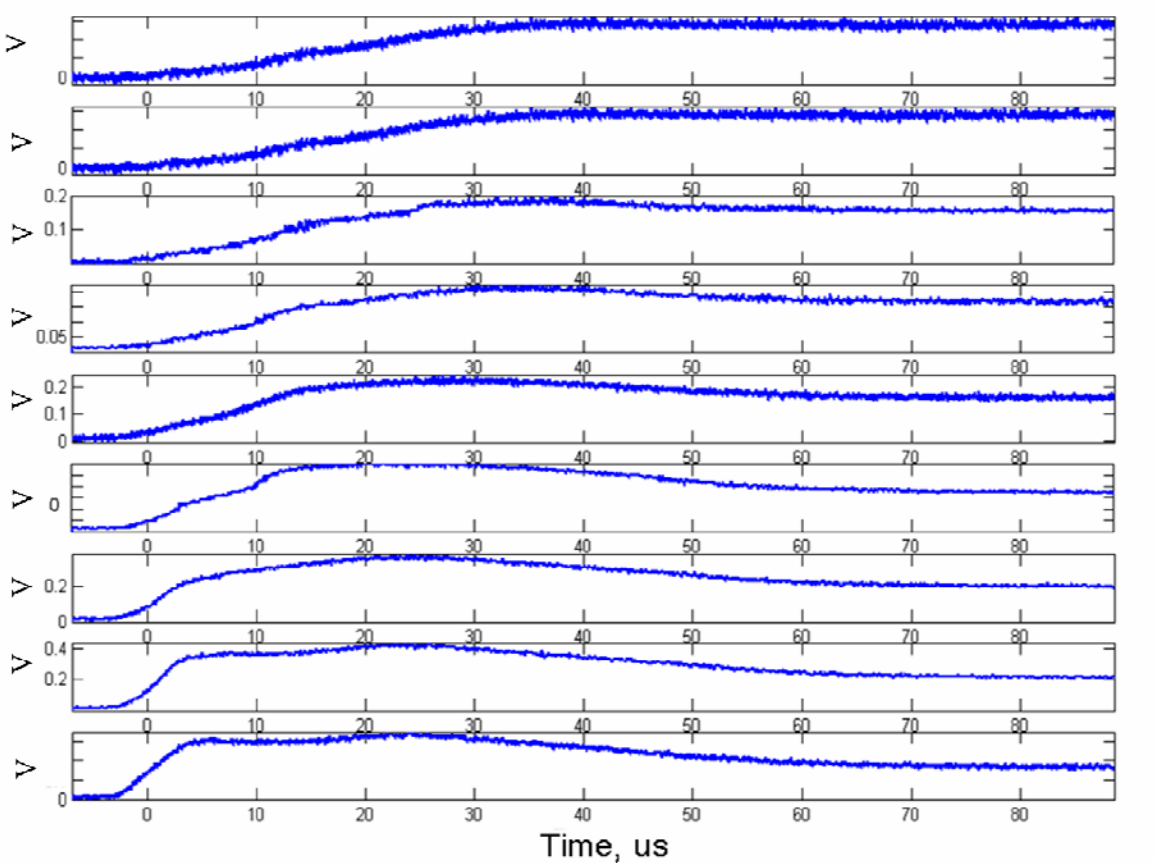

Figure 4-41 Event NAT0523, stroke 1, photodiode array record. The vertical scale indicates relative light intensity in terms of voltage at the oscilloscope input. The distance to the termination point is unknown, and therefore the height viewed by each sensor cannot be determined.

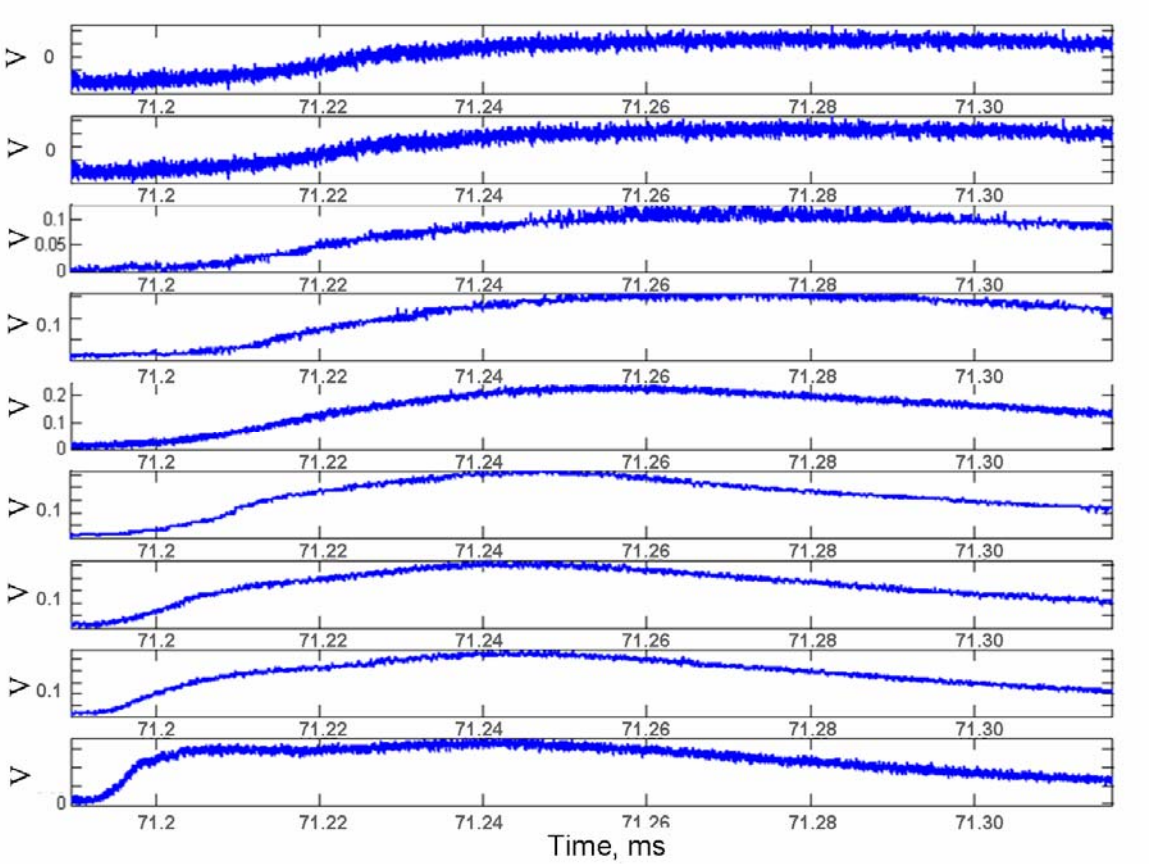

Figure 4-42 Event NAT0523, stroke 2, photodiode array record. The vertical scale indicates relative light intensity in terms of voltage at the oscilloscope input. The distance to the termination point is unknown, and therefore the height viewed by each sensor cannot be determined.

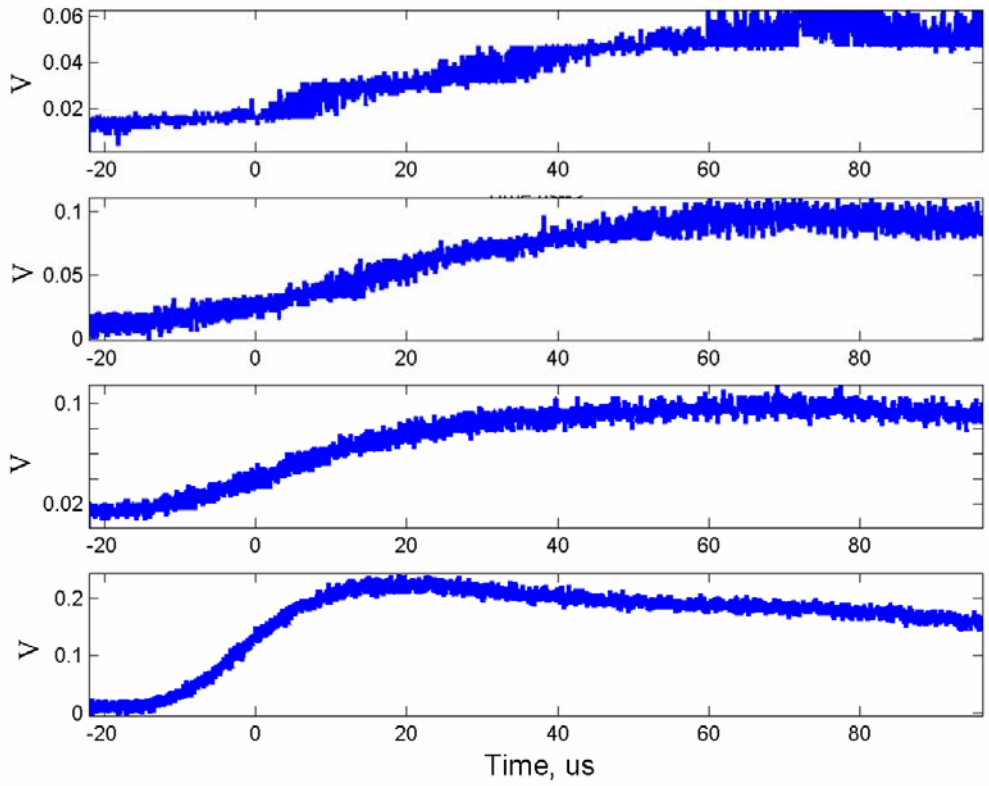

Figure 4-43 Event NAT0524 photodiode array record. The vertical scale indicates relative light intensity in terms of voltage at the oscilloscope input. The distance to the termination point is unknown, and therefore the height viewed by each sensor cannot be determined.

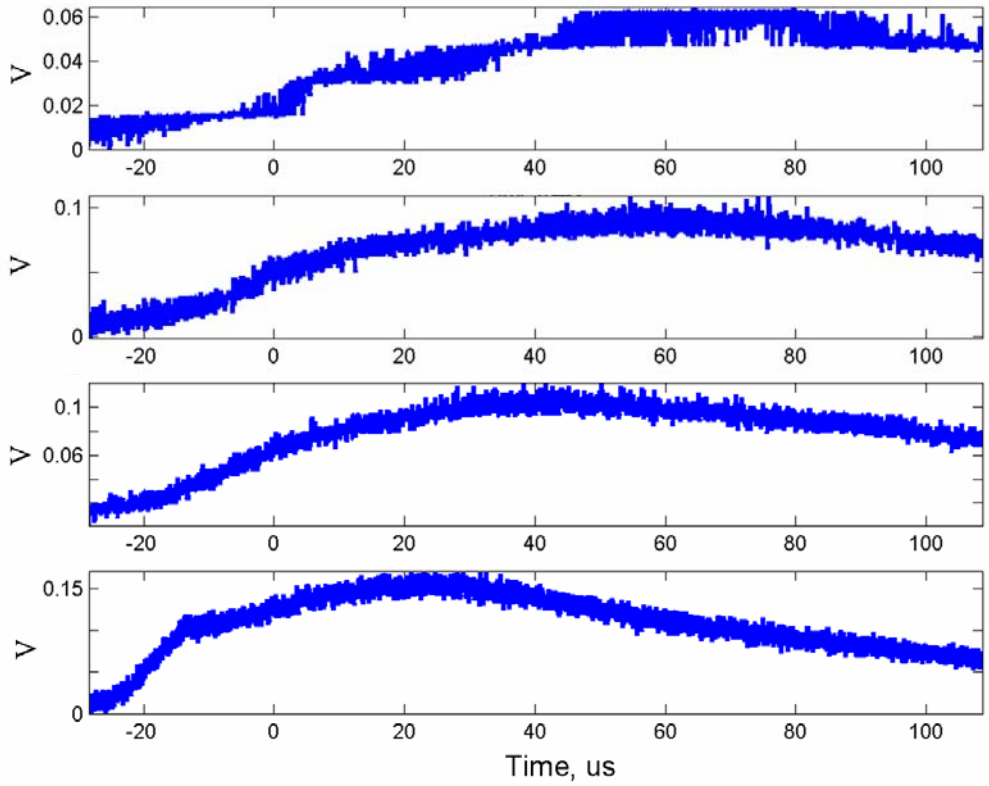

Figure 4-44 Event NAT0524 photodiode array record. The vertical scale indicates relative light intensity in terms of voltage at the oscilloscope input. The distance to the termination point is unknown, and therefore the height viewed by each sensor cannot be determined.

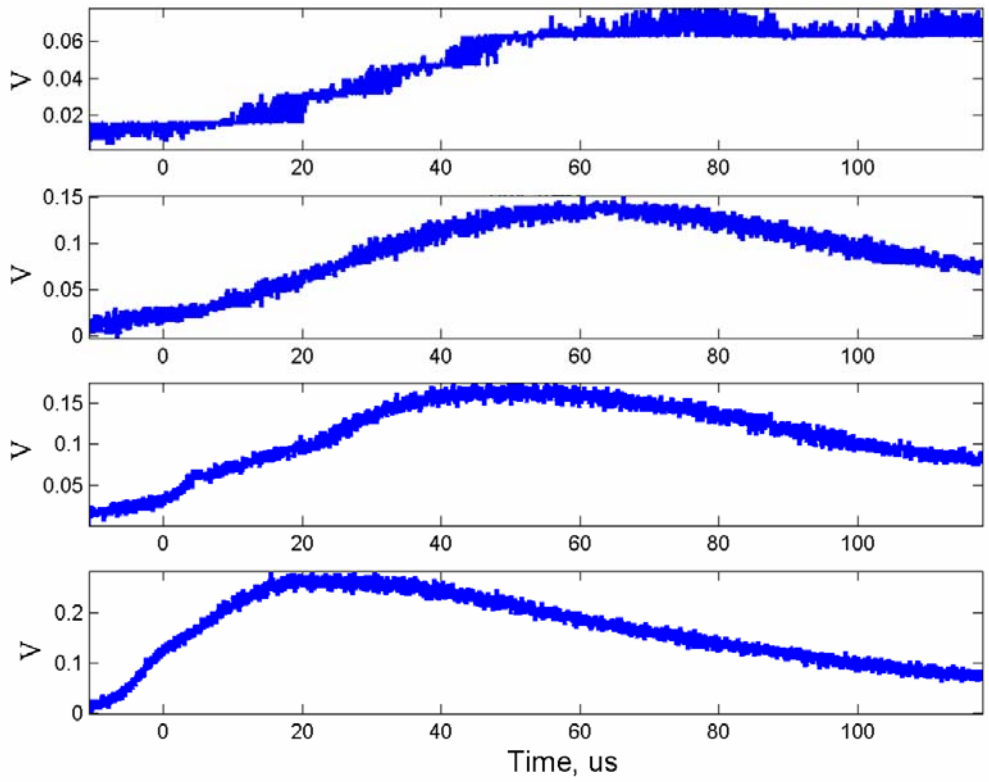

Figure 4-45 Event NAT0526 photodiode array record. The vertical scale indicates relative light intensity in terms of voltage at the oscilloscope input. The distance to the termination point is unknown, and therefore the height viewed by each sensor cannot be determined.

Table 4-1: Optical Dataset for Natural Lightning, Summer 2005

Flash ID	Date	Time (UTC)	Number of Return Strokes	Photo-diode Array	K004M
NAT0503	July.2,2005	23:29:13	1	Y	N
NAT0504	July.2,2005	23:33:24	1	Y	N
NAT0506	July.14,2005	21:05:37	1	Y	N
NAT0507	July.14,2005	21:06:05	1	Y	N
NAT0508	July.14,2005	21:13:14	1	Y	N
NAT0509	July.14,2005	21:14:02	2	Y	N
NAT05010	July.14,2005	21:14:23	1	Y	N
NAT05011	July.14,2005	21:16:17	1	Y	N
NAT05012	July.14,2005	21:16:59	2	Y	N
NAT05013	July.14,2005	21:28:47	1	Y	N
NAT05014	July.14,2005	21:31:25	1	Y	N
NAT05015	July.22,2005	23:13:58	1	Y	N
NAT05016	July.22,2005	23:19:46	1	Y	N
NAT05017	July.22,2005	23:20:40	1	Y	N
NAT05018	July.23,2005	23 :31 :24	1	Y	N
NAT05019	July.29,2005	16:56:57	1	Y	N
NAT05020	July.29,2005	17:06:24	1	Y	N
NAT05021	July.29,2005	17:21:56	1	Y	N
NAT05022	July.29,2005	17:23:58	1	Y	N
NAT05023	July.29,2005	17:25:22	2	Y	N
NAT05024	July.29,2005	17:54:46	1	Y	N
NAT05025	July.29,2005	17:59:42	1	Y	N
NAT05026	July.29,2005	18:01:11	1	Y	N

Table 4-2: Optical Dataset for Triggered Lightning, Summer 2005

Flash ID	Date	Time (UTC)	Number of Return Strokes	Photodiode Array	K004M
F0501	July 2,2005	23:22:46	1	YES	NO
F0503	July 2,2005	23:37:27	4	YES	NO
F0510	July 31,2005	20:03:33	1	YES	NO
F0512	July 31,2005	20:14:47	1	YES	NO
F0514	August 4,2005	18:44:38	1	YES	NO
F0517	August 4,2005	19:32:47	2	YES	NO
F0520	August 5,2005	21:24:50	1	YES	NO
F0521	August 5,2005	21:30:57	1	YES	NO

Table 4-3: Event F0501 and F0503 Slit Tube Angles and Viewed Heights

Sensor No.	Tube Angle, Degrees	Height Above Ground, m
9	32.6	451
8	27	360
7	24	314
6	19.1	245
5	13.6	171
4	9.3	116
3	6.8	84
2	3.6	44

Table 4-4: Event F0510, F0512, F0514, F0517, F0520 and F0521 Slit Tube Angles and Viewed Heights

Sensor No.	Tube Angle, Degrees	Height Above Ground, m
9	32.6	304
8	27	242
7	24	212
6	19.1	165
5	13.6	115
4	9.3	78
3	6.8	57
2	3.6	30

CHAPTER 5
DATA ANALYSIS AND RESULTS

5.1 Methodology

Olsen (2003) analyzed the return-stroke propagation speeds of five strokes from a seven stroke triggered lightning flash using a vertical array of photodiodes with a 2 ns sampling interval. The seven stroke lightning flash was triggered at Camp Blanding, Florida during the summer of 2003. Using the photodiode array, the one-dimensional speeds of return-stroke propagation were measured in the lowest 170 m of the lightning channel for five out of the seven return strokes, all of which transported negative charge to ground. The triggering rocket was launched from a mobile launcher located approximately 300 m from the photodiode array. At this distance, each of the diodes was able to view a vertical section of lightning channel approximately 1 m in length. Various methods to determine the reference points were explored, and the speeds were observed to vary by an order of magnitude depending on chosen method. Speeds computed using these different reference points are presented in Table 2.1.

Usually, reference points to be tracked on the return-stroke waveforms are chosen to represent as closely as possible the time at which the wave-front first passes the viewed area. The choice of the reference points affects the measured speed, as the shape and the amplitude of the waveform change as it propagates up the channel. Thus it is necessary to select a reference point that is identifiable in all the waveforms and is independent of these waveform characteristics. One reasonable method was to detect the time when the waveform reached 10% of the maximum optical intensity level (Olsen, 2003). This area of initial deflection is usually covered with noise and so was not considered by Olsen (2003), whereas, the 20% of the peak optical intensity is less affected by noise and was hence was chosen as one of the reference points. The 90% and the maximum peak optical intensity time points have also been chosen as reference points with the

drawback that, these points occur towards the peak of the waveform, usually characterized by slower rise times (more affected by dispersion). As a result, when these points were chosen as references the speeds computed were much lower than expected. Another reference point was located at the peak of the time derivative of the rising portion of the return-stroke waveform. Since the 20% point is apparently, the least affected by either waveform noise or dispersion, only the 20% point was used as a reference when computing the return stroke propagation speed profile along the lightning channel. The 10%, 90%, maximum peak intensity, and light intensity derivative peak points were used to only compute the overall return-stroke propagation speeds.

Olsen (2003) also used another technique called the slope-intercept method, intended to determine the reference point for the return-stroke reasonably well even in the presence of noise. As illustrated in the Figure 5-1, a straight, horizontal line was drawn on the waveform. The vertical level of this line was chosen to pass through the center of the noise amplitude in the region of minimum signal intensity just prior to the return-stroke waveform. In waveforms which exhibit leader signatures, the region of lowest signal intensity between the leader peak and return stroke peak (not shown in Figure 5-1) was chosen to be the region of minimum signal intensity. This line was labeled as the "Reference Level Line". Next, a slanted line was drawn parallel and congruent with the slope of the return-stroke rising portion, approximating as closely as possible the mean of the waveform front over as long an interval as possible. This line is labeled "Average Slope Line" in Figure 5-1. The intersection of these two lines, marked "R.S Beginning" was taken to be the beginning of the return stroke waveform for each segment of the channel.

5.2 Calibration of the Data Analysis Tools

In order to "calibrate" the analysis tools that were used in the analysis of the summer 2005 data, I re-computed the overall return stroke speeds computed by Olsen et al. (2003) for F0336.

Table 5-1 shows the percentage errors relative to the return-stroke propagation speeds previously computed by Olsen et. al. (2003). Most of the errors are within 10 percent, with a few exceptions. Also, it is important to note that the errors were apparently random in nature, which confirms the accuracy (absence of bias) of the data analysis tools used in this thesis. A systematic error in the analysis would often be either always positive or always negative. Figure 5-2 shows that the errors found do not follow such patterns, thus suggesting the absence of systematic errors.

5.3 Filters Used for the Summer 2005 Data Analysis

A typical lightning light waveform is noisy, which makes the analysis of data for the purpose of return stroke speed measurements very difficult. Therefore, filtering the lightning data was essential Also, as seen in the spectrum of a typical lightning return stroke light waveform shown in Figure 5-3; there is not much useful information above 12 MHz or so. This corresponds to a rise time of 30 nanoseconds, whereas return stroke waveforms have rise times typically of the order a few microseconds. The spectrum of all light waveforms considered here was similar to that shown in Figure 5-3. Hence, filtering out information above 12 MHz did not affect the rise time portion of any of the analyzed return-strokes. The following three filters were used for the lightning data analysis, applied depending on noisiness of the waveform.

A moving average filter with the window size of 11 samples was used to filter F0336, stroke 1 (captured at a height of 7 m above termination, Olsen (2003)) lightning waveform as illustrated in Figure 5-4.The unfiltered and filtered waveforms are compared to check for any changes in the initial rising portion of the return stroke. As one can see, the moving average filter works well in averaging out the noise and providing a smooth waveform, while preserving all the salient features of the waveform.

A 47th order low pass filter (Filter 1) with the stop band (the filter response goes from 0 db attenuation to 98 db attenuation) extending from 3.75 MHz to12 MHz was used to filter same F0336, stroke 1 lightning waveform described above. The filtered and unfiltered waveforms were overlaid to nullify the gain provided by the filter and to check for faithful reproduction of salient feature of the initial rising portion of the return stroke waveform, as shown in Figure 5-5. This filter was used whenever the moving average filter failed to provide a sufficiently smooth waveform.

A 1011th order low pass filter (Filter 2) with a stop band extending from 1 MHz to 1.75 MHz was also used to filter F0336, stroke 1 lightning waveform. This filter was used only for smoothing especially noisy waveforms, an example of which is shown in Figure 5-6. The filtered and unfiltered waveforms in all the cases were overlaid on top of each other to check the quality of filtering.

When using the above mentioned low pass filters, I scaled down all the filtered waveforms to the original amplitude to nullify the gains and shifted to nullify the delays caused by the respective filters.

5.4 Results of the Summer 2005 Data Analysis

In this section, the return-stroke propagation speeds of all the 2005 triggered lightning strokes are presented. Light profiles of a total of 11 triggered lightning strokes were recorded on the LeCroy DSOs and those of a total of 8 strokes were recorded on both LeCroy DSOs and Yokogawa oscilloscopes.

The overall return-stroke speeds were computed only using LeCroy data because of their higher sampling rate of 500 MHz, which corresponds to 2 nanoseconds between data points. The Yokogawa DSO has a sampling rate of 10 MHz, which corresponds to a time interval of 100 nanoseconds between data points. As explained in Chapter 3, although the LeCroy Scope 6

trigger timing was somewhat uncertain, this leads to an inaccuracy of not more than 6% in the overall return-stroke speeds in the case of F0517, Stroke 1, F0517, Stroke 2 and F0521, Stroke 1. The LeCroy data were also used to compute the return-stroke speed profiles as a function of height. Yokogawa data were compared to the LeCroy data.

In computing return-stroke speeds at different heights using the 2005 LeCroy data, the following two groups of channels were considered for computing two separate speed profiles. Sensor 2 to Sensor 3 (44 m to 84 m), Sensor 3 to Sensor 4 (84 m to 116 m), Sensor 4 to Sensor 6 (116 m to 245 m), and Sensor 6 to Sensor 9 (245 m to 451 m) comprised one profile set. Sensor 5 to Sensor 7 (171 m to 314 m) and Sensor 7 to Sensor 8 (314 m to 360 m) comprised the second profile set. These two profiles were then overlapped onto each other for comparison.

5.4.1 Event F0501

Event F0501 was triggered on July 2, 2005 at 23:22:46 UTC. One stroke was observed for this event on the photodiode array following the initial stage The overall return-stroke speeds for this event using the different reference points explained in section 5-1 is given in Table 5-2. The return-stroke speeds at various heights, measured using LeCroy data for this event are given in Table 5-3. The speed profile is shown in Figure 5-7 with the 20% point as reference and in Figure 5-8 with the slope intercept point as the reference. The profiles shown in Figures 5-7 and 5-8 in blue are based on data from channels 2,3,4,6, and 9, whereas the overlaid profiles in red are based on data from channels 5, 7, and 8. The average of two profiles is given in Table 5-4. The average speed profile is shown in Figure 5-9 with the 20% point as reference and in Figure 5-10 using the slope intercept point as reference. The average of these two profiles is given in Table 5-5 and in Figure 5-11.

The return-stroke speeds at various heights, measured using Yokogawa data for this event are given in Table 5-6. The corresponding speed profiles are shown in Figure 5-12 using the 20%

point as reference and in Figure 5-13 using the slope intercept point as reference. The average of these two profiles is given in Table 5-7 and the corresponding average return-stroke speed profile based on Yokogawa data is shown in Figure 5-14.

Table 5-8 gives the leader propagation speeds at various heights based on the LeCroy data and computed using the 20% point as reference. In contrast with the return-stroke speeds, leader speeds were estimated using all LeCroy channels without segregating them into two groups .We notice that for the same event, the leader propagation speeds are an order of magnitude lower than the observed two-dimensional return-stroke speeds.Table 5-9 gives the return stroke optical risetimes at various heights for event F0501, Stroke 1, recorded by the LeCroy oscilloscope.

5.4.2 Event F0503

Event F0503 was triggered on July 2, 2005 at 23:37:27 UTC. Four strokes were observed for this event on the photodiode array following the initial stage. The segments which were recorded correspond to strokes 1, 2, 3 and 4. The overall return-stroke speeds for this event using the different reference points explained in Section 5-1 are given in Table 5-10. The return-stroke speeds at various heights, measured using LeCroy data for event F0503, stroke 1 are given in Table 5-11. The speed profile is shown in Figure 5-16 with the 20% point as reference and in Figure 5-17 with the slope intercept point as the reference. The profiles shown in Figures 5-16 and 5-17 in blue are based on data from channels 2, 3, 4, 6, and 9, whereas the overlaid profiles in red are based on data from channels 5, 7, and 8. The average of two profiles is given in Table 5-12. The corresponding average speed profile is shown in Figure 5-18 with the 20% point as reference and in Figure 5-19 using the slope intercept point as reference using LeCroy data. The average of these two profiles is given in Table 5-13 and in Figure 5-19.

The return-stroke speeds at various heights, measured using Yokogawa data for this event are given in Table 5-14. The corresponding speed profiles are shown in Figure 5-20 using the

20% point as reference and in Figure 5-21 using the slope intercept point as reference. The average of these two profiles is given in Table 5-15. The corresponding average return-stroke speed profile based on Yokogawa data is shown in Figure 5-22. Table 5-16 gives the return stroke optical risetimes at various heights for the event F0503, Stroke 1, recorded by the LeCroy oscilloscope.

The return-stroke speeds at different heights, measured using LeCroy data for event F0503, stroke 2 are given in Table 5-17. Te speed profile is shown in Figure 5-25 with the 20% point as reference and in Figure 5-26 with the slope intercept point as the reference. The profiles shown in Figures 5-25 and 5-26 in blue are based on data from channels 2, 3, 4, 6, and 9, whereas the overlaid profiles in red are based on data from channels 5, 7, and 8. The average of two profiles is given in Table 5-18. The average speed profile is shown in Figure 5-27 with the 20% point as reference and in Figure 5-28 using the slope intercept point as reference using LeCroy data. The average of these two profiles is given in Table 5-19 and in Figure 5-27.

The return-stroke speeds at various heights, measured using Yokogawa data for this event are given in Table 5-20. The corresponding speed profiles are shown in Figure 5-28 using the 20% point as reference and in Figure 5-29 using the slope intercept point as reference. The average of these two profiles is given in Table 5-21. The corresponding average return-stroke speed profile based on Yokogawa data is shown in Figure 5-30.

Table 5-22 gives the leader propagation speeds at various heights based on the LeCroy data and computed using the 20% point as reference. In contrast with the return-stroke speeds, leader speeds were estimated using all LeCroy channels without segregating them into two groups. We notice that for the same event, the leader propagation speeds are an order of magnitude lower than the observed two-dimensional return-stroke speeds. Table 5-23 gives the

return stroke optical risetimes at various heights for event F0503, Stroke 2, recorded by the LeCroy oscilloscope.

The return-stroke speeds at different heights, measured using LeCroy data for event F0503, stroke 3 are given in Table 5-24. The speed profile is shown in Figure 5-31 with the 20% point as reference and in Figure 5-32 with the slope intercept point as the reference. The profile shown in Figures 5-31 and 5-32 in blue are based on data from channels 2, 3, 4, 6, and 9, whereas the overlaid profiles in red are based on data from channels 5, 7, and 8. The average of two profiles is given in Table 5-25. The average speed profile is shown in Figure 5-33 with the 20% point as reference and in Figure 5-34 using the slope intercept point as reference using LeCroy data. The average of these two profiles is given in Table 5-26 and in Figures 5-35.

The return-stroke speeds at various heights, measured using Yokogawa data for this event are given in Table 5-26. The corresponding speed profiles are shown in Figure 5-36 using the 20% point as reference and in Figure 5-37 using the slope intercept point as reference. The average of these two profiles is given in Table 5-28. The corresponding average return-stroke speed profile using Yokogawa data is shown in Figure 5-38. Table 5-29 gives the return stroke optical risetimes at various heights for the event F0503, Stroke 3, recorded by the LeCroy oscilloscope.

The return-stroke speeds at different heights, measured using LeCroy data for event F0503, stroke 4 are given in Table 5-30. The speed profile is shown in Figure 5-39 with the 20% point as reference and in Figure 5-40 with the slope intercept point as the reference. The profile shown in Figures 5-39 and 5-40 in blue are based on data from channels 2, 3, 4, 6, and 9, whereas the overlaid profiles in red are based on data from channels 5, 7, and 8. The average of two profiles is given in Table 5-31. The average speed profile is shown in Figure 5-41 with the 20% point as

reference and in Figure 5-42 using the slope intercept point as reference using LeCroy data. The average of these two profiles is given in Table 5-32 and inFigure 5-43.

The return-stroke speeds at different heights, measured using Yokogawa data for this event are given in Table 5-33. The corresponding speed profiles are shown in Figure 5-44 using the 20% point as reference and in Figure 5-45 using the slope intercept point as reference. The average of these two profiles is given in Table 5-34. The corresponding average return-stroke speed profile based on Yokogawa data is shown in Figure 5-46. Table 5-35 gives the return stroke optical risetimes at various heights for event F0503, Stroke 4, recorded by the LeCroy oscilloscope.

5.4.3 Event F0510

Event F0510 was triggered on July 31, 2005 at 20:03:33 UTC. One stroke was observed for this event by the photodiode array following the initial stage. The overall return-stroke speeds for this event using the different reference points explained in section is given in Table 5-36. The return-stroke speeds at various heights, measured using LeCroy data for this event are given in Table 5-37. The speed profile is shown in Figure 5-47 with the 20% point as reference and in Figure 5-48 with the slope intercept point as the reference. The profile shown in Figures 5-47 and 5-48 in blue are based on data from channels 2,3,4,6, and 9, whereas the overlaid profiles in red are based on data from channels 5, 7, and 8. The average of two profiles is given in Table 5-38. The average speed profile is shown in Figure 5-49 with the 20% point as reference and in Figure 5-50 using the slope intercept point as reference using LeCroy data. The average of these two profiles is given in Table 5-39 and in Figure 5-51. Table 5-40 gives the return stroke optical risetimes at various heights for event F0510, Stroke 1 recorded by the LeCroy oscilloscope.

5.4.4 Event F0512

Event F0512 was triggered on July 31, 2005 at 20:14:47 UTC. One stroke was observed for this event by the photodiode array. The overall return-stroke speeds for this event using the different reference points explained in section is given in Table 5-41. The return-stroke speeds at various heights, measured using LeCroy data for this event are given in Table 5-42. The speed profile is shown in Figure 5-52 with the 20% point as reference and in Figure 5-53 with the slope intercept point as the reference. The profile shown in Figures 5-52 and 5-53 in blue are based on data from channels 2, 3, 4, and 6, whereas the overlaid plot in red are based on data from channels 5, 7, and 8. The average of two profiles is given in Table 5-43. The average speed profile is shown in Figure 5-54 with the 20% point as reference and in Figure 5-55 using the slope intercept point as reference using LeCroy data. The average of these two profiles is given in Table 5-44 and in Figure 5-56.

Table 5-45 gives the leader propagation speeds at various heights based on the LeCroy data and computed using the 20% point as reference. In contrast with the return-stroke speeds, leader speeds were estimated using all LeCroy channels without segregating them into two groups. We notice that for the same event, the leader propagation speeds are an order of magnitude lower than the observed two-dimensional return-stroke speeds.

Table 5-46 gives the return stroke optical risetimes at various heights for event F0512, Stroke 1 recorded by the LeCroy oscilloscope.

5.4.5 Event F0514

Event F0514 was triggered on August 4, 2005 at 18:44:38 UTC. One stroke was observed for this event by the photodiode array. The overall return-stroke speeds for this event using the different reference points explained in section is given in Table 5-47. The return-stroke speeds at various heights, measured using LeCroy data for this event are given in Table 5-48. The speed

profile is shown in Figure 5-57 with the 20% point as reference and in Figure 5-58 with the slope intercept point as the reference. The profile shown in Figures 5-57 and 5-58 in blue are based on data from channels 2, 3, 4, and 6, whereas the overlaid profiles in red are based on data from channels 5, 7, and 8. The average of two profiles is given in Table 5-49. The corresponding average speed profile is shown in Figure 5-59 with the 20% point as reference and in Figure 5-60 using the slope intercept point as reference using LeCroy data. The average of these two profiles is given in Table 5-50 and in Figure 5-61.

The return-stroke speeds at various heights, measured using Yokogawa data for this event are given in Table 5-51. The corresponding speed profiles are shown in Figure 5-62 using the 20% point as reference and in Figure 5-63 using the slope intercept point as reference. The average of these two profiles is given in Table 5-52. The corresponding average return-stroke speed profile based on Yokogawa data is shown in Figure 5-64.

Table 5-53 gives the leader propagation speeds at various heights based on the LeCroy data and computed using the 20% point as reference. In contrast with the return-stroke speeds, leader speeds were estimated using all LeCroy channels without segregating them into two groups. We notice that for the same event, the leader propagation speeds are an order of magnitude lower than the observed two-dimensional return-stroke speeds.

Table 5-54 gives the return stroke optical risetimes at various heights for event F0514, Stroke 1, recorded by the LeCroy oscilloscope.

5.4.6 Event F0517

Event F0517 was triggered on August 4, 2005 at 19:32:47 UTC. Two strokes was observed for this event by the photodiode array. The segments which were recorded correspond to strokes 1, and 2. The overall return-stroke speeds for this event using the various reference points explained in section is given in Table 5-55. The return-stroke speeds at different heights,

measured using LeCroy data for this event are given in Table 5-56. The speed profile is shown in Figure 5-65 with the 20% point as reference and in Figure 5-66 with the slope intercept point as the reference. The profile shown in Figures 5-65 and 5-66 in blue are based on data from channels 2, 3, 4, and 6, whereas the overlaid profiles in red are based on data from channels 5, 7, and 8. The average of two profiles is given in Table 5-57. The average speed profile is shown in Figure 5-67 with the 20% point as reference and in Figure 5-68 using the slope intercept point as reference using LeCroy data. The average of these two profiles is given in Table 5-58 and in Figure 5-69.

The return-stroke speeds at various heights, measured using Yokogawa data for this event are given in Table 5-59. The corresponding speed profiles are shown in Figure 5-70 using the 20% point as reference and in Figure 5-71 using the slope intercept point as reference. The average of these two profiles is given in Table 5-60. The corresponding average return-stroke speed profile based on Yokogawa data is shown in Figure 5-72.

Table 5-61 gives the return stroke optical risetimes at various heights for event F0514, Stroke 1, recorded by the LeCroy oscilloscope.

The return-stroke speeds at different heights, measured using LeCroy data for event F0517, stroke 2 are given in Table 5-62. The speed profile is shown in Figure 5-73 with the 20% point as reference and in Figure 5-74 with the slope intercept point as the reference. The profile shown in Figures 5-73 and 5-74 in blue are based on data from channels 2, 3, 4, and 6, whereas the overlaid profiles in red are based on data from channels 5, 7, and 8. The average of two profiles is given in Table 5-63. The average speed profile is shown in Figure 5-75 with the 20% point as reference and in Figure 5-76 using the slope intercept point as reference using LeCroy data. The average of these two profiles is given in Table 5-64 and in Figure 5-77.

The return-stroke speeds at various heights, measured using Yokogawa data for this event are given in Table 5-65. The corresponding speed profiles are shown in Figure 5-78 using the 20% point as reference and in Figure 5-79 using the slope intercept point as reference. The average of these two profiles is given in Table 5-66 and in Figure 5-80.

Table 5-67 gives the leader propagation speeds at various heights based on the LeCroy data and computed using the 20% point as reference. In contrast with return-stroke speeds, leader speeds were estimated using all the LeCroy channels without segregating them into two groups. We notice that for the same event, the leader propagation speeds are an order of magnitude lower than the observed two-dimensional return-stroke speeds.

Table 5-68 gives the return stroke optical risetimes at various heights for event F0517, Stroke 2, recorded by the LeCroy oscilloscope.

5.4.7 Event F0521

Event F0521 was triggered on August 5, 2005 at 21:30:57 UTC. One strokes was observed for this event by the photodiode array. The overall return-stroke speeds for this event using the different reference points explained in section is given in Table 5-69. The return-stroke speeds at various heights, measured using LeCroy data for this event are given in Table 5-70. The speed profile is shown in Figure 5-81 with the 20% point as reference and in Figure 5-82 with the slope intercept point as the reference. The profile shown in Figures 5-81 and 5-82 in blue are based on data from channels 2, 3, 4, and 6, whereas the overlaid profiles in red are based on data from channels 5, 7, and 8. The average of two profiles is given in Table 5-71. The average speed profile is shown in Figure 5-83 with the 20% point as reference and in Figure 5-84 using the slope intercept point as reference using LeCroy data. The average of these two profiles is given in Table 5-72 and in Figure 5-85.

Table 5-73 gives the return stroke optical risetimes at various heights for event F0521, Stroke 1, recorded by the LeCroy oscilloscope.

5.5 Summary

The results from the above data analysis have been summarized in this section.

5.5.1 Return-Stroke Speeds

The return-stroke speed profiles for different groups of LeCroy channels, but the same reference point were compared. Specifically, the 'solid red line' LeCroy return-stroke speed profile obtained using the 20% point as reference was compared to the 'dashed blue line' LeCroy return-stroke speed profile obtained using the 20% point as reference. The percentage differences were found to be less than 30% in all the cases except for the cases listed in Table 5-74. Similarly, the 'solid red line' LeCroy return-stroke speed profile obtained using the slope intercept point as reference was compared to the 'dashed blue line' LeCroy return-stroke speed profile obtained using the slope intercept point as reference. The percentage differences were found to be less than 30% in all the cases again, except for the cases listed in Table 5-74.

The averaged LeCroy return-stroke speed profiles, obtained by averaging the 'solid red line' and the 'dashed blue line' return-stroke speed profiles, using the 20% point as reference were compared to the return-stroke speed profiles, obtained by averaging the 'solid red line' and the 'dashed blue line' return-stroke speed profiles, using the slope intercept point as reference. The percentage differences were found to be less than 30% in all the cases except for the events listed in Table 5-75.

The return-stroke speed profiles measured using Yokogawa data, with the 20% as reference were compared with the return-stroke speed profiles measured using Yokogawa data, with the slope intercept point as reference. The percentage differences were less than 30% in all the cases.

The return-stroke speed profiles obtained by computing the average of the speeds from the two groups of LeCroy channels with the 20% point as reference were compared to the Yokogawa data with the 20% point as reference. The percentage difference was less than 30% for all the events. Similarly, the return-stroke speed profiles obtained by computing the average of the speeds measured using LeCroy data with the slope intercept point as reference were compared to the Yokogawa data with the 20% point as reference. The percentage differences were less than 30% in all the cases.

The return-stroke speed profiles obtained by computing the average of the speeds obtained using LeCroy data, with the 20% point and slope intercept point as reference, were compared to the average return-stroke speeds computed similarly using Yokogawa data. The percentage difference was less than 30% for the all the cases except for the events listed in Table 5-76.

In the slope-intercept method, the starting point will be reported earlier in time as the risetime of the waveform gets slower. For this reason, it is believed that the speeds measured using the slope intercept method overestimate the actual speed whereas the 20% of peak method is believed to underestimate the actual 1-D speed (Olsen et al., 2004). Accordingly, the lower and upper bounds on the mean return-stroke speeds using LeCroy and Yokogawa data. The mean return-stroke speeds obtained using LeCroy data are found to vary between 1.48×10^8 m/s and 1.59×10^8 m/s. Whereas, the mean return-stroke speeds obtained using the Yokogawa data are found to vary between 1.53×10^8 m/s and 1.61×10^8 m/s.

The mean return-stroke speed, obtained by computing the average of the return-speeds using the 20% and slope intercept reference points, was 1.51×10^8 m/s in the case of LecCroy data and 1.57×10^8 m/s in the case of Yokogawa data.

The return-stroke speed profiles had non-monotonic profiles in all of the events analyzed in this chapter. The return-stroke speeds found to be higher in the middle of the lightning channel and lower in either the bottom or the top portions of the lightning channel. Accordingly the speeds were seen to vary between 1 x 10^8 m/s and 2 x 10^8 m/s using the LeCroy data, whereas the seeds were seen to vary between 1 x 10^8 m/s and 2.2 x 10^8 m/s using the Yokogawa data.

5.5.2 Leader Speeds

Four triggered lightning events, F0501-Stroke 1 (July 2), F0512-Stroke 1 (July 31), F0514-Stroke 1 (August 4) and F0503-Stroke 2 (July 2) exhibited distinct leader pulses before the onset of the return-stroke pulse. The leader propagation speeds in all the cases were found to follow the trend of lower speeds in the top portion of the lightning channel (452 m before July 13, 2005, and 304 m after that) and higher speeds at the bottom of the channel (44 m before July 13, 2005, and 30 m after that). The mean leader speeds are found to vary between 1.3 x 10^7 m/s and 2.5 x 10^7 m/s.

5.5.3 Optical Risetimes

Return-stroke optical risetimes were computed for the summer 2005 triggered lightning events. The optical risetimes in all the cases were found to follow the trend of smaller risetimes in the bottom of the lightning channel (44 m before July 13 2005, and 30 m after that) and larger risetimes in the top (452 m before July 13 2005, and 304 m after that) of the lightning channel. The mean optical rise times were found to vary from 0.81 μs at the bottom to 2.83 μs at the top of the channel.

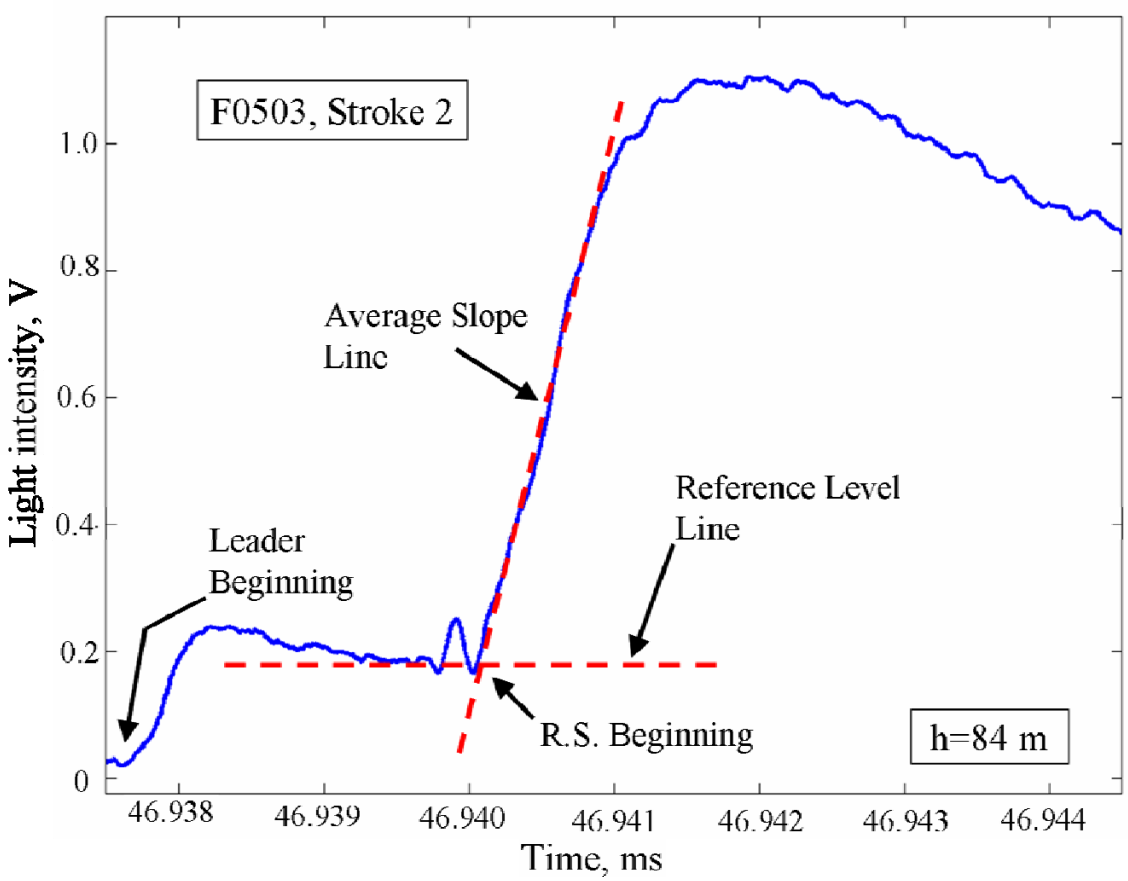

Figure 5-1: Illustration of the "slope-intercept" method. The optical waveform of Flash F0503, Stroke 2 at a height of 84 m above the termination point is shown on a 7-μs time-scale. The beginning of the return-stroke is taken to be inter-section of the two (red) dashed lines. This intersection point was tracked in estimating the return stroke speed by the "slope-intercept" method on unfiltered waveforms. Vertical axis represents the optical intensity in volts at the input of the oscilloscope.

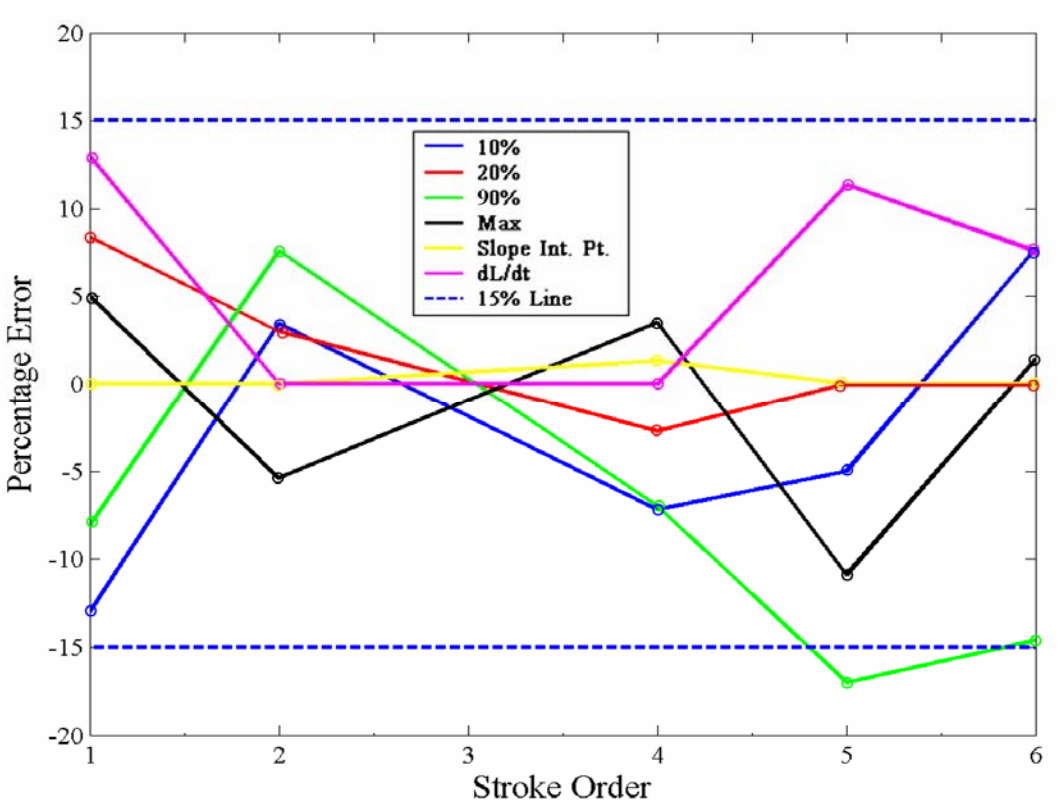

Figure 5-2: Calibration of the data analysis tools used in this thesis. None of the errors cross the 20% level. The analysis was carried out for the summer 2003 F0336 flash which had 5 return strokes for which speeds were measured. No data for stroke 3 are available. The y-axis indicates the percentage error in the overall return-stroke propagation speed values computed in this thesis relative to the corresponding values computed by Olsen et. al. (2003).

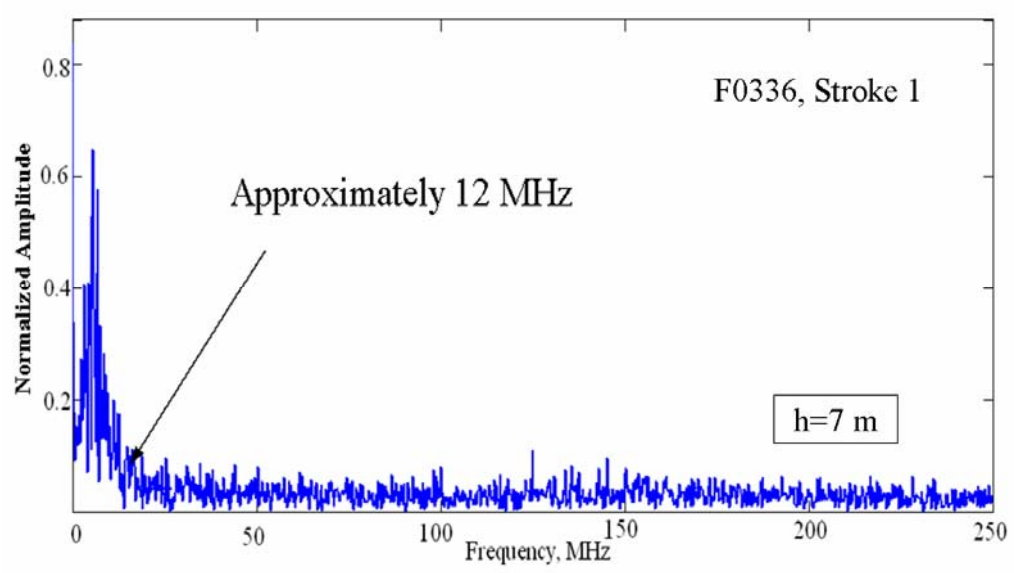

Figure 5-3: Spectrum of light waveform of flash F0336, Stroke 1 (at a height of 7 m above termination) lightning waveform. The event was triggered at Camp Blanding, Florida during the summer of 2003 and was subsequently analyzed by Olsen (2003).

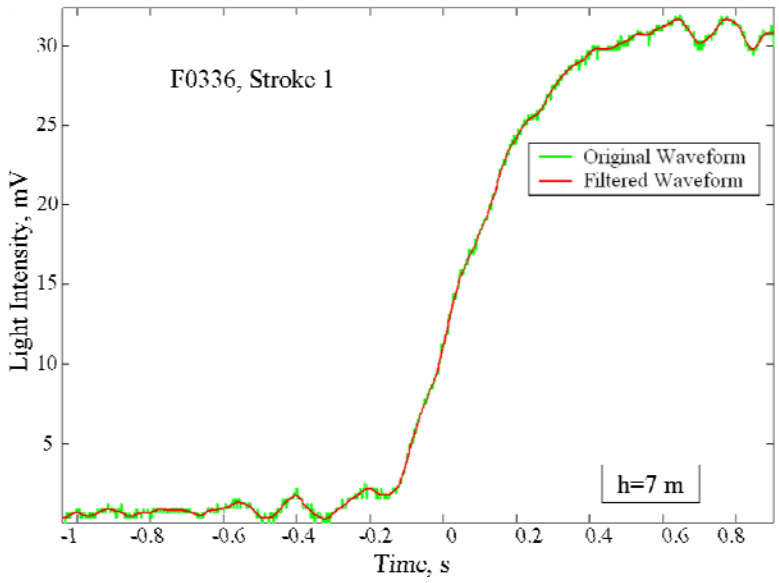

Figure 5-4: Event F0336, Stroke 1 (at a height of 7 m above termination) from Summer 2003, filtered using a moving average filter (with window size of 11 samples). The filtered waveform is overlaid over the original waveform to check the quality of filtering. Vertical axis represents the optical intensity in volts at the input of the oscilloscope.

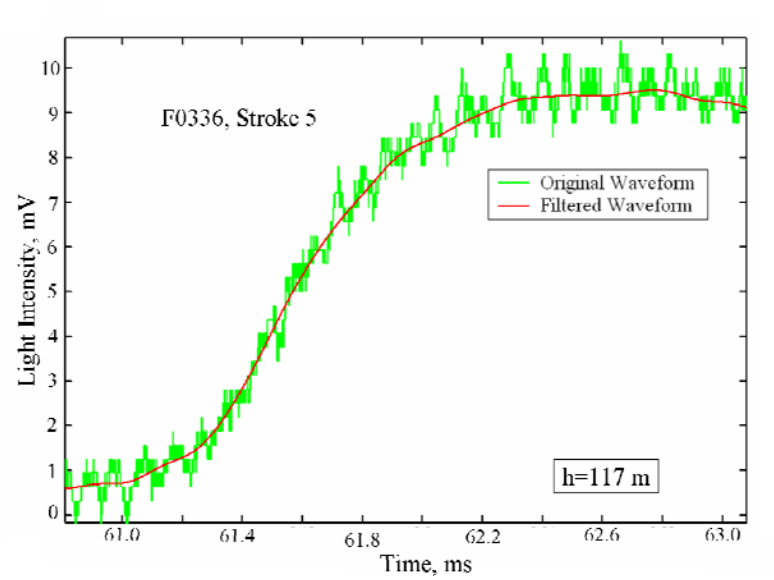

Figure 5-5: Event F0336, Stroke 5 (at a height of 117 m above termination) from Summer 2003, filtered using Filter 1. The filtered waveform is overlaid over the original waveform to check the quality of filtering. Vertical axis represents the optical intensity in volts at the input of the oscilloscope.

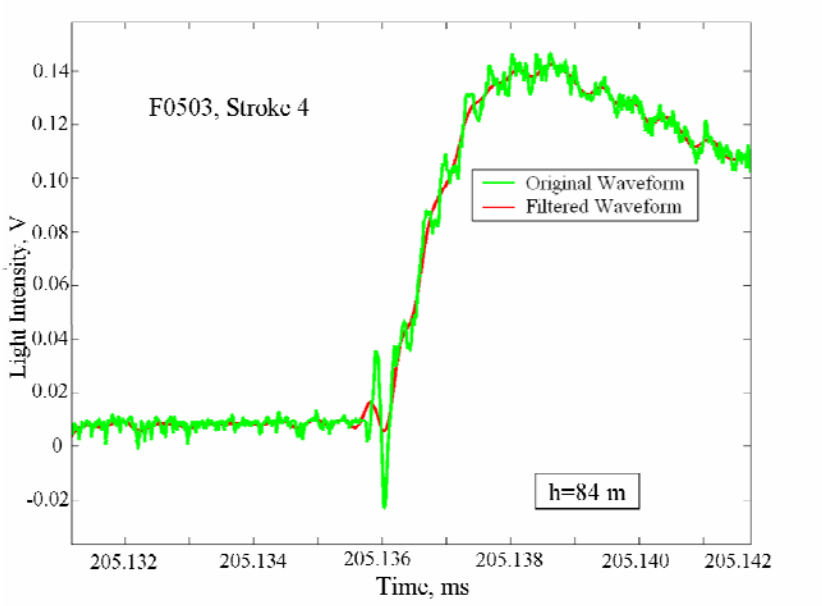

Figure 5-6: Event F0504, Stroke 4 (at a height of 84 m above termination) from Summer 2005 filtered using Filter 2. The filtered waveform is overlaid over the original waveform to check the quality of filtering. Vertical axis represents the optical intensity in volts at the input of the oscilloscope.

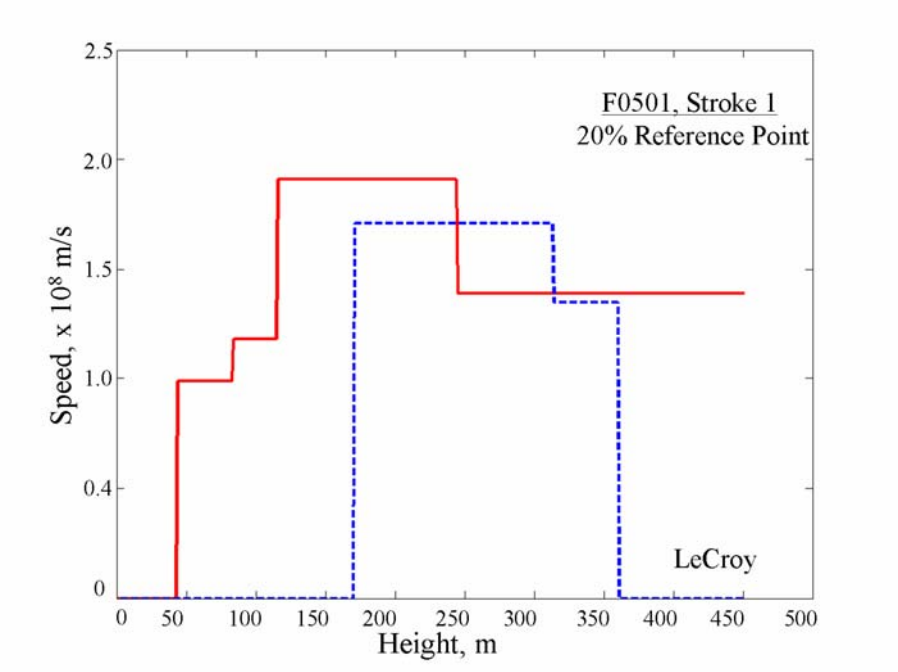

Figure 5-7: Return-stroke speed profiles obtained using the 20% reference point for event F0501, Stroke 1. Solid red line corresponds to data from LeCroy channels 2,3,4,6, and 9, and dashed blue line to data from LeCroy channels 5, 7, and 8.

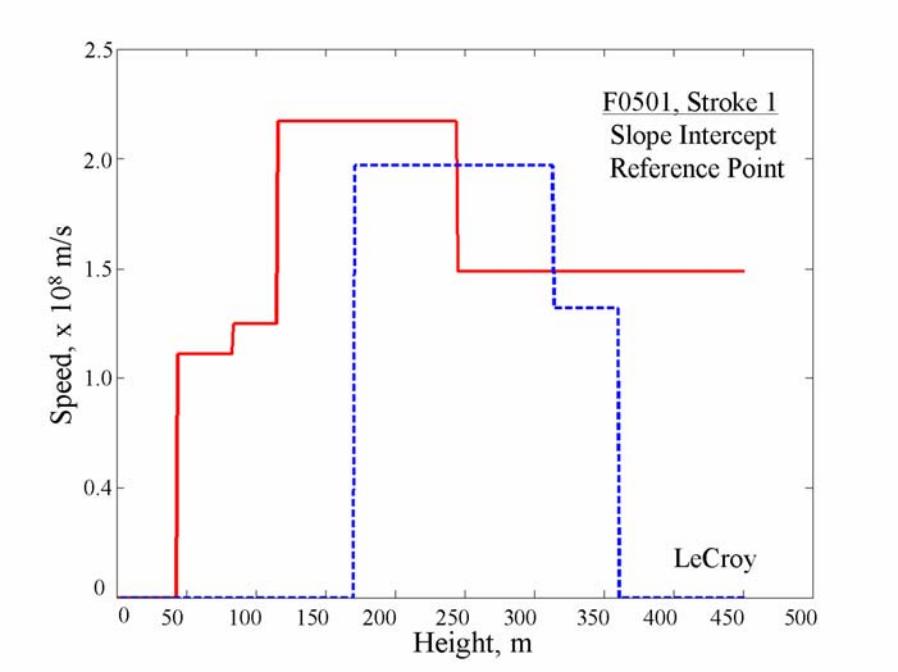

Figure 5-8: Return-stroke speed profiles obtained using the slope intercept reference point for event F0501, Stroke 1. Solid red line corresponds to data from LeCroy channels 2,3,4,6, and 9, and dashed blue line to data from LeCroy channels 5, 7, and 8.

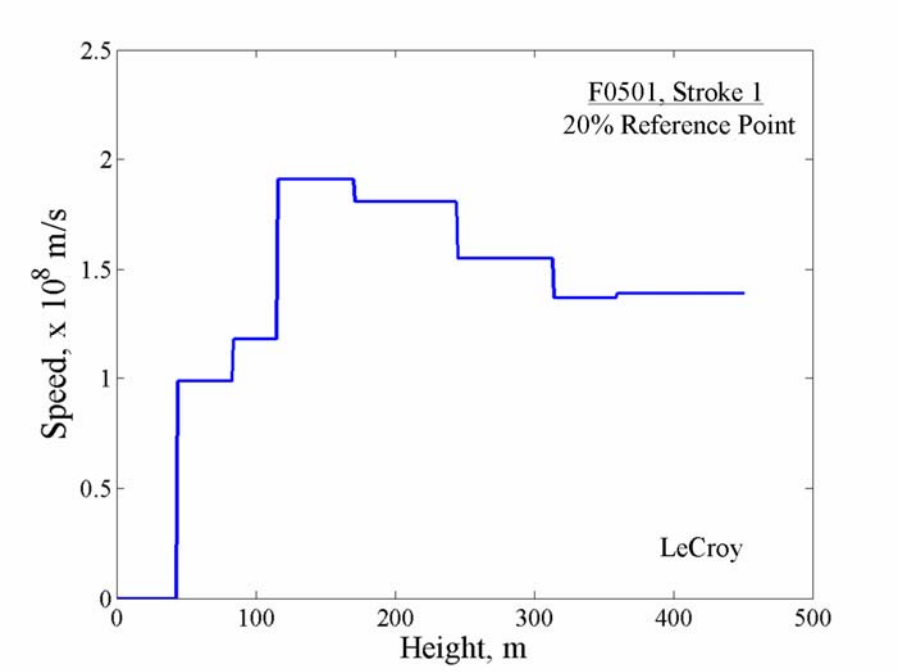

Figure 5-9: Return-stroke speed profile obtained using the 20% reference point for event F0501, Stroke 1, based on all the LeCroy data (combination of the two profiles shown in Figure 5-7).

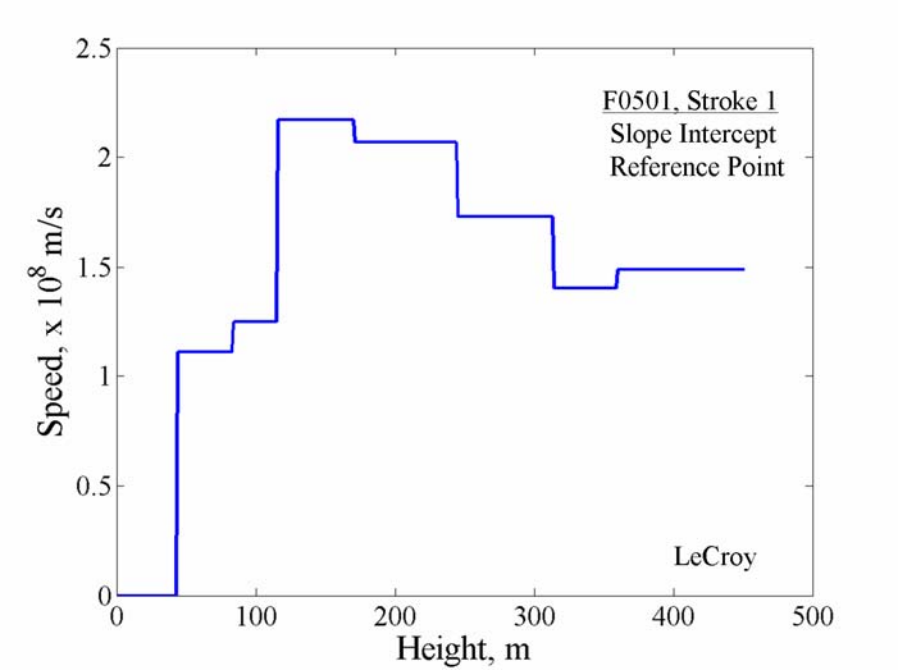

Figure 5-10: Return-stroke speed profile obtained using the slope intercept point as reference for event F0501, Stroke 1, based on all the LeCroy data (combination of two profiles shown in Figure 5-8).

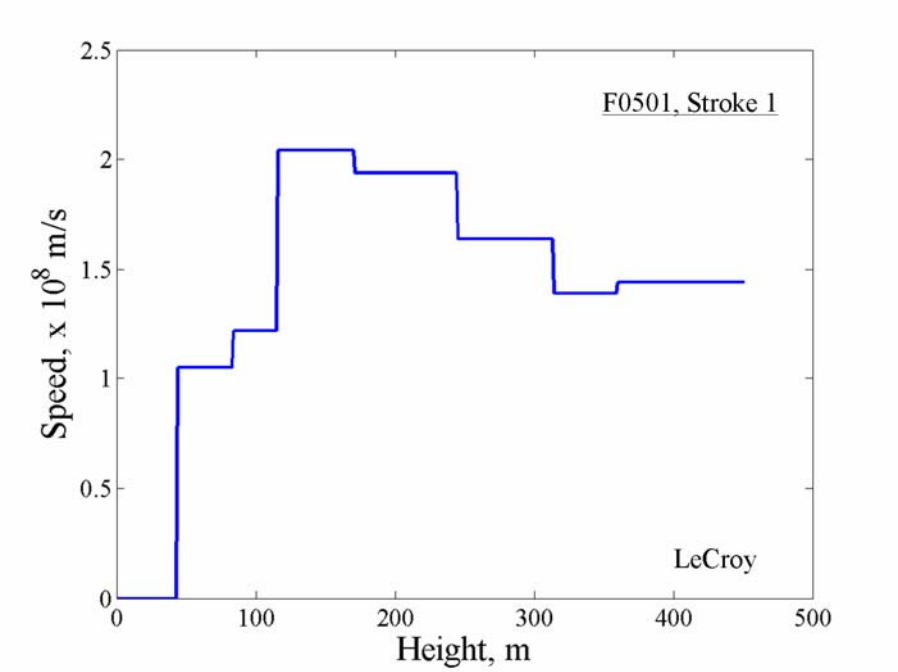

Figure 5-11: Return-stroke speed profile obtained by computing average of the speeds computed using the 20% and slope intercept methods, based on LeCroy data, shown in Figures 5-9 and 5-10, for event F0501, Stroke 1.

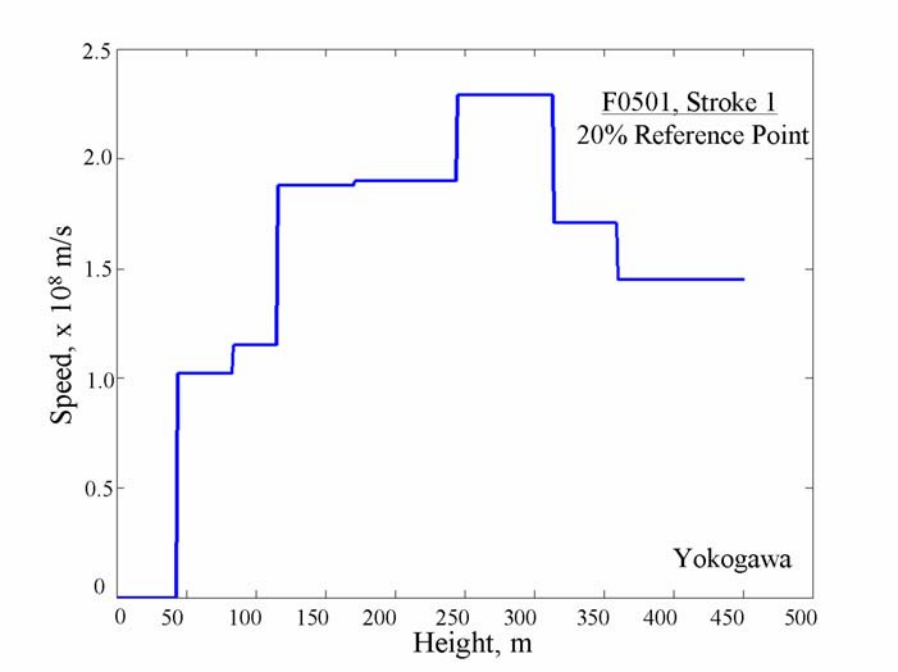

Figure 5-12: Return-stroke speed profile obtained using the 20% reference point for event F0501, Stroke 1, based on Yokogawa data.

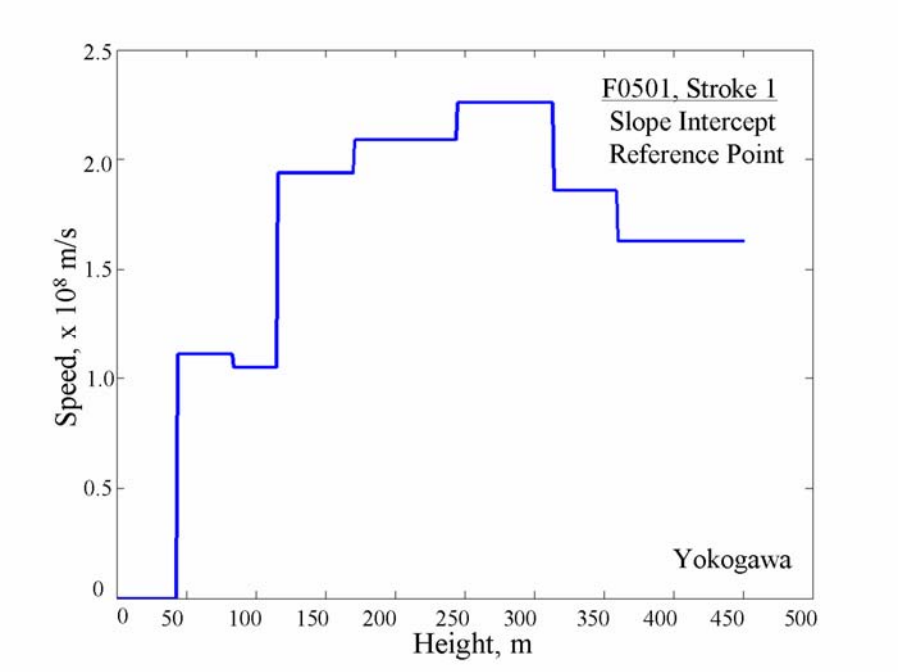

Figure 5-13: Return-stroke speed profile obtained using the slope intercept point as reference for event F0501, Stroke 1, based on Yokogawa data.

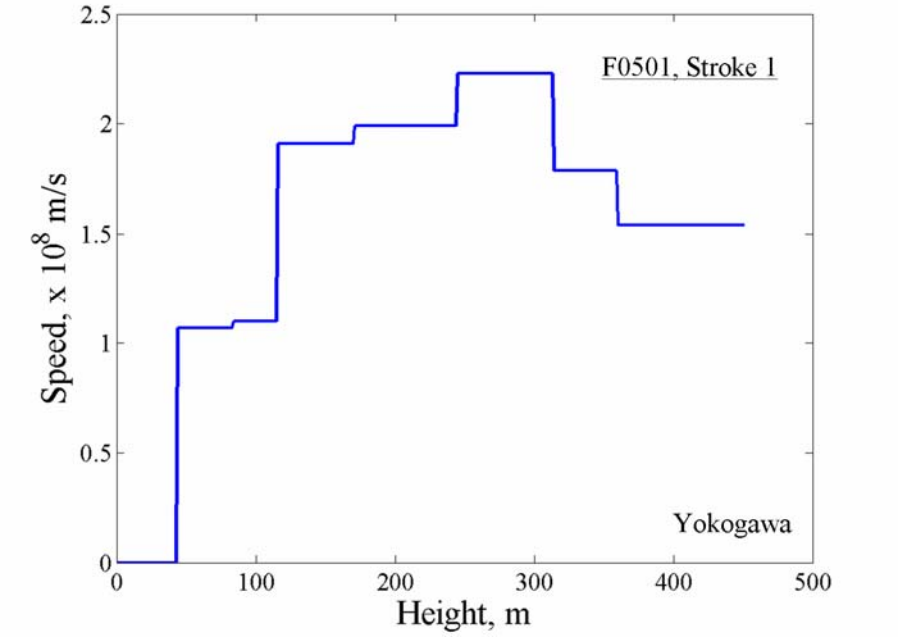

Figure 5-14: Return-stroke speed profile obtained by computing average of the speeds computed using the 20% and slope intercept methods, based on Yokogawa data, shown in Figures 5-12 and 5-13, for event F0501, Stroke 1.

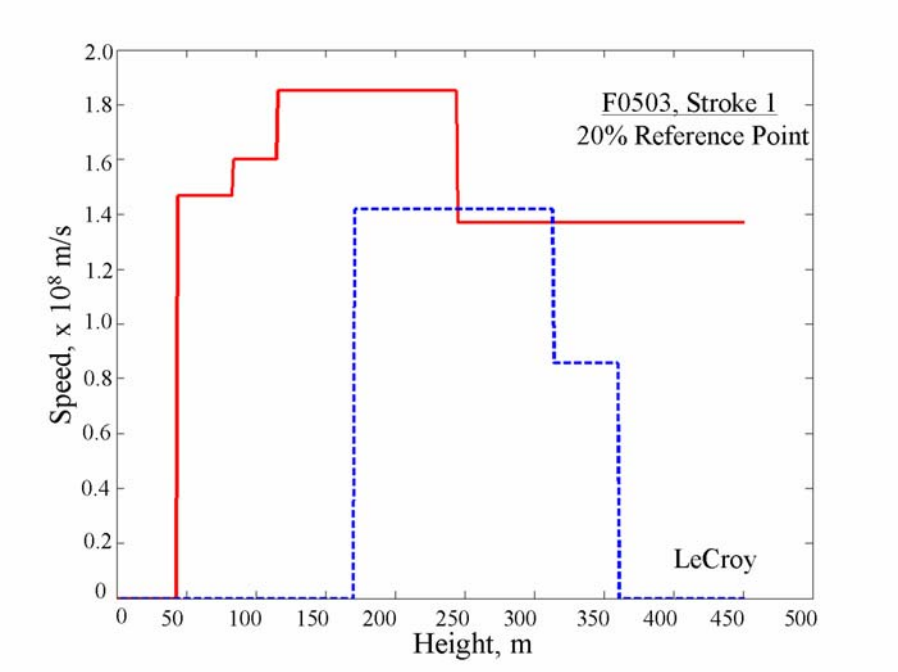

Figure 5-15: Return-stroke speed profiles obtained using the 20% reference point for event F0503, Stroke 1. Solid red line corresponds to data from LeCroy channels 2, 3, 4, 6, and 9, and dashed blue line to data from LeCroy channels 5, 7, and 8.

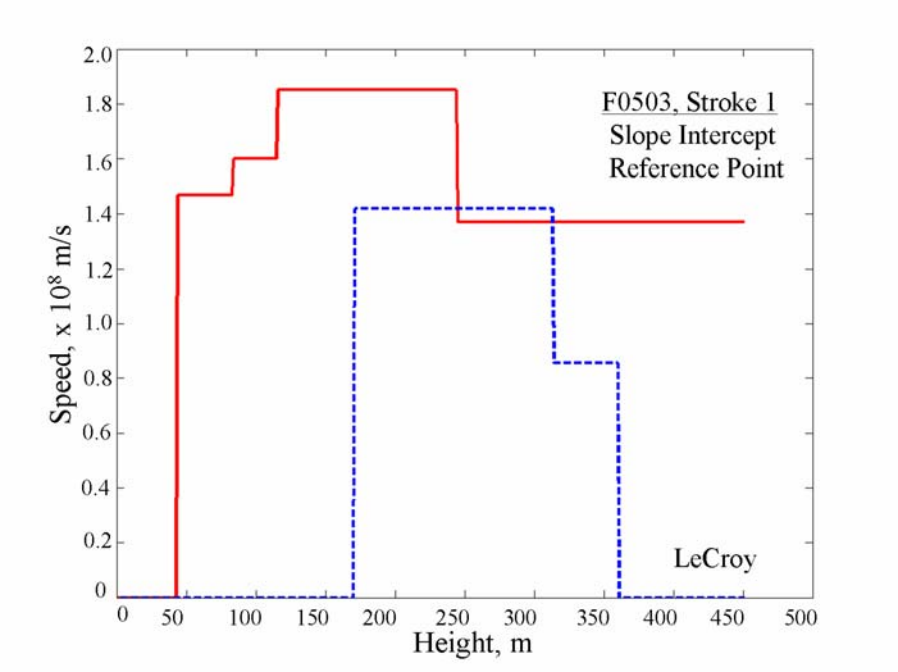

Figure 5-16: Return-stroke speed profiles obtained using the slope intercept reference point for event F0503, Stroke 1. Solid red line corresponds to data from LeCroy channels 2, 3, 4, 6, and 9, and dashed blue line to data from LeCroy channels 5, 7, and 8.

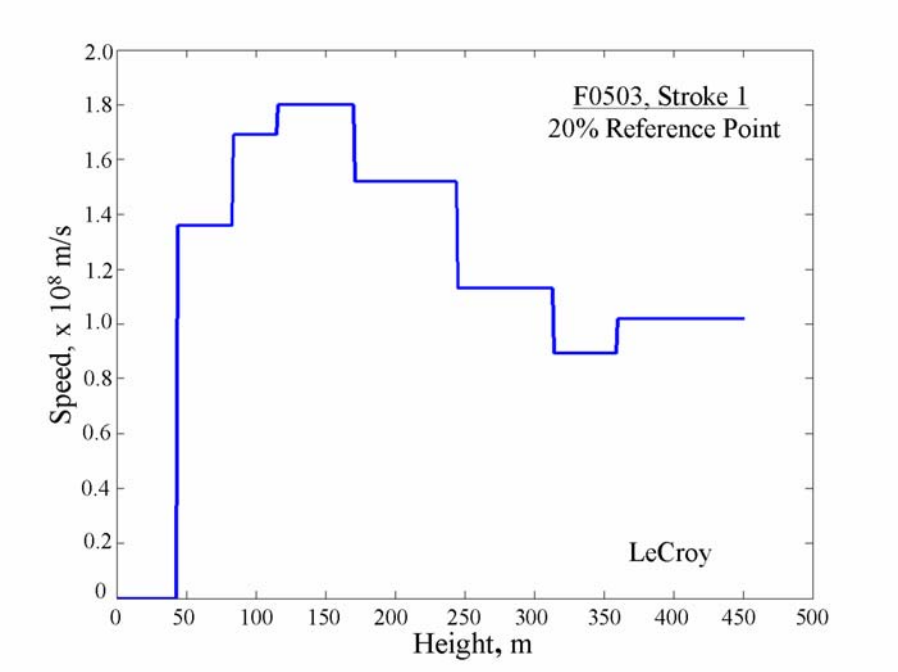

Figure 5-17: Return-stroke speed profile obtained using the 20% reference point for event F0503, Stroke 1, based on all the LeCroy data (combination of the two profiles shown in Figure 5-15).

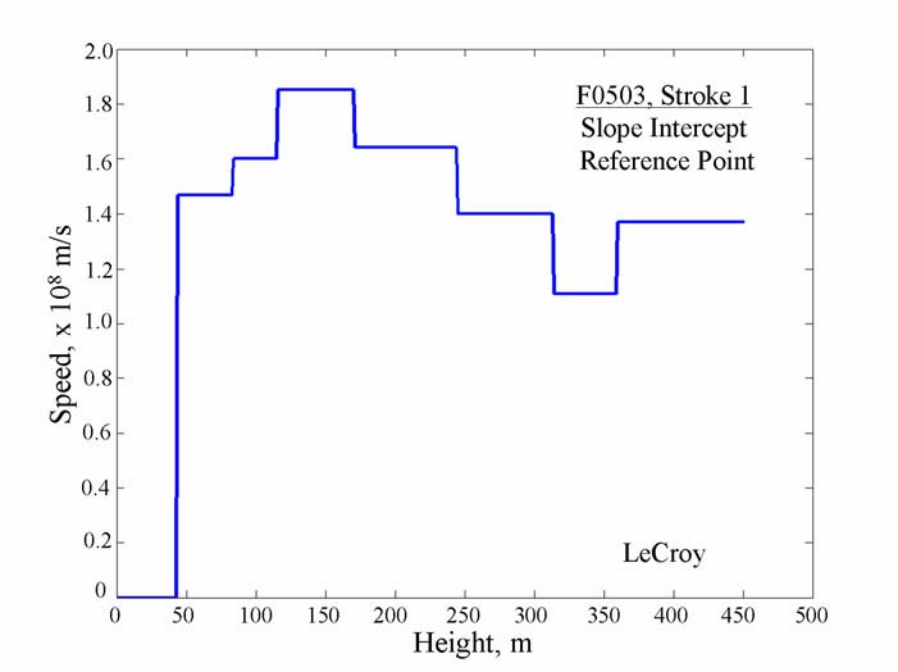

Figure 5-18: Return-stroke speed profile obtained using the slope intercept point as reference for event F0503, Stroke 1, based on all the LeCroy data (combination of the two profiles shown in Figure 5-16).

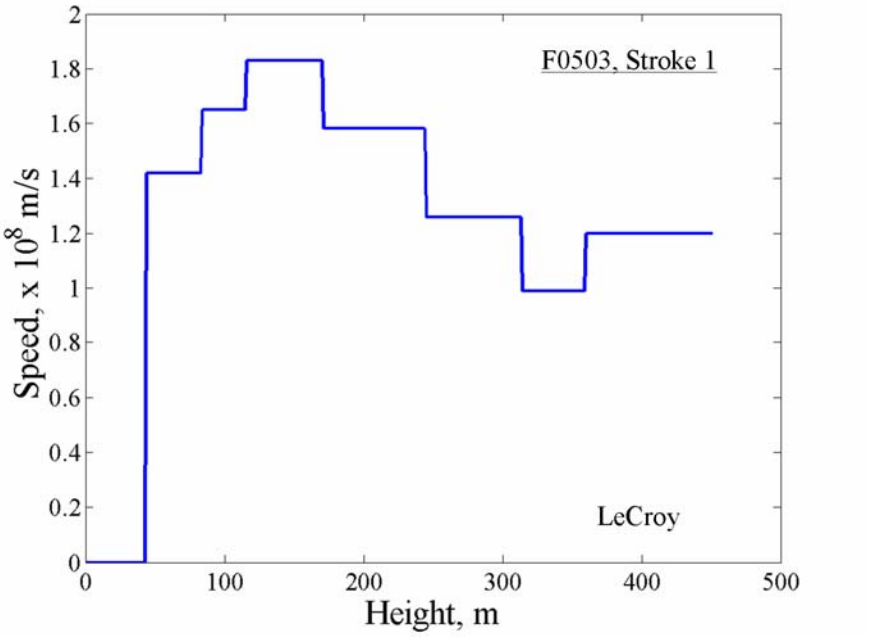

Figure 5-19: Return-stroke speed profile obtained by computing average of the speeds computed using the 20% and slope intercept methods, based on LeCroy data, shown in Figures 5-17 and 5-18, for event F0503, Stroke 1.

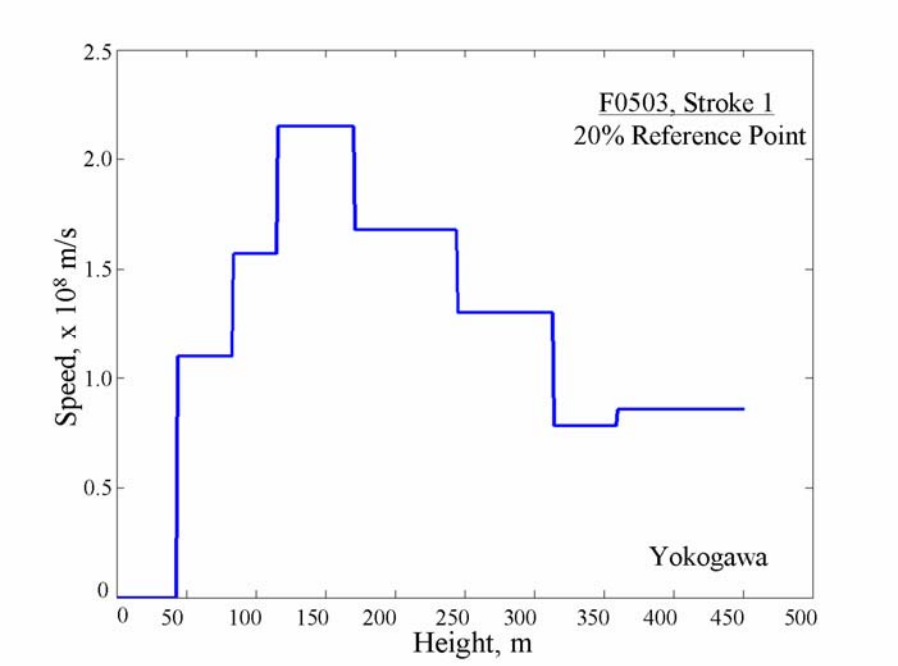

Figure 5-20: Return-stroke speed profile using the 20% Point as Reference for Event F0503, Stroke1, based on Yokogawa data.

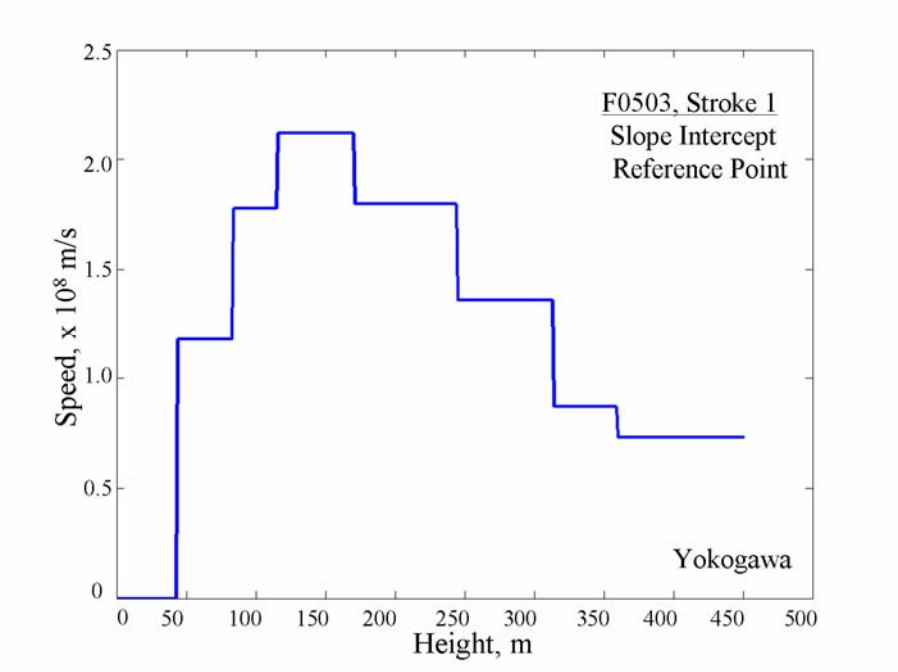

Figure 5-21: Return-stroke speed profile using the slope point as reference for event F0503, Stroke1, based on Yokogawa data.

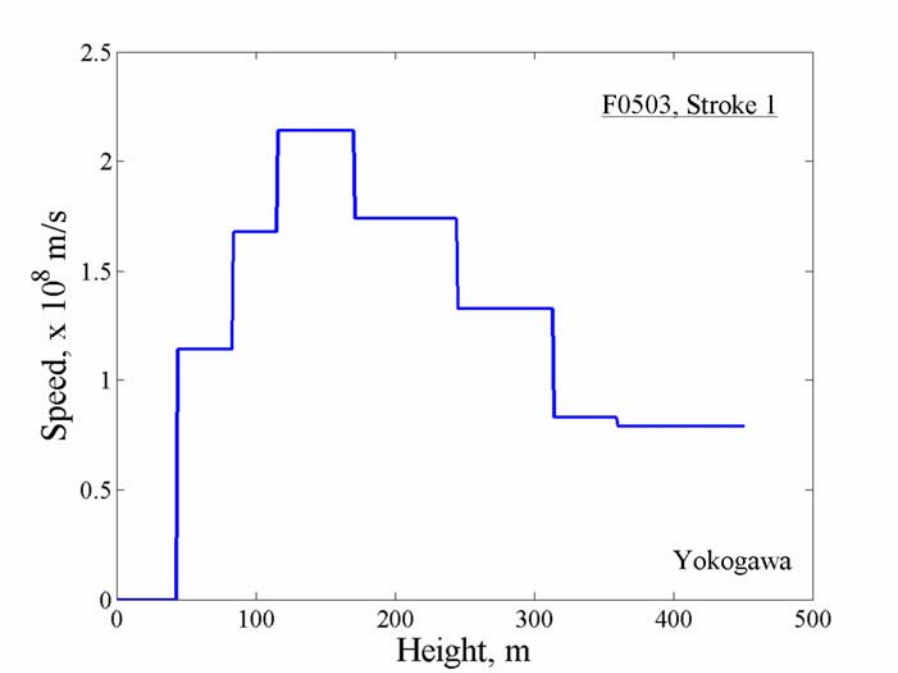

Figure 5-22: Return-stroke speed profile obtained by computing average of the speeds computed using the 20% and slope intercept methods, based on Yokogawa data, shown in Figures 5-20 and 5-21, for event F0503, Stroke 1.

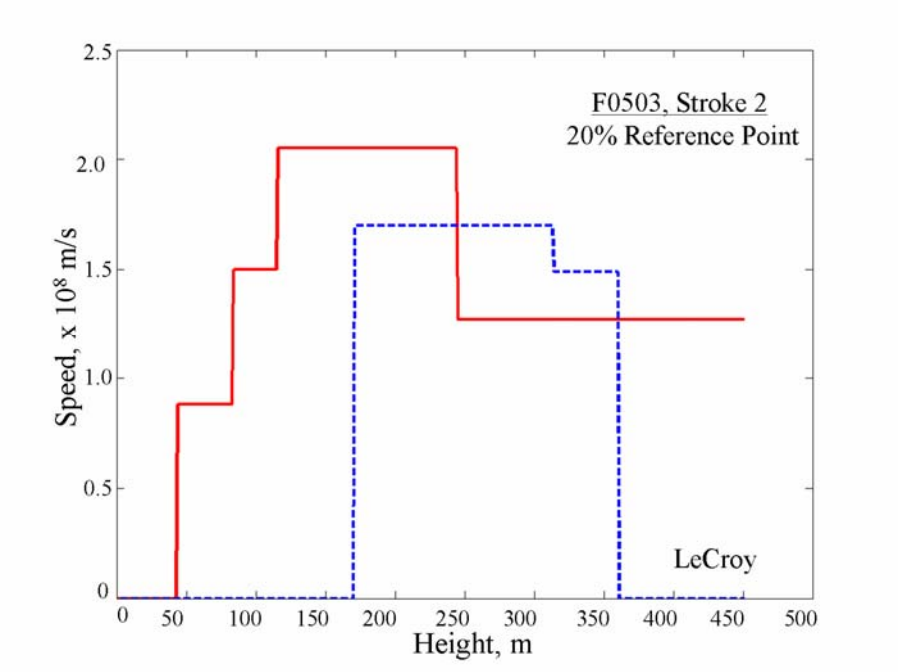

Figure 5-23: Return-stroke speed profiles obtained using the 20% reference point for event F0503, Stroke 2. Solid red line corresponds to data from LeCroy channels 2, 3, 4, 6, and 9, and dashed blue line to data from LeCroy channels 5, 7, and 8.

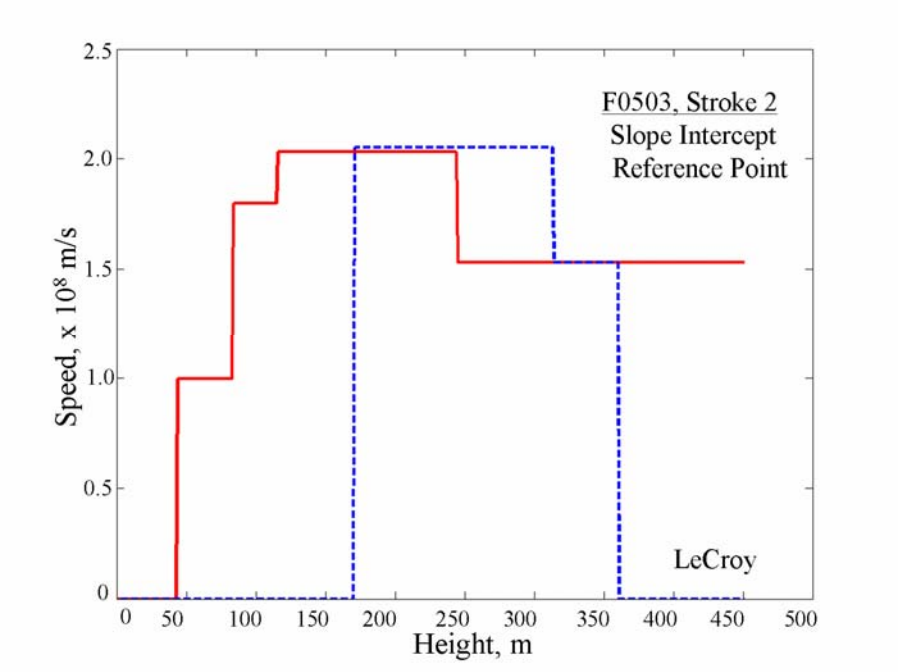

Figure 5-24: Return-stroke speed profiles obtained using the slope intercept reference point for event F0503, Stroke 2. Solid red line corresponds to data from LeCroy channels 2, 3, 4, 6, and 9, and dashed blue line to data from LeCroy channels 5, 7, and 8.

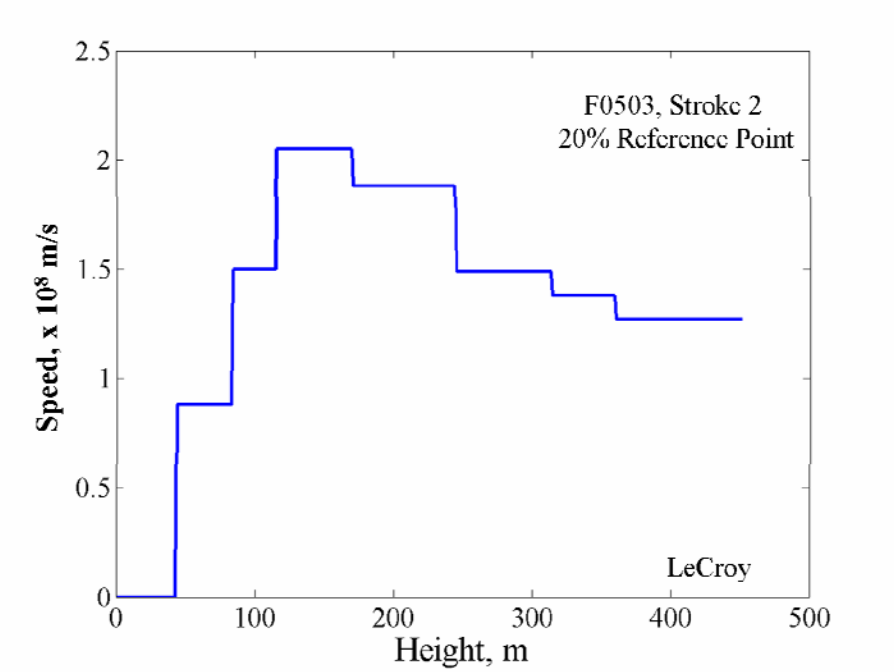

Figure 5-25: Return-stroke speed profile obtained using the 20% reference point for event F0503, Stroke 2, based on all the LeCroy data (combination of the two profiles shown in Figure 5-23).

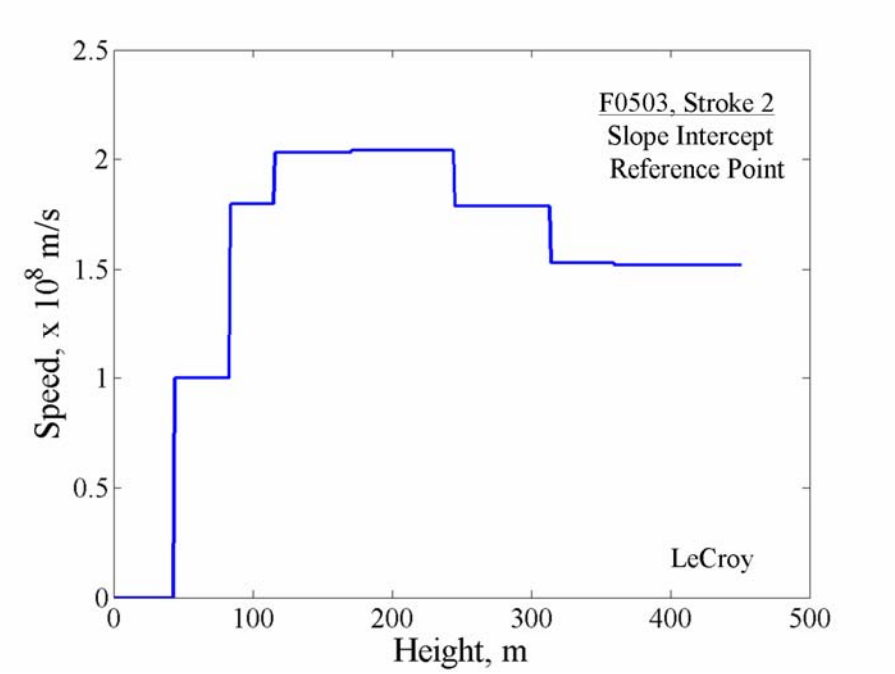

Figure 5-26: Return-stroke speed profile obtained using the slope intercept point as reference for event F0503, Stroke 2, based on all the LeCroy data (combination of the two profiles shown in Figure 5-24).

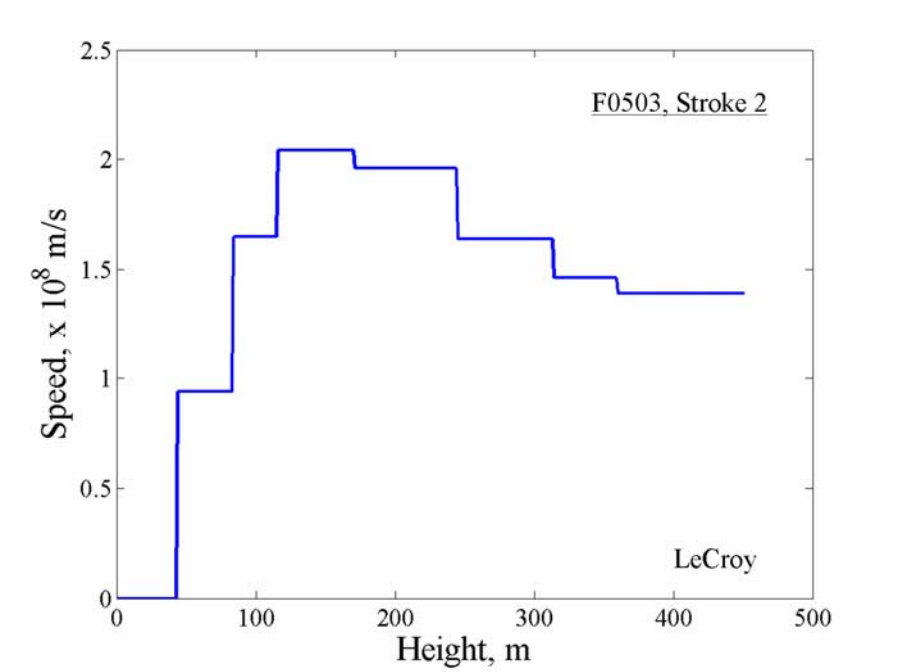

Figure 5-27: Return-stroke speed profile obtained by computing average of the speeds computed using LeCroy data, shown in Figures 5-25 and 5-26, for event F0503, Stroke 2.

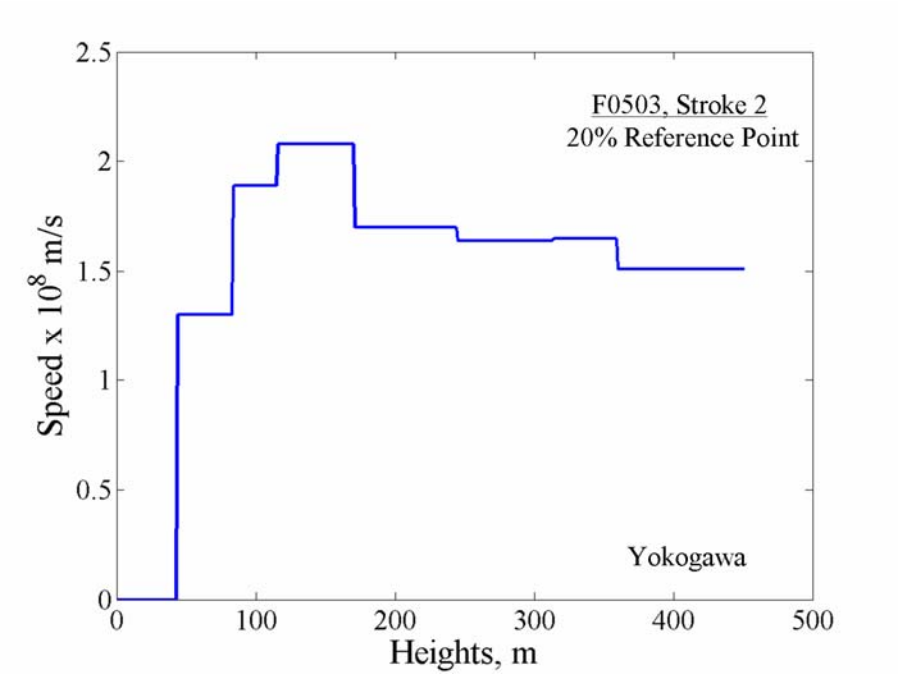

Figure 5-28: Return-stroke speed profile using the 20% Point as Reference for Event F0503, Stroke 2, based on Yokogawa data.

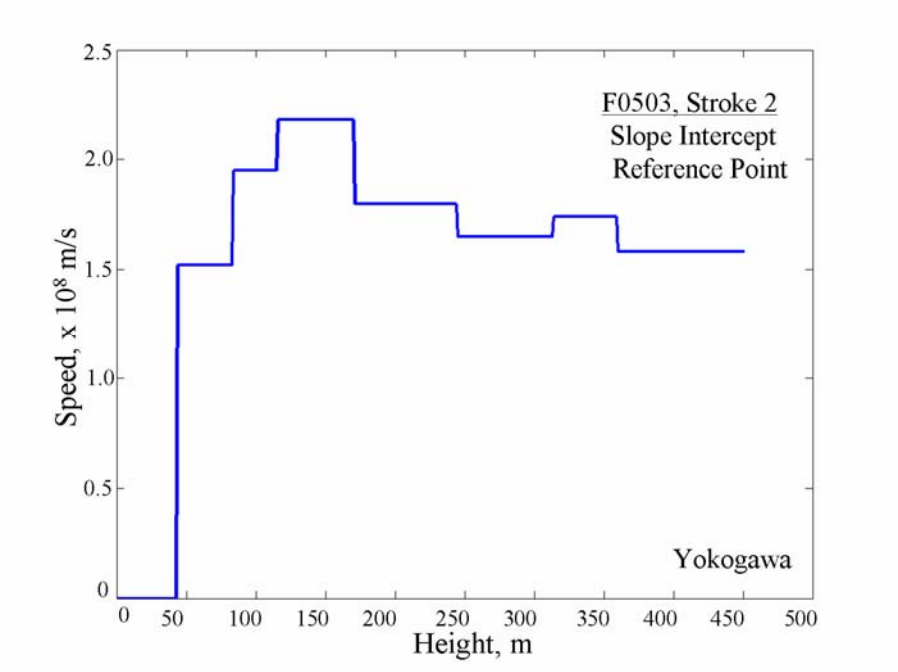

Figure 5-29: Return-stroke speed profile using the slope point as reference for event F0503, Stroke 2, based on Yokogawa data.

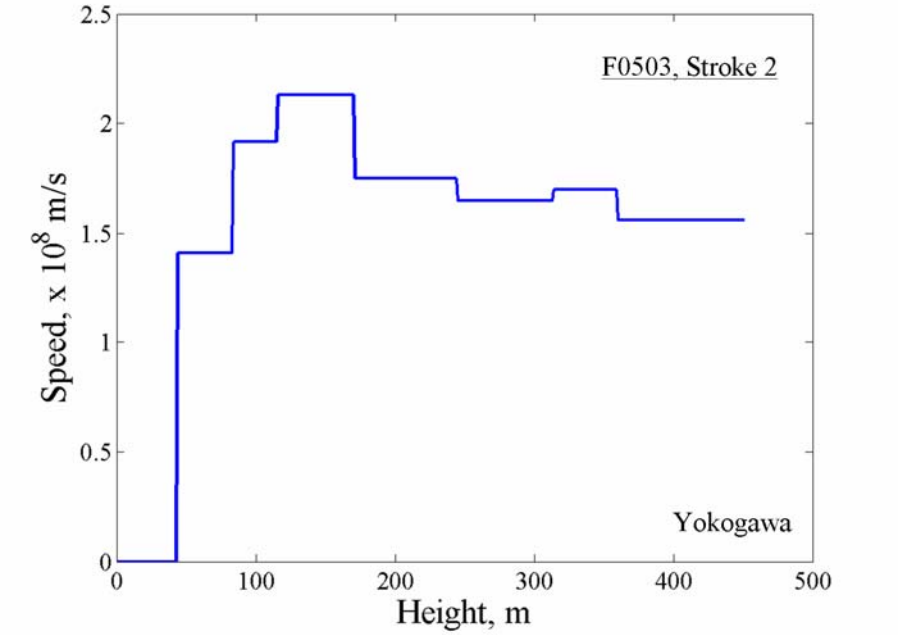

Figure 5-30: Return-stroke speed profile obtained by computing average of the speeds computed using the 20% and slope intercept methods, based on Yokogawa data, shown in Figures 5-28 and 5-29, for event F0503, Stroke 2.

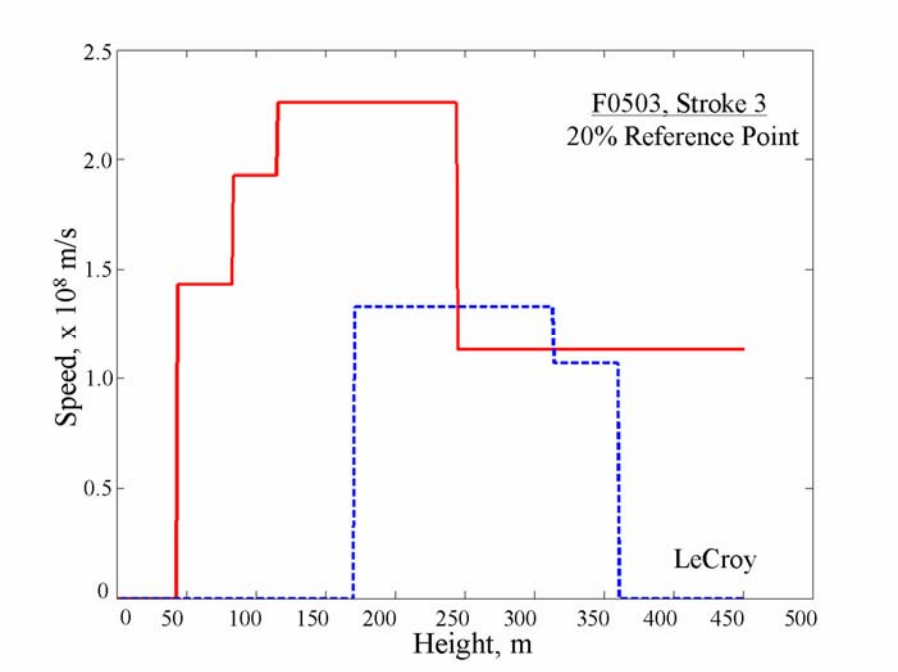

Figure 5-31: Return-stroke speed profiles obtained using the 20% reference point for event F0503, Stroke 3. Solid red line corresponds to data from LeCroy channels 2, 3, 4, 6, and 9, and dashed blue line to data from LeCroy channels 5, 7, and 8.

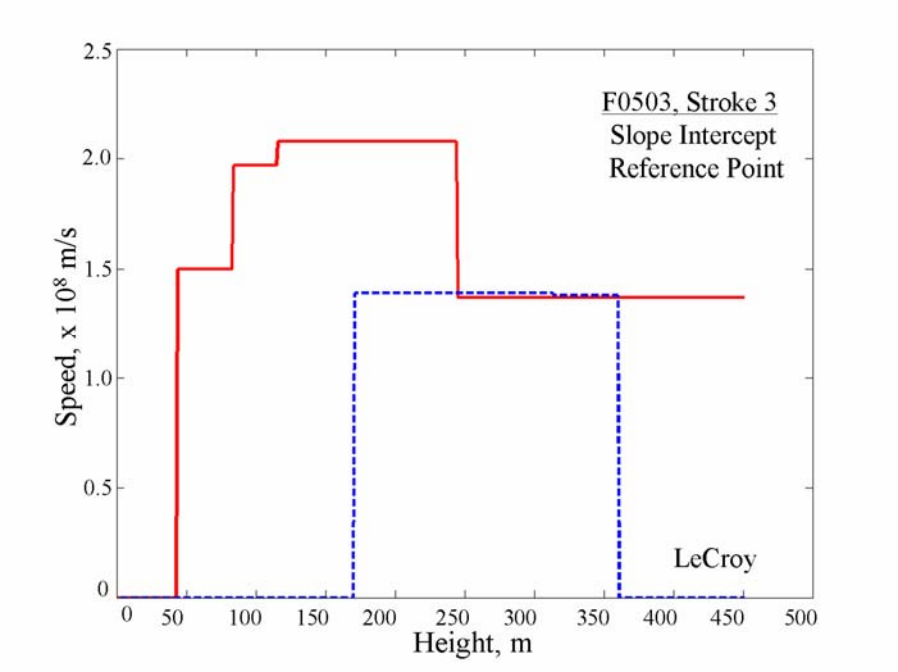

Figure 5-32: Return-stroke speed profiles obtained using the slope intercept reference point for event F0503, Stroke 3. Solid red line corresponds to data from LeCroy channels 2, 3, 4, 6, and 9, and dashed blue line to data from LeCroy channels 5, 7, and 8.

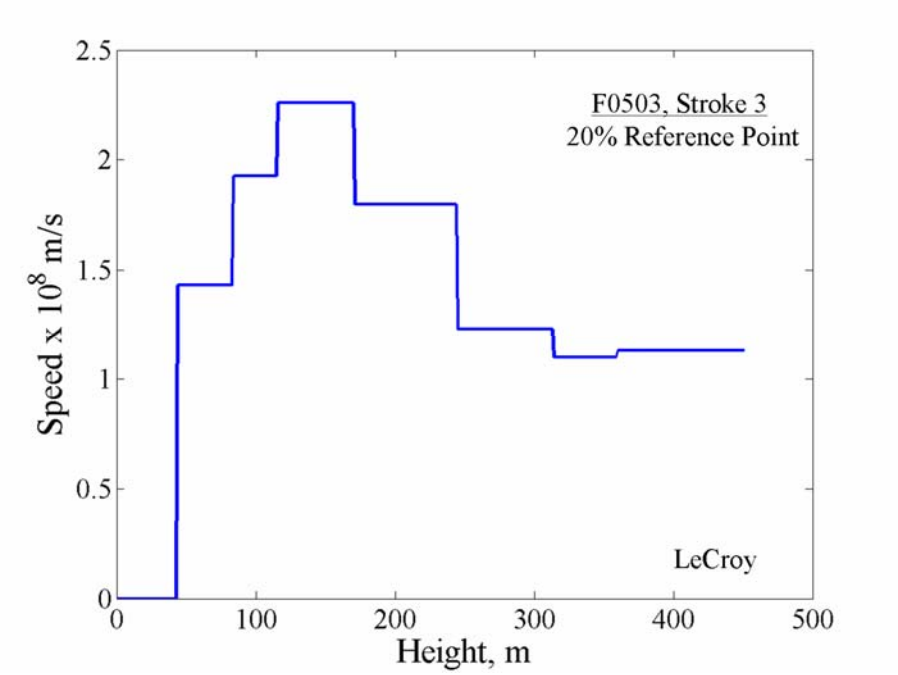

Figure 5-33: Return-stroke speed profile obtained using the 20% reference point for event F0503, Stroke 3, based on all the LeCroy data (combination of the two profiles shown in Figure 5-31).

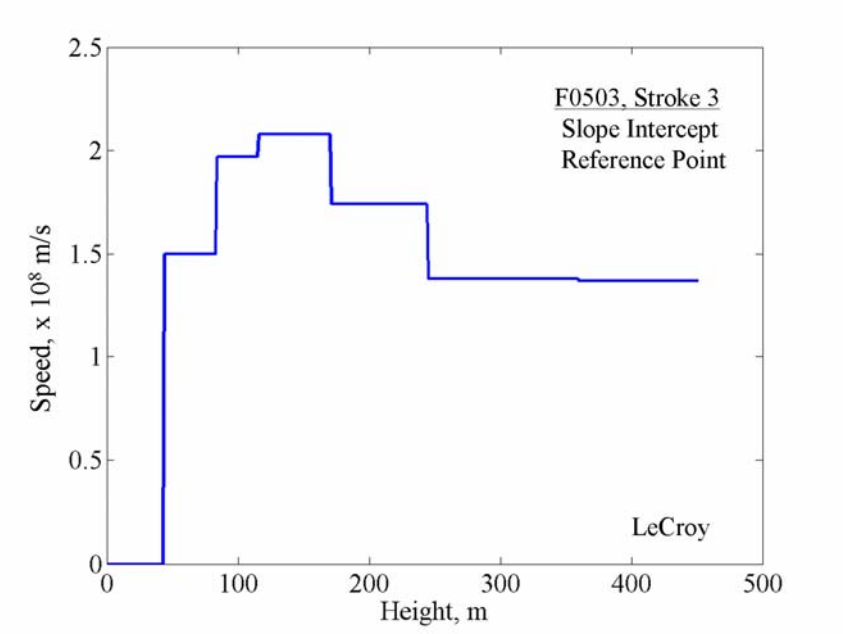

Figure 5-34: Return-stroke speed profile obtained using the slope intercept point as reference for event F0503, Stroke 3, based on all the LeCroy data (combination of the two profiles shown in Figure 5-32).

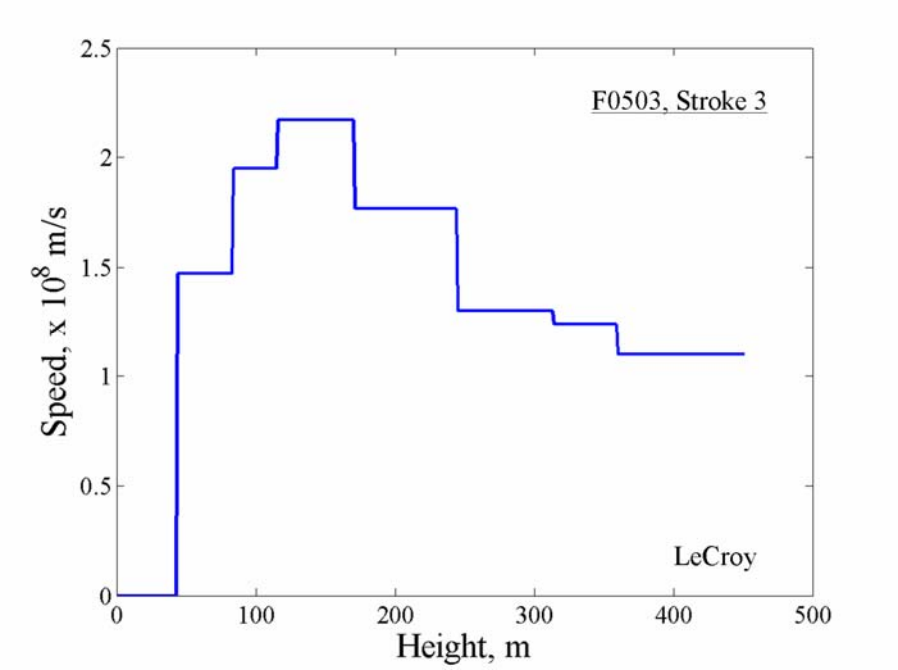

Figure 5-35: Return-stroke speed profile obtained by computing average of the speeds computed using the 20% and slope intercept methods, based on LeCroy data, shown in Figures 5-33 and 5-34, for event F0503, Stroke 3.

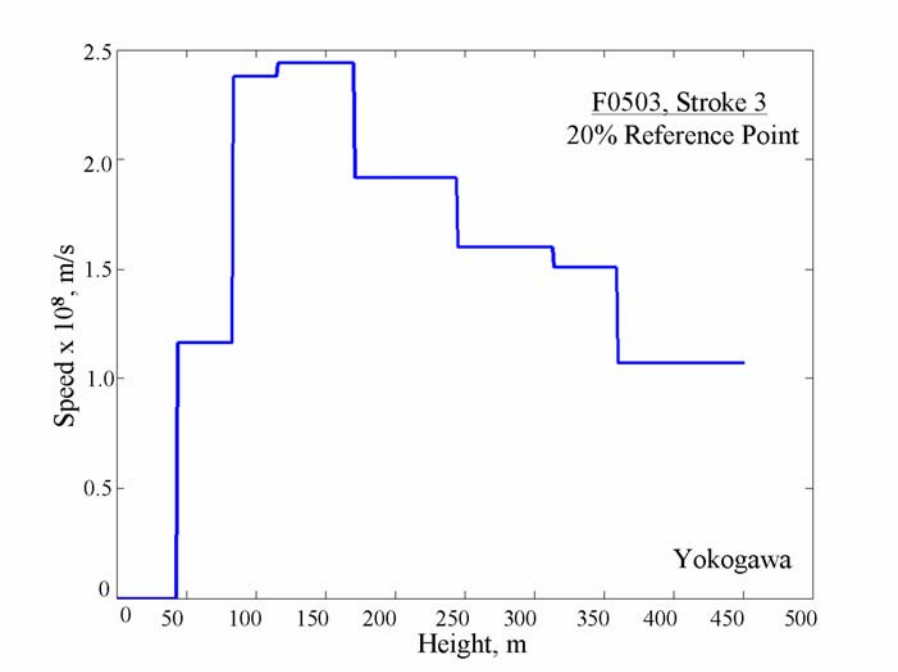

Figure 5-36: Return-stroke speed profile using the 20% Point as Reference for Event F0503, Stroke 3, based on Yokogawa data.

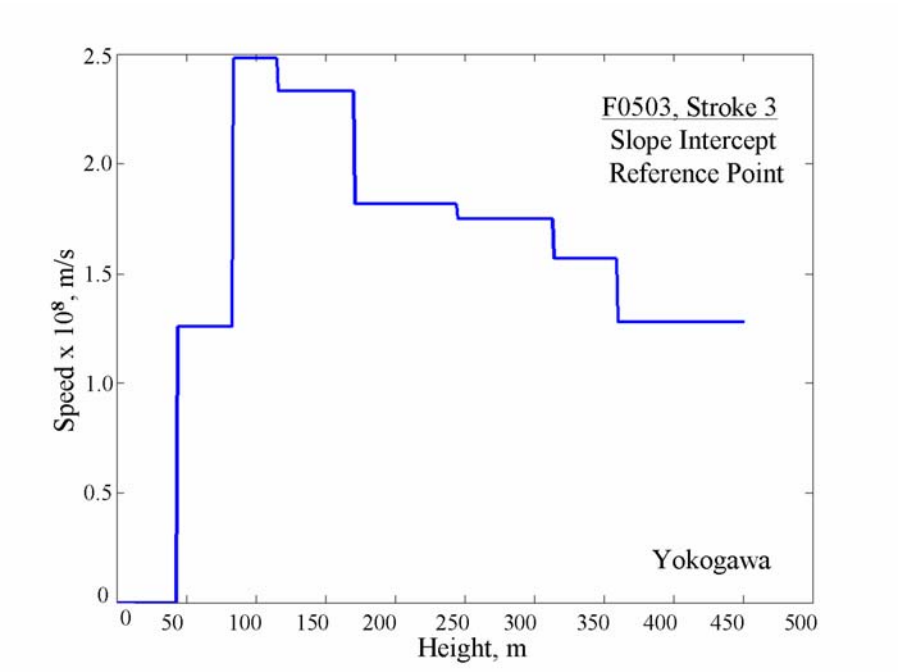

Figure 5-37: Return-stroke speed profile using the slope point as reference for event F0503, Stroke 3, based on Yokogawa data.

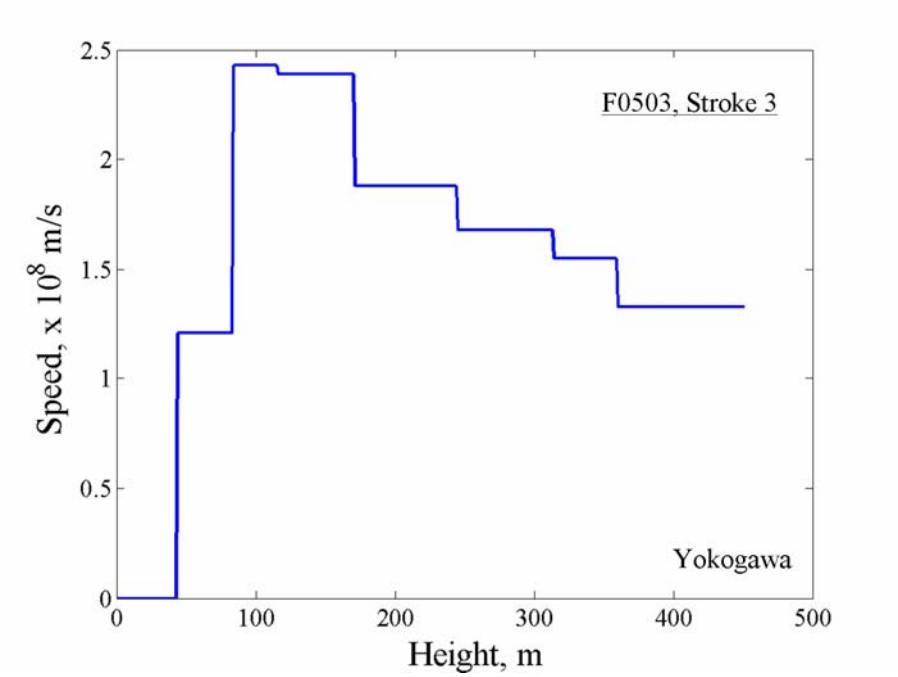

Figure 5-38: Return-stroke speed profile obtained by computing average of the speeds computed using the 20% and slope intercept methods, based on Yokogawa data, shown in Figures 5-36 and 5-37, for event F0503, Stroke 3.

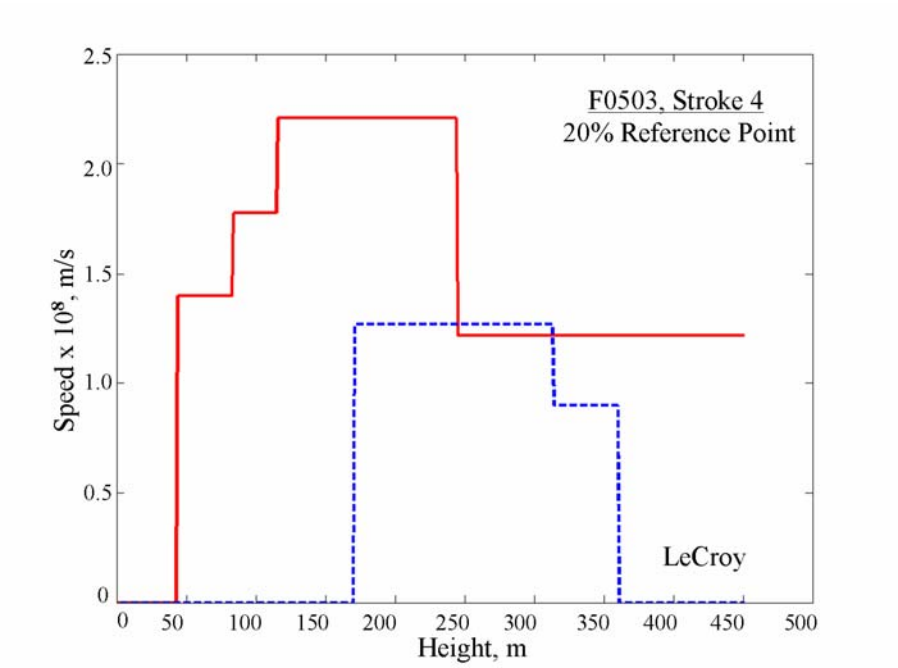

Figure 5-39: Return-stroke speed profiles obtained using the 20% reference point for event F0503, Stroke 4. Solid red line corresponds to data from LeCroy channels 2, 3, 4, 6, and 9, and dashed blue line to data from LeCroy channels 5, 7, and 8.

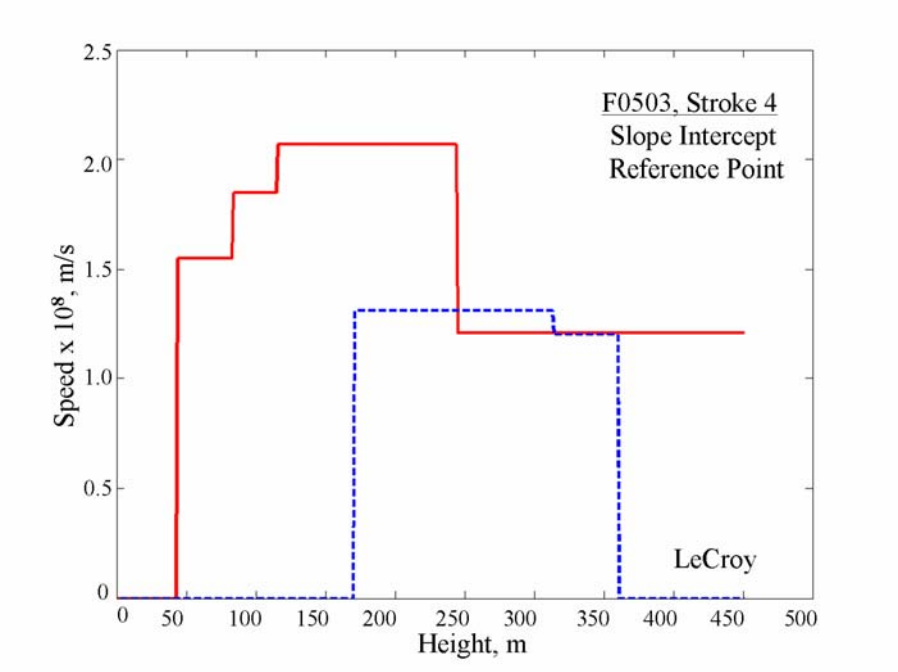

Figure 5-40: Return-stroke speed profiles obtained using the slope intercept reference point for event F0503, Stroke 4. Solid red line corresponds to data from LeCroy channels 2, 3, 4, 6, and 9, and dashed blue line to data from LeCroy channels 5, 7, and 8.

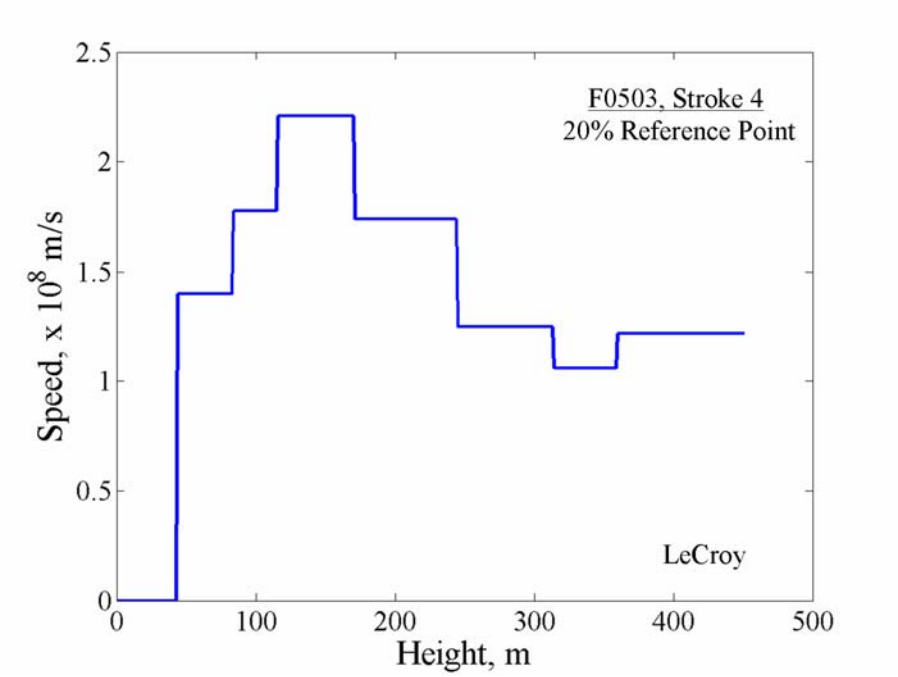

Figure 5-41: Return-stroke speed profile obtained using the 20% reference point for event F0503, Stroke 4, based on all the LeCroy data (combination of the two profiles shown in Figure 5-39).

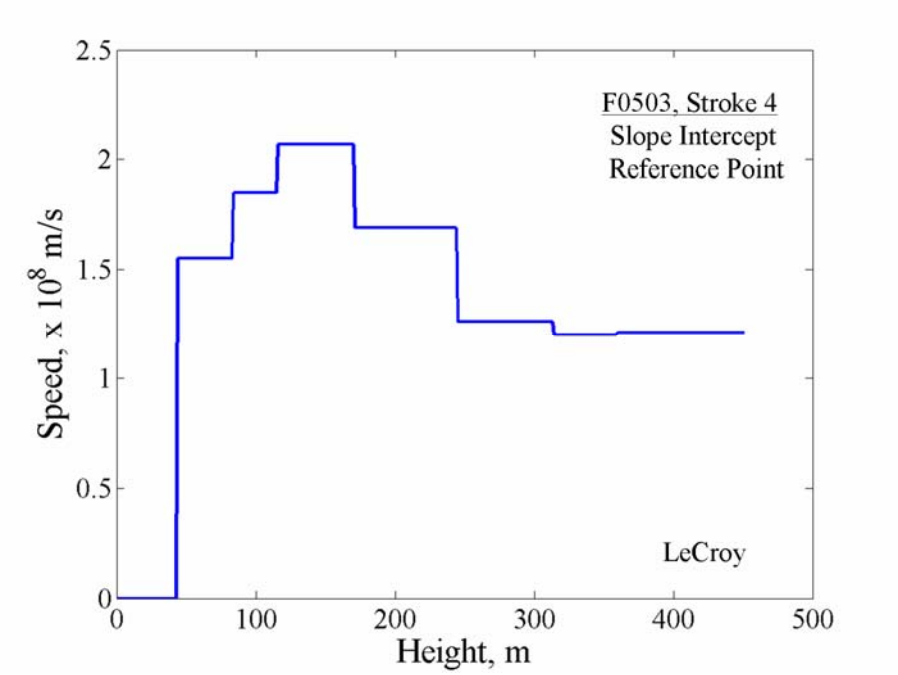

Figure 5-42: Return-stroke speed profile obtained using the slope intercept point as reference for event F0503, Stroke 4, based on all the LeCroy data (combination of the two profiles shown in Figure 5-40).

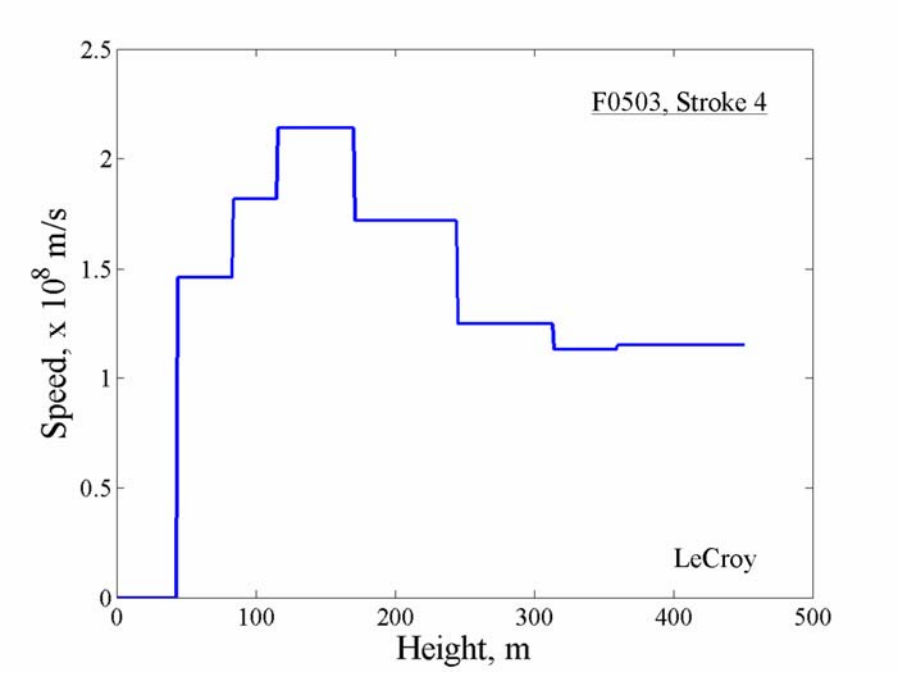

Figure 5-43: Return-stroke speed profile obtained by computing average of the speeds computed using the 20% and slope intercept methods, based on LeCroy data, shown in Figures 5-41 and 5-42, for event F0503, Stroke 4.

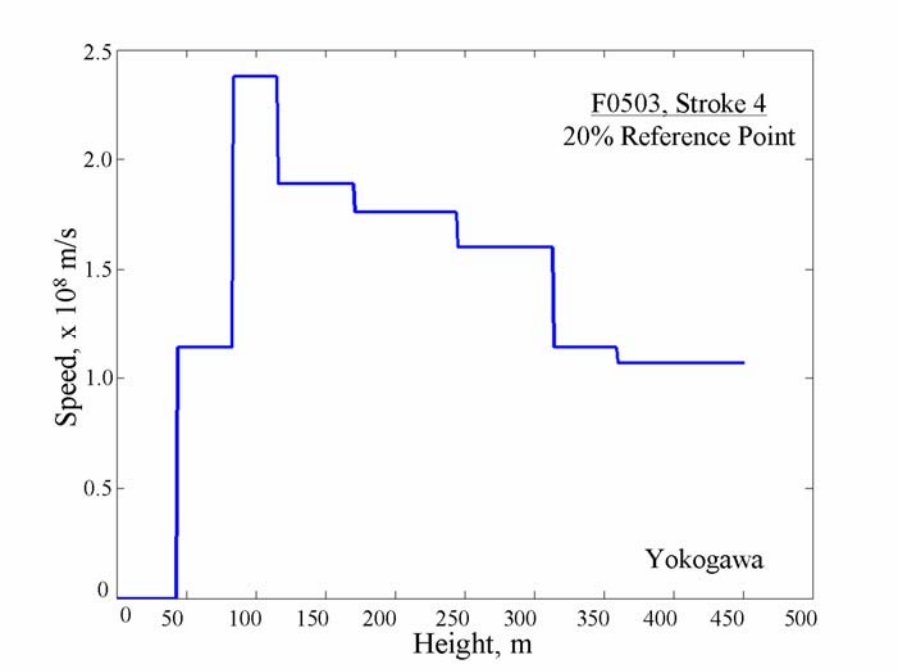

Figure 5-44: Return-stroke speed profile using the 20% Point as Reference for Event F0503, Stroke 4, based on Yokogawa data.

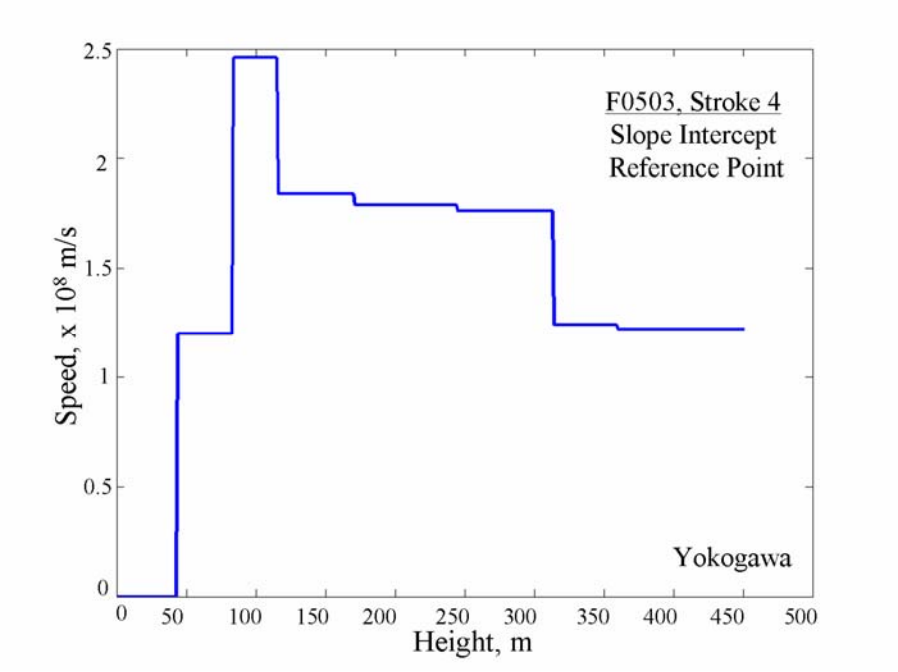

Figure 5-45: Return-stroke speed profile using the slope point as reference for event F0503, Stroke 4, based on Yokogawa data.

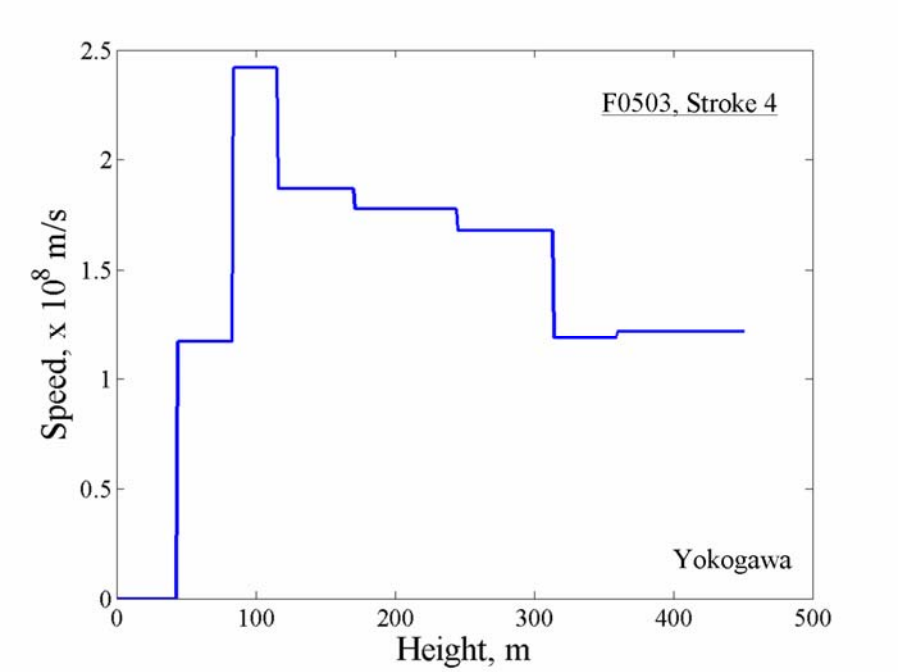

Figure 5-46: Return-stroke speed profile obtained by computing average of the speeds computed using the 20% and slope intercept methods, based on Yokogawa data, shown in Figures 5-44 and 5-45, for event F0503, Stroke 4.

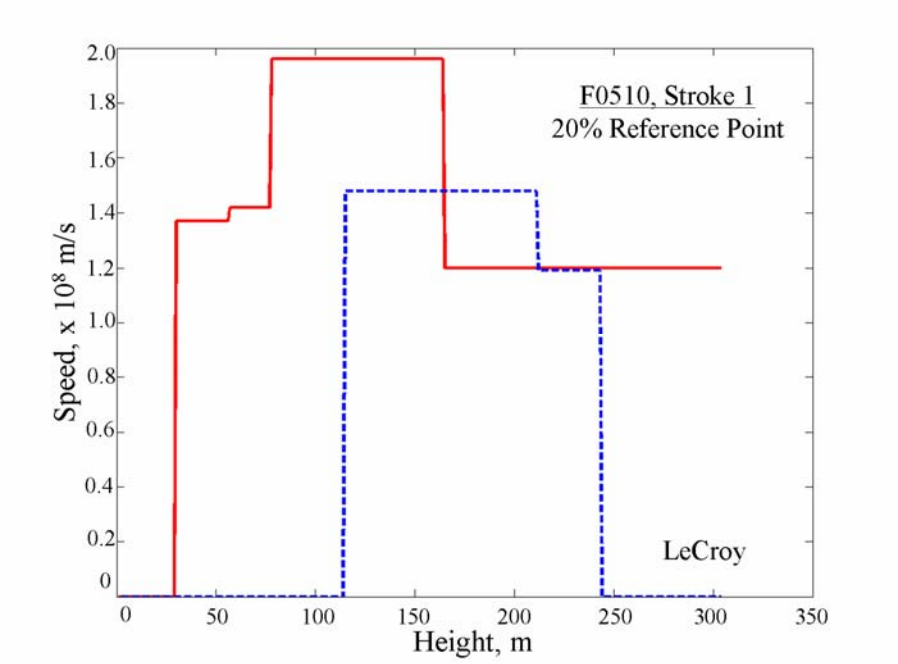

Figure 5.47: Return-stroke speed profiles obtained using the 20% reference point for event F0510, Stroke 1. Solid red line corresponds to data from LeCroy channels 2, 3, 4, 6, and 9, and dashed blue line to data from LeCroy channels 5, 7, and 8.

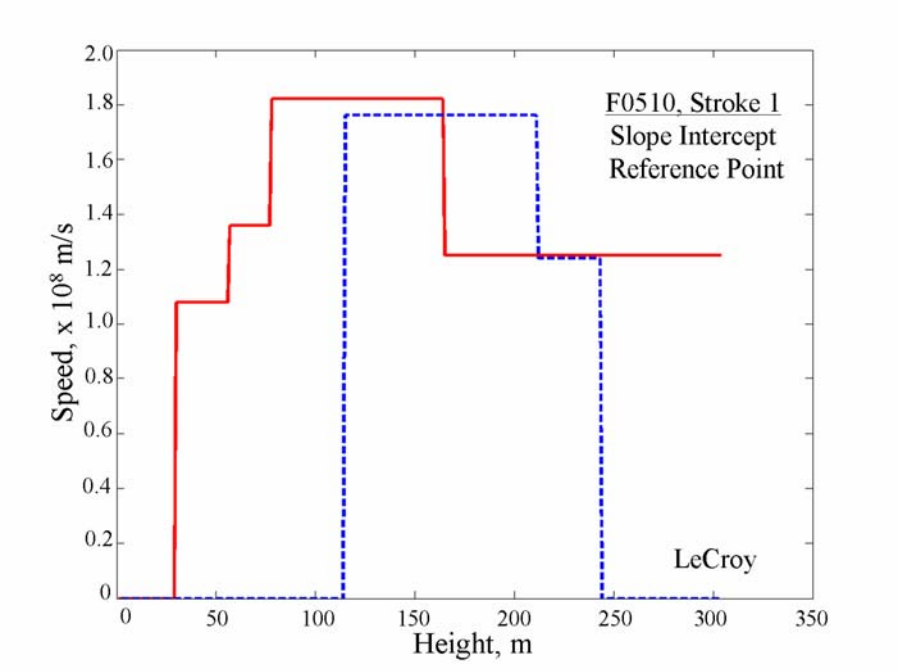

Figure 5.48: Return-stroke speed profiles obtained using the slope intercept reference point for event F0510, Stroke 1. Solid red line corresponds to data from LeCroy channels 2, 3, 4, 6, and 9, and dashed blue line to data from LeCroy channels 5, 7, and 8.

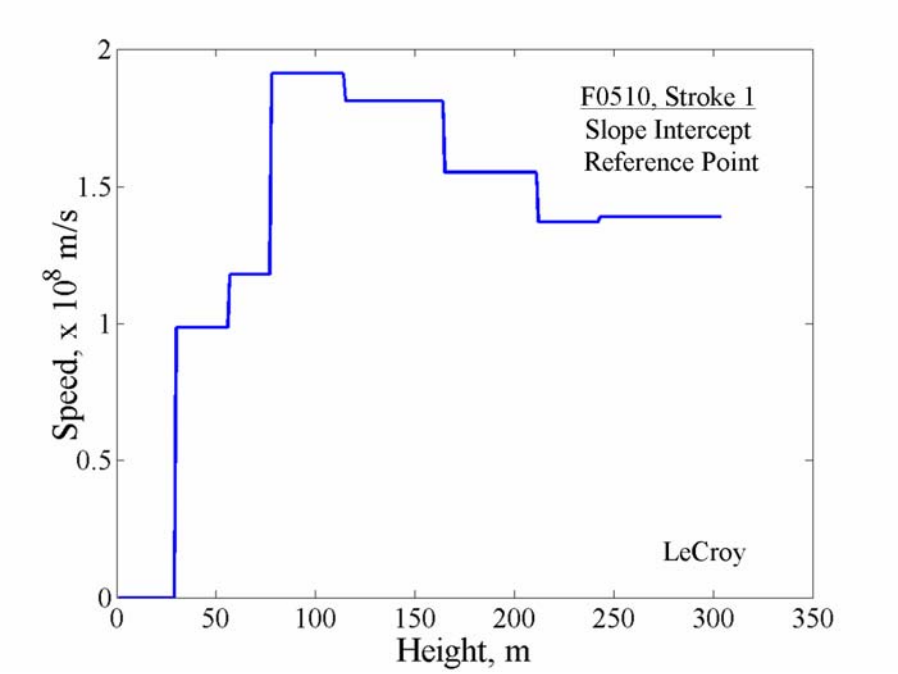

Figure 5-49: Return-stroke speed profile obtained using the 20% reference point for event F0510, Stroke 1, based on all the LeCroy data (combination of the two profiles shown in Figure 5-47).

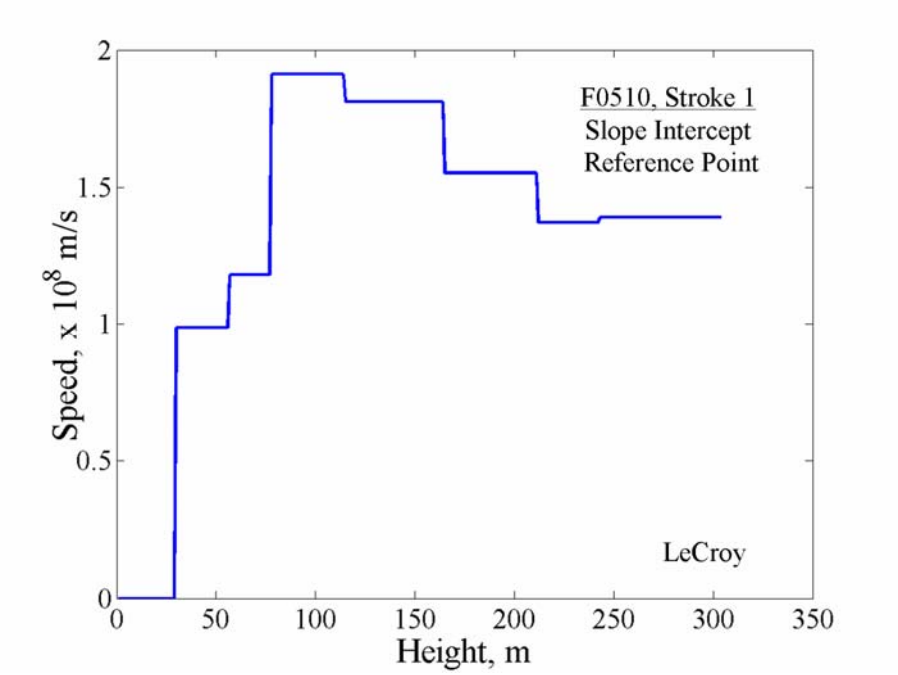

Figure 5-50: Return-stroke speed profile obtained using the slope intercept point as reference for event F0510, Stroke 1, based on all the LeCroy data (combination of the two profiles shown in Figure 5-48).

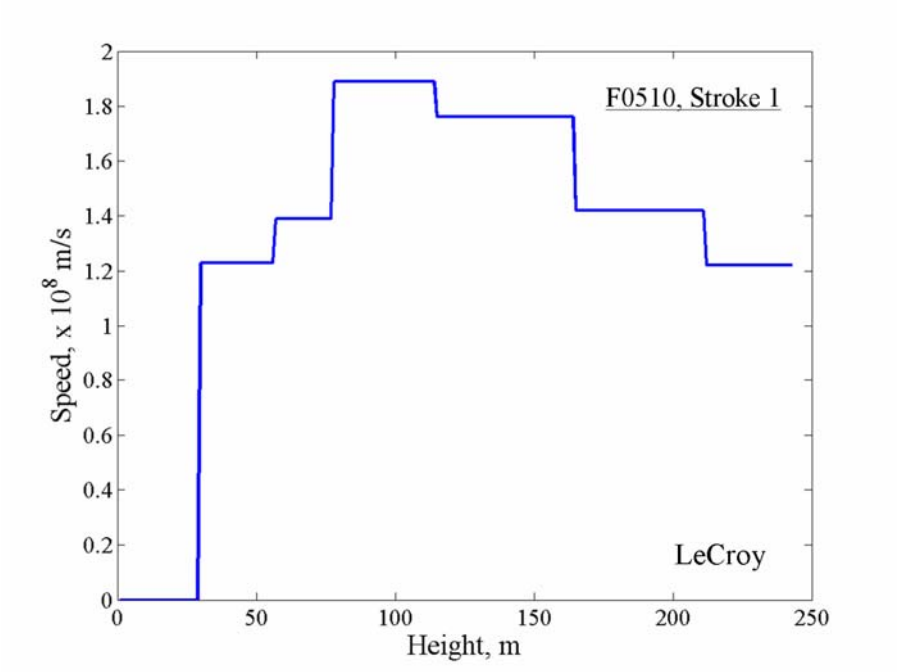

Figure 5-51: Return-stroke speed profile obtained by computing the average of speeds computed using the 20% and slope intercept methods, based on LeCroy data, shown in Figures 5-54 and 5-55, for event F0510, Stroke 1.

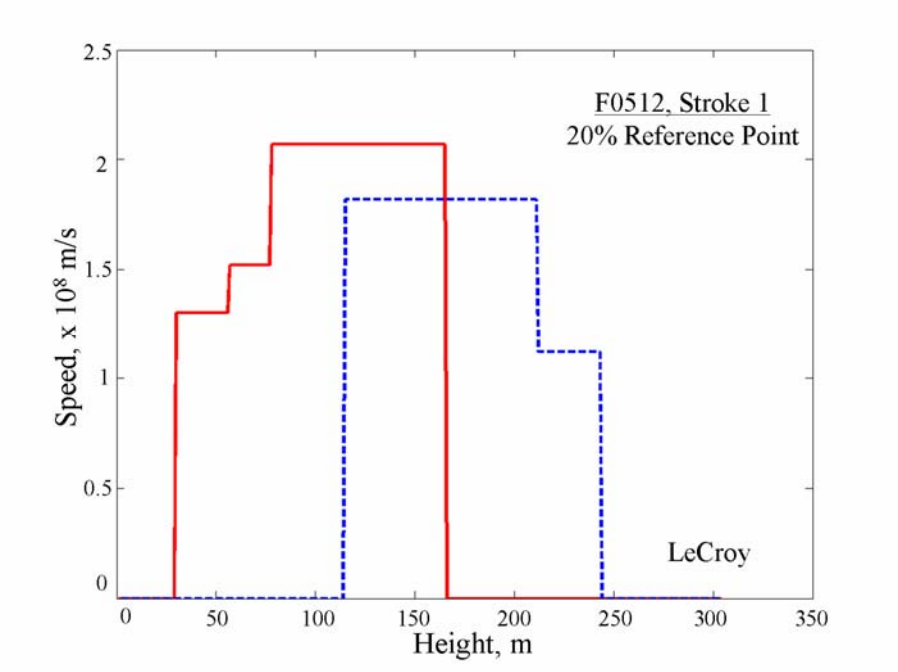

Figure 5.52: Return-stroke speed profiles obtained using the 20% reference point for event F0512, Stroke 1. Solid red line corresponds to data from LeCroy channels 2, 3, 4, and 6, and dashed blue line to data from LeCroy channels 5, 7, and 8.

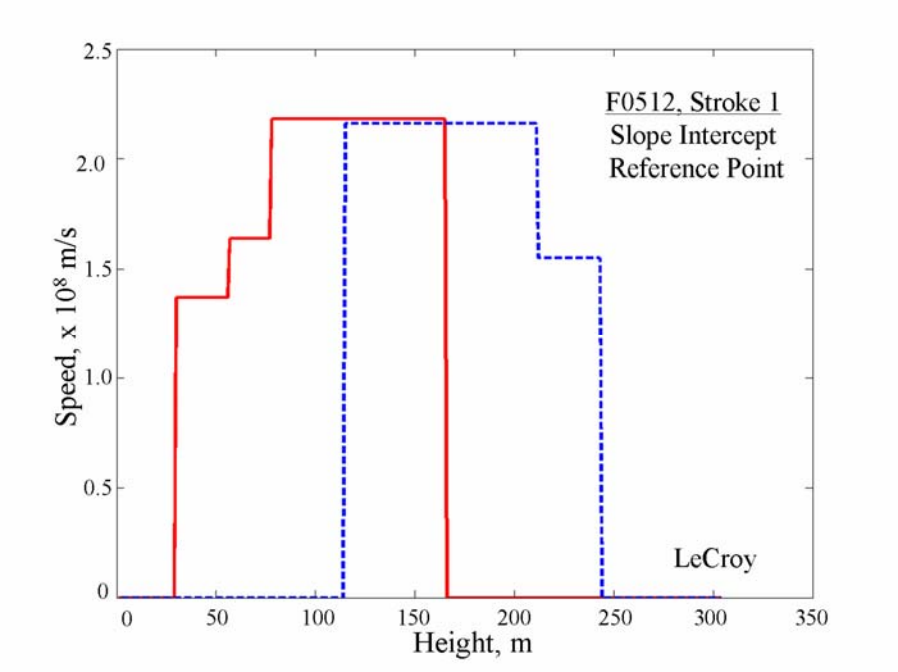

Figure 5-53: Return-stroke speed profiles obtained using the slope intercept reference point for event F0512, Stroke 1. Solid red line corresponds to data from LeCroy channels 2, 3, 4, and 6, and dashed blue line to data from LeCroy channels 5, 7, and 8.

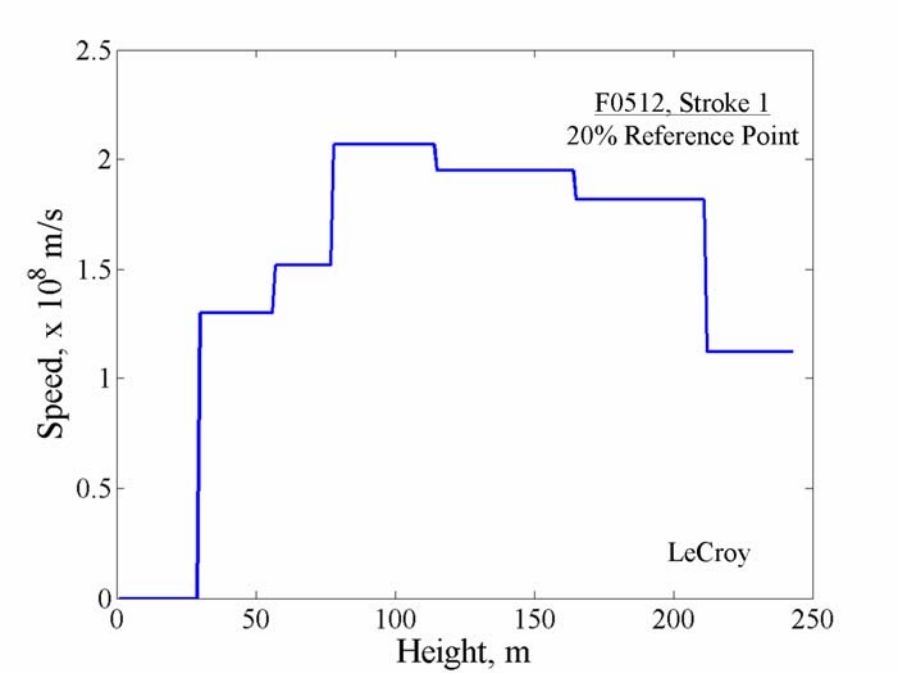

Figure 5-54: Return-stroke speed profile obtained using the 20% reference point for event F0512, Stroke 1, based on all the LeCroy data (combination of the two profiles shown in Figure 5-52).

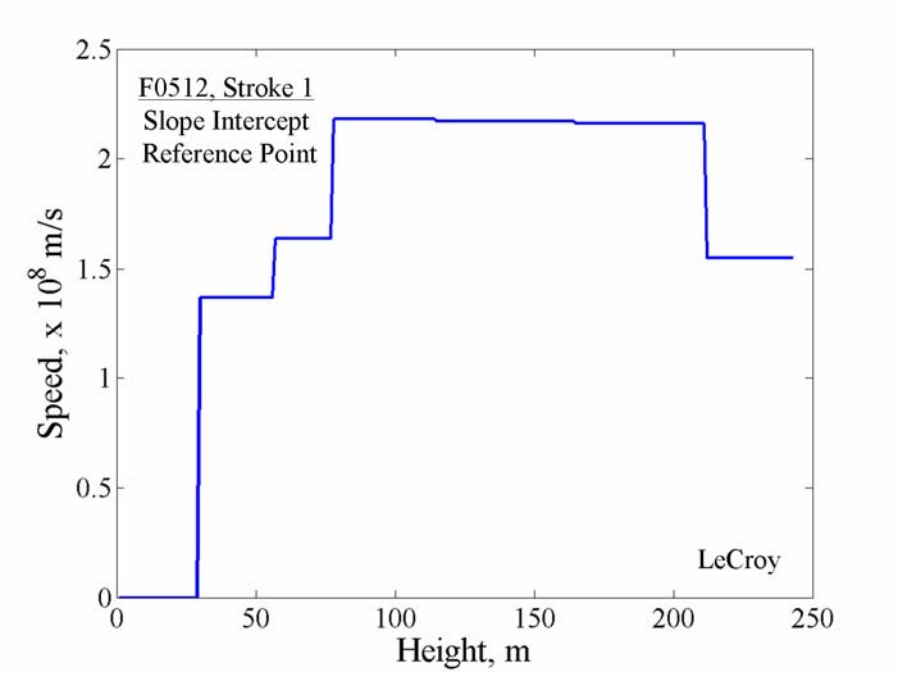

Figure 5-55: Return-stroke speed profile obtained using the slope intercept point as reference for event F0512, Stroke 1, based on all the LeCroy data (combination of the two profiles shown in Figure 5-53).

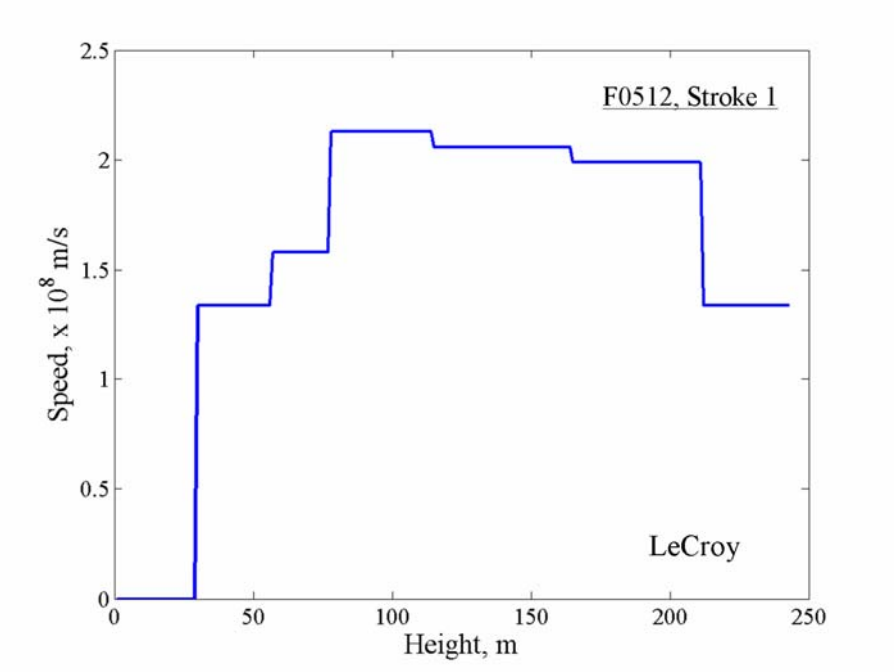

Figure 5-56: Return-stroke speed profile obtained by computing the average of speeds computed using the 20% and slope intercept methods, based on LeCroy data, shown in Figures 5-59 and 5-60, for event F0512, Stroke 1.

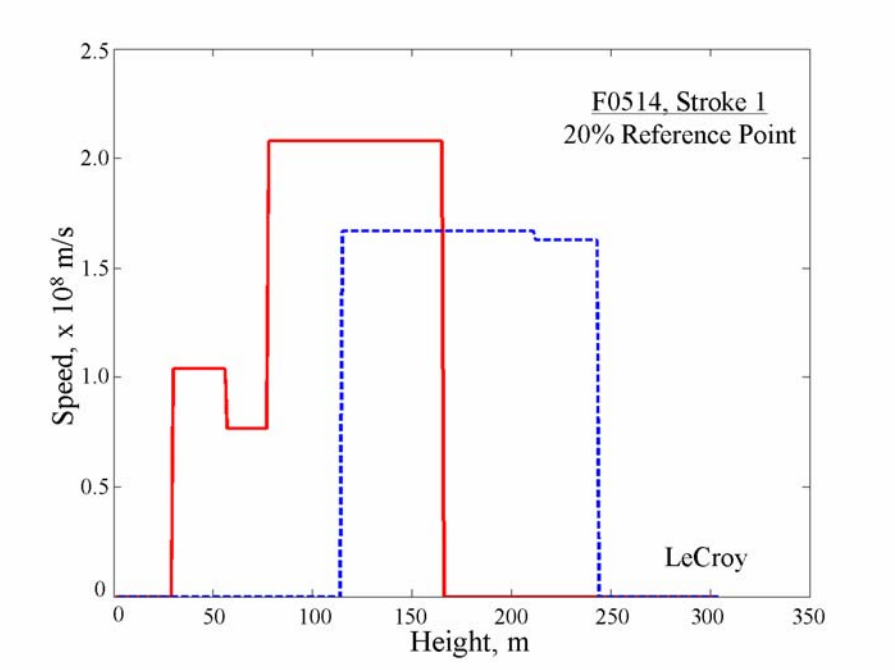

Figure 5-57: Return-stroke speed profiles obtained using the 20% reference point for event F0514, Stroke 1. Solid red line corresponds to data from LeCroy channels 2, 3, 4, and 6, and dashed blue line to data from LeCroy channels 5, 7, and 8.

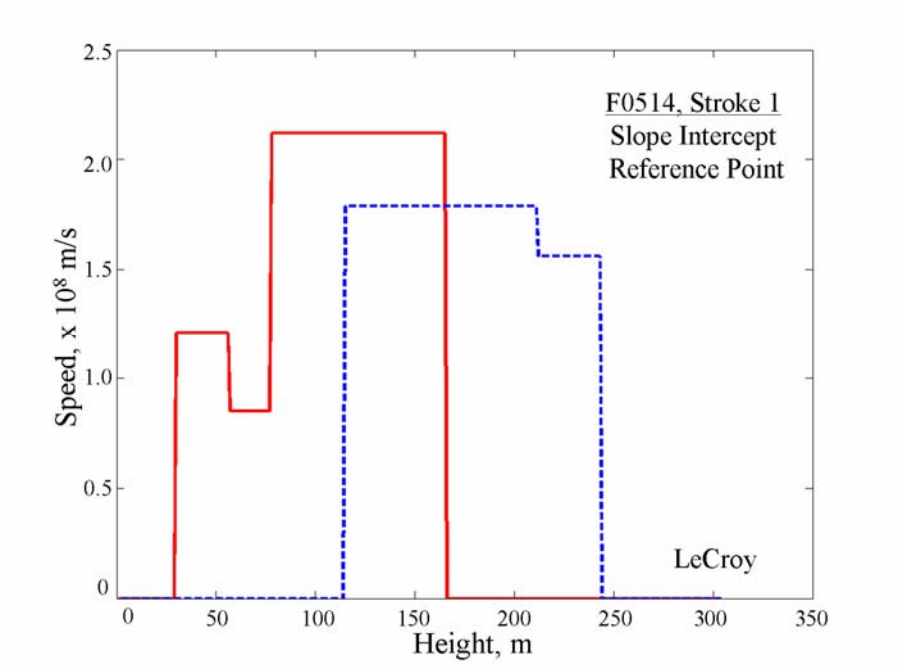

Figure 5-58: Return-stroke speed profiles obtained using the slope intercept reference point for event F0514, Stroke 1. Solid red line corresponds to data from LeCroy channels 2, 3, 4, and 6, and dashed blue line to data from LeCroy channels 5, 7, and 8.

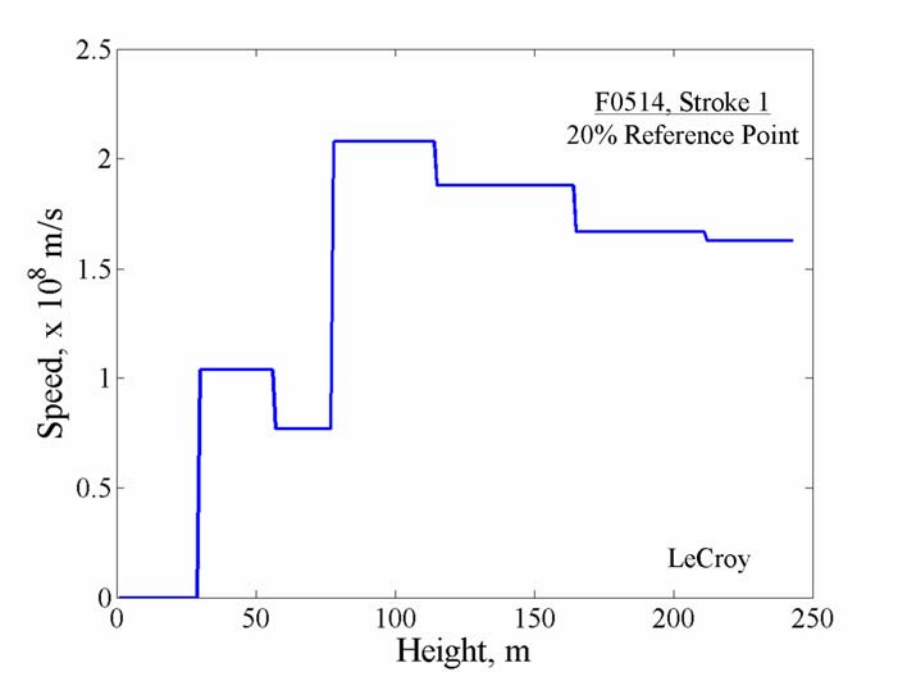

Figure 5-59: Return-stroke speed profile obtained using the 20% reference point for event F0514, Stroke 1, based on all the LeCroy data (combination of the two profiles shown in Figure 5-57).

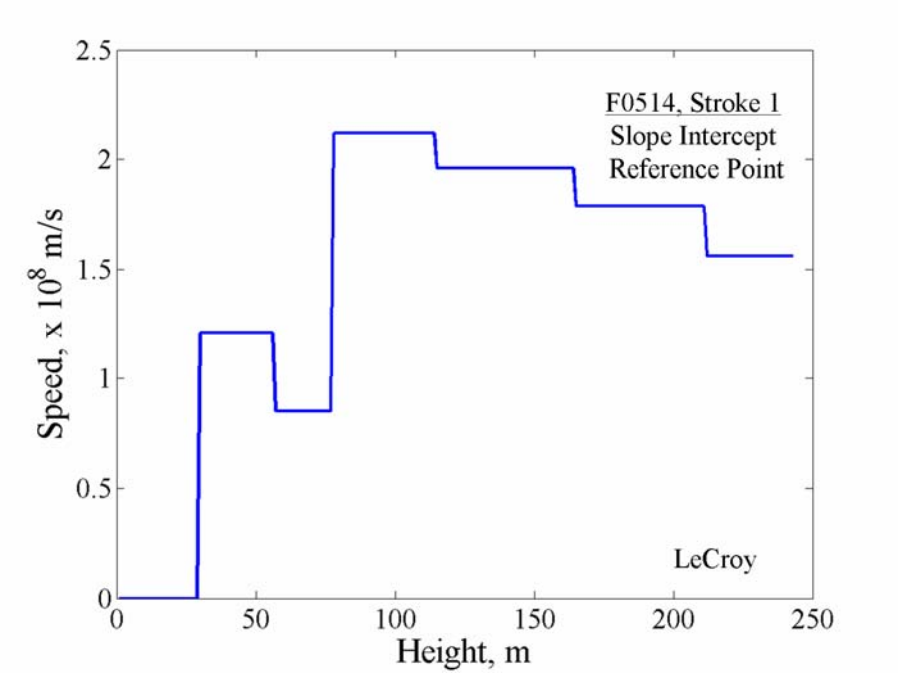

Figure 5-60: Return-stroke speed profile obtained using the slope intercept point as reference for event F0514, Stroke 1, based on all the LeCroy data (combination of the two profiles shown in Figure 5-58).

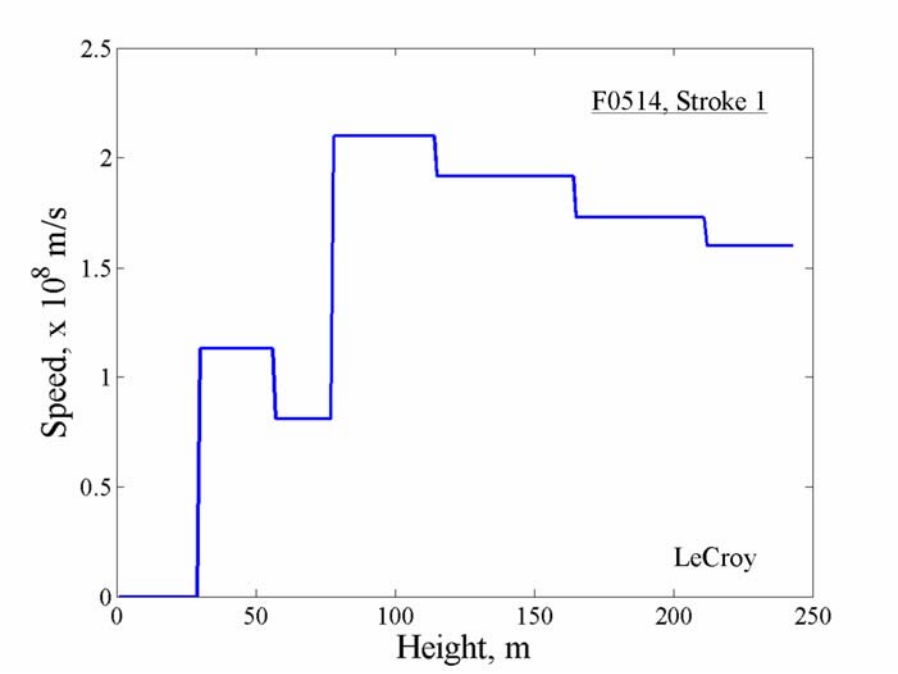

Figure 5-61: Return-stroke speed profile obtained by computing average of the speeds computed using the 20% and slope intercept methods, based on LeCroy data, shown in Figures 5-59 and 5-60, for event F0514, Stroke 1.

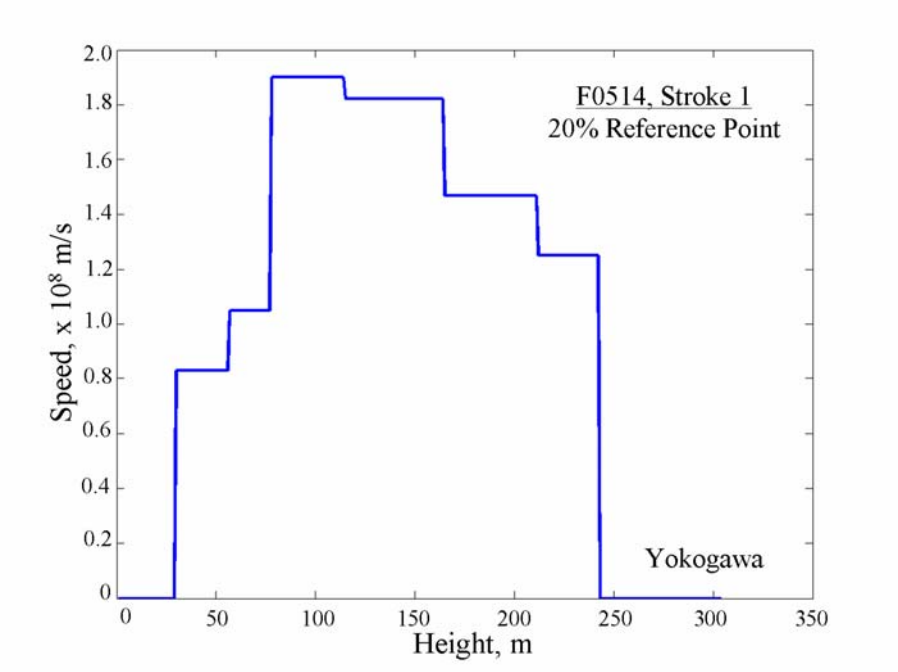

Figure 5-62: Return-stroke speed profile using the 20% Point as Reference for Event F0514, Stroke 1, based on Yokogawa data.

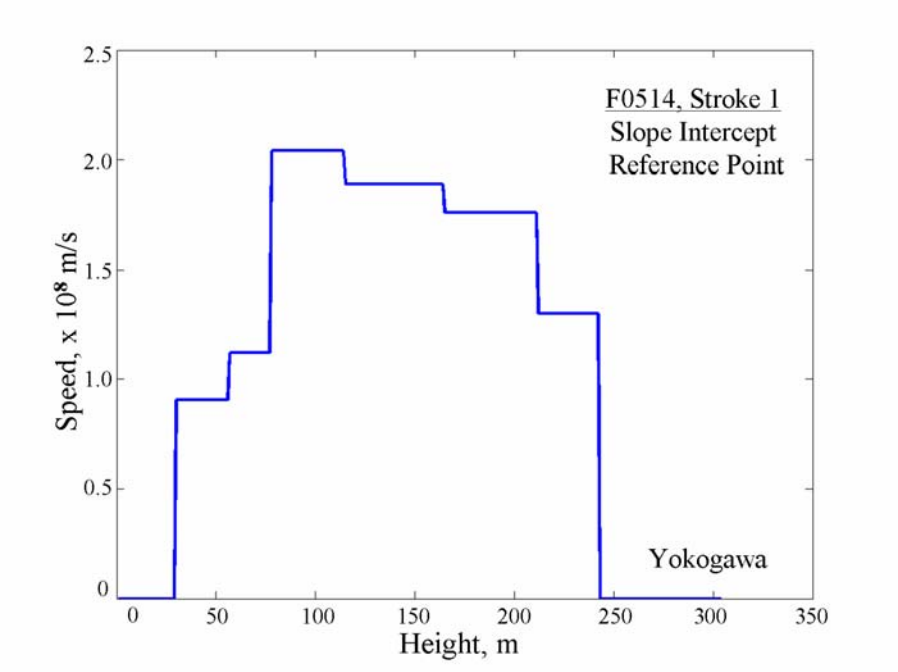

Figure 5-63: Return-stroke speed profile using the slope point as reference for event F0514, Stroke 1, based on Yokogawa data.

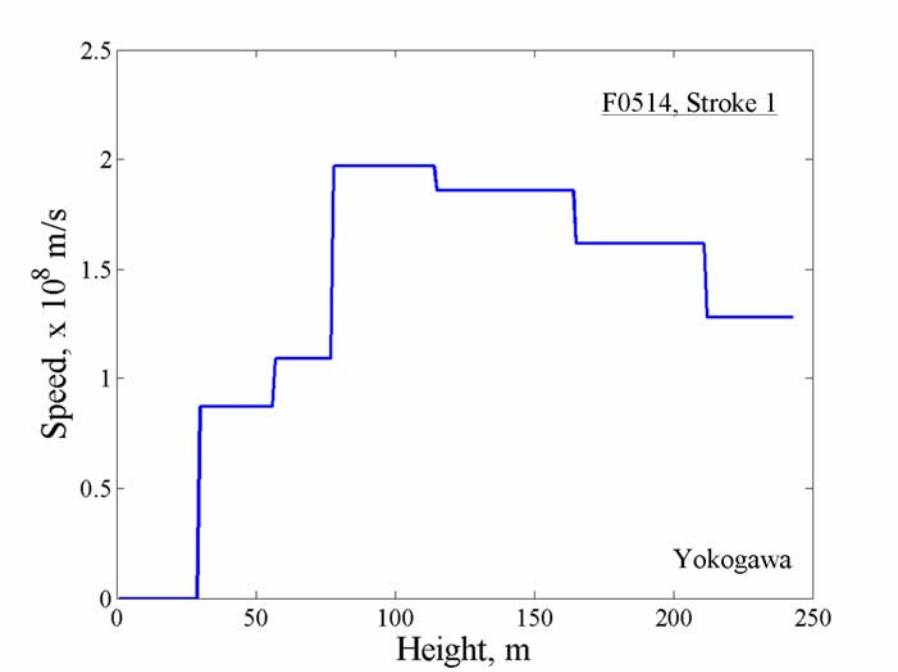

Figure 5-64: Return-stroke speed profile obtained by computing average of the speeds computed using the 20% and slope intercept methods, based on Yokogawa data, shown in Figures 5-62 and 5-63, for event F0514, Stroke 1.

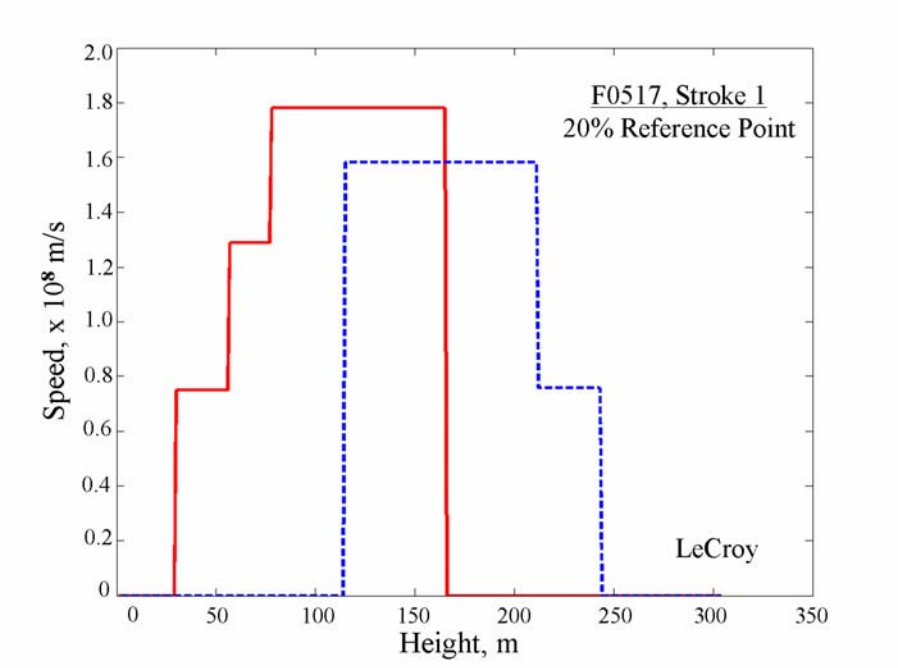

Figure 5-65: Return-stroke speed profiles obtained using the 20% reference point for event F0517, Stroke 1. Solid red line corresponds to data from LeCroy channels 2, 3, 4, and 6, and dashed blue line to data from LeCroy channels 5, 7, and 8.

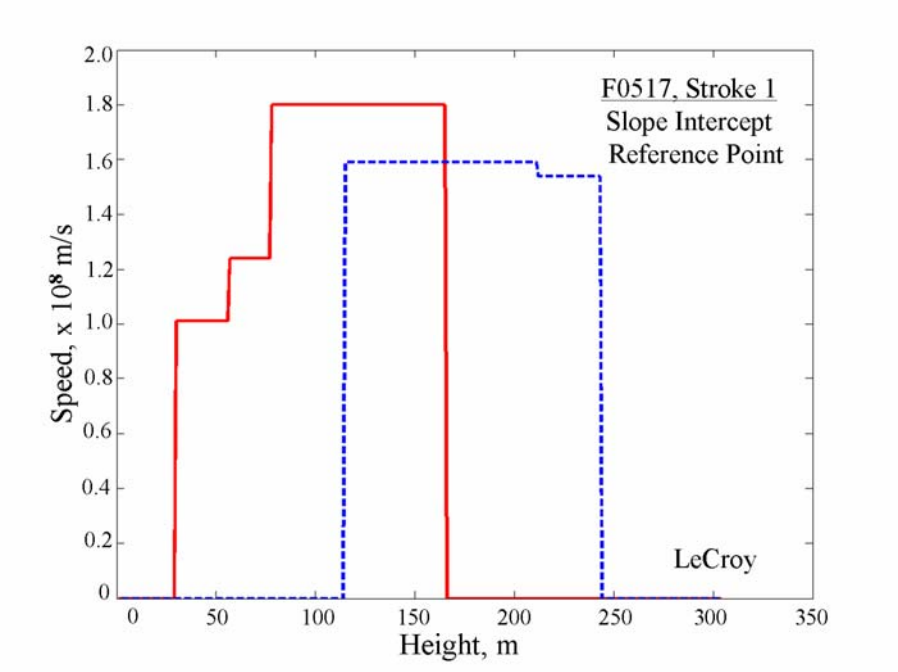

Figure 5-66: Return-stroke speed profiles obtained using the slope intercept reference point for event F0517, Stroke 1. Solid red line corresponds to data from LeCroy channels 2, 3, 4, and 6, and dashed blue line to data from LeCroy channels 5, 7, and 8.

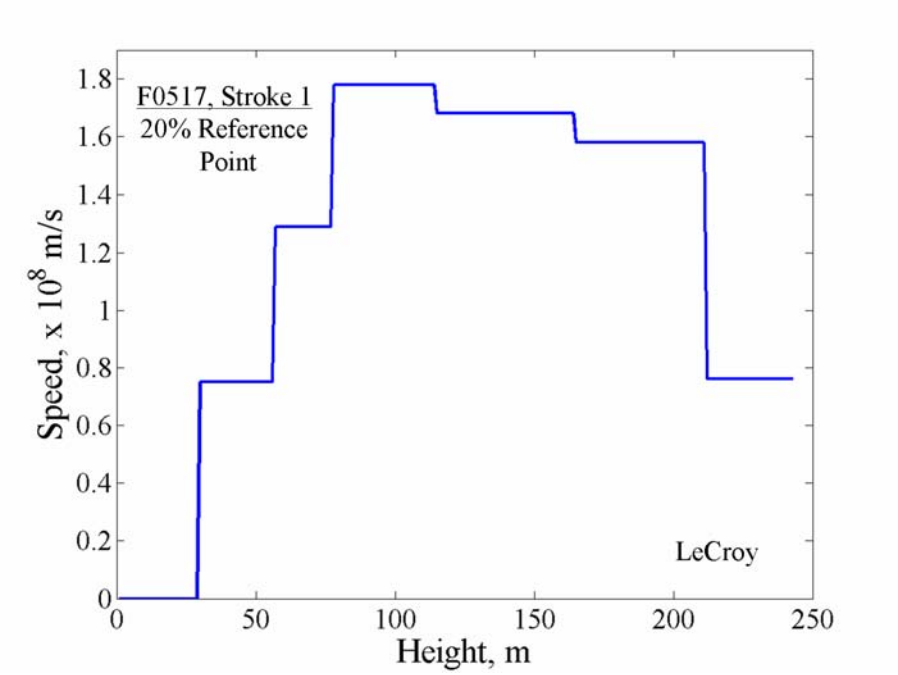

Figure 5-67: Return-stroke speed profile obtained using the 20% reference point for event F0517, Stroke 1, based on all the LeCroy data (combination of the two profiles shown in Figure 5-65).

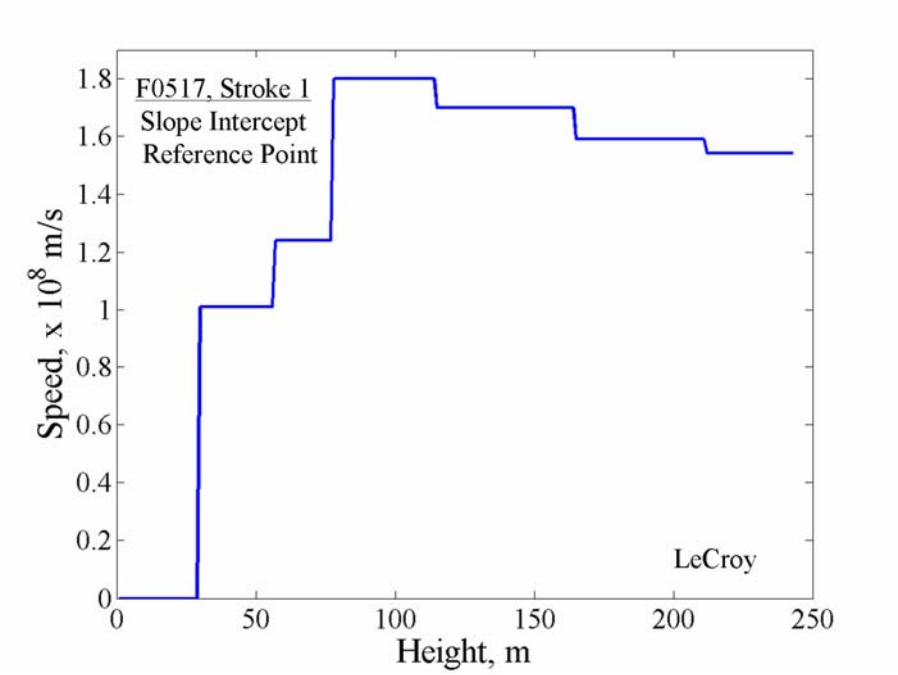

Figure 5-68: Return-stroke speed profile obtained using the slope intercept point as reference for event F0517, Stroke 1, based on all the LeCroy data (combination of the two profiles shown in Figure 5-66).

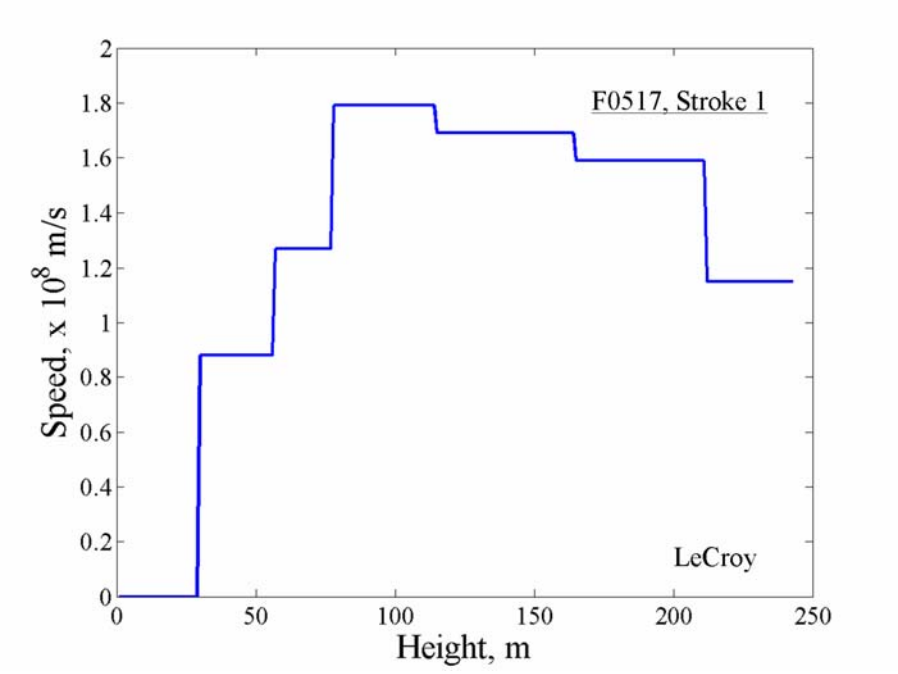

Figure 5-69: Return-stroke speed profile obtained by computing average of the speeds computed using the 20% and slope intercept methods, based on LeCroy data, shown in Figures 5-67 and 5-68, for event F0517, Stroke 1.

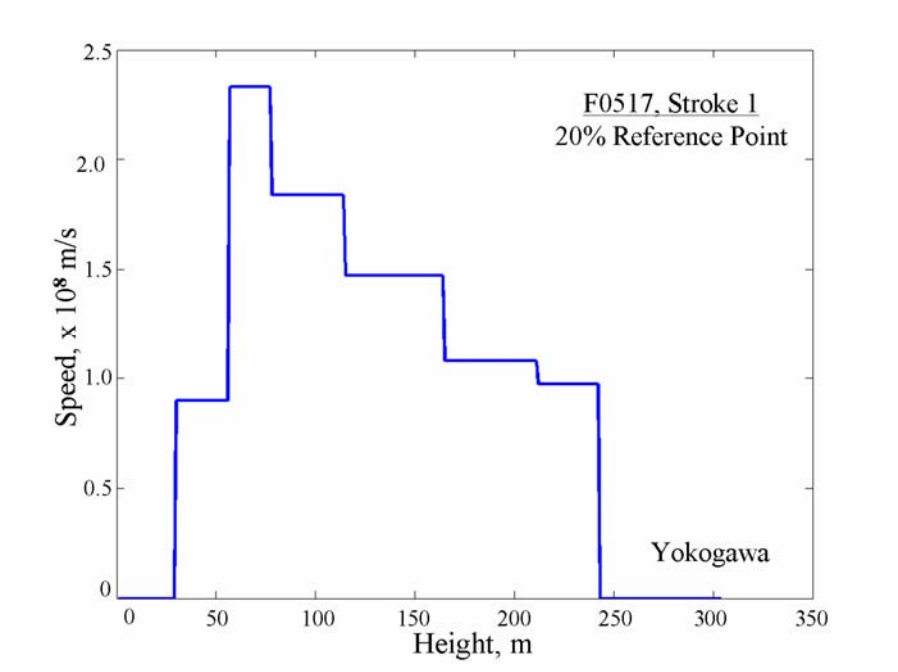

Figure 5-70: Return-stroke speed profile using the 20% Point as Reference for Event F0517, Stroke 1, based on Yokogawa data.

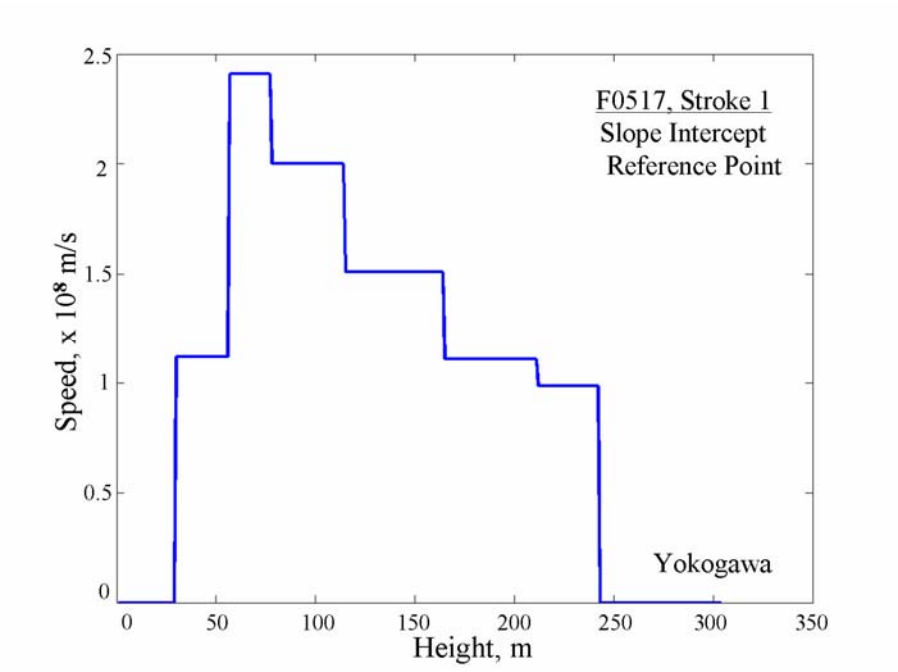

Figure 5-71: Return-stroke speed profile using the slope point as reference for event F0517, Stroke 1, based on Yokogawa data.

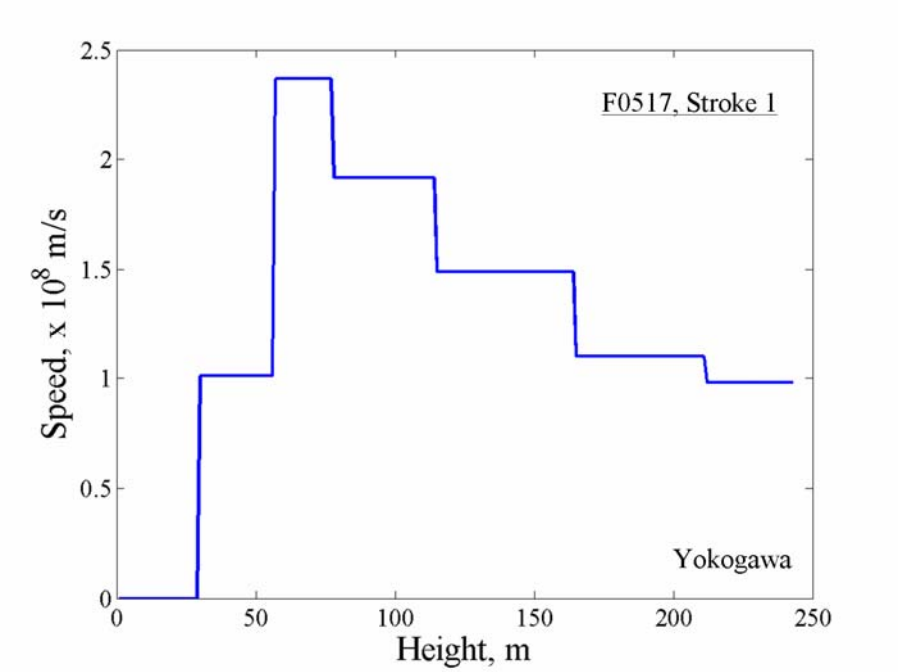

Figure 5-72: Return-stroke speed profile obtained by computing average of the speeds computed using the 20% and slope intercept methods, based on Yokogawa data, shown in Figures 5-70 and 5-71, for event F0517, Stroke 1.

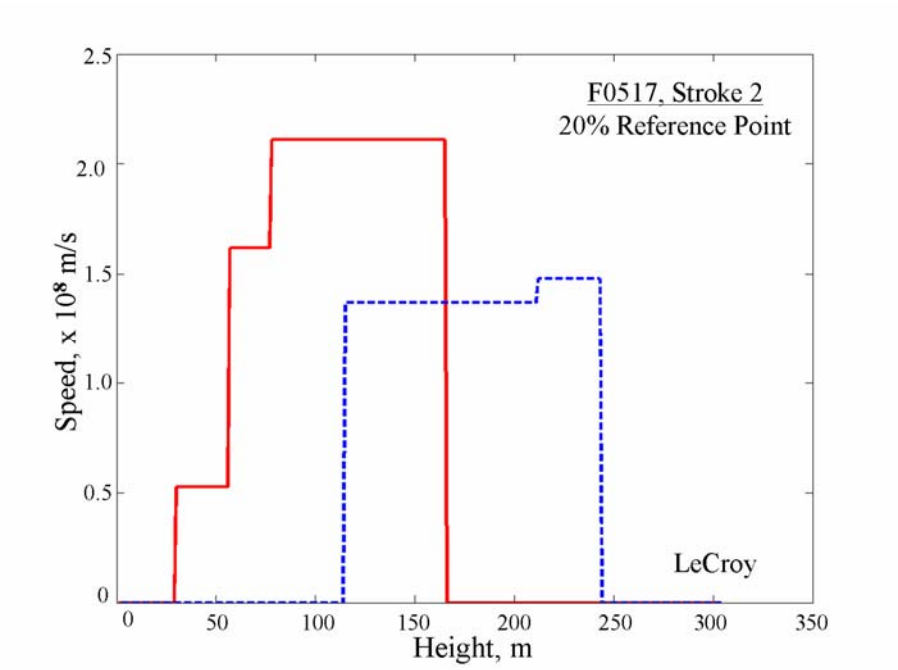

Figure 5-73: Return-stroke speed profiles obtained using the 20% reference point for event F0517, Stroke 2. Solid red line corresponds to data from LeCroy channels 2, 3, 4, and 6, and dashed blue line to data from LeCroy channels 5, 7, and 8.

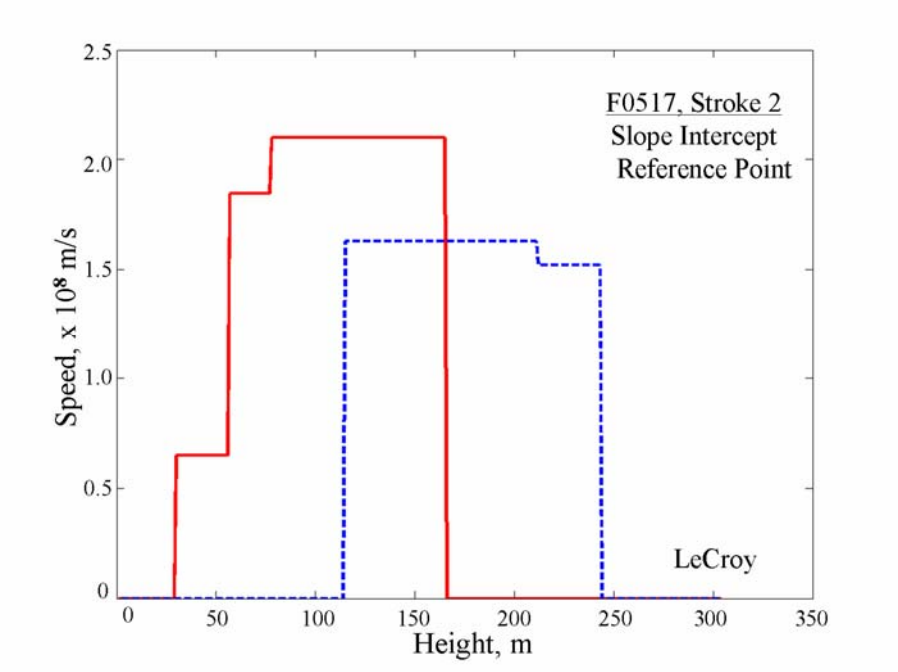

Figure 5-74: Return-stroke speed profiles obtained using the slope intercept reference point for event F0517, Stroke 2. Solid red line corresponds to data from LeCroy channels 2, 3, 4, and 6, and dashed blue line to data from LeCroy channels 5, 7, and 8.

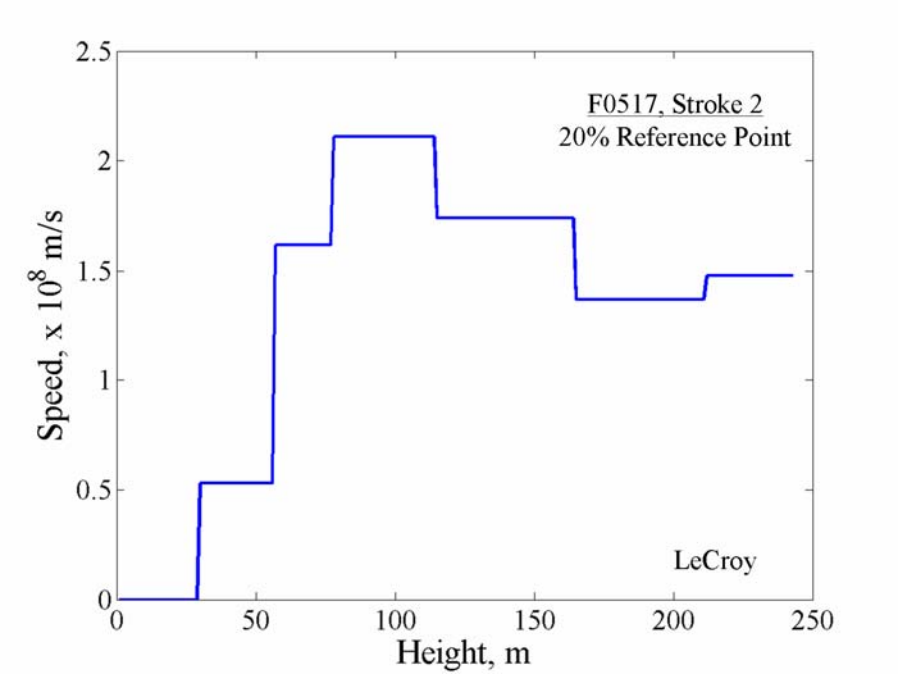

Figure 5-75: Return-stroke speed profile obtained using the 20% reference point for event F0517, Stroke 2, based on all the LeCroy data (combination of the two groups of channels shown in Figure 5-73).

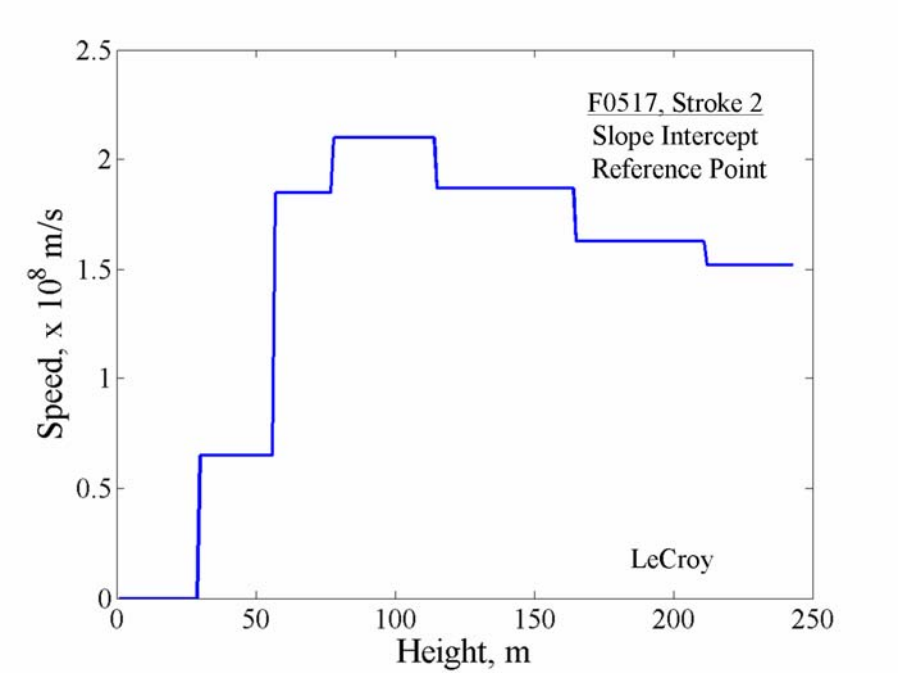

Figure 5-76: Return-stroke speed profile obtained using the slope intercept point as reference for event F0517, Stroke 2, based on all the LeCroy data (combination of the two groups of channels shown in Figure 5-74).

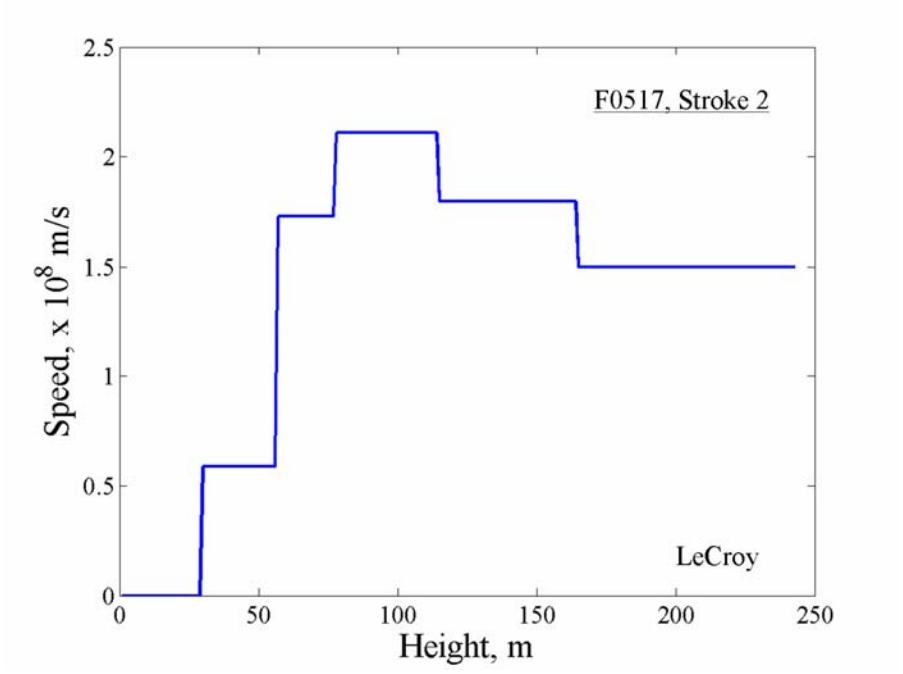

Figure 5-77: Return-stroke speed profile obtained by computing average of the speeds computed using the 20% and slope intercept methods, based on LeCroy data, shown in Figures 5-75 and 5-76, for event F0517, Stroke 2.

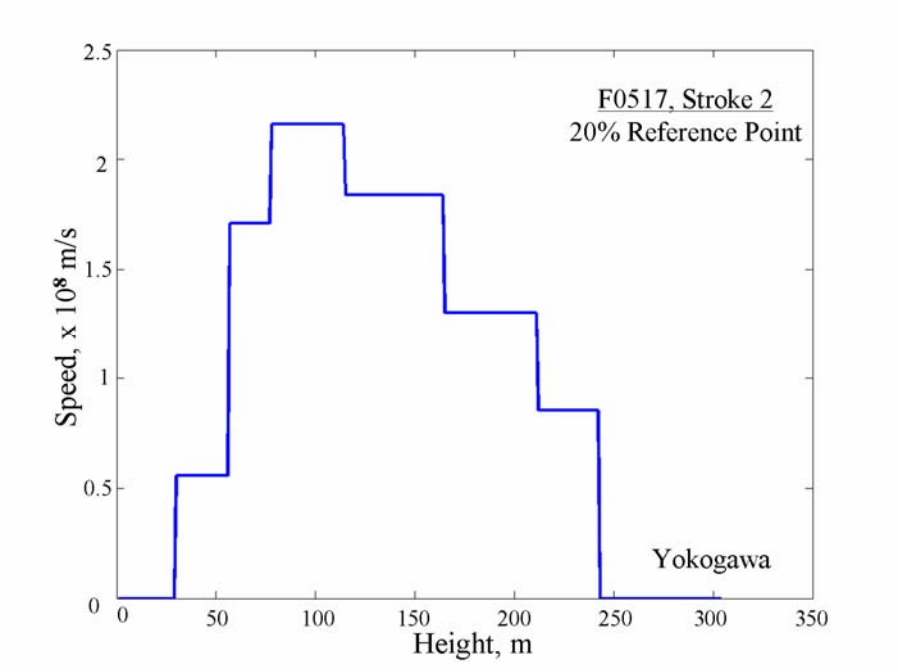

Figure 5-78: Return-stroke speed profile using the 20% Point as Reference for Event F0517, Stroke 2, based on Yokogawa data.

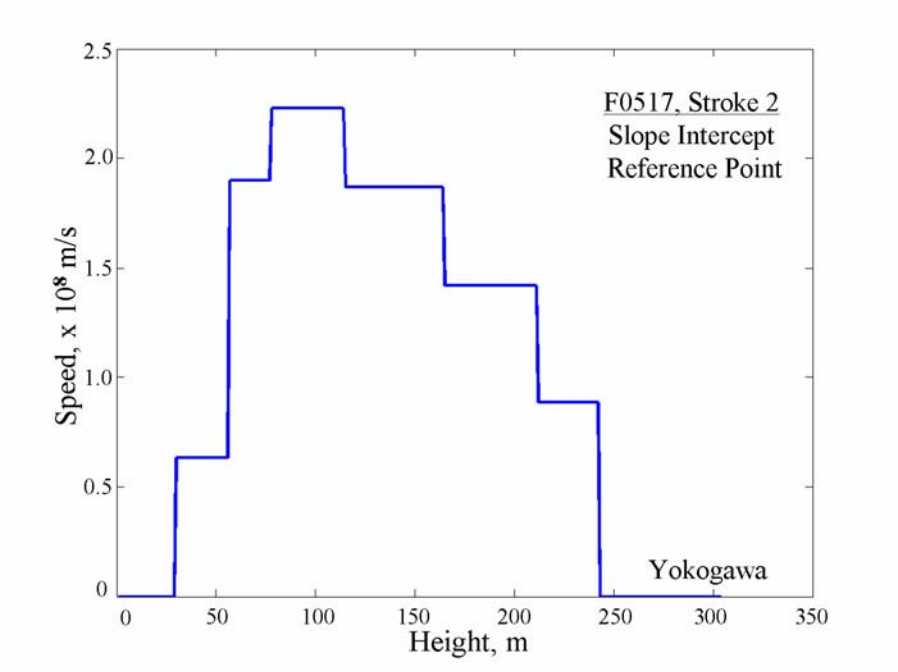

Figure 5-79: Return-stroke speed profile using the slope point as reference for event F0517, Stroke 2, based on Yokogawa data.

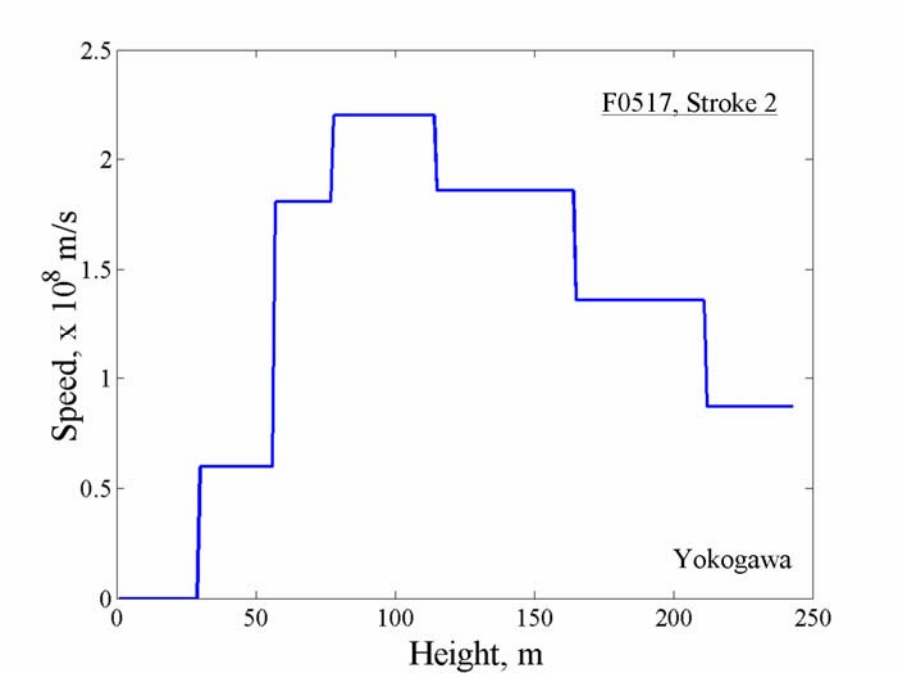

Figure 5-80: Return-stroke speed profile obtained by computing average of the speeds computed using the 20% and slope intercept methods, based on Yokogawa data, shown in Figures 5-78 and 5-79, for event F0517, Stroke 2.

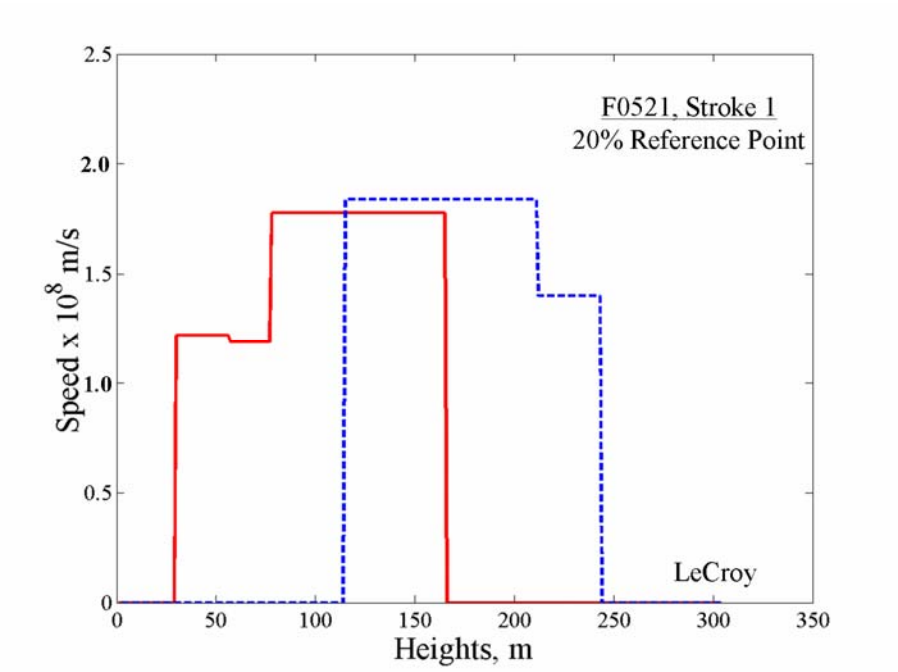

Figure 5-81: Return-stroke speed profiles obtained using the 20% reference point for event F0521, Stroke 1. Solid red line corresponds to data from LeCroy channels 2, 3, 4, and 6, and dashed blue line to data from LeCroy channels 5, 7, and 8.

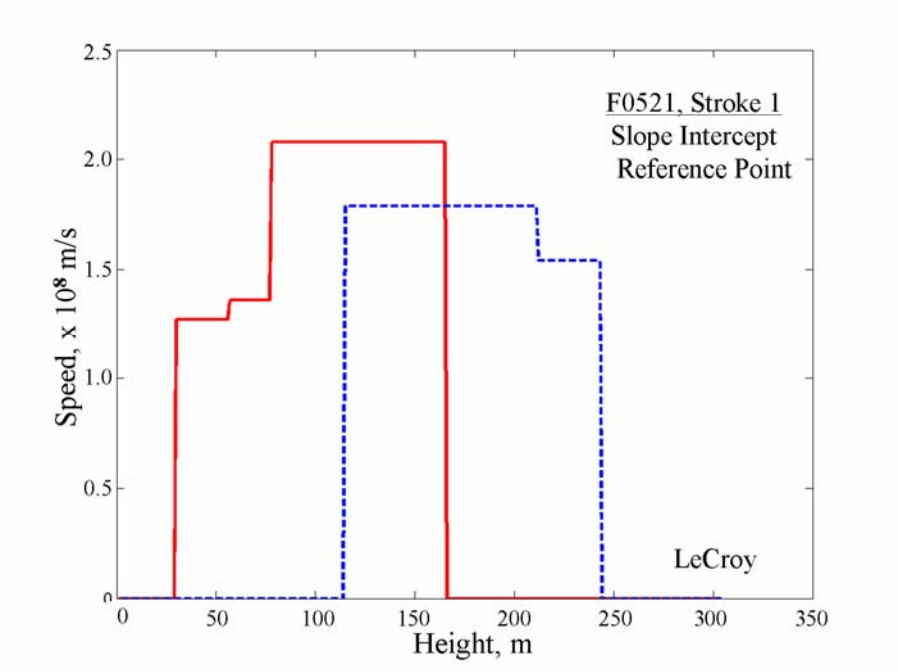

Figure 5-82: Return-stroke speed profiles obtained using the slope intercept reference point for event F0521, Stroke 1. Solid red line corresponds to data from LeCroy channels 2, 3, 4, and 6, and dashed blue line to data from LeCroy channels 5, 7, and 8.

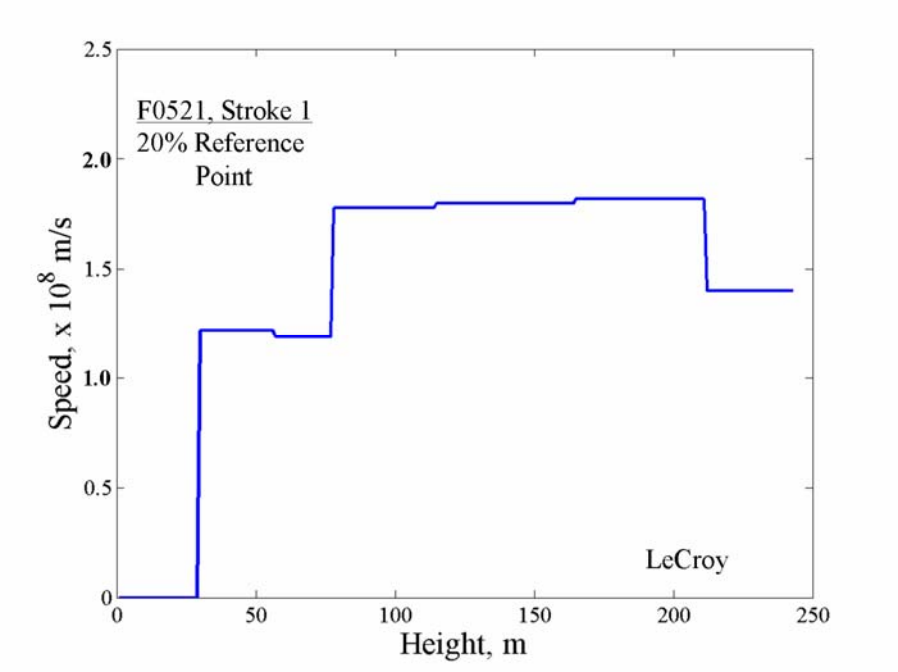

Figure 5-83: Return-stroke speed profile obtained using the 20% reference point for event F0521, Stroke 1, based on all the LeCroy data (combination of the two profiles shown in Figure 5-81).

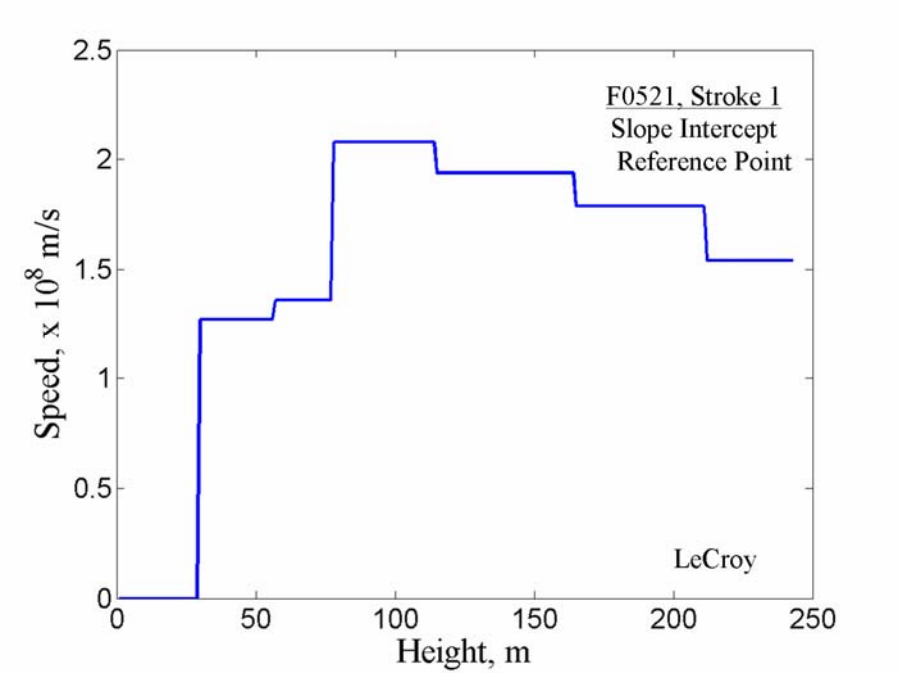

Figure 5-84: Return-stroke speed profile obtained using the slope intercept point as reference for event F0521, Stroke 1, based on all the LeCroy data (combination of the two profiles shown in Figure 5-82).

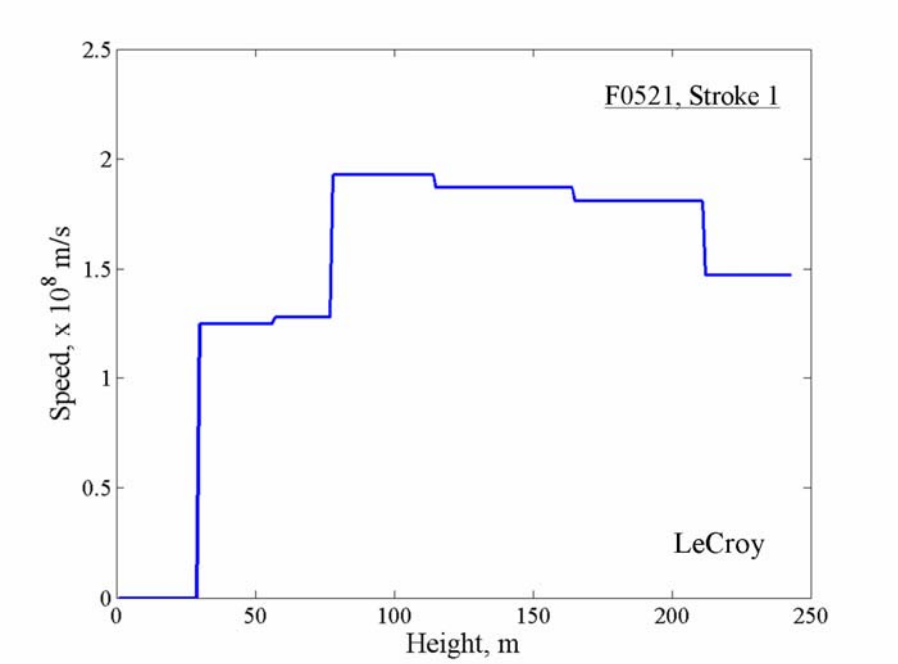

Figure 5-85: Return-stroke speed profile obtained by computing the average of speeds computed using the 20% and slope intercept methods, based on LeCroy data, shown in Figures 5-91 and 5-92, for event F0521, Stroke 1.

Table 5-1: Percent error in the RS speeds computed in this thesis relative to those obtained by Olsen et. al. (2003). The errors appear to be random in nature, suggesting that there is no systematic bias introduced by the data analysis tools adopted in this thesis.

	10% Point (% Error)	20% Point (% Error)	90% Point (% Error)	Max Point (% Error)	Slope Intercept Point (% Error)	Peak dL/dt (% Error)
Stroke 1	+13.0	-8.4	+8.1	-5.0	0.0	-13.0
Stroke 2	-3.5	-3.0	-7.6	+5.4	0.0	0.0
Stroke 4	+7.2	+2.7	+7.0	-3.5	-1.3	0.0
Stroke 5	+5.0	0.0	+17.0	+11	0.0	-11.4
Stroke 6	-7.7	0.0	+15	-1.4	0.0	-7.6

Table 5-2: Overall return-stroke speeds (estimated using LeCroy channels 2 and 9) for Event F0501, Stroke 1.

Reference Point	Speed, $x10^8$ m/s
10%	2.39
20%	1.73
90%	1.07
Max	0.69
Slope Intercept	2.13
Max d/dt	1.37

Table 5-3: Return-stroke speed profiles for event F0501, Stroke 1, obtained using LeCroy data from two groups of channels.

Channels	Height Range, m	Speed, x 10^8 m/s		Graphical representation in Figures 5-7 and 5-8
		20% Reference Point	Slope Intercept Reference Point	
2-3	44-84	0.99	1.11	Solid red line
3-4	84-116	1.18	1.25	
4-6	116-245	1.91	2.17	
6-9	245-451	1.39	1.49	
5-7	171-314	1.71	1.97	Dashed blue line
7-8	314-360	1.35	1.32	

Table 5-4: Return-stroke speed profile for event F0501, Stroke 1, obtained by averaging data from the two groups of LeCroy channels shown in Table 5-3.

Height Range, m	Speed, x 10^8 m/s	
	20% Reference Point	Slope Intercept Reference Point
44-84	0.99	1.11
84-116	1.18	1.25
116-171	1.91	2.17
171-245	1.81	2.07
245-314	1.55	1.73
314-360	1.37	1.41
360-451	1.39	1.49

Table 5-5: Return-stroke speeds at various heights for event F0501, Stroke 1, obtained using LeCroy data, found by computing the average of the speeds shown in Table 5-4 (see also Figure 5-11).

Height Range, m	Speed, x 10^8 m/s
44-84	1.05
84-116	1.22
116-171	2.04
171-245	1.94
245-314	1.64
314-360	1.39
360-451	1.44

Table 5-6: Return-stroke speeds at various heights for event F0501, Stroke 1, obtained using Yokogawa data (see also Figure 5-14).

Height Range, m	Speed, x 10^8 m/s	
	20% Reference Point	Slope Intercept Reference Point
44-84	1.02	1.11
84-116	1.15	1.05
116-171	1.88	1.94
171-245	1.90	2.09
245-314	2.29	2.26
314-360	1.71	1.86
360-451	1.45	1.63

Table 5-7: Return-stroke speeds at various heights for event F0501, Stroke 1, obtained using Yokogawa data, found by computing the average of the speeds shown in Table 5-6.

Height Range, m	Speed, x 10^8 m/s
44-84	1.07
84-116	1.10
116-171	1.91
171-245	2.00
245-314	2.28
314-360	1.79
360-451	1.54

Table 5-8: Leader speeds at various heights for event F0501, Stroke 1, measured using LeCroy data.

Height Range, m	Leader Speed, x10^6 m/s
44-84	29.40
84-116	33.10
116-171	28.20
171-245	21.10
245-314	12.00
314-360	13.40
360-451	14.70

Table 5-9: The optical return-stroke risetimes based on LeCroy measurements for event F0501, Stroke 1.

Height Above Ground, m	Return Stroke Risetime, μs
44	0.69
84	1.07
116	1.14
171	1.92
245	1.97
314	2.32
360	2.53
451	3.50

Table 5-10: Overall return-stroke speeds (estimated using LeCroy channels 2 and 9) for Event F0503. This event had four return strokes.

Reference Point	Stroke 1 Speed, $x10^8$ m/s	Stroke 2 Speed, $x10^8$ m/s	Stroke 3 Speed, $x10^8$ m/s	Stroke 4 Speed, $x10^8$ m/s
10%	0.89	1.42	1.06	1.17
20%	0.79	1.08	0.93	0.97
90%	0.55	0.67	0.68	0.65
Max	0.38	0.38	0.51	0.57
Slope Intercept	0.99	1.34	1.26	1.39
Max d/dt	1.00	1.07	1.02	1.08

Table 5-11: Return-stroke speed profiles at various heights for event F0503, Stroke 1, obtained using LeCroy data from two groups of channels.

Channels	Height Range, m	Speed, x 10^8 m/s		Graphical representation in Figures 5-10 and 5-11
		20% Reference Point	Slope Intercept Reference Point	
2-3	44-84	1.36	1.47	Solid red line
3-4	84-116	1.69	1.60	
4-6	116-245	1.80	1.85	
6-9	245-451	1.02	1.37	
5-7	171-314	1.23	1.42	Dashed blue line
7-8	314-360	0.75	0.86	

Table 5-12: Return-stroke speed profile for event F0503, Stroke 1, obtained by averaging data from the two groups of LeCroy channels.

Height Range, m	Speed, x 10^8 m/s	
	20% Reference Point	Slope Intercept Reference Point
44-84	1.36	1.47
84-116	1.69	1.60
116-171	1.80	1.85
171-245	1.52	1.64
245-314	1.13	1.40
314-360	0.89	1.11
360-451	1.02	1.37

Table 5-13: Return-stroke speeds at various heights for event F0503, Stroke 1, obtained using LeCroy data, found by computing the average of the speeds shown in Table 5-12 (see also Figure 5-19).

Height Range, m	Speed, x 10^8 m/s
44-84	1.42
84-116	1.65
116-171	1.83
171-245	1.58
245-314	1.26
314-360	1.00
360-451	1.20

Table 5-14: Return-stroke speeds at various heights for event F0503, Stroke 1, obtained using Yokogawa data.

Height Range, m	Speed, x 10^8 m/s	
	20% Reference Point	Slope Intercept Reference Point
44-84	1.10	1.18
84-116	1.57	1.78
116-171	2.15	2.12
171-245	1.68	1.80
245-314	1.30	1.36
314-360	0.78	0.87
360-451	0.86	0.73

Table 5-15: Return-stroke speeds at various heights for event F0503, Stroke 1, obtained using Yokogawa data, found by computing the average of the speeds shown in Table 5-14 (see also Figure 5-22).

Height Range, m	Speed, x 10^8 m/s
44-84	1.14
84-116	1.68
116-171	2.14
171-245	1.74
245-314	1.33
314-360	0.83
360-451	0.80

Table 5-16: The optical return-stroke risetimes based on LeCroy measurements for event F0503, Stroke 1.

Height Above Ground, m	Return Stroke Risetime, μs
44	1.05
84	1.62
116	1.59
171	1.72
245	2.16
314	2.84
360	2.71
451	3.63

Table 5-17: Return-stroke speed profiles at various heights for event F0503, Stroke 2, obtained using LeCroy data from two groups of channels.

Channel	Height Range, m	Speed, x 10^8 m/s		Graphical representation in Figures 5-18 and 5-19
		20% Reference Point	Slope Intercept Reference Point	
2-3	44-84	0.88	1.00	Solid line in red
3-4	84-116	1.50	1.80	
4-6	116-245	2.05	2.03	
6-9	245-451	1.27	1.53	
5-7	171-314	1.70	2.05	Dashed blue line
7-9	314-360	1.49	1.52	

Table 5-18: Return-stroke speed profile for event F0503, Stroke 2, obtained by averaging data from the two groups of LeCroy channels.

Height Range, m	Speed, x 10^8 m/s	
	20% Reference Point	Slope Intercept Reference Point
44-84	0.88	1.00
84-116	1.50	1.80
116-171	2.05	2.03
171-245	1.88	2.04
245-314	1.49	1.79
314-360	1.38	1.53
360-451	1.27	1.53

Table 5-19: Return-stroke speeds at various heights for event F0503, Stroke 2, obtained using LeCroy data, found by computing the average of the speeds shown in Table 5-18 (see also Figure 5-27).

Height Range, m	Speed, x 10^8 m/s
44-84	0.94
84-116	1.65
116-171	2.04
171-245	1.96
245-314	1.64
314-360	1.46
360-451	1.39

Table 5-20: Return-stroke speeds at various heights for event F0503, Stroke 2, obtained using Yokogawa data.

Height Range, m	Speed, x 10^8 m/s	
	20% Reference Point	Slope Intercept Reference Point
44-84	1.30	1.52
84-116	1.89	1.95
116-171	2.08	2.18
171-245	1.70	1.80
245-314	1.64	1.65
314-360	1.65	1.74
360-451	1.51	1.58

Table 5-21: Return-stroke speeds at various heights for event F0503, Stroke 2, obtained using Yokogawa data, found by computing the average of the speeds shown in Table 5-20 (see also Figure 5-30).

Height Range, m	Speed, x 10^8 m/s
44-84	1.41
84-116	1.92
116-171	2.13
171-245	1.75
245-314	1.65
314-360	1.70
360-451	1.56

Table 5-22: Leader speeds at various heights for event F0503, Stroke 2, measured using LeCroy data.

Height Range, m	Leader Speed, x10^6 m/s
44-84	28.65
84-116	34.98
116-171	31.47
171-245	30.51
245-314	29.17
314-360	11.72
360-451	14.40

Table 5-23: The optical return-stroke risetimes based on LeCroy measurements for event F0503, Stroke 2.

Height Above Ground, m	Return Stroke Risetime, μs
44	0.63
84	1.01
116	1.33
171	1.57
245	2.06
314	2.55
360	2.59
451	3.66

Table 5-24: Return-stroke speed profiles at various heights for event F0503, Stroke 3, obtained using LeCroy data from two groups of channels.

Channels	Heights Range, m	Speed, x 10^8 m/s		Graphical representation shown in Figures 5-26 and 5-27
		20% Reference Point	Slope Intercept Reference Point	
2-3	44-84	1.43	1.50	Solid red line
3-4	84-116	1.93	1.97	
4-6	116-245	2.26	2.08	
6-9	245-451	1.13	1.37	
5-7	171-314	1.34	1.39	Dashed line in blue
7-8	314-360	1.07	1.38	

Table 5-25: Return-stroke speed profile for event F0503, Stroke 3, obtained by averaging data from the two groups of LeCroy channels.

Height Range, m	Speed, x 10^8 m/s	
	20% Reference Point	Slope Intercept Reference Point
44-84	1.43	1.50
84-116	1.93	1.97
116-171	2.26	2.08
171-245	1.80	1.74
245-314	1.23	1.38
314-360	1.10	1.38
360-451	1.13	1.37

Table 5-26: Return-stroke speeds at various heights for event F0503, Stroke 3, obtained using LeCroy data, found by computing the average of the speeds shown in Table 5-25 (see also Figure 5-35).

Height Range, m	Speed, x 10^8 m/s
44-84	1.47
84-116	1.95
116-171	2.17
171-245	1.77
245-314	1.31
314-360	1.24
360-451	1.10

Table 5-27: Return-Stroke speeds at various heights for event F0503, Stroke 3, obtained using Yokogawa data.

Heights Range, m	Speed, x 10^8 m/s	
	20% Reference Point	Slope Intercept Reference Point
44-84	1.16	1.26
84-116	2.38	2.48
116-171	2.44	2.33
171-245	1.93	1.83
245-314	1.60	1.75
314-360	1.52	1.58
360-451	1.07	1.28

Table 5-28: Return-stroke speeds at various heights for event F0503, Stroke 3, obtained using Yokogawa data, found by computing the average of the speeds shown in Table 5-27 (see also Figure 5-38).

Height Range, m	Speed, x 10^8 m/s
44-84	1.21
84-116	2.43
116-171	2.39
171-245	1.88
245-314	1.68
314-360	1.55
360-451	1.33

Table 5-29: The optical return-stroke risetimes based on LeCroy measurements for event F0503, Stroke 3.

Height Above Ground, m	Return Stroke Risetime, μs
44	0.79
84	1.28
116	1.41
171	1.64
245	1.84
314	2.43
360	2.47
451	3.13

Table 5-30: Return-stroke speed profiles at various heights for event F0503, Stroke 4, obtained using LeCroy data from two groups of channels.

Channels	Heights Range, m	Speed, x 10^8 m/s		Graphical representation in Figures 5-34 and 5-35
		20% Reference Point	Slope Intercept Reference Point	
2-3	44-84	1.40	1.55	Solid line in red
3-4	84-116	1.79	1.85	
4-6	116-245	2.22	2.07	
6-9	245-451	1.22	1.21	
5-7	171-314	1.27	1.31	Dashed blue line
7-8	314-360	0.90	1.20	

Table 5-31: Return-stroke speed profile for event F0503, Stroke 4, obtained by averaging data from the two groups of LeCroy channels

Height Range, m	Speed, x 10^8 m/s	
	20% Reference Point	Slope Intercept Reference Point
44-84	1.40	1.55
84-116	1.78	1.85
116-171	2.21	2.07
171-245	1.74	1.69
245-314	1.25	1.26
314-360	1.06	1.20
360-451	1.22	1.21

Table 5-32: Return-stroke speeds at various heights for event F0503, Stroke 4, obtained using LeCroy data, found by computing the average of the speeds shown in Table 5-31 (see also Figure 5-43).

Height Range, m	Speed, x 10^8 m/s
44-84	1.48
84-116	1.82
116-171	2.14
171-245	1.72
245-314	1.25
314-360	1.13
360-451	1.15

Table 5-33: The Return-Stroke speeds at various heights for event F0503 Stroke 4, obtained using Yokogawa data.

Height Range, m	Speed, x 10^8 m/s	
	20% Reference Point	Slope Intercept Reference Point
44-84	1.14	1.20
84-116	2.38	2.46
116-171	1.89	1.84
171-245	1.76	1.79
245-314	1.60	1.76
314-360	1.14	1.24
360-451	1.07	1.22

Table 5-34: Return-stroke speeds at various heights for event F0503, Stroke 4, obtained using Yokogawa data, found by computing the average of the speeds shown in Table 5-33 (see also Figure 5-46).

Height Range, m	Speed, x 10^8 m/s
44-84	1.17
84-116	2.42
116-171	1.87
171-245	1.78
245-314	1.68
314-360	1.19
360-451	1.22

Table 5-35: The optical return-stroke risetimes based on LeCroy measurements for event F0503, Stroke 4.

Height Above Ground, m	Return Stroke Risetime, μs
44	0.98
84	1.34
116	1.50
171	1.75
245	2.20
314	3.41
360	3.13
451	3.63

Table 5-36: Overall return-stroke speeds (estimated using LeCroy channels 2 and 9) for Event F0510, Stroke 1, measured using data from LeCroy channels.

Reference Point	Speed, x10^8 m/s
10%	1.60
20%	1.50
90%	1.00
Max	0.78
Slope Intercept	1.67
Max d/dt	1.47

Table 5-37: Return-stroke speed profile at various heights for event F0510, Stroke 1, obtained using LeCroy data from two groups of channels.

Channels	Heights, m	Speed, x 10^8 m/s		Graphical representation in Figures 5-42 and 5-43
		20% Reference Point	Slope Intercept Reference Point	
2-3	30-57	1.37	1.08	Solid line in red
3-4	57-78	1.42	1.36	
4-6	78-165	1.96	1.82	
6-9	165-304	1.20	1.25	
5-7	115-212	1.48	1.76	Dashed blue line
7-8	212-243	1.19	1.24	

Table 5-38: Return-stroke speed profile for event F0510, Stroke 1, obtained by averaging data from the two groups of LeCroy channels.

Height Range, m	Speed, x 10^8 m/s	
	20% Reference Point	Slope Intercept Reference Point
30-57	1.37	1.08
57-78	1.42	1.36
78-115	1.96	1.82
115-165	1.72	1.79
165-212	1.34	1.51
212-243	1.19	1.24
243-304	1.20	1.25

Table 5-39: Return-stroke speeds at various heights for event F0510, Stroke 1, obtained using LeCroy data, found by computing the average of the speeds shown in Table 5-38 (see also Figure 5-51).

Height Range, m	Speed, x 10^8 m/s
30-57	1.23
57-78	1.39
78-115	1.89
115-165	1.76
165-212	1.42
212-243	1.22
243-304	1.23

Table 5-40: The optical return-stroke risetimes based on LeCroy measurements for event F0510, Stroke 1.

Height Above Ground, m	Return Stroke Risetime, μs
30	0.69
57	1.14
78	1.38
115	1.29
165	1.64
212	1.83
243	1.82
304	2.05

Table 5-41: Overall return-stroke speeds (estimated using LeCroy channels 2 and 8) for Event F0512, Stroke 1.

Reference Point	Speed, $x10^8$ m/s
10%	2.33
20%	2.26
90%	1.31
Max%	0.84
Slope Intercept	2.32
Max d/dt	2.23

Table 5-42: Return-stroke speed profile at various heights for event F0512, Stroke 1, obtained using LeCroy data from two groups of channels.

Channels	Height Range, m	Speed, x 10^8 m/s		Graphical representation in Figures 5-46 and 5-47
		20 Reference Point	Slope Intercept Reference Point	
2-3	30-57	1.30	1.37	Solid line in red
3-4	57-78	1.52	1.64	
4-6	78-165	2.07	2.18	
5-7	115-212	1.82	2.16	Dashed blue line
7-8	212-243	1.12	1.55	

Table 5-43: Return-stroke speed profile for event F0512, Stroke 1, obtained by averaging data from the two groups of LeCroy channels.

Height Range, m	Speed, x 10^8 m/s	
	20% Reference Point	Slope Intercept Reference Point
30-57	1.30	1.37
57-78	1.52	1.64
78-115	2.07	2.18
115-165	1.95	2.17
165-212	1.82	2.16
212-243	1.12	1.55

Table 5-44: Return-stroke speeds at various heights for event F0512, Stroke 1, obtained using LeCroy data, found by computing the average of the speeds shown in Table 5-43 (see also Figure 5-56).

Height Range, m	Speed, x 10^8 m/s
30-57	1.34
57-78	1.58
78-115	2.13
115-165	2.06
165-212	1.99
212-243	1.34

Table 5-45: Leader speeds at various heights for event F0512, Stroke 1, obtained using LeCroy data.

Height Range, m	Leader Speed, x10^6 m/s
30-57	29.36
57-78	31.09
78-115	15.73
115-165	17.03
165-212	12.53
212-243	12.19
243-360	13.72

Table 5-46: The optical return-stroke risetimes based on LeCroy measurements for event F0512, Stroke 1.

Height Above Ground, m	Return Stroke Risetime, μs
30	0.71
57	0.99
78	1.21
115	1.41
165	1.88
212	1.90
243	2.16
304	2.38

Table 5-47 Overall return-stroke speeds (estimated using LeCroy channels 2 and 8) for Event F0514, Stroke 1.

Reference Point	Speed, $x10^8$ m/s
10%	1.46
20%	1.58
90%	0.50
Max%	0.75
Slope Intercept	2.18
Max d/dt	1.30

Table 5-48: Return-stroke speed profile at various heights for event F0514, Stroke 1, obtained using LeCroy data from two groups of channels.

Channels	Heights, m	Speed, x 10^8 m/s		Graphical representation in Figures 5-50 and 5-51
		20 Reference Point	Slope Intercept Reference Point	
2-3	30-57	1.04	1.21	Solid line in red
3-4	57-78	0.77	0.85	
4-6	78-165	2.08	2.12	
5-7	115-212	1.67	1.79	Dashed blue line
7-8	212-243	1.63	1.56	

Table 5-49 Return-stroke speed profile for event F0514, Stroke 1, obtained by averaging data from the two groups of LeCroy channels.

Height Range, m	Speed, x 10^8 m/s	
	20% Reference Point	Slope Intercept Reference Point
30-57	1.04	1.21
57-78	0.77	0.85
78-115	2.08	2.12
115-165	1.86	1.96
165-212	1.67	1.79
212-243	1.63	1.56

Table 5-50: Return-stroke speeds at various heights for event F0514, Stroke 1, obtained using LeCroy data, found by computing the average of the speeds shown in Table 5-49 (see also Figure 5-61).

Height Range, m	Speed, x 10^8 m/s
30-57	1.13
57-78	0.81
78-115	2.10
115-165	1.92
165-212	1.73
212-243	1.60

Table 5-51: The Return-Stroke speeds at various heights for event F0514, Stroke 1, obtained using Yokogawa data.

Height Range, m	Speed, x 10^8 m/s	
	20% Reference Point	Slope Intercept Reference Point
30-57	0.83	0.91
57-78	1.05	1.12
78-115	1.90	2.04
115-165	1.82	1.89
165-212	1.47	1.76
212-243	1.25	1.30

Table 5-52: Return-stroke speeds at various heights for event F0514, Stroke 1, obtained using Yokogawa data, found by computing the average of the speeds shown in Table 5-51 (see also Figure 5-64).

Height Range, m	Speed, x 10^8 m/s
30-57	0.87
57-78	1.09
78-115	1.97
115-165	1.86
165-212	1.62
212-243	1.28

Table 5-53: Leader speeds at various heights for event F0514, Stroke 1, obtained using LeCroy data.

Height Range, m	Leader Speed, x10^6 m/s
30-57	27.44
57-78	28.50
78-115	27.59
115-165	23.69
165-212	19.01
212-243	18.81

Table 5-54: The optical return-stroke risetimes based on LeCroy measurements for event F0514, Stroke 1.

Height Above Ground, m	Return Stroke Risetime, μs
30	0.69
57	1.13
78	1.13
115	1.34
165	1.68
212	1.91
243	2.02

Table 5-55: Overall return-stroke speeds (estimated using LeCroy channels 2 and 8) for Event F0517, Stroke 1.

Reference Point	Stroke 1 Speed, $x10^8$ m/s	Stroke 2 Speed, $x10^8$ m/s
10%	1.45	1.47
20%	1.37	1.35
90%	0.93	0.85
Max%	0.71	0.55
Slope Intercept	1.48	1.47
Max d/dt	1.21	1.35

Table 5-56: Return-stroke speed profile at various heights for event F0517, Stroke 1, obtained using LeCroy data from two groups of channels.

Channels	Heights, m	Speed, x 10^8 m/s		Graphical representation shown in Figures 5-58 and 5-59
		20 Reference Point	Slope Intercept Reference Point	
2-3	30-57	0.75	1.01	Solid line in red
3-4	57-78	1.29	1.24	
4-6	78-165	1.78	1.80	
5-7	115-212	1.58	1.59	Dashed blue line
7-8	212-243	0.76	1.54	

Table 5-57: Return-stroke speed profile for event F0517, Stroke 1, obtained by averaging data from the two LeCroy channels.

Height Range, m	Speed, x 10^8 m/s	
	20% Reference Point	Slope Intercept Reference Point
30-57	0.75	1.01
57-78	1.29	1.24
78-115	1.78	1.80
115-165	1.68	1.70
165-212	1.58	1.59
212-243	0.76	1.54

Table 5-58: Return-stroke speeds at various heights for event F0517, Stroke 1, obtained using LeCroy data, found by computing the average of the speeds shown in Table 5-57 (see also Figure 5-69).

Height Range, m	Speed, x 10^8 m/s
30-57	0.88
57-78	1.27
78-115	1.79
115-165	1.69
165-212	1.59
212-243	1.15

Table 5-59: The Return-Stroke speeds at various heights for event F0514, Stroke 1, obtained using Yokogawa data.

Height Range, m	Speed, x 10^8 m/s	
	20% Reference Point	Slope Intercept Reference Point
30-57	0.90	1.12
57-78	2.33	2.41
78-115	1.84	2.00
115-165	1.47	1.51
165-212	1.08	1.11
212-243	0.97	0.99

Table 5-60: Return-stroke speeds at various heights for event F0517, Stroke 1, obtained using Yokogawa data, found by computing the average of the speeds shown in Table 5-59 (see also Figure 5-72).

Height Range, m	Speed, x 10^8 m/s
30-57	1.01
57-78	2.37
78-115	1.92
115-165	1.49
165-212	1.10
212-243	0.91

Table 5-61: The optical return-stroke risetimes based on LeCroy measurements for event F0517, Stroke 1.

Height Above Ground, m	Return Stroke Risetime, μs
30	1.06
57	1.41
78	1.65
115	1.71
165	2.16
212	2.47
243	3.00

Table 5-62: Return-stroke speed profile at various heights for event F0517, Stroke 2, obtained using LeCroy data from two groups of channels.

Channels	Heights, m	Speed, x 10^8 m/s		Graphical representation shown in Figures 5-66 and 5-67
		20 Reference Point	Slope Intercept Reference Point	
2-3	30-57	0.53	0.65	Solid line in red
3-4	57-78	1.62	1.85	
4-6	78-165	2.11	2.10	
5-7	115-212	1.37	1.63	Dashed blue line
7-8	212-243	1.48	1.52	

Table 5-63: Return-stroke speed profile for event F0517, Stroke 2, obtained by averaging data from the two LeCroy channels.

Height Range, m	Speed, x 10^8 m/s	
	20% Reference Point	Slope Intercept Reference Point
30-57	0.53	0.65
57-78	1.62	1.85
78-115	2.11	2.10
115-165	1.74	1.87
165-212	1.37	1.63
212-243	1.48	1.52

Table 5-64: Return-stroke speeds at various heights for event F0517, Stroke 2, obtained using LeCroy data, found by computing the average of the speeds shown in Table 5-63 (see also Figure 5-77).

Height Range, m	Speed , x 10^8 m/s
30-57	0.59
57-78	1.73
78-115	2.11
115-165	1.80
165-212	1.50
212-243	1.50

Table 5-65: The Return-Stroke speeds at various heights for event F0517, Stroke 2, obtained using Yokogawa data.

Heights, m	Speed, x 10^8 m/s	
	20% Reference Point	Slope Intercept Reference Point
30-57	0.56	0.63
57-78	1.71	1.90
78-115	2.16	2.23
115-165	1.84	1.87
165-212	1.30	1.42
212-243	0.85	0.88

Table 5-66: Return-stroke speeds at various heights for event F0517, Stroke 2, obtained using Yokogawa data, found by computing the average of the speeds shown in Table 5-65 (see also Figure 5-80).

Height Range, m	Speed , x 10^8 m/s
30-57	0.60
57-78	1.81
78-115	2.20
115-165	1.86
165-212	1.36
212-243	0.87

Table 5-67: Leader speeds at various heights for event F0517, Stroke 2, obtained using LeCroy data.

Height Range, m	Leader Speed, $x10^6$ m/s
30-57	7.94
57-78	6.16
78-115	5.24
115-165	4.18
165-212	4.29
212-243	4.90

Table 5-68: The optical return-stroke risetimes based on LeCroy measurements for event F0517, Stroke 2.

Height Above Ground, m	Return Stroke Risetime, μs
30	0.78
57	1.14
78	1.35
115	1.44
165	1.67
212	1.86
243	2.07

Table 5-69: Overall return-stroke speeds (estimated using LeCroy channels 2 and 8) for Event F0521, Stroke 1, measured using data from LeCroy channels.

Reference Point	Speed, $x10^8$ m/s
10%	1.80
20%	1.86
90%	0.91
Max%	0.69
Slope Intercept	2.11
Max d/dt	1.50

Table 5-70: Return-stroke speed profile at various heights for event F0521, Stroke 1, obtained using LeCroy data from two groups of channels.

Channels	Heights, m	Speed, x 10^8 m/s		Graphical representation in Figures 5-74 and 5-75
		20 Reference Point	Slope Intercept Reference Point	
2-3	30-57	1.22	1.27	Solid line in red
3-4	57-78	1.19	1.36	
4-6	78-165	1.78	2.08	
5-7	115-212	1.82	1.79	Dashed blue line
7-8	212-243	1.40	1.54	

Table 5-71: Return-stroke speed profile for event F0521, Stroke 1, obtained by averaging data from the two LeCroy channels.

Height Range, m	Speed, x 10^8 m/s	
	20% Reference Point	Slope Intercept Reference Point
30-57	1.22	1.27
57-78	1.19	1.36
78-115	1.78	2.08
115-165	1.80	1.94
165-212	1.82	1.79
212-243	1.40	1.54

Table 5-72: Return-stroke speeds at various heights for event F0521 Stroke 1, obtained using LeCroy data, found by computing the average of the speeds shown in Table 5-71 (see also Figure 5-85).

Height Range, m	Speed, x 10^8 m/s
30-57	1.25
57-78	1.28
78-115	1.93
115-165	1.87
165-212	1.81
212-243	1.47

Table 5-73: The optical return-stroke risetimes based on LeCroy measurements for event F0521, Stroke 1.

Height Above Ground, m	Return Stroke Risetime, μs
30	0.80
57	1.35
78	1.67
115	1.88
165	1.88
212	1.94
243	2.02

Table 5-74: Return-stroke speed profiles based on data from the two groups of LeCroy channels with differences exceeding 30%.

LeCroy Event	Channels Under Comparison		Reference Point	Percentage Difference Between Two Profiles
F0503, Stroke 1	4-6	5-7	20%	46%
	6-9	7-8	Slope Intercept	38%
F0503, Stroke 3	4-6	5-7	20%	69%
	4-6	5-7	Slope Intercept	49%
F0503, Stroke 4	4-6	5-7	20%	74%
	4-6	5-7	Slope Intercept	58%
F0510, Stroke 1	4-6	5-7	20%	32%
F0517, Stroke 2	4-6	5-7	20%	35 %

Table 5-75: Return-stroke speed profile based on averaging data from the two groups of LeCroy channels using the 20% and slope intercept points as references with percentage difference above 30%.

LeCroy Event	Channel	Reference Points Under Comparison	Percentage Difference
F0517, Stroke 1	7-8	20% and Slope Intercept Reference Points	50%

Table 5-76: Return-stroke speed profiles based on averaging data from the LeCroy and Yokogawa channels with percentage difference above 30%.

Event	Channel	Percentage Difference
F0503, Stroke 1	8-9	51%
F0517, Stroke 1	3-4	47%
F0517, Stroke 2	7-8	73%

CHAPTER 6
DISCUSSION AND CONCLUSIONS

In the summer 2005 experimental setup block diagram, shown in Figure 3-8, the LeCroy Scope 16 was used to trigger the LeCroy Scope 6 which would then trigger the LeCroy Scope 17. The oscilloscopes had their own internal finite time delays which resulted in an inter-scope delay when one scope was used to trigger another. The time delays between the LeCroy DSOs were computed as shown in Table 3-2. and the return-stroke speed equation was modified to take the finite inter-scope time delays along with the time correction factors as described in section 3.6.

Optical records of 31 lightning flashes were obtained in Summer 2005. Of these 31, 8 were triggered lightning and the remaining 23 were natural lightning events. The natural lightning optical records could not be analyzed for return-stroke speeds because the distance to the channel termination was unknown. But the natural-lightning light profiles (a light profile represents a set of light waveforms recorded for each lightning event at various heights) have been presented for visual analysis in chapter 4.

A novel trigger circuit (functional block diagram is shown in Figure 3-6) was prototyped and designed by the author in Fall 2007. This simple trigger circuit allows full control over the triggering light levels. The triggering levels can be changed suitably to use either leader or return-stroke as trigger event for the K004M Image Converter Camera.

The BIFO K004M Image Converter Camera (ICC) was operated in University of Florida lightning experiments in 2006. The K004M and its original triggering device PS001 settings along with the captured natural lightning streak images are shown in Appendix A. The record length was 10.67 um for all the captured events. There were no avalanche photodiode records that corresponded to the natural lightning recorded by the BIFO K004M camera. The height of

the channel could not be estimated, because the distance to the channel was unknown in all the cases. Also, the images were either highly saturated or barely visible in most of the cases, therefore rendering them not suitable for any sort of detailed data analysis or image processing for characterization of the lightning channel. The shape of the lightning channel however was identifiable in some of the cases.

Five triggered-lightning events, F0501-Stroke 1 (July 2, 2005), F0503-Stroke 2 (July 2, 2005), F0512-Stroke 1 (July 31, 2005), F0514-Stroke 1 (August 4, 2005) and F0517-Stroke2 (August 4, 2005) exhibited distinct leader pulses before the onset of the return-stroke pulse. The leader propagation speeds in all the cases were found to follow the trend of lower values in the top portion of the lightning channel (452 m before July,13 2005, and 304 m after that) and higher values at the bottom (44 m before July,13 2005, and 30 m after that) of the lightning channel. The mean leader speeds are found to vary between 1.3×10^7 m/s and 2.5×10^7 m/s.

Return-stroke optical risetimes were measured for the summer 2005 triggered lightning events. The optical risetimes in all the cases were found to follow the trend of smaller values in the bottom section of the lightning channel (44 m before July,13 2005, and 30 m after that) and larger values in the top section (452 m before July, 13 2005, and 304 m after that) of the lightning channel. The mean optical risetimes were found to vary from 0.81 μs to 2.83 μs at the channel bottom and top, respectively.

The mean return-stroke speeds based on 11 triggered-lightning events in Summer 2005, obtained by computing the average of the return-speeds based on the 20% and slope intercept reference point methods, was 1.51×10^8 m/s in the case of LecCroy data and 1.57×10^8 m/s in the case of Yokogawa data.

As explained in section 5.5.1, return-stroke speeds measured using the 20% and slope intercept methods can be viewed as a lower bound and an upper bound, respectively. Accordingly, the mean return-stroke speeds obtained using LeCroy data are found to vary between 1.48×10^8 m/s and 1.59×10^8 m/s. Similarly, the mean return-stroke speeds obtained using the Yokogawa data are found to vary between 1.53×10^8 m/s and 1.61×10^8 m/s.

Return-stroke speed profiles based on the 11 triggered-lightning events from Summer 2005 were computed using data captured using the LeCroy as well as the Yokogawa DSOs, as explained in chapter 3, section 3.5. The LeCroy DSOs have a high sampling rate of 500 MHz or 2 nanoseconds between data points, whereas the Yokogawa DSO has a lower sampling rate of 10 MHz or 100 nanoseconds between data points, as explained in section 5.4,. Therefore, the return-stroke speeds obtained using the LeCroy data have a higher degree of accuracy as compared to the return-stroke speeds computed using the Yokogawa data. The only purpose of computing the return-stroke speeds using Yokogawa data (presented in chapter 5) was to check against the more accurate return-stroke speed profiles obtained using the LeCroy DSOs.
The percentage difference between the average return-stroke speed profiles based on the LeCroy and Yokogawa data was found to be within 30% in all the cases, except for 3 cases shown in Table-5-76.

Therefore, in the following we will only discuss the more accurate LeCroy return-stroke speed profiles. An interesting trend was observed in the return-stroke speeds obtained by computing the average of speeds. This trend concerns the variation in measured return-stroke speeds in the seven channel segments between 44 m and 451 m (before July 13, 2005) and six channel segments between 30 m and 243 m (after July 13, 2005), as listed in Tables 6-1 and 6-2. The speed profile was non-monotonic with height in all the cases presented in Tables 6-1

and 6-2. This observation is consistent with the 2003 results previously published by Olsen et al. (2004). For the strokes listed in Table 6-1, it was observed that the measured speed was greatest in the 116-171 m segment, and lowest in 314-451 m and 44-84 m segments. This suggests that the speed reaches a maximum value at a height between 116 m and 171 m in these five strokes. The speed gradually increases with increasing height starting from the 84-116 m segment, and gradually decreases with decreasing height starting from the 171-245 m segment.

For the strokes listed in Table 6-2, it was observed that the measured speed was greatest in the third segment between 78-115 m, and lowest in the segments between 212-243 m and 30-57 m. This suggests that the speed reaches a maximum value at a height between 78-165 m in these six strokes. The speed gradually increases from the second segment, between 57-78 m, and gradually decreases from the fifth segment between 165-212 m and is the lowest in the uppermost segment between 212-243 m.

Table 6-1: Return-stroke speeds at various heights, obtained by computing the average of the speeds based on the 20% and slope intercept methods, found using the LeCroy data for triggered-lightning events before July 13, 2005. The speeds listed for the various events are to be multiplied by 10^8 m/s.

Event ID	Height Range, m						
	44-84	84-116	116-171	171-245	245-314	314-360	360-451
F0501,S1,	1.04	1.22	2.04	1.94	1.64	1.39	1.44
F0503,S1	1.42	1.65	1.83	1.58	1.26	1.00	1.20
F0503,S2	0.94	1.65	2.04	1.96	1.64	1.46	1.39
F0503,S3	1.47	1.95	2.17	1.77	1.31	1.24	1.10
F0503,S4	1.48	1.82	2.14	1.72	1.25	1.13	1.15

Table 6-2: Return-stroke speeds at various heights obtained by computing the average of the speeds based on the 20% and slope intercept methods, found using the LeCroy data computed for triggered-lightning events after July 13, 2005. The speeds listed for the various events are to be multiplied by 10^8 m/s.

Event ID	Height Range, m						
	30-57	57-78	78-115	115-165	165-212	212-243	243-304
F0510,S1	1.23	1.39	1.89	1.76	1.42	1.22	1.23
F0512,S1	1.34	1.58	2.13	2.06	1.99	1.34	-
F0514,S1	1.13	0.81	2.10	1.92	1.73	1.60	-
F0517,S1	0.88	1.27	1.79	1.69	1.59	1.15	-
F0517,S2	0.59	1.73	2.11	1.80	1.50	1.50	-
F0521,S1	1.22	1.19	1.78	1.8	1.82	1.4	-

CHAPTER 7
RECOMMENDATIONS FOR FUTURE RESEARCH

The primary purpose of the BIFO K04M camera was to obtain images of the lightning attachment process for natural lighting as well as triggered-lightning events. However, operating the K004M camera was a non-trivial task during both the Summer 2006 natural-lightning experiments at the University of Florida by the author and the Summer 2005 triggered-lightning experiments at Camp Blanding, Florida, by Robert Olsen. This could mainly be attributed to the inability of accurately determining the optimal exposure settings on the K004M camera during triggered-lightning events in Summer 2005 at Camp Blanding, Florida. In the case of capturing natural lightning events, this was further exacerbated by the variability of brightness in lightning flashes as well as the variability of the distance to the channel terminations. Thus, the same gain settings would not yield useful images for different natural lightning events. During the Summer 2006 lightning experiments, a triangular platform with wheels was prototyped and built by the author upon which, PS001 photosensor was mounted on top of the K004M camera, as shown in Figure 3-10. The platform made it possible to quickly re-orient the K004M camera depending on the nature of the lightning storm in Summer 2006. The oscilloscopes were mounted on a different rack and had to be repositioned near the K004M camera for easy access. In future, the apparatus could be improved by providing a means of mounting the K004M camera, the photosensor as well as the oscilloscopes onto the same platform so that the process of reorientation would become less time consuming, thus yielding a higher number of natural lightning captures.

During the summer 2006 lightning experiments, the PS001 was seen to be incapable of triggering the K004M based on leader optical intensity irrespective of position of the gain setting knobs. Modifying the internal circuitry of the PS001 was as a non-trivial job. Therefore the

author prototyped and build a simple and novel triggering circuit that has easy accessibility to the on-chip potentiometers which provide flexibility of setting different reference voltages for the leader and return-stroke channels. This provides the capability of triggering the K004M based on the leader optical intensity. A detailed description of the circuit topology and its operation has been given in section 3.3.1 and Figure 3-6. The circuit can now replace the PS001 photosensor and can be set to trigger the K004M camera on leader (high gain) as well as return-stroke stage. Deciding on appropriate lightning levels is not an easy task. Field testing of the new trigger circuit is planned for Summer 2008.

This circuit could be further improved as shown in Figure 7.1. A microcontroller such as a member of Microchip's PIC family (PICF816FFA) of low power, high speed microcontrollers may be employed. An LCD , keypad and a high-speed digital-to-analog controller (DAC) could be interfaced with the microcontroller. The microcontroller could be programmed and configured in such a way, that all the bias voltages for each of the avalanche photodiodes could be set accurately via the keypad without having to adjust it manually. The bias voltages could then be monitored via the LCD display instead of checking the bias voltage by manually probing with the aid of a voltmeter/multi-meter. The reference voltage levels (V_{ref1} and V_{ref2}) could also be set accurately in a similar manner. These voltage reference levels can be quickly set with the aid of the keypad to either increase or decrease the sensitivity of the triggering circuit (formed by the avalanche photodiode and pre-amp stage). The above circuit could be integrated on-chip using careful layout techniques to ensure proper symmetry. This could then be mounted into a case upon which the keypad and LCD could be firmly mounted.

The spatial resolution of the K004M system is currently limited by the resolution of the camera readout (640x480 pixels), which is lower than the K004M resolution in the vertical

dimension. Several commercially-available cameras have image resolution greater than the K004M's inherent physical resolution, and many are available with digital connections such as USB2 and FireWire (IEEE1394) which allow for the direct connection of the camera to a PC for recording and archiving purposes. Also, the software used by the K004M camera, KLEN could be replaced by a robust and easy to use graphical user interface using Labview. Additional features like automatic triggering and simple image processing functionalities could be build into such a graphical user interface.

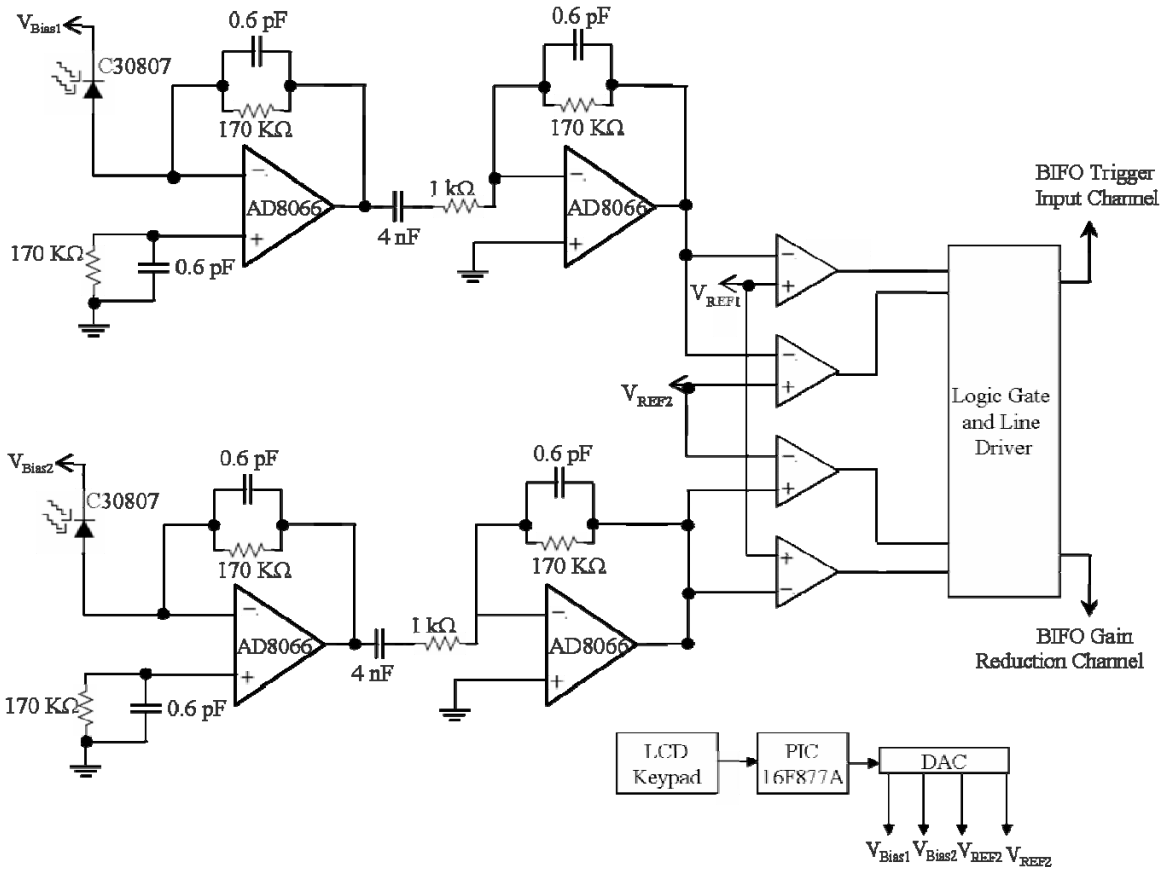

Figure 7-1: Recommended trigger circuit for the BIFO K004M camera.

APPENDIX A
THE BIFO K004M IMAGES CAPTURED IN SUMMER 2006 IN GAINESVILLE.

The BIFO K004M Image Converter Camera (ICC) was operated in University of Florida lightning experiments in 2006. All the images of the lightning events captured by the K004M are shown in figures below. The captions on each image indicate the date of the capture. The K004M was operating in streak mode, with a linear sweep rate of 3 μs/cm this corresponded with a record length of 10.67 us. The objective lens was an Industar-61 50 mm, f2.8 lens. The focus was adjusted for maximum resolution at the launch tower. The trigger level on the camera was set to approximately 4.5. The MCP1 DYN GAIN knob was set to maximum. The MCP1 STAT GAIN was set to an angle similar to the hour hand of a clock reading 3:30. The MCP2 STAT GAIN knob was set to an angle similar to 3:30, and the MCP2 DYN GAIN knob was set fractionally higher than zero. The PS001 trigger unit was adjusted so that both trigger level knobs were at their minimum settings. Each photo-sensor on the PS001 was operated with a 28 mm lens, and both slit adjusters were set to +1.5. There were no avalanche photodiode records that corresponded to the natural lightning events captured on the K004M camera, therefore the time range of the captured streak images could not be estimated. Also, the images were either highly saturated or barely visible in most of the cases, therefore rendering them unsuitable for any sort of detailed data analysis or image processing for characterization of the natural lightning channel. The shape of the lightning channel, however was identifiable in some of the cases.

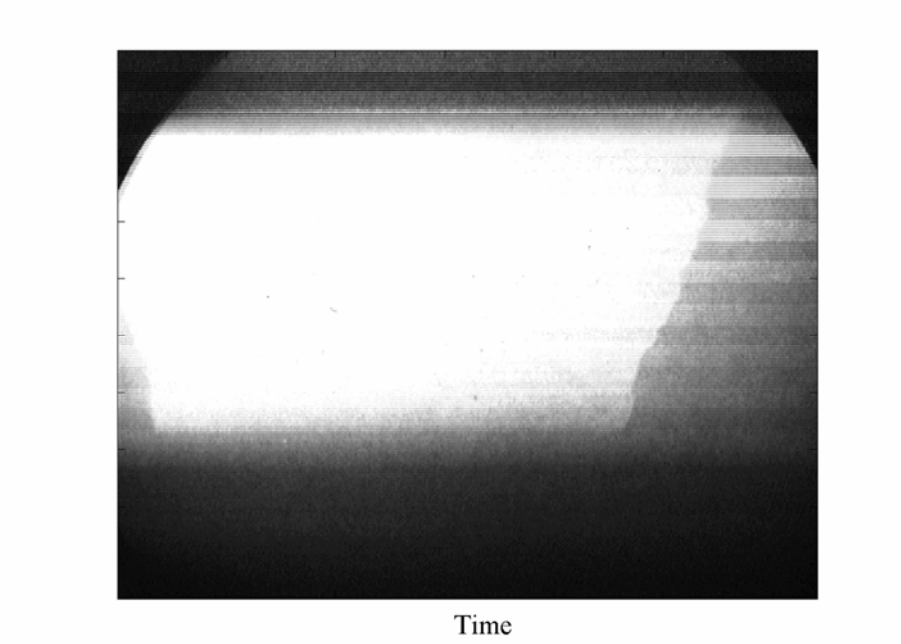

Figure A-1: Natural lightning record captured on the BIFO K004M Image Converter Camera in April 21, 2006.

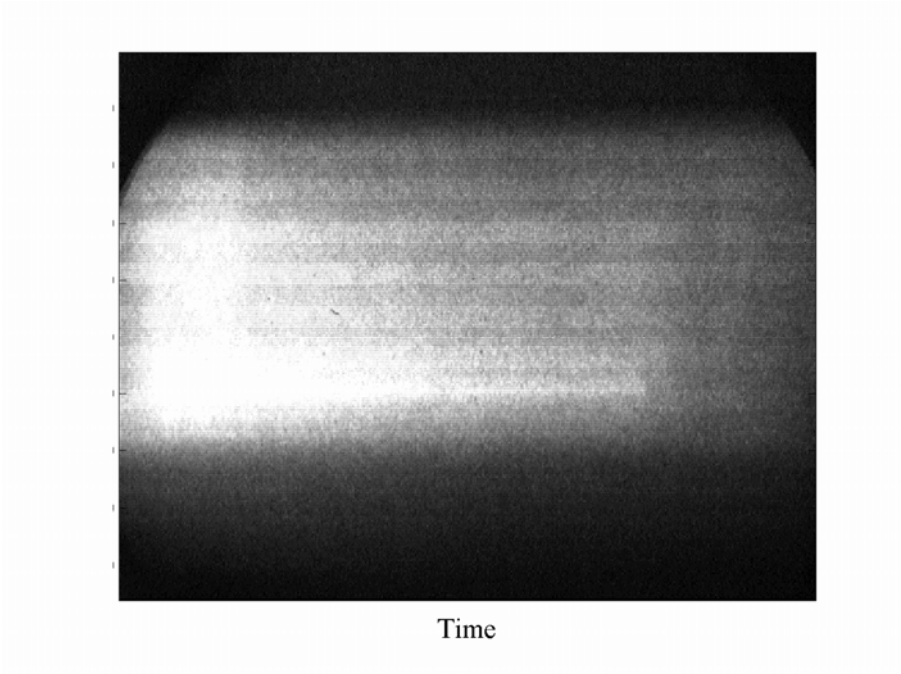

Figure A-2: Natural lightning record captured on the BIFO K004M Image Converter Camera in April 21, 2006.

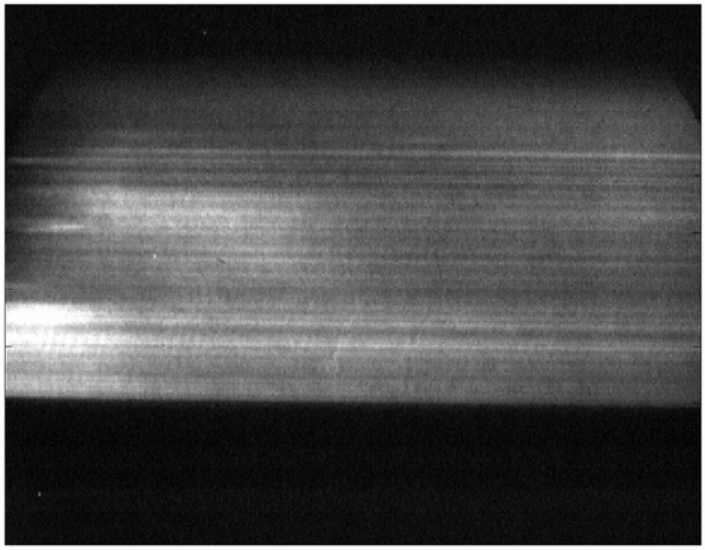

Time

Figure A-3: Natural lightning record captured on the BIFO K004M Image Converter Camera in July 17, 2006.

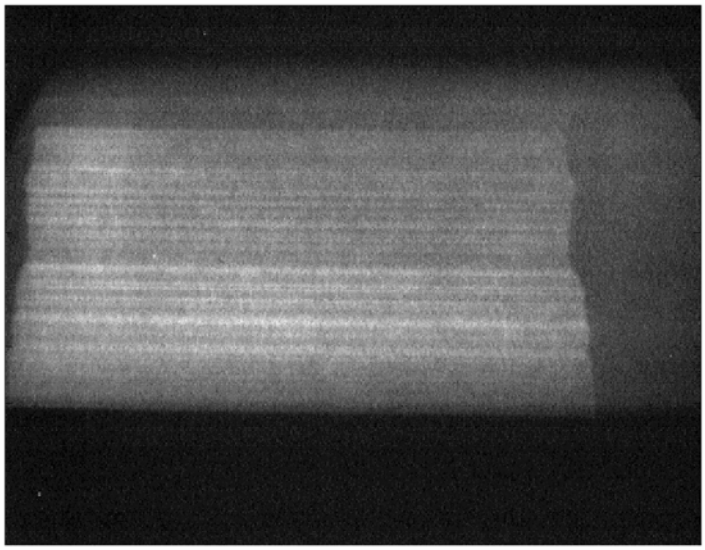

Time

Figure A-4: Natural lightning record captured on the BIFO K004M Image Converter Camera in July 17, 2006.

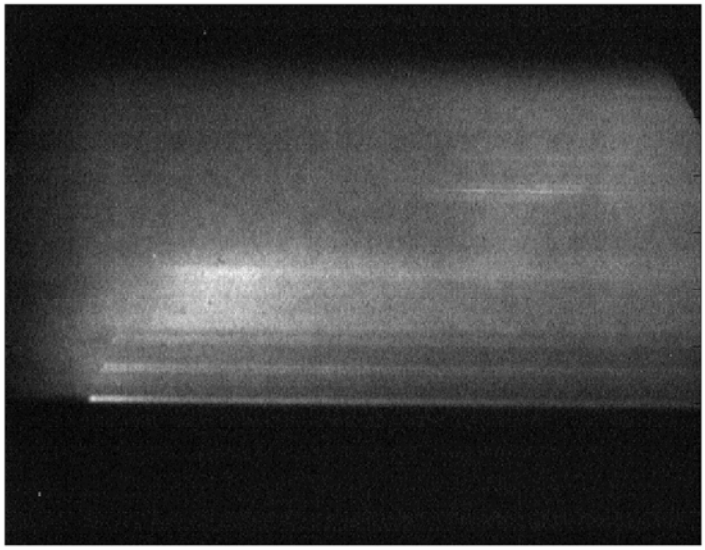

Time

Figure A-5: Natural lightning record captured on the BIFO K004M Image Converter Camera in July 17, 2006.

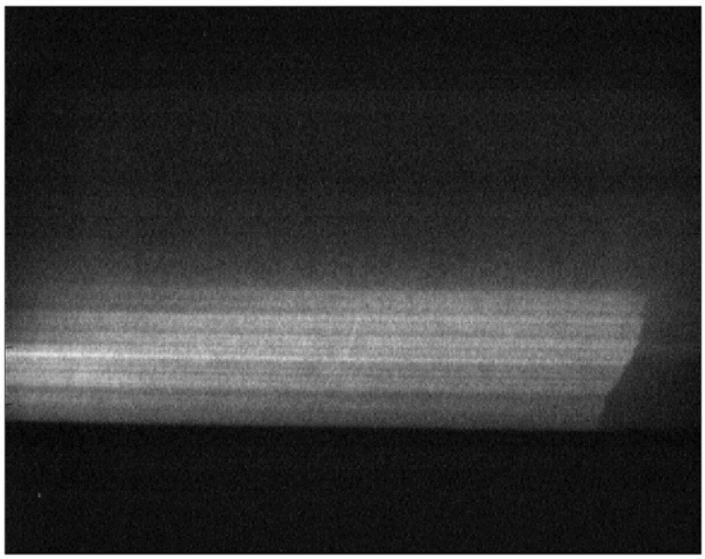

Time

Figure A-6: Natural lightning record captured on the BIFO K004M Image Converter Camera in July 17, 2006.

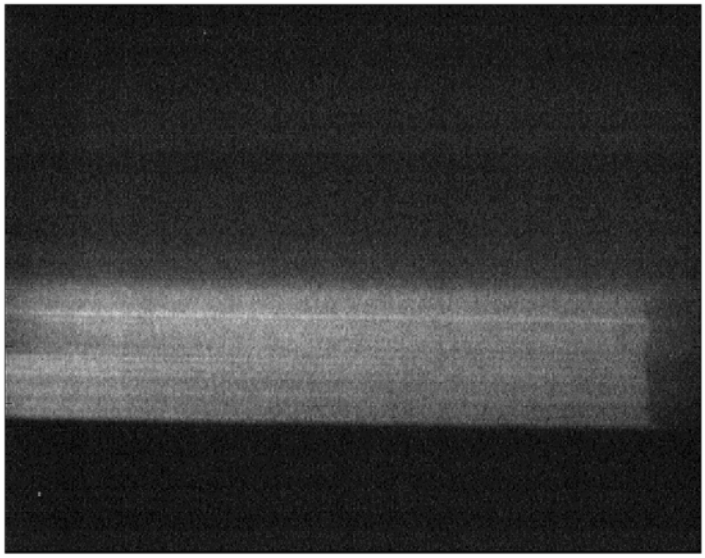

Time

Figure A-7: Natural lightning record captured on the BIFO K004M Image Converter Camera in July 17, 2006.

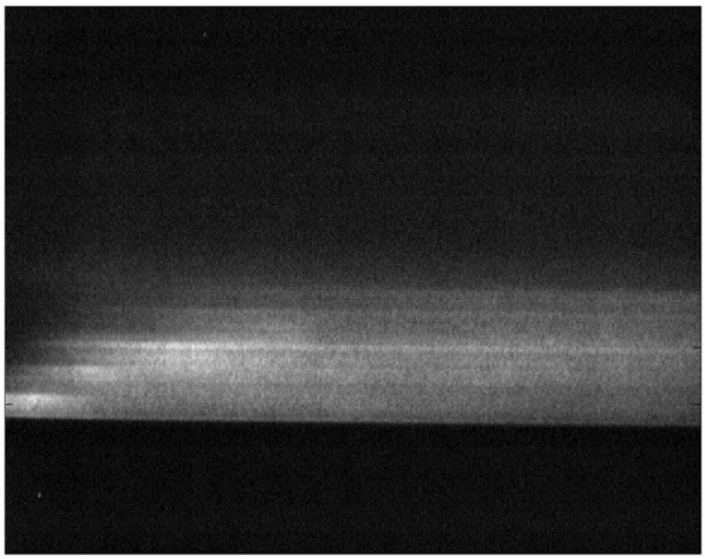

Time

Figure A-8: Natural lightning record captured on the BIFO K004M Image Converter Camera in July 17, 2006.

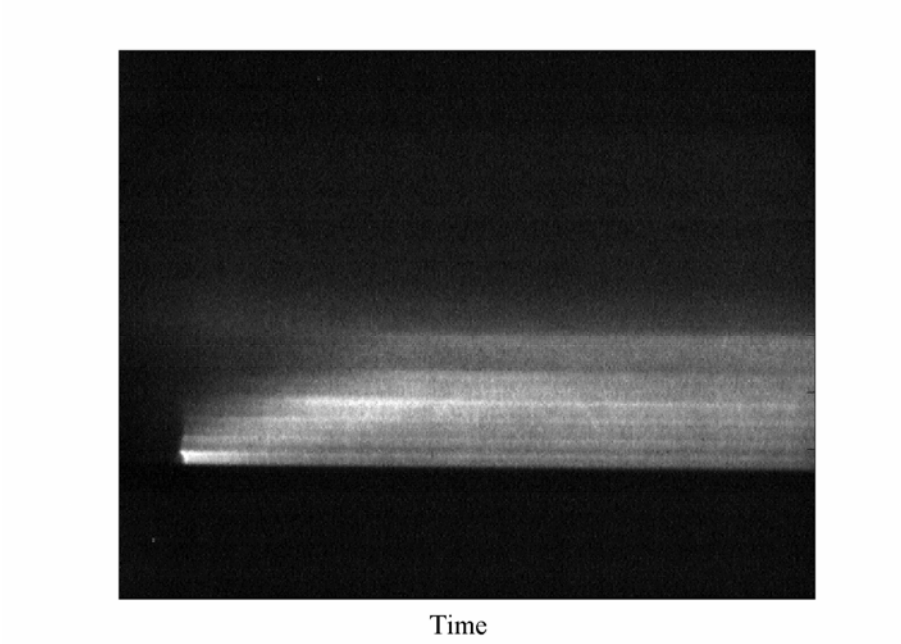

Figure A-9: Natural lightning record captured on the BIFO K004M Image Converter Camera in July 17, 2006.

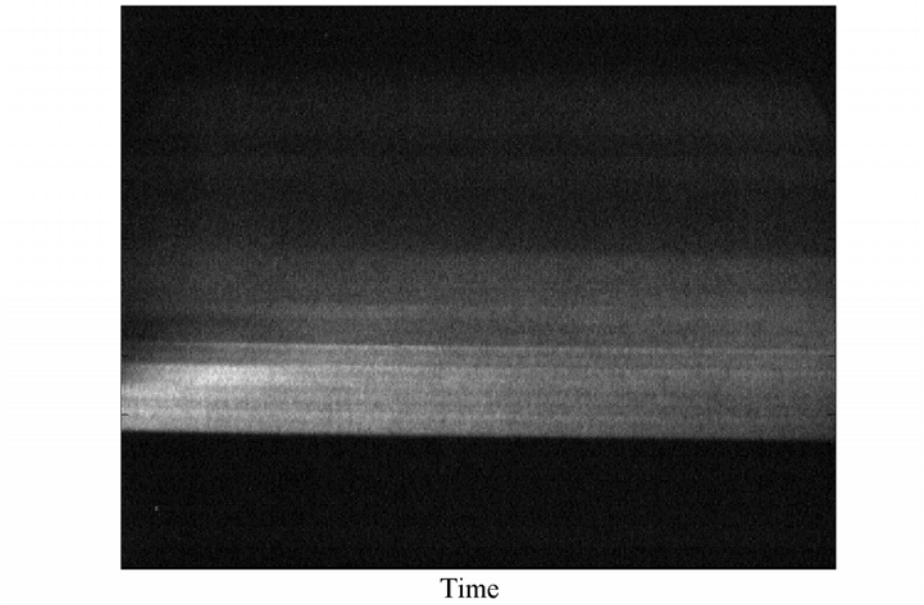

Figure A-10: Natural lightning record captured on the BIFO K004M Image Converter Camera in July 17, 2006.

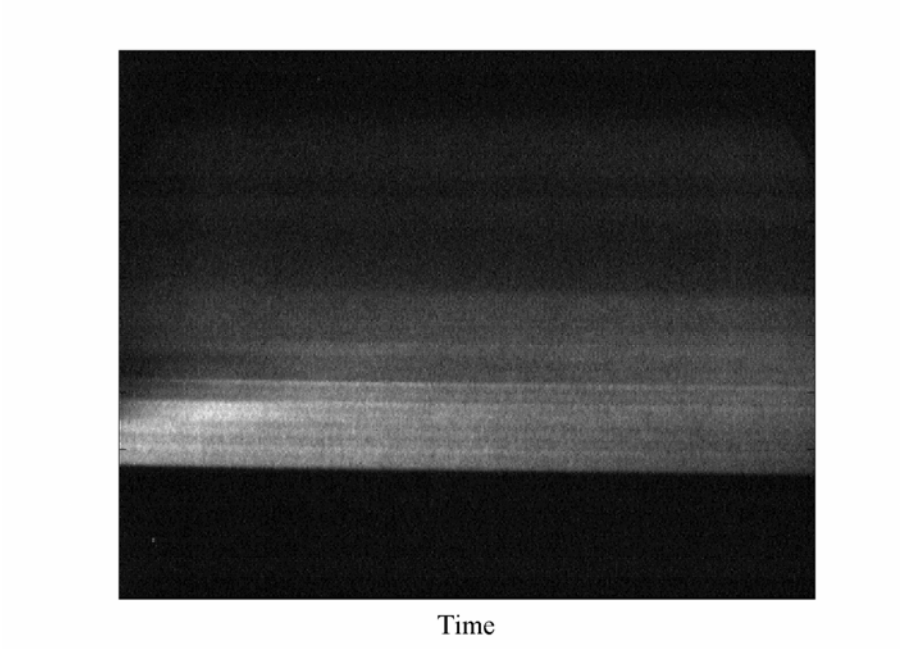

Figure A-11: Natural lightning record captured on the BIFO K004M Image Converter Camera in July 17, 2006.

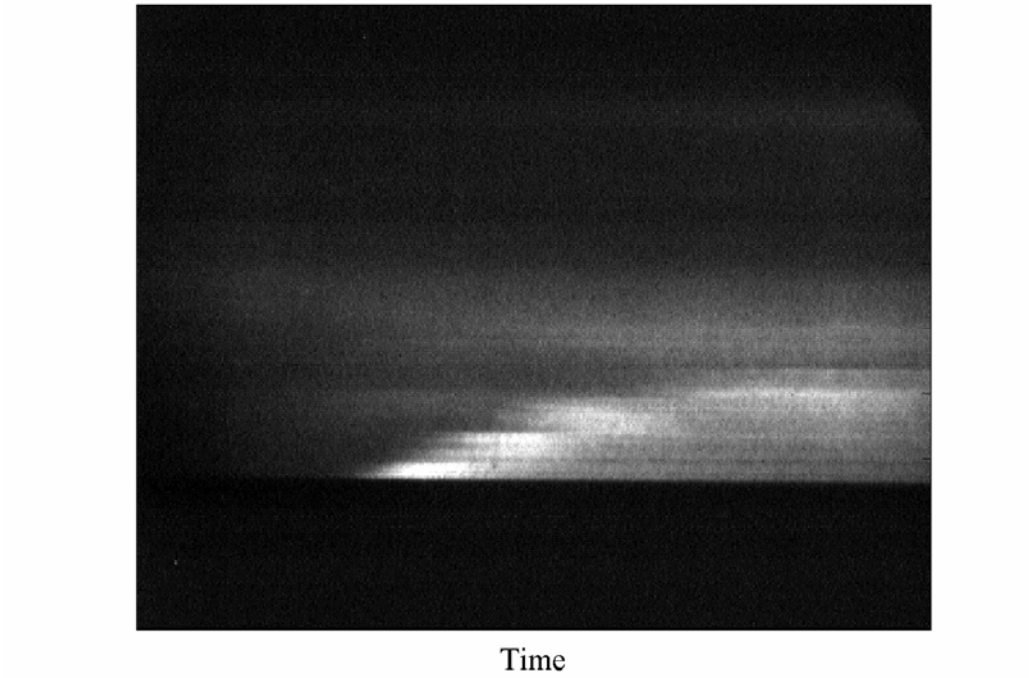

Figure A-12: Natural lightning record captured on the BIFO K004M Image Converter Camera in July 17, 2006.

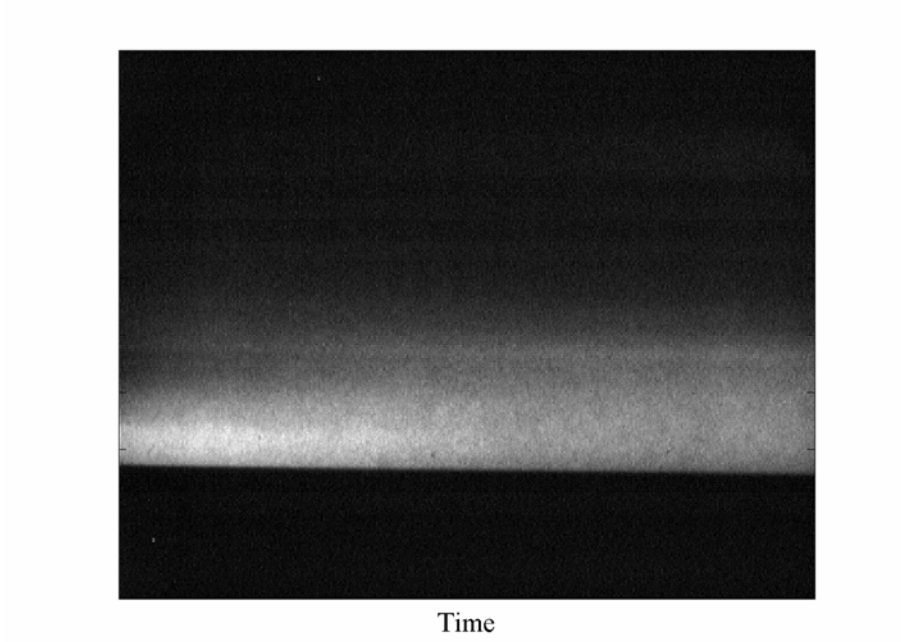

Figure A-13: Natural lightning record captured on the BIFO K004M Image Converter Camera in July 17, 2006.

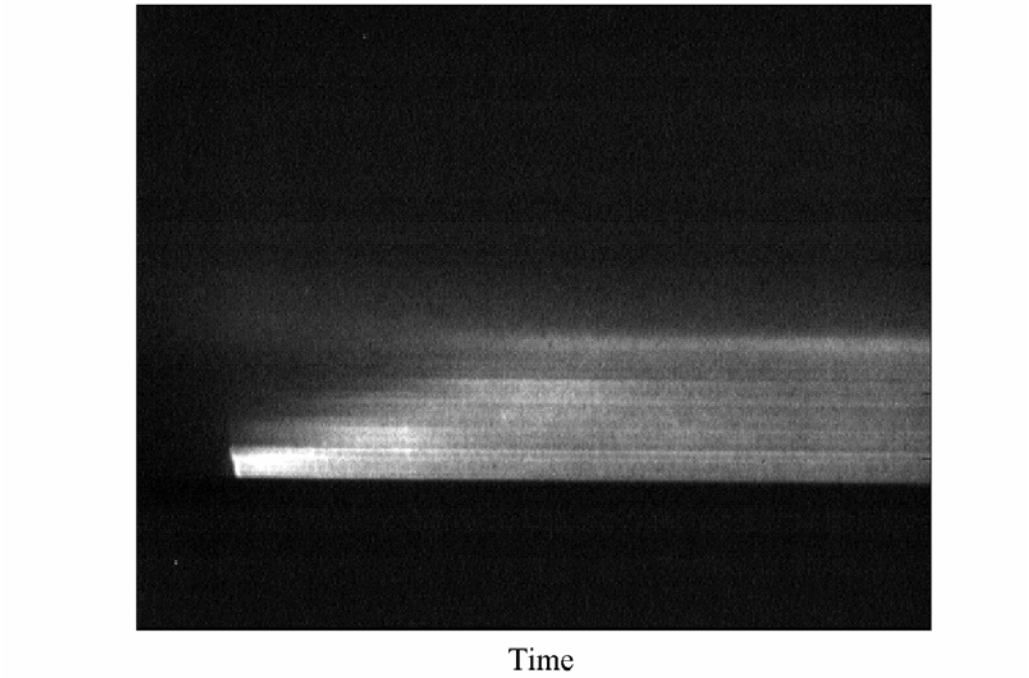

Figure A-14: Natural lightning record captured on the BIFO K004M Image Converter Camera in July 17, 2006.

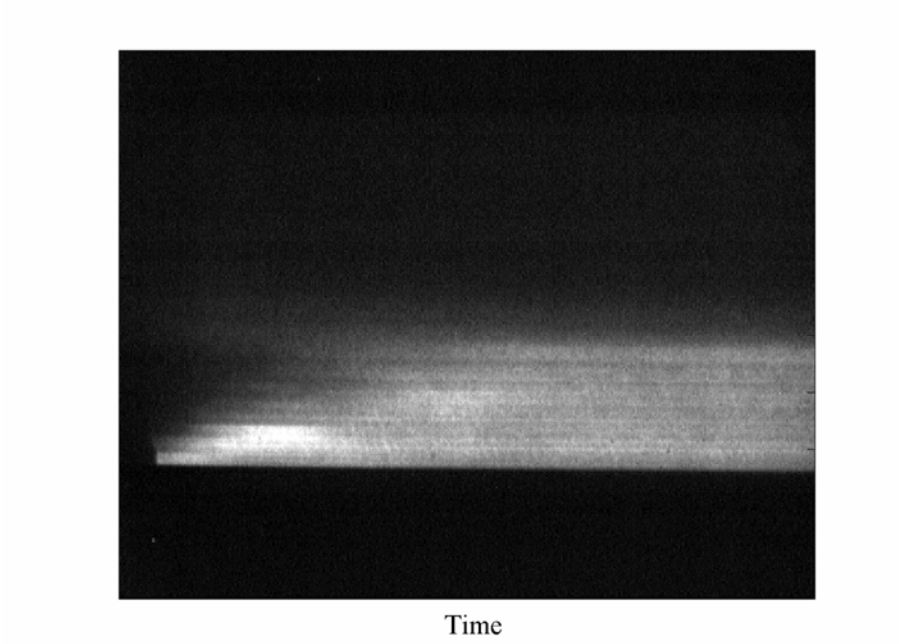

Figure A-15: Natural lightning record captured on the BIFO K004M Image Converter Camera in July 17, 2006.

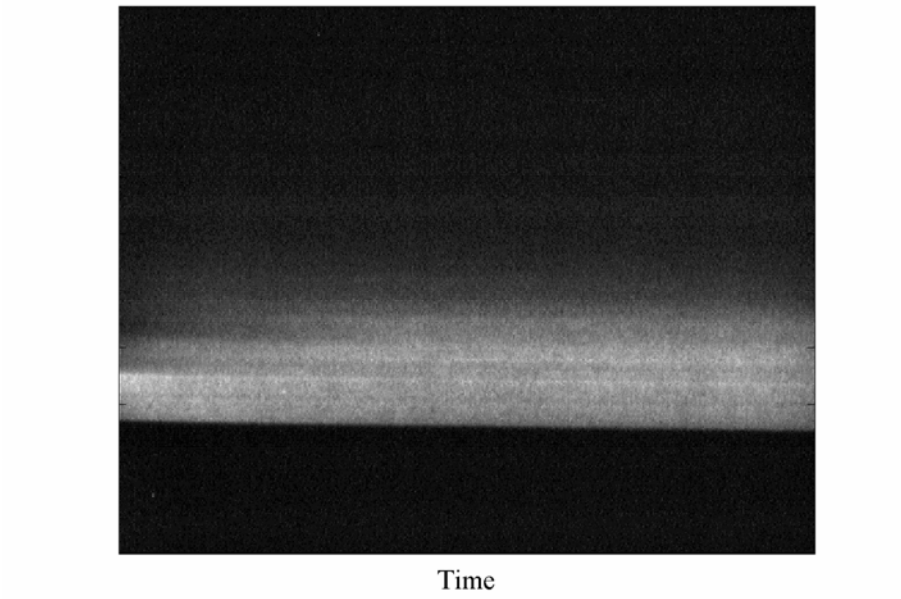

Figure A-16: Natural lightning record captured on the BIFO K004M Image Converter Camera in July 17, 2006.

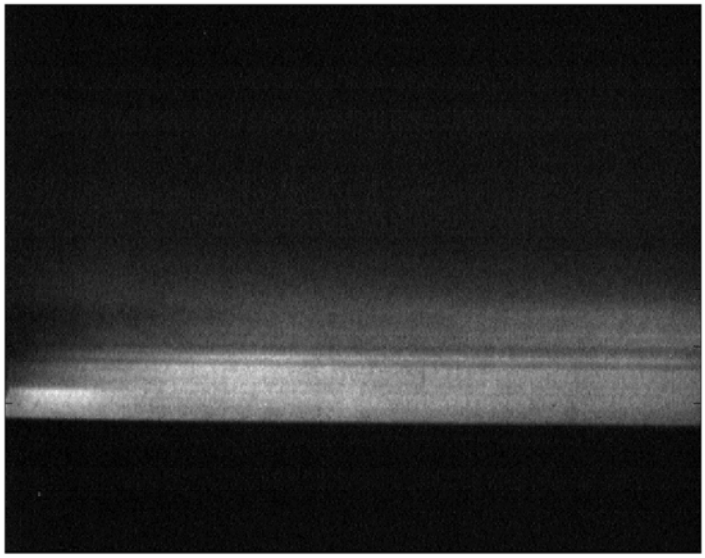

Figure A-17: Natural lightning record captured on the BIFO K004M Image Converter Camera in July 17, 2006.

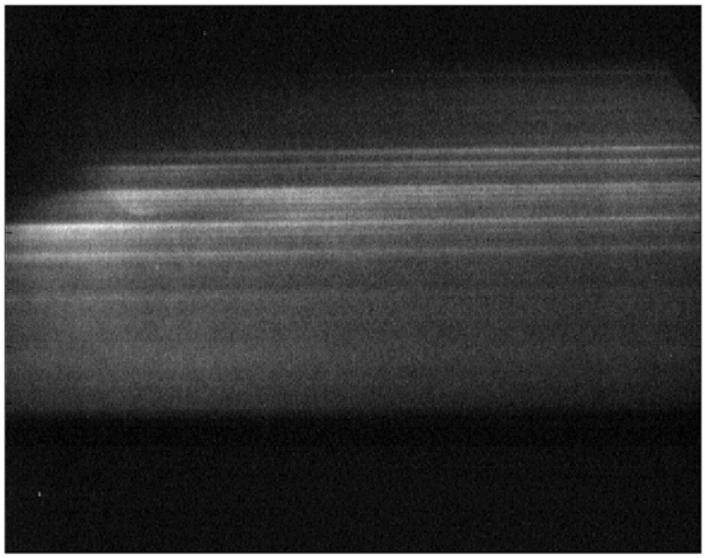

Figure A-18: Natural lightning record captured on the BIFO K004M Image Converter Camera in August 4, 2006.

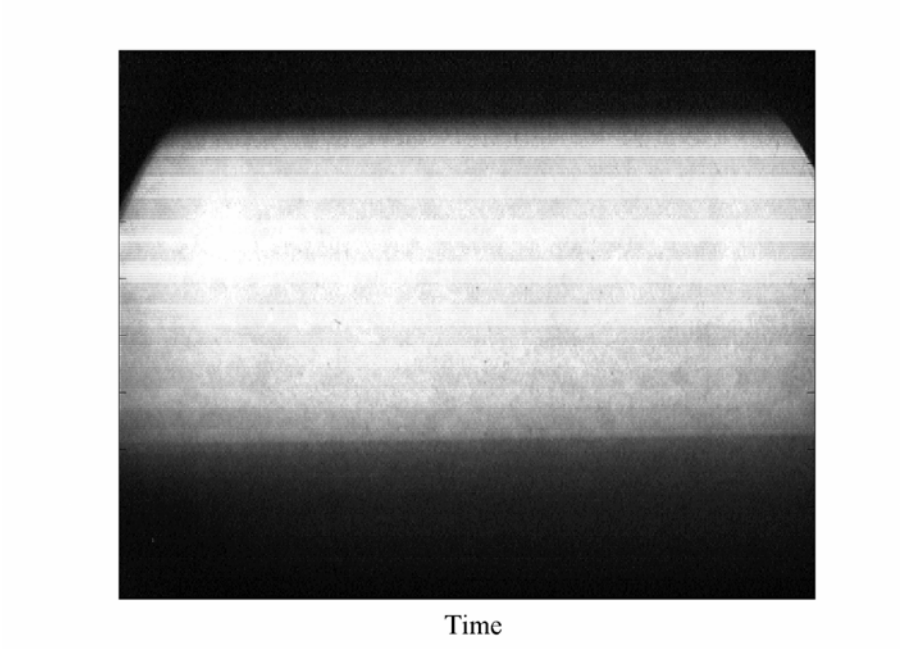

Figure A-19: Natural lightning record captured on the BIFO K004M Image Converter Camera in August 21, 2006.

APPENDIX B
FILTERS USED FOR PROCESSING THE SUMMER 2005 LIGHTNING DATA

As mentioned in chapter 5, a typical lightning light waveform is noisy, which makes the analysis of data for the purpose of return stroke speed measurements very difficult. Therefore, filtering the lightning data without affecting the risetimes of the waveforms was essential. Accordingly, three filters, the moving average filter, the low pass filter 1 and the low pass filter 2, were used when computing the return-stroke propagation speeds for the summer 2005 data captured on the LeCroy and Yokogawa oscilloscopes at various heights along the lightning channel as shown in the tables below.

Table B-1: Filters used for return-stroke speed calculation at various heights for event F0501, Stroke 1 measured using LeCroy data.

Height Range, m	Filter	
	20% Reference Point	Slope Intercept Reference Point
44-84	Low Pass Filter-2	Moving Average
84-116	Low Pass Filter-2	Moving Average
116-171	Low Pass Filter-2	Moving Average
171-245	Low Pass Filter-1	Moving Average
245-314	Low Pass Filter-1	Moving Average
314-360	Low Pass Filter-1	Moving Average
360-451	Low Pass Filter-1	Moving Average

Table B-2: Filters used for return-stroke speed calculation at various heights for event F0503, Stroke 1 measured using LeCroy data.

Height Range, m	Filter	
	20% Reference Point	Slope Intercept Reference Point
44-84	Low Pass Filter-1	Moving Average
84-116	Low Pass Filter-1	Moving Average
116-171	Low Pass Filter-1	Moving Average
171-245	Low Pass Filter-1	Moving Average
245-314	Low Pass Filter-1	Moving Average
314-360	Low Pass Filter-1	Moving Average
360-451	Low Pass Filter-1	Moving Average

Table B-3: Filters used for return-stroke speed calculation at various heights for event F0503, Stroke 2 measured using LeCroy data.

Height Range, m	Filter	
	20% Reference Point	Slope Intercept Reference Point
44-84	Low Pass Filter-2	Moving Average
84-116	Low Pass Filter-2	Moving Average
116-171	Low Pass Filter-1	Moving Average
171-245	Low Pass Filter-1	Moving Average
245-314	Low Pass Filter-1	Moving Average
314-360	Low Pass Filter-1	Moving Average
360-451	Low Pass Filter-1	Moving Average

Table B-4: Filters used for return-stroke speed calculation at various heights for event F0503, Stroke 3 measured using LeCroy data.

Height Range, m	Filter	
	20% Reference Point	Slope Intercept Reference Point
44-84	Low Pass Filter-2	Moving Average
84-116	Low Pass Filter-1	Moving Average
116-171	Low Pass Filter-1	Moving Average
171-245	Low Pass Filter-1	Moving Average
245-314	Low Pass Filter-1	Moving Average
314-360	Low Pass Filter-1	Moving Average
360-451	Low Pass Filter-1	Moving Average

Table B-5: Filters used for return-stroke speed calculation at various heights for event F0503, Stroke 4 measured using LeCroy data.

Height Range, m	Filter	
	20% Reference Point	Slope Intercept Reference Point
44-84	Low Pass Filter-1	Moving Average
84-116	Low Pass Filter-1	Moving Average
116-171	Low Pass Filter-1	Moving Average
171-245	Low Pass Filter-1	Moving Average
245-314	Low Pass Filter-1	Moving Average
314-360	Low Pass Filter-1	Moving Average
360-451	Low Pass Filter-1	Moving Average

Table B-6: Filters used for return-stroke speed calculation at various heights for event F0510, Stroke 1 measured using LeCroy data.

Height Range, m	Filter	
	20% Reference Point	Slope Intercept Reference Point
44-84	Low Pass Filter-1	Moving Average
84-116	Low Pass Filter-1	Moving Average
116-171	Low Pass Filter-1	Moving Average
171-245	Low Pass Filter-1	Moving Average
245-314	Low Pass Filter-1	Moving Average
314-360	Low Pass Filter-1	Moving Average
360-451	Low Pass Filter-1	Moving Average

Table B-7: Filters used for return-stroke speed calculation at various heights for event F0512, Stroke 1 measured using LeCroy data.

Height Range, m	Filter	
	20% Reference Point	Slope Intercept Reference Point
44-84	Low Pass Filter-1	Moving Average
84-116	Low Pass Filter-1	Moving Average
116-171	Low Pass Filter-1	Moving Average
171-245	Low Pass Filter-1	Moving Average
245-314	Low Pass Filter-1	Moving Average
314-360	Low Pass Filter-1	Moving Average
360-451	Low Pass Filter-1	Moving Average

Table B-8: Filters used for return-stroke speed calculation at various heights for event F0514, Stroke 1 measured using LeCroy data.

Height Range, m	Filter	
	20% Reference Point	Slope Intercept Reference Point
44-84	Low Pass Filter-1	Moving Average
84-116	Low Pass Filter-1	Moving Average
116-171	Low Pass Filter-1	Moving Average
171-245	Low Pass Filter-1	Moving Average
245-314	Low Pass Filter-1	Moving Average
314-360	Low Pass Filter-1	Moving Average
360-451	Low Pass Filter-1	Moving Average

Table B-9: Filters used for return-stroke speed calculation at various heights for event F0517, Stroke 1 measured using LeCroy data.

Height Range, m	Filter	
	20% Reference Point	Slope Intercept Reference Point
44-84	Low Pass Filter-1	Moving Average
84-116	Low Pass Filter-1	Moving Average
116-171	Low Pass Filter-1	Moving Average
171-245	Low Pass Filter-1	Moving Average
245-314	Low Pass Filter-1	Moving Average
314-360	Low Pass Filter-1	Moving Average
360-451	Low Pass Filter-1	Moving Average

Table B-10: Filters used for return-stroke speed calculation at various heights for event F0517, Stroke 2 measured using LeCroy data.

Height Range, m	Filter	
	20% Reference Point	Slope Intercept Reference Point
44-84	Low Pass Filter-2	Moving Average
84-116	Low Pass Filter-1	Moving Average
116-171	Low Pass Filter-1	Moving Average
171-245	Low Pass Filter-1	Moving Average
245-314	Low Pass Filter-1	Moving Average
314-360	Low Pass Filter-1	Moving Average
360-451	Low Pass Filter-1	Moving Average

Table B-11: Filters used for return-stroke speed calculation at various heights for event F0521, Stroke 1 measured using LeCroy data.

Height Range, m	Filter	
	20% Reference Point	Slope Intercept Reference Point
44-84	Low Pass Filter-1	Moving Average
84-116	Low Pass Filter-1	Moving Average
116-171	Low Pass Filter-1	Moving Average
171-245	Low Pass Filter-1	Moving Average
245-314	Low Pass Filter-1	Moving Average
314-360	Low Pass Filter-1	Moving Average
360-451	Low Pass Filter-1	Moving Average

LIST OF REFERENCES

BIFO Company, K004M Universal Image Converter Camera Documentation, BIFO Company, Moscow, Russia, 2002.

Idone, V. P., and R.E. Orville (1984), Three Unusual strokes in a Triggered Lightning Flash, *J. Geophysis. Res.*,*89*, 7311-7316.

Idone, V. P., R.E. Orville, Pierre Hubert, Louis Barret and Andre Eybert-Berard (1984), Correlated Observations of Three Triggered Lightning Flashes, *J. Geophysis. Res.*, *89*, 1385-1394.

Idone, V. P., and R.E. Orville (1987), The Propagation Speed of a Positive Lightning Return Stroke, *J. Geophysis.* Res., *14*, 1150-1153.

Idone, V. P., and R.E. Orville (1992), Return stroke velocities in the Thunderstorm Research International Program (TRIP), *J. Geophysis. Res.*, *87*, 12, 23-28.

Jordan, D. M. (1990), Relative light intensity and electric field intensity of cloud to ground lightning, *Ph. D. thesis*, *Univ. of Fla.*, Gainesville.

Jordan, D. M., V. A. Rakov, William H. Beasley, and Marting A. Uman (1997), Luminosity characteristics of dart leaders and return strokes in natural lightning, *J. Geophysis. Res.*, *102*, 22025-22032

Jordan, D. M., V. P. Idone, V. A. Rakov, M. A. Uman, W. H. Beasley and H. Jurenka (1992), Observed Dart Leader Speed in Natural and Triggered Lightning, *J. Geophysis. Res.*, *97*, 9951-9957.

Mach, D. M., and W. D. Rust (1989a), Photoelectric return-stroke velocity and peak current estimates in natural and triggered lightning, *J. Geophysis. Res.*, *94(D11)*, 13,237-13,247.

Mach, D. M., and W. D. Rust (1989b), A photoelectric technique for measuring lightning-channel propagation velocities from a mobile laboratory, *J. Atmos. Oceanic Technol.*, *6*, 439-445.

Mach, D. M., and W. D. Rust (1997), Two dimensional speeds and optical risetime estimates for natural and triggered dart leaders, *J.Geophys. Res.*, *102*, 13,673-13,684.

McEachron, K. (1939), Lightning to the Empire State Building, *J. Franklin Inst.*, *227*,149-217.

Olsen, R. C. III (2003), Optical Characterization of Rocket-Triggered Lightning at Camp Blanding, Florida, *Master's Thesis*, *Univ. of Fla.*, Gainesville.

Olsen, R. C. III, D. M. Jordan, V. A. Rakov, M. A. Uman, N. Grimes (2004), Observed one-dimensional return stroke propagation speeds in the bottom 170 m of a rocket-triggered lightning channel, *Geophys. Res. Letters*, *31*, L1607.

Rakov V. A., and M. A. Uman (2003), Lightning: Physics and Effects, *Cambridge University Press*, *Cambridge*

Schonland, B. (1956), The Lightning Discharge, *Handb. Phys*.

Thomson, E. M., M. A. Uman and W. H. Beasley (1985), Speed and Current for Lightning Stepped Leaders Near Ground as Determind From Electric Field Records, *J. Geophysis. Res.*, *90*, 8136-8142.

Uman, M. A. (1987), The Lightning Discharge, *Academic*, *San Diego*, *Califonia.*

Wang, D., N. Takagi, T. Watanabe, V. A. Rakov, and M. A. Uman (199b), Observed leader and return stroke propagation characteristics in the bottom 400 m of a rocket-triggered lightning channel, *J. Geophys. Res.*, *104*, 14,369-14,376.

BIOGRAPHICAL SKETCH

Sandip Nallani C. was born in Mumbai, India, in 1983. He graduated with a Bachelor of Science degree in electronics and telecommunication engineering from K. J. Somaiya Institute of Engineering and Information Technology in India, in 2005. In Fall 2005, he went to the USA to pursue a Master of Science degree in electrical engineering at the University of Florida, Gainesville.